UNIVERSITY OF SOUTHAMPTON

Faculty of Natural and Environmental Sciences
Ocean and Earth Science

National Oceanography Centre, University of Southampton

WAVE DISSIPATION PATTERNS AS AN INDICATOR OF RIP CURRENT HAZARD

By

SEBASTIAN JOHN PITMAN

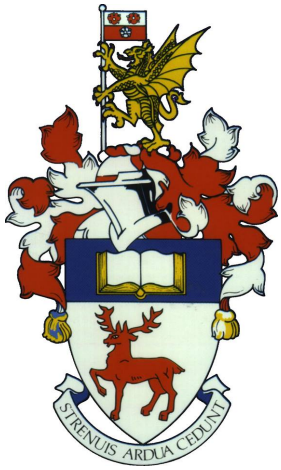

Thesis for the degree of Doctor of Philosophy

March 2017

UNIVERSITY OF SOUTHAMPTON

ABSTRACT

FACULTY OF NATURAL AND ENVIRONMENTAL SCIENCES

Ocean and Earth Sciences

Doctor of Philosophy

WAVE DISSIPATION PATTERNS AS AN INDICATOR OF RIP CURRENT HAZARD

by Sebastian John Pitman

Rip currents (rips) are hazardous offshore-directed flows in the surfzone of beaches worldwide. Rips are a major hazard for recreational beach use and are the dominant cause of beach rescues and drownings. It is therefore important to understand what conditions make a rip most hazardous, in order for beach safety practitioners to mitigate the risk. The aim of this thesis was to determine how patterns of wave breaking influence rip channel hazard on beaches. In order to quantify wave breaking, video imagery from three hydrodynamically diverse case studies was used, and validated at two sites against Lagrangian GPS drifter data. This thesis first developed pre-processing techniques for video imagery which then subsequently improved the reliability of rip channel detection. Hitherto, the noise inherent in such signals has made automated detection of rip currents problematic. Wave breaking patterns could then be identified with the novel application of synoptic typing methods to the imagery, resulting in a classification scheme for rip currents based on wave breaking. Two dominant types were identified: (1) open channels, whereby the rip channel has free connectivity to the region beyond the surfzone; and (2) closed channels, where wave breaking across the seaward extent of the channel effectively closes this connectivity to the offshore region. Investigation of Lagrangian data for each of the prevailing states shows that under open conditions, drifters were highly likely to be transported beyond the edge of the surfzone by the rip current, with exit rates reaching 100 % at times. Under closed conditions, drifters were more likely to be retained in the surfzone, with typical exit rates between 0 and 35 %. A rip current that exits the surfzone is more hazardous to bathers, and therefore, this thesis subsequently investigated the prevalence of open and closed rip channels in records of rip rescue events. Over two sites for which data were available, upwards of two thirds of major rip rescues occurred when the channel could be classified by this new method as open. Furthermore, the majority of surfer and bodyboarder rescues occurred under open conditions. Despite their over-representation in the rip rescue record, the overall prevalence of open channels over a year is only around 40 %. Normalising the number of rescues in open rips by their occurrence shows open rips to be twice as hazardous as closed channels. This new approach provides a quick and inexpensive means to assess high risk surf conditions at rip beaches worldwide, with the deployment of only a small (often mobile) imaging system.

Contents

List of Figures

List of Tables

DECLARATION OF AUTHORSHIP

I, **SEBASTIAN JOHN PITMAN** declare that this thesis entitled **Wave dissipation patterns as an indicator of rip current hazard**, and the work presented in it are my own and has been generated by me as the result of my own original research.

1. This work was done wholly or mainly while in candidature for a research degree at this University;
2. Where any part of this thesis has previously been submitted for a degree or any other qualification at this University or any other institution, this has been clearly stated;
3. Where I have consulted the published work of others, this is always clearly attributed;
4. Where I have quoted from the work of others, the source is always given. With the exception of such quotations, this thesis is entirely my own work;
5. I have acknowledged all main sources of help;
6. Where the thesis is based on work done by myself jointly with others, I have made clear exactly what was done by others and what I have contributed myself;
7. Parts of this work have been published as:
   (a) Parts of Chapter 5 were published as Pitman, S.J.; Gallop, S.L.; Haigh, I.D.; Mahmoodi, S.; Masselink, G., and Ranasinghe, R., 2016. Synthetic imagery for the automated detection of rip currents. **In:** Vila-Concejo, A.; Bruce, E.; Kennedy, D.M., and McCarroll, R.J. (eds.), Proceedings of the 14th International Coastal Symposium (Sydney, Australia). Journal of Coastal Research, Special Issue, No. 75, pp. 912-916. Coconut Creek (Florida), ISSN 0749-0208.
   (b) Parts of Chapters 7 were published as Pitman, S.J.; Gallop, S.L.; Haigh, I.D.; Masselink, G., and Ranasinghe, R., 2016. Wave breaking patterns control rip current flow regimes and surfzone retention. Marine Geology 382: 176 - 190.

Sebastian John Pitman Date

Acknowledgements

> Research is to see what everyone else has seen, and to think what nobody else has thought.
>
> *Albert Szent-Gyorgi*

The PhD journey has been far from simple, and nor could I consider it to be linear in nature. I am indebted to my supervisory team for keeping me on track, challenging my thought process, and ensuring I can justify and defend my findings. To Dr. Ivan Haigh I am most grateful for his dedication to supervision, his ability to motivate and keep things in perspective, and his excellent technical tuition in all things coding. To Dr. Shari Gallop I am indebted for initially inspiring in me an active interest in rip currents, and therein for dedicated supervision and support both in person and remotely. Shari has engendered in me the ability to critically assess my methods, results, and more importantly, my interpretations and conclusions. To Prof. Gerd Masselink I owe thanks for inspiring my initial interest in coastal morphology. During this research, Gerd has been on hand to provide fresh insight, geomorphological expertise, and most important for the course of this PhD, frank opinion. To both Prof. Rosh Ranasinghe and Dr. Sasan Mahmoodi I am thankful for early discussions on the approach to automated rip detection, and for critical reviews of draft manuscripts through the course of the project.

To The University of Southampton, I acknowledge the receipt of a studentship, enabling the project to take place. Furthermore, grants from the Royal Geographical Society and the British Society for Geomorphology enabled both fieldwork and travel during the project. To Kelvin Aylett I am most grateful for dedicated support and patience in the manufacture of our GPS drifters. I thank Dr. Tim Scott for the many discussions around data, fieldwork, and rip current hazard. I would like to thank both the RNLI and also Surf Lifesaving New Zealand for the free provision of rip current incident data, and in particular Nick Mulcahy and Meagan Lowe for facilitating the provision of SLSNZ data. I would like to thank the National Institute of Water and Atmospheric Research (NZ), and Oregon State University for the provision of field site imagery. I'd also like to extend thanks to Dr. Karin Bryan, Dean Sandwell, Raglan Coastguard and all the field teams for both of our experiments, of whom there are far too many to name here.

My family have been most supportive through the PhD, offering both motivation, perspective and a genuine interest in my work. Thanks to Dad (Mike), Mum (Sue), and my Grandad (John) for all their support throughout. I owe an enormous debt of gratitude to my partner, Emilie, who has picked me up from the deepest lows, offered unconditional support, shown compassion and care by the bucket load, and kept my work-life balance on track throughout. It's been most refreshing to come back to you after the bad days, only to be whisked out into the forest to a nice pub with our two dogs to forget it all!

Definitions and abbreviations

ATV	All–terrain vehicle
BODC	British Oceanographic Data Centre [UK]
CCO	Channel Coast Observatory [UK]
CD	Chart Datum [m]
D_{50}	Medium diameter of grain size distribution [mm]
F_N	Normalised frequency distribution
Γ	Horizontal vorticity $[s^{-1}]$
GUI	Graphical User Interface
GPS	Global Positioning System
GNSS	Global Navigation Satellite System
H_m	Maximum wave height [m]
H_s	Significant wave height [m]
IRB	Inshore rescue boat
λ	Rip current spacing [m]
LIDAR	Light Direction and Ranging
LW	Low water
MLW	Mean Low Water
MLWN	Mean Low Water Neaps
MLWS	Mean Low Water Springs
MSL	Mean Sea Level
NIWA	National Institute of Water and Atmospheric Research [New Zealand]
O	On the order of
ODN	Ordnance Datum Newlyn [m]
θ	Mean incident wave direction [°]
RADAR	Radio Direction and Ranging
RNLI	Royal National Lifeboat Institution [UK]

RTK-GPS	Realtime kinematic GPS
SAR	Synthetic Aperture RADAR
SLSNZ	Surf Life Saving New Zealand
τ	Threshold
T_p	Peak wave period [s]
U	Wind speed [m s^{-1}]
VLF	Very Low Frequency
W_{Dir}	Wind direction [°]
X_s	Surfzone width [m]

Chapter 1

Introduction

This chapter offers a broad overview of rip current formation, and sets the aims and objectives of the thesis. It is important for the reader to be aware of subtle differences in terminology used throughout the thesis, outlined below:

1. **Rip current** refers to an established active offshore flow, with the term often shortened to *'rip'*.
2. **Rip channel** refers to a morphological depression, which given the right environmental conditions, may contain a *rip current*.

1.1 Background

Rip currents (rips) are hazardous narrow currents in the surfzone (Figure 1.1) of beaches worldwide, that generally head seawards. They typically have velocities of 0.5—0.8 m s^{-1}, and can exceptionally reach 2 m s^{-1} (MacMahan et al., 2006). Rips are a major hazard to recreational beach users, as bathers can be transported seaward and often require rescue (Figure 1.2). These rescue events and associated fatalities were key drivers behind early rip current research (Shepard et al., 1941), focused on the Californian

coastline. Shepard (1936) detailed discussions held with lifeguards in Los Angeles, whom described rips carrying bathers far offshore. Rips still present a global problem for recreational beach use; in the U.K., 68 % of incidents on beaches patrolled by the Royal National Lifeboat Institution (RNLI) are attributed to rips (Scott et al., 2008), in Australia, rips were a factor in 44 % of recorded beach drownings over a seven-year period (Brighton et al., 2013), and in Japan they were a factor in 45 % of rescues (Ishikawa et al., 2014). Indeed, the rip current hazard has been heralded as the greatest danger to users of recreational beaches worldwide (Brander and MacMahan, 2011), and therefore a good understanding of the processes controlling their formation, behaviour, and decay is of paramount importance. Rips are also seen as key drivers of cross-shore shore sediment transport (Aagaard et al., 1997), and have been observed to move significant amounts of sediment offshore to the inner continental shelf (Cook, 1970), with obvious implications for storm erosion and post storm recovery.

There are multiple types of rip currents, broadly categorised into: (1) bathymetric rips, driven by hydrodynamics but strongly influenced in alongshore morphological variability; (2) hydrodynamic rips driven by solely by hydrodynamic forcing in the absence of any morphological control; and (3) boundary rips controlled by solid structures (Castelle et al., 2016b). These types are discussed in detail in Section 2.2.2. This thesis focusses on channel rips which are a type of bathymetric rip formed in deeper channels incised through sand bars (Castelle et al., 2016b). Beaches that are considered as pleasant recreationally are often replete with the physical conditions under which bathymetric rip channels will likely form. For example, it is common on straight, sandy beaches for a submerged bar to develop, over which the majority of the incident wave field will break. Rip currents can then be generated by alongshore variations in bathymetrically-controlled breaking wave heights over this bar (Bowen, 1969; Bruneau et al., 2011). Longshore variability in wave breaking intensity acts to create gradients in radiation stress (Sonu, 1972); the excess flow of momentum due to the presence of waves (Longuet-Higgins and Stewart, 1964). Negligible influence is exerted by unbroken waves propagating through incised channels in the bar, whereas high landward-directed stresses

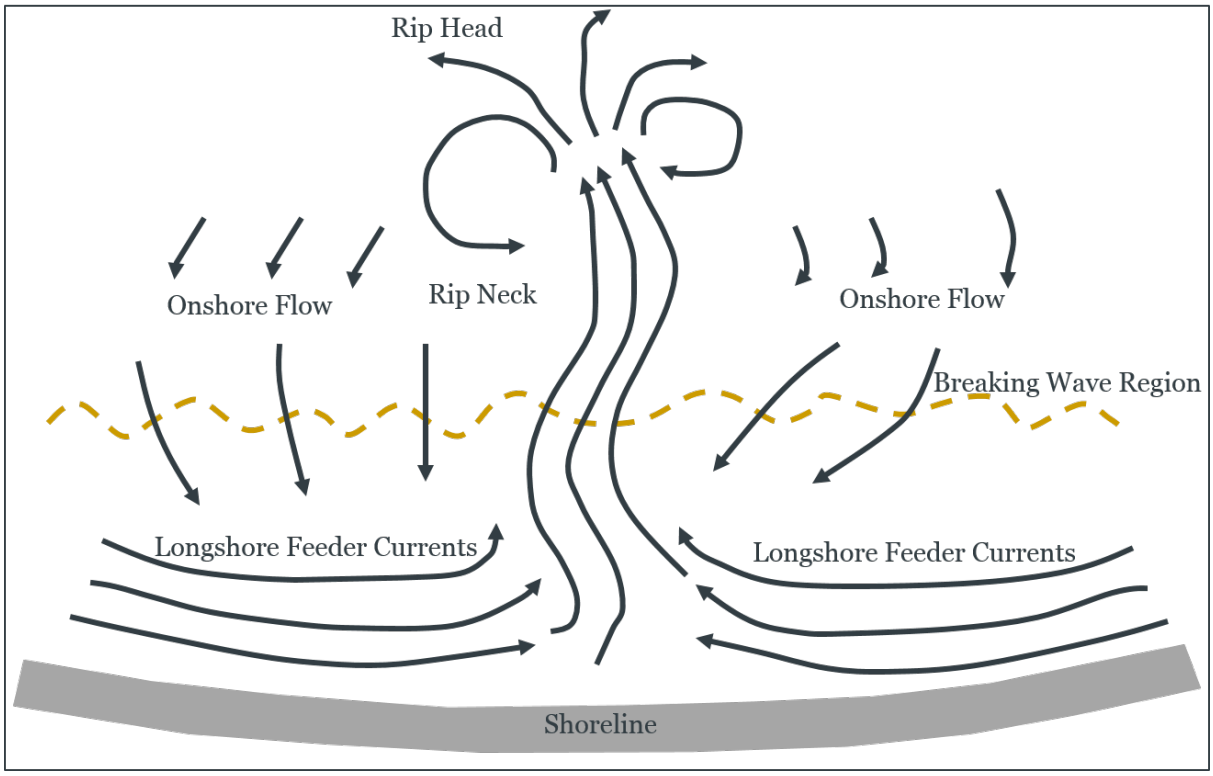

Figure 1.1: A schematic of a generalised rip current and associated nearshore circulations. Adapted from MacMahan et al. (2006) and based on early observations.

form when waves break over the bar, forming a longshore gradient directed towards the channels, driving the rip current (Austin et al., 2009).

Shorelines often exhibit rhythmic rip channel spacing as a result of the hydrodynamic (wave/tide) forcing, with spacing of $O(100$ m) (Aagaard et al., 1997). Early observations (Shepard and Inman, 1950, 1951; Bowen, 1969) identified four component parts to a generalised rip current system: (1) shoreward mass transport due to wave motion through the surfzone, (2) a longshore feeder current, (3) a seaward, laterally confined flow (the rip neck), and (4) the dispersive rip head (Figure 1.1). Although this early conceptualisation still persists, recent research (Austin et al., 2010; MacMahan et al., 2010) has shown that often, much more complex patterns are regularly present. In particular, there is a tendency for circulation cells to form, whereby the current does not

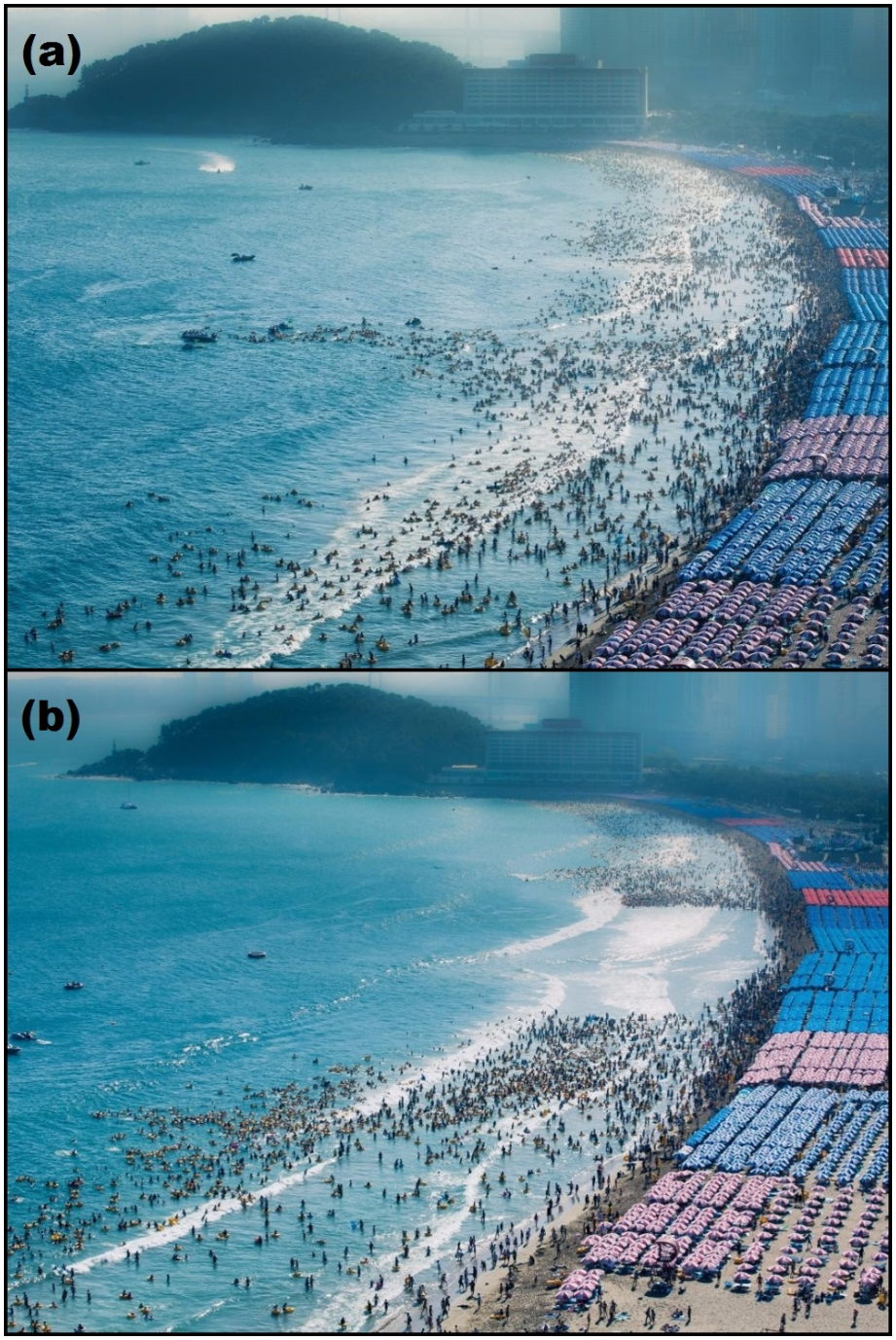

Figure 1.2: (a) A mass rescue from a rip current at Busan beach, South Korea, and (b) the aftermath of the rescue whereby lifeguards have cleared the area of the beach associated with the rip current. Photo credit: J. Lee.

disperse in the rip head, but instead circulates back onshore, creating a cell-like circulation (Austin et al., 2010; MacMahan et al., 2010).

Circulation of rip current cells is horizontally segregated, with depth-uniform onshore flows over the bar and depth-uniform offshore flows through the channel (Inman and Quinn, 1952; Bowen, 1969; Bowen and Inman, 1969). Rip current magnitude is proportional to the percentage of water depth occupied by the bar, i.e. the bar height as a percentage of water depth over the bar trough (Dean and Thieke, 2011). This explains why many studies (e.g. Shepard et al., 1941; Aagaard et al., 1997; Brander and Short, 2000; Austin et al., 2009, 2010; Scott et al., 2014) show tidal modulation of the rip current, with the strongest velocities at or around low tide. At mid- or high-tide, the water depth may be too deep for waves to break over the bar, whereas at lower water levels, breaking occurs and longshore gradients in radiation stress are created. This is often referred to as the expression of the morphological template (Scott et al., 2014), with lower water levels creating morphologically constricted flows.

Our understanding of controls on rip circulation have been gained through many studies using *in situ* measurements (Austin et al., 2009, 2010, 2014; MacMahan et al., 2010; McCarroll et al., 2014; Scott et al., 2014), and video imagery (Ranasinghe et al., 1999; Bogle et al., 2000; Whyte et al., 2005; Holman et al., 2006; Turner et al., 2007; Gallop et al., 2009, 2011). The use of video imagery to measure rips was an important step as it allows for near continual acquisition of data (discussed in Section 2.1). However, a key consideration of video systems is the creation of massive datasets that need an efficient means of analysis. Therefore, there is a drive for automation (Ranasinghe et al., 1999; Holman et al., 2006) of rip channel detection from video imagery in order to extract only the pertinent information. However, attempts to completely automate the process thus far have been unsuccessful.

As a result of the difficulty in extracting rip information from imagery, very little research has attempted to combine *in situ* measurement of rips with video images for quantitative means. One such study addressing this was by Austin et al. (2010), which quantified wave roller dissipation over the sand bar at Perranporth, U.K., and linked the intensity of breaking to rip pulsations. The patterns of wave breaking they identified

were subject to rapid change, and they were only able to qualitatively describe the wave roller dissipation. Since wave breaking patterns can exert control on rip current circulation, it is important to classify different types of wave breaking pattern in order to compare against circulatory response. This is an approach to classification not previously attempted, as most rip classifications describe instead the formation mechanisms of rip currents, and thus do not focus on temporal changes in circulation within each rip type (discussed in Section 2.2).

The Austin et al. (2010) study determined how changes in the intensity of wave dissipation activated the rip, but not how patterns of dissipation influenced circulation pattern, i.e., if a rip is retained within, or exits the surfzone. A link between readily observable phenomena, such as wave breaking, and the danger level of prevailing rip currents could have practical benefits, yet this control is yet to be quantified. The implications are discussed in Section 2.3. This investigation of wave breaking patterns could provide an indication of whether rip currents are likely to be retained within, or exit, the surfzone based purely on real time video imagery. Such information would prove useful to beach safety practitioners. Rips exiting the surfzone are likely more dangerous as they carry bathers further offshore, therefore, beach practitioners may elect to increase coverage or patrols on days where rips appear more dangerous in imagery.

1.2 Aims and objectives

The overall aim of this thesis is to determine how patterns of wave breaking influence rip channel hazards on beaches. In order to quantify wave breaking, a novel combination of video imagery and *in situ* measurement is used as a means to quantify surfzone processes. The overall aim is achieved through the following four objectives:

1. To develop pre-processing image techniques to improve the reliability of automated rip channel detection in video imagery.
2. To establish a classification of rip channel morphology based on wave breaking patterns.

3. To assess the control exerted by differing wave breaking patterns on rip current flow regimes.

4. To identify the hydrodynamic and morphologic conditions most conducive to formation of hazardous rip currents.

These objectives were achieved using three study sites; Tairua (New Zealand), Perranporth (U.K.), and Ngarunui (New Zealand). Tairua is used purely for video imagery analysis in Objective 1. Perranporth and Ngarunui are two hydrodynamically diverse sites, offering different tidal ranges (macro- and mesotidal, respectively), and differing morphological states (low tide bar/rip, and double barred, respectively). Therefore, they are both used for *in situ* measurement and video analysis, contributing towards Objectives, 2, 3, and 4. All three sites, including the rationale behind their selection, are detailed in Chapter 3.

To address Objective 1, new image processing techniques are applied in order to allow automated rip current detection in video imagery. Subsequently, the effect of pre-filtering imagery on subsequent processing is investigated to develop a simplified binary image for rip channel detection.

In Objective 2, the binary images are used as a measure of wave breaking patterns. Here, a synoptic typing algorithm is applied to images from two study sites, in order to identify the dominant patterns of wave breaking. From here, the thesis investigates the degree to which hydrodynamic parameters control the observed patterns of wave breaking and establishes the controls on temporal change in wave breaking patterns.

Having classified the wave breaking patterns, in Objective 3 the general hydrodynamics of the GPS drifters are quantified over the course of the experiment, after which a comparison to the two dominant regimes of wave breaking (open or closed rip channels) can be made. This allows determination of whether a change in wave breaking pattern influences the rip current circulation.

For Objective 4, an existing analysis of high risk hydrodynamic conditions for Perranporth is compared against new hydrodynamic analysis at Ngarunui. Subsequently,

a comparison between rip current rescue data and the patterns of wave breaking observed from the video imagery is made. This establishes whether one of the two dominant wave breaking regimes outlined in Objective 3 can be considered as more hazardous to bathers.

1.3 Thesis structure

The structure of the thesis is as follows: **Chapter 2** consists of a literature review, with sections that mirror the thesis objectives. **Chapters 3** and **4** outline the study sites and the generic methods used for data collection. **Chapters 5**, **6**, **7** & **8** are then used to address the four objectives in turn. The key findings of the study are summarised and discussed in **Chapter 9**, along with recommendations for further research.

Chapter 2

Literature review

This chapter gives an overview of the current state of the art, and identifies the knowledge gaps leading to the creation of the four research objectives: Automated rip detection is considered in Section 2.1; Section 2.2 discusses coastal and rip classification; Section 2.3 considers surfzone retention; and Section 2.4 looks at surfzone hazard. The key knowledge gaps are summarised in Section 2.5. In each of the main results chapters, the key literature for that section will again be summarised.

2.1 Automated detection of rip currents

This section discusses literature pertinent to objective one; the development of an automated means of rip current detection.

The *in situ* measurement of swash- and surfzone processes, such as rip currents, is inherently difficult and complex (Blenkinsopp et al., 2011), proving challenging for even the most robust and advanced hydrodynamic equipment (Masselink and Puleo, 2006). In addition, achieving high spatial and temporal coverage is also problematic using *in situ* methods (Holman and Stanley, 2007; Guedes et al., 2011). One of the primary knowledge gaps regarding rip currents surrounds their behaviour under storm conditions,

for which the usual Lagrangian and Eulerian measurement methods are generally considered too dangerous to attempt (Castelle et al., 2016b). A combination of these factors has driven advancement in the field of remote sensing of coastal processes. A major benefit of such systems is that continuous logging can be achieved for relatively little cost and risk, and it is often accessible in real time. This creates large archives of data, and it quickly becomes unrealistic to manually sift through all the data to find events of interest. With regard to rip currents, there is much desire to create a system capable of automatically detecting rip channels in remotely sensed data as they are some of the hardest nearshore features to effectively instrument.

2.1.1 Video remote sensing

Remote sensing systems (e.g. video imagery, RADAR, LiDAR, satellite imagery, etc.,) are capable of monitoring multiple coastal processes over large areas for long periods of time. The most common approaches to remotely sensing rip currents are through the use of land based Radio Direction And Ranging (RADAR) (Haller et al., 2014), satellite mounted Synthetic Aperture RADAR (SAR) (da Silva et al., 2006), or more commonly, video imagery which (Ranasinghe et al., 1999; Bogle et al., 2000; Whyte et al., 2005; Holman et al., 2006; Turner et al., 2007; Gallop et al., 2009, 2011; Quartel, 2009; Orzech et al., 2010; Murray et al., 2013) which is discussed further here.

Video imaging is by far the most prevalent method for remote sensing rip currents, making use of signal in the optical spectrum. Video imaging has been used to remotely sense the nearshore for about 30 years. Lippmann and Holman (1989) first realised the utility of time-lapse imagery in identifying the position of offshore sand bars, using areas of high light intensity generated by waves breaking over the bar. The development of bespoke coastal imaging methods such as Argus (Holman and Stanley, 2007) or CamEra (NIWA), allows extraction of quantitative data from images. These differing types of camera system operate in a similar manner and create similar products, but are different commercial entities and as a result run slightly different algorithms to achieve the same image outputs. These outputs include information useful for measuring bar position

Figure 2.1: The three-camera monitoring system installed at Droskyn Point to monitor Perranporth. Picture taken at high tide, with cameras orientated to capture low tide intertidal beach area. Photo credit: S Pitman.

(Lippmann and Holman, 1989), wave period and nearshore bathymetry (Stockdon and Holman, 2000; Ranasinghe et al., 2004), wave incidence angle (Lippmann and Holman, 1991), and alongshore rip channel locations (Ranasinghe et al., 1999; Bogle et al., 2000; Whyte et al., 2005; Holman et al., 2006).

Progress in this area is driven, in no minor part, by the aforementioned difficulties in obtaining in-situ measurements. Video imaging systems have developed to a stage whereby they typically comprise of a cluster of up to 5 cameras positioned overlooking the coast (Figure 2.1). Images are captured at regular time intervals and are then uploaded to a computer-based archive and control system (Holman and Stanley, 2007). Imaging stations typically sample once or twice every hour, generally producing three outputs: (1) snapshot; (2) time exposure (timex); and (3) time variance images (variance) (Figure 2.2). Snapshot images are rarely used for quantitative analysis, but give a good qualitative overview of the study area (Holman and Stanley, 2007). Timex images have become the most used image output. These are generally collected hourly

and record the mean of all frames over a sample period (typically ∼600 images collected at 1 Hz), which represents a 10 min time frame (Guedes et al., 2011). These images are useful in giving an overview of persistent processes by averaging out moving components, such as breaking waves, into a distinct white band. Variance images are perhaps the least used image type, and are comprised of the variance in image intensities over the sample period, or otherwise, the standard deviation in pixel intensity over the sample period. These images are characterised by bright areas representing high variability in pixel intensity over time (such as the surf and swash zones), whereas dark areas represent low variability in intensities (such as subaerial beach or the region seaward of the surfzone).

2.1.2 Quantitative use of video imagery

To employ a remote sensing system in the coastal zone, it is first important to understand how nearshore processes can be sampled with a coastal imaging system. Many of these processes exhibit a visual signature on the sea surface which can be remotely monitored (Smit et al., 2007), for example, breaking waves over shallow areas will produce white water due to air bubbles. Furthermore, it can be inferred that the existence of this breaking region is indicative of a submerged sandbar (Lippmann and Holman, 1989). In order to quantify this signature, the pixel intensity value of the image can be used, whether it be extracted as brightness in gray-scale images or the relative balance of red-green-blue reflectivity in full colour images (Holman et al., 1993). These signatures are generally representative of processes that are uniform with depth (excepting undertow), meaning analysis of ocean surface signatures are appropriate to measure nearshore processes (Holman et al., 2003). Quantitative analysis of these images is normally undertaken after georectification of the image co-ordinates $[u, v]$ to resolve the three-dimensional $[x, y, z]$ real-world position (Figure 2.3), henceforth referred to as rectified images (Turner et al., 2006).

This process works well for straight beaches, but is complicated on embayed, curved beaches. Such locations require an understanding of the transformations applied to the image to resolve alongshore distance (Komar, 1998). When calibrating the images, the

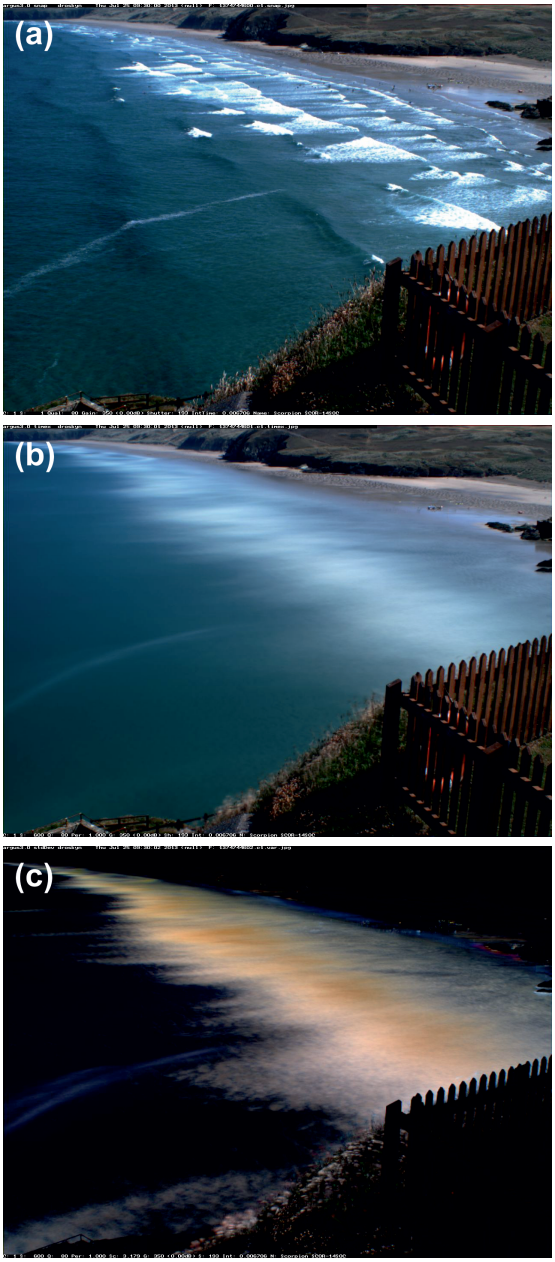

Figure 2.2: Examples of (a) snapshot, (b) timex, and (c) variance images collected by the Argus camera at Droskyn Point on 25 Jul 2013.

rectification requires fixed ground control points (GCPs) within the view of the camera that can be surveyed and monitored, to accurately convert between real world and image co-ordinate systems. This is non-trivial in the coastal zone, as a large portion of the image incorporates the ocean, with only a small amount of land and often a lack of permanent, well-defined features. Even on the land portions of the image, the dynamic nature of the beach makes the location of stable reference points that are constantly visible in the image problematic (Holland et al., 1997). GCPs need to be resurveyed whenever there is a shift in the camera (such as due to high winds), and periodically to check accuracy. To overcome the problem of few well defined static features in the field of view, temporary GCPs that are clearly visible in the images can be surveyed (Figure 2.4). This approach is favoured when temporary camera stations are installed for a short defined field experiment.

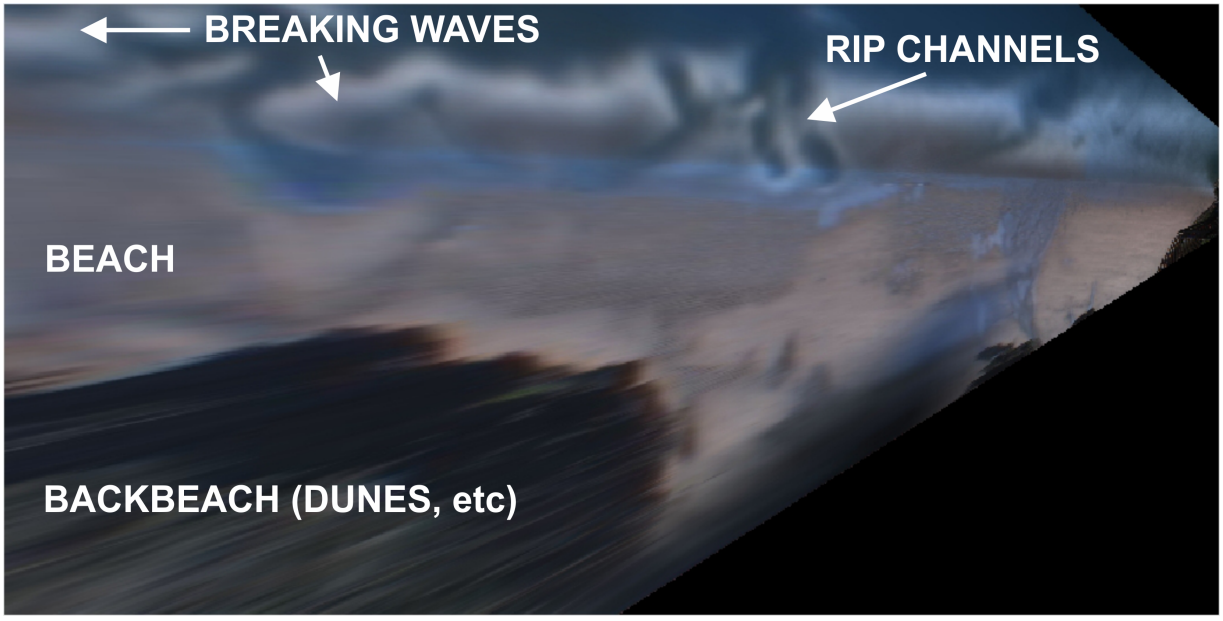

Figure 2.3: An example of a rectified and merged image from the Droskyn Point camera, Perranporth, with prominent features labelled. The black corners are areas outside the field of view of the camera. A seam is visible running alongshore near the waters edge, where images from two different fields of view have been merged together.

2.1.3 Attempts to automate rip detection

Automated detection of rip channels would decrease the subjectivity inherent in manual detection processing time, and cost. There have been few recent attempts to automatically detect rip channels in video imagery. Much progress was made with the increasing availability of Argus systems 10 years ago, but few studies were able to move beyond semi-automated or manual approaches to rip detection. The shortcomings of such studies were generally as a result of the employment of site-specific thresholds necessary to achieve results, and the noisy nature of video imagery, resulting in erroneous detection. These shortcomings are found in rip detection studies using all types of camera system (Argus, Cam-Era, etc.,) and are outlined below, along with the various progression routes for rip channel detection algorithms since the advent of video imaging.

The first attempt to use video imagery to quantify nearshore processes was by Lippmann and Holman (1989), where light intensity profiles in time exposure images were successfully used to indicate the cross-shore location of an offshore bar. Ranasinghe et al. (1999) then used this methodology to remotely sense rip currents, utilising 2 years of time exposure images on Palm Beach, Australia. Their algorithm delineated the surfzone and then made pixel intensity measurements along shore-normal transects within this area. Rip currents were clearly visible as troughs in the longshore filtered intensity profiles. The limitations of the method included the fact that they could only detect alongshore location and there was no indication of size or orientation in the rip current. The method described worked well for simplistic, calm scenarios but was unable to perform effectively in more complex situations. The method was also deemed sensitive to thresholds selected in the data analysis (Holman et al., 2006). As a result of these complications with the automation of rip detection, studies that followed typically used various manual (and thus, subjective and time consuming) rip detection methods (e.g. Bogle et al., 2000; Whyte et al., 2005; Holman et al., 2006; Turner et al., 2007; Quartel, 2009; Orzech et al., 2010; Murray et al., 2013).

Despite the inherent problems with automation, pixel intensity was deemed a good indicator of rip location. Therefore Bogle et al. (2000) nominally identified the surfzone,

Figure 2.4: Example use of temporary GCPs (when no permanent features are visible in the image) at Perranporth, U.K. This image depicts checker boards placed on the beach (black circles), providing easily identifiable static positions in the image. Additionally, the static RNLI truck has also been used as an extra GCP. Photo extract from Argus archive.

before averaging cross-shore transects of intensity. This resulted in one intensity value per cross-shore location, which could then be mapped in the alongshore direction. From this alongshore transect, manual selection of the minima in intensity were made and deemed to be the location of rip channels.

However, the prevailing approach to date has been manual selection of rip current locations in rectified images, using a graphical user interface (GUI) that translates the

users input into cross- and along-shore location (e.g. Whyte et al., 2005; Holman et al., 2006; Turner et al., 2007; Orzech et al., 2010). The following Root Mean Square (RMS) errors in alongshore location have been reported with the use of a GUI for rip detection: 13.2 m (Holman et al., 2006), and 10.1 m (Orzech et al., 2010). These errors are comparable to the width of the rip channel itself, and perhaps suitable for measurements of rip spacing along a 2-3 km beach, although the error is large when considering rip channels in isolation. These studies have also typically used day-timex images (an average of all daylight timex images collected during the course of one day) to average out tidal variations. However, this method will not be applicable on macrotidal beaches where the high tide surfzone is displaced onshore to such an extent that the intensity values may obscure or negate the low tide dominant rip current signal. An alternative option, however, is to select low tide images for that particular site.

Gallop et al. (2009, 2011) undertook the most recent attempt to develop an automated method to detect rip currents from video imagery. Unlike previous efforts, this method was designed to take into account the entire surfzone rather than just one shore-normal transect. The method again relied on pixel intensity gradients, however, the algorithm was designed to cluster observations of pixel intensity minima into distinct rips, therefore providing information on orientation and size as well as longshore position. However, various thresholds in the algorithm made it site specific and the data required a large degree of manual cleaning, for example to remove longshore-orientated clusters of minima. It is widely accepted that a good approach to detect rips is using the local minima (Lippmann and Holman, 1989; Ranasinghe et al., 1999; Bogle et al., 2000; Gallop et al., 2009, 2011), and therefore this approach will form the focus of developments within this thesis.

2.1.4 Constraints and possible solutions

The majority of research using video images uses the raw image products (snapshot, timex, daytime, etc.) output from the cameras, which can often be inherently noisy, hindering robust rip channel detections. The methods discussed in Section 2.1.3

(alongshore intensity profiles e.g., Ranasinghe et al. (1999)) are appropriate for simple scenarios where rip channels are orientated in shore-normal directions. They are inappropriate for complex bathymetries (Holman et al., 2006) such as the common cases where rip channels cut across the surfzone diagonally to form acute angles with the shoreline because the detected location does not give a true indication of the rip location when orientated at acute angles.

The intensity profiles generated have typically been subject to visual classification in order to ascertain rip locations (e.g. Bogle et al., 2000). This is due to the resultant image intensity profiles containing a degree of noise or fouling that can act to obscure the main features. In this context, noise refers to artefacts introduced to the image during processing. Fouling refers to anything undesirably captured by the camera, such as rain drops and fog. Noise can be present in the image for a variety of reasons, such as environmental factors (i.e. sensor temperature) during image acquisition (Russ, 2011).

Yet more noise is introduced during the production of a digital image; analogue signals of the natural world are continuous (Bovik, 2005) and therefore need to be quantized to produce digital images before computer processing. In the literature pertaining to image-based rip detection and surfzone studies, pixel values known as intensities are usually quantized into 256 discrete levels [0—255]. This quantization process introduces a uniform noise to the digital image (Gonzalez and Woods, 2008). A common approach to reduce such noise in the field of image processing is to filter the image, yet this is rarely discussed in literature pertaining to image-based rip detection, or surfzone studies.

To the author's knowledge, simple image filtering prior to detection of surfzone features has not been widely used before, because the prevalent image type used for analysis is the so called timex image, which represents the time-mean of intensity in all frames collected at 2 Hz over a 10-minute period (Holman and Stanley, 2007). This constitutes a form of average filtering during the image acquisition stage; however, the resultant image may still include background noise or erroneous data. One such example is raindrops on the lens covering, which would appear in the rectified image, giving a false intensity signature for the pixel(s) concerned. Studies using video images tend to reject imagery where raindrops are visible on the lens for this reason. One of the only studies

to investigate pre-processing for noise removal was that of Holman et al. (2013), where they described how consecutive images in a time series can be used to create a running-average estimate (cBathy). cBathy uses wave celerity to estimate bathymetry, and the use of this running-average filter has been successful in removing fouling from subsequent images, such as rain drops or sun glare.

Despite the assumption that a timex image is already prefiltered, it still contains noisy signals, representative of a very dynamic surfzone. Furthermore, inclement weather still appears as fouling in the imagery. Therefore, there is a need to pre-filter the image before processing, rather than relying on filtering the signal that is extracted as a result of processing. In this thesis, in an attempt to create an algorithm capable of automated rip detection, the benefit of pre-processing images for noise reduction is investigated.

2.2 Rip channel classification

This section discusses literature pertinent to objective two; the classification of nearshore flow regimes.

2.2.1 Objective surfzone classification

There are obvious benefits to coastal classification schemes, such as the ability to communicate the main characteristics of a particular site succinctly, or the ability to make inferences about specific behaviours based on relatively small amounts of information. Furthermore, you can make inference about the characteristics of an unstudied site based on just a few parameters. Therefore, such classifications are integral to coastal management and planning. The most widely used beach classification scheme is Wright and Short (1984), which classifies morphodynamic beach state on wave-dominated sandy beaches (Figure 2.5). This scheme was based on visual subjective observation of the beach state, to ascertain similarity against a set of 6 defined beach types, ranging from dissipative, through various intermediate stages, to reflective. The

classification scheme has found most of its success as a result of its ability to infer large amounts of morphological information within each beach state. For example, on a beach classified as reflective under the scheme, one would expect to see a dominance of surging breakers, a steep beachface, a pronounced step and a wide berm, with a largely linear, low-gradient nearshore profile. The scheme was later updated by Masselink and Short (1993) who created a conceptual beach model (as oppose to classification scheme), that estimated beach state based on a combination of relative tide range, and dimensionless fall velocity (Gourlay, 1968; Dean, 1973). This development provided a good estimate of how a beach may look, based on quantitative parameters, however, classification of an actual beach at a given time remained subjective based on observation of features.

The earliest attempt to objectively classify the beach states in the Wright and Short (1984) model was by Wright et al. (1987), with the result being low (36 %) agreement between visual and objectively-derived beach states. Ranasinghe et al. (2004) later found some success using a combination of surfzone width and alongshore pixel intensity variance. This method was able to differentiate between the four intermediate beach states, with reported success rates of 90 % when compared to expert operator classification. Improving on both these methods was the study by Browne et al. (2006). Their study was able to successfully classify images as falling into one of three observed intermediate beach states using higher order statistics (e.g., variance, skewness, and kurtosis) of pixel intensities. Their study drew conclusions from a comparatively smaller dataset than previous studies, but they successfully showed that the use of parameters other than just pixel intensity resulted in a higher rate of correct classifications.

The Wright and Short (1984) model dealt objectively with rip channels, and was more concerned with bar morphologies, and the associated change in position and extent. In all of their depictions of rip channels (Figure 2.5), there was the presence of a rip head outside the surfzone, suggesting that the rip current exited. Rip circulation is varied, and there is often a dominance of surfzone retention (see full discussion in Section 2.3), meaning the Wright and Short (1984) model is incapable of differentiating between a rip that exits, or is retained within the surfzone. Rip currents, however, were not the main

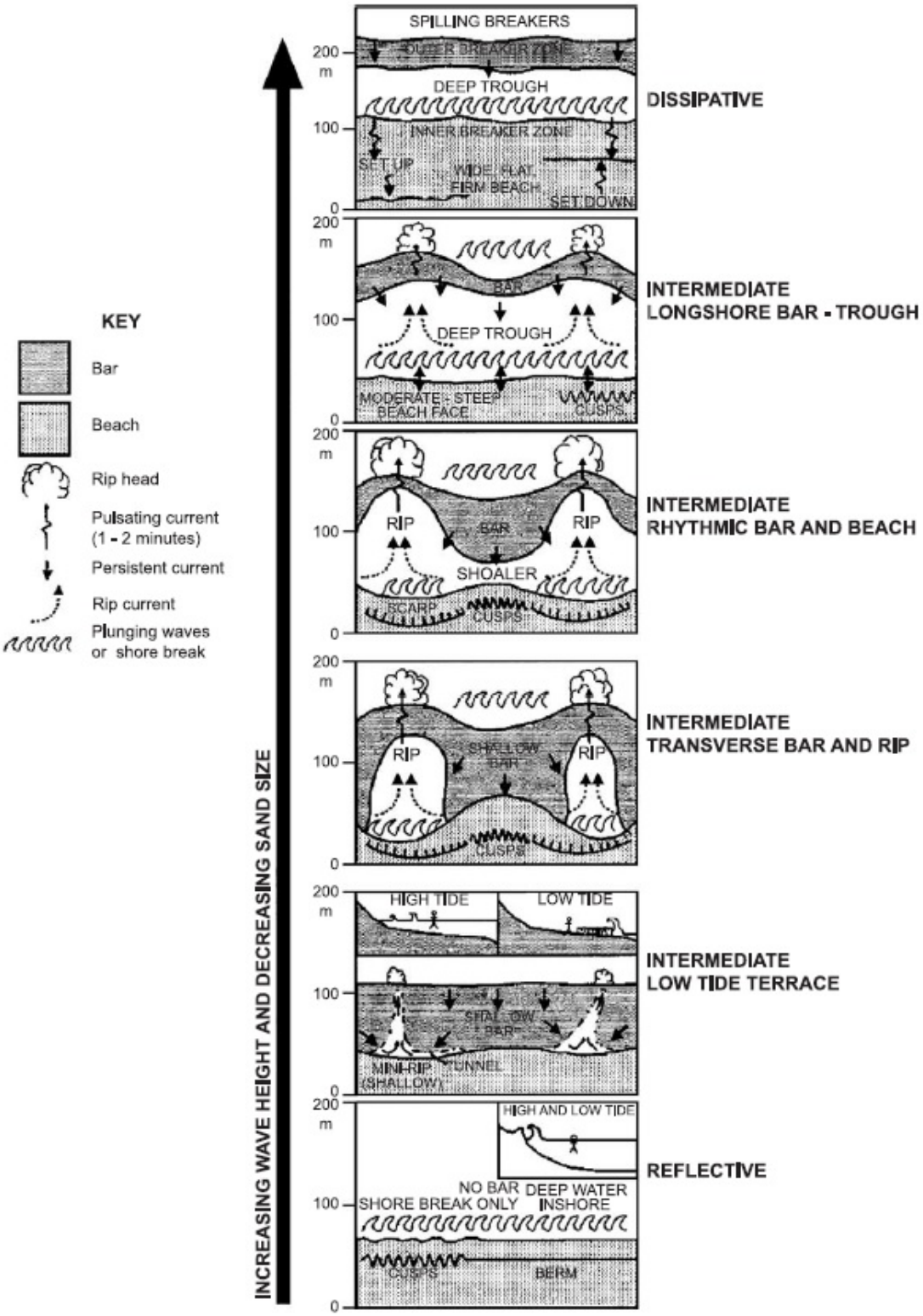

Figure 2.5: Wright and Short (1984) beach state classification scheme. Illustration from Ranasinghe et al. (2004).

focus of their approach, and there are a number of classification schemes concerned primarily with the classification of rip systems, detailed below.

2.2.2 Rip current classification

There has been much less work on the classification of rip current types, compared to overall beach states, despite rip currents being an integral feature used in discriminating between beach states. Short (1979, 1985) was the first to highlight the importance of being able to distinguish between different types of rips. Until recently, the dominant differentiations have been that of 'open-coast' or 'embayed beach' rip currents (McCarroll et al., 2014; Scott et al., 2014), 'fixed' or 'transient' rip currents (Vos, 1976; Johnson and Pattiaratchi, 2004), or 'accretive' and 'erosive' rips (Short, 1979, 1985). MacMahan et al. (2006) defined a rip classification system based on energy as a function of wave-current interaction, using the Froude number and a measure of rip shear. They divided their scheme into low, intermediate and high energy rip regimes, with low energy systems having negligible wave-current interaction, and high energy regimes experiencing interaction of sufficient strength to induce significant wave dissipation through the channel. Price and Ruessink (2011) was the first study to quantitatively track rip channel development in a double-barred environment, with observations indicating that rip currents were often more persistent in the outer of the two bars. They mapped development and infilling of rip channels, but made no attempt to classify the rip current type. Castelle et al. (2016b) recently highlighted how the descriptions previously applied to rip classifications can be misleading. For example, in the case of 'open coast' and 'embayed' rip currents, they note that an embayed beach may exhibit rips not directly controlled by physical boundaries, but instead more akin to open coast rips. Instead, they propose a classification with three broad types (hydrodynamically, bathymetrically, and boundary controlled rips), distinguished by the main forcing mechanism. Their classification is discussed briefly below, and despite being somewhat subjective, it is the most comprehensive approach to date:

Hydrodynamic rips

Hydrodynamic rips occur purely as a result of incident wave forcing, irrespective of bathymetric conditions. Castelle et al. (2016b) reports their occurrence is confined purely to featureless beaches or planar sections of beach. There are two types of hydrodynamic rip: (i) flash rips; and (ii) shear instability rips, described below:

i. Flash rips. These are perhaps the most short-lived rips observed, with lifespans typically $O(5$ mins$)$, with low temporal frequency (Murray et al., 2013). Often referred to as transient rips, these currents often have smaller offshore flow velocities and extent compared to some bathymetrically influenced rips (Dalrymple et al., 2011). Feddersen (2014) describes the formation of migrating surfzone eddies as a result of gradients in vorticity after the passage of individual short-crested breaking waves. Flash rips are the offshore jets of water produced by these eddies (Castelle et al., 2016b).

ii. Shear instability rips. Whereas flash rips are predominantly a result of shore-normal incident waves, shear instability rips form under highly oblique waves. They are uncommon, and form as a result of instabilities in the alongshore directed current, as a result of cross-shore shear (Castelle et al., 2016b).

Bathymetric & boundary rips

These are types of rips controlled by something other than purely the hydrodynamics. As a result they are comparatively more fixed in terms of location. Bathymetrically controlled rips have a degree of mobility, but boundary rips form as a result of a solid synthetic structure (e.g., groynes) or a naturally occurring feature, such as rocky headland, and are therefore generally more spatially fixed.

i. Channel rips. Channel rips, the focus of this thesis, are a bathymetrically controlled rip, and have received most attention in the literature. They are the main rip type discussed in research pertaining to 'open coast' rips, and have received so much attention as a result of their accessibility and predictability (Castelle et al., 2016b). Channel rips require some form of undulating nearshore bathymetry, such as longshore bar-trough

beach states (Figure 2.5). Channel rips subsequently form in incised channels between sand bars as a result of alongshore variations in breaking wave heights (Bowen, 1969; Scott et al., 2014).

ii. Focused rips. Like channel rips, focused rips also form as a result of bathymetry-induced alongshore variations in breaking wave height. However, instead of nearshore variations, as with channel rips, focused rips form as a result of offshore bathymetric variation, such as submarine canyons that incise into the nearshore (Castelle et al., 2016b). The alongshore variation is as a result of refraction (and hence, focussing) of incoming waves, which drive offshore flows in the same manner as channel rips (Long and Ozkan-Haller, 2005).

iii. Shadow rips. Shadow rips are a boundary controlled rip. They occur in the lee of rigid structures, as a result of wave shadowing around the feature. The result of wave shadowing is a boundary-hugging offshore jet on the lee side of the structure (Castelle et al., 2016b).

iv. Deflection rips. Deflection rips occur on the stoss side of rigid structures, as opposed to shadow rips on the lee side. Alongshore flows meet a physical boundary and are forced offshore, forming the deflection rip (Castelle et al., 2016b). They exhibit offshore speeds that match those of channelled rips, but under much lower wave conditions (Scott et al., 2016).

Although this rip classification scheme is comprehensive in terms of rip formation, it is unable to account for any changes in a given rip current over tidal cycle. It offers no information on how rip current circulation is likely to operate. In order to investigate rip circulation, there is potential to measure channel shape using video imagery, which may give information on how a rip current circulates, discussed below.

2.2.3 The effect and quantification of rip channel shape

It is already understood that factors such as a well-defined low-tide bar/rip morphology produces a more established channel rip than would be the case with subtler topographic

variations (Scott et al., 2011). It follows that the geometry of the channel, in this case the cross-shore profile, exerts a control on the circulation dynamics. Therefore, it is possible that the plan view form of a channel could also exert control on circulation, something not considered by the classification scheme of Castelle et al. (2016b). In lieu of regular *in situ* bathymetric surveys, which are often expensive, video imaging can be used as a proxy for channel shape. In time exposure imagery, waves breaking over shallower areas show as a persistent white band in the imagery, and the inference can be made that this white band is therefore co-located with submerged sandbars (Lippmann and Holman, 1989). Conversely, distinct breaks in this band can be interpreted as rip channels (Ranasinghe et al., 1999), and often the shape of the channel is evident. Indeed, most attempts to objectively classify the coastal zone favour this use of video imagery, as it provides a means of quantifying the entire imaged area, through pixel intensities.

It is therefore of interest to find a means to classify rip channel shapes in video imagery. Outside of the coastal processes field, synoptic typing has been used as a means to identify statistically similar environmental variables (Hemer et al., 2008). Synoptic typing was originally developed as a means of comparing meteorological phenomena, such as the change in 500 millibar isoline patterns over Europe (Kirchofer, 1974), and has since been used to investigate other meteorological phenomena such as airborne pollutants (McGregor and Bamzelis, 1995) and cloud cover (Barry et al., 1981). The method has not been applied to either coastal processes or to video imagery before. It could prove useful as a means to assesses the visual similarity in the form of the rip channel, as expressed through wave breaking in timex images. In particular, the use of an adapted Kirchofer sum-of-squares technique (Kirchofer, 1974; Yarnal, 1992) which was modified by Hemer et al. (2008) may be useful to categorise rip imagery. The original Kirchofer (1974) method was successful in quantifying overall similarity in grids, however, it was unable to differentiate whether there were significant sub-grid level differences (Blair, 1998). The Hemer et al. (2008) adaptation allows the method to take account of sub-grid differences by assigning a similarity rating for each row and each column within the grid, and checking that it passes a given threshold. This would

ultimately provide a good indication of whether two independent rip channel images could be considered similar, and is explored in this thesis.

2.3 Controls on surfzone retention

This section discusses literature pertinent to objective three; different types of rip current circulation, and the processes deemed to control circulation.

2.3.1 Rip current circulation

There is a longstanding view that rip currents always extend and disperse well seaward of the wave breaking region. This ideology is based on early studies and observations, such as that of Shepard (1936) whereby he described discussions held with lifeguards in Los Angeles, whom described rips carrying bathers far offshore (Figure 1.1). Thus the typical description of a rip current became that of an offshore directed flow, perpendicular to the shore, which exits the surfzone into deeper water (Shepard et al., 1941). This behaviour is herein referred to as a *rip exit*. However, Lagrangian measurement of rips over the last decade (Austin et al., 2009, 2010, 2014; MacMahan et al., 2010; McCarroll et al., 2014; Scott et al., 2014) have shown that there is a wide variety of rip circulation patterns, including circulatory (Figure 2.6), and angular flow (i.e., not perpendicular to shore).

2.3.2 Controls on circulation

Rip activation (defined here as the establishment of a depth-uniform offshore-directed flow) has been attributed largely to alongshore gradients in the radiation stresses of breaking waves (Longuet-Higgins, 1970), and variations in nearshore bathymetry that induces spatially variable patterns of wave breaking (Bowen and Inman, 1969). The requirement for wave breaking on offshore bars is widely accepted as a pre-requisite for topographic rip activation, with increasing intensities of wave breaking creating stronger

rip circulations (Sonu, 1972; Dalrymple, 1975; Wright et al., 1979; Aagaard et al., 1997; MacMahan et al., 2006). Rip flow is also tidally-modulated, with water level controlling the degree to which waves interact with bathymetry. This interaction transforms wave breaking patterns and varies flow constriction through channels over the tidal cycle (Austin et al., 2010). Maximum rip speeds are generally observed around low tide, when the interaction of breaking waves with the morphology is greatest (Aagaard et al., 1997; Brander, 1999; Austin et al., 2010, 2014; McCarroll et al., 2014; Scott et al., 2014). In macrotidal environments, higher tidal levels can switch off rip circulation entirely as a result of the cessation of wave breaking over the bar (Austin et al., 2014). The combination of these controls on nearshore circulation create one of two responses in an active rip: 1) rip exit, or 2) recirculation within the surfzone.

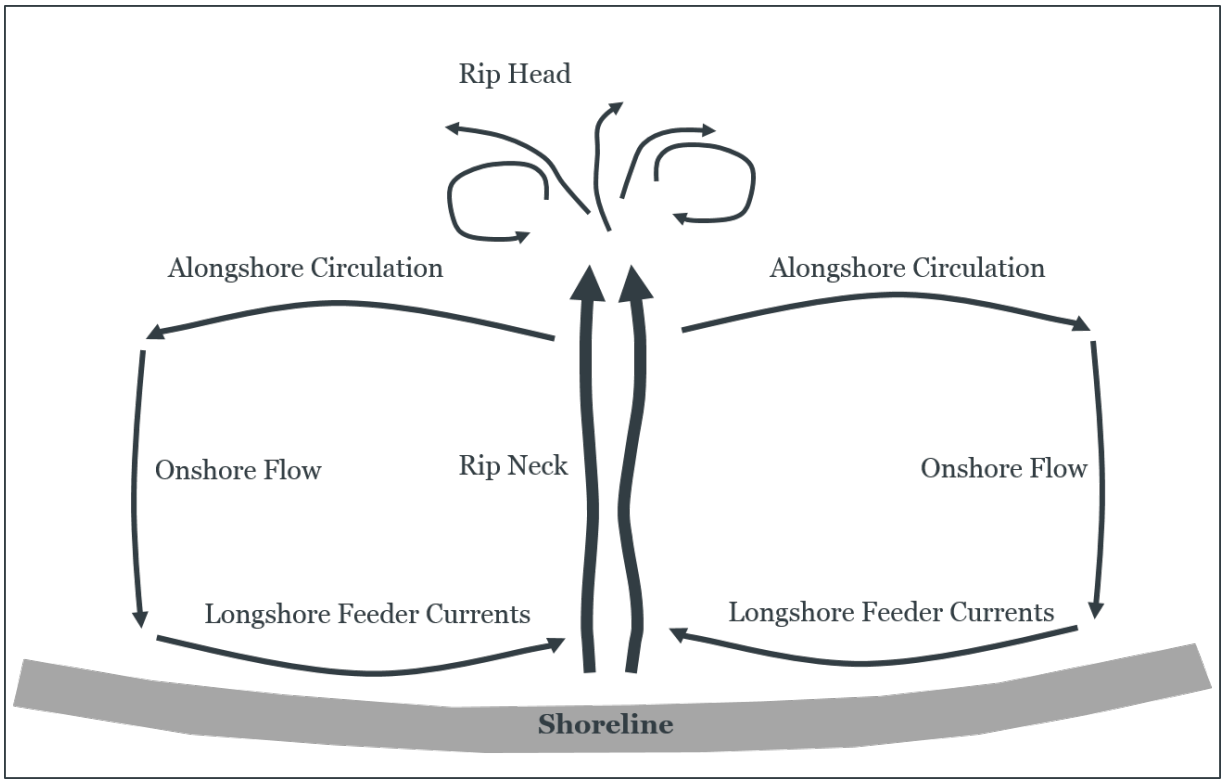

Figure 2.6: Contemporary view of rip current circulation, indicating the propensity for recirculatory flow, in addition to exits. Following the work of Austin et al. (2010) and MacMahan et al. (2010).

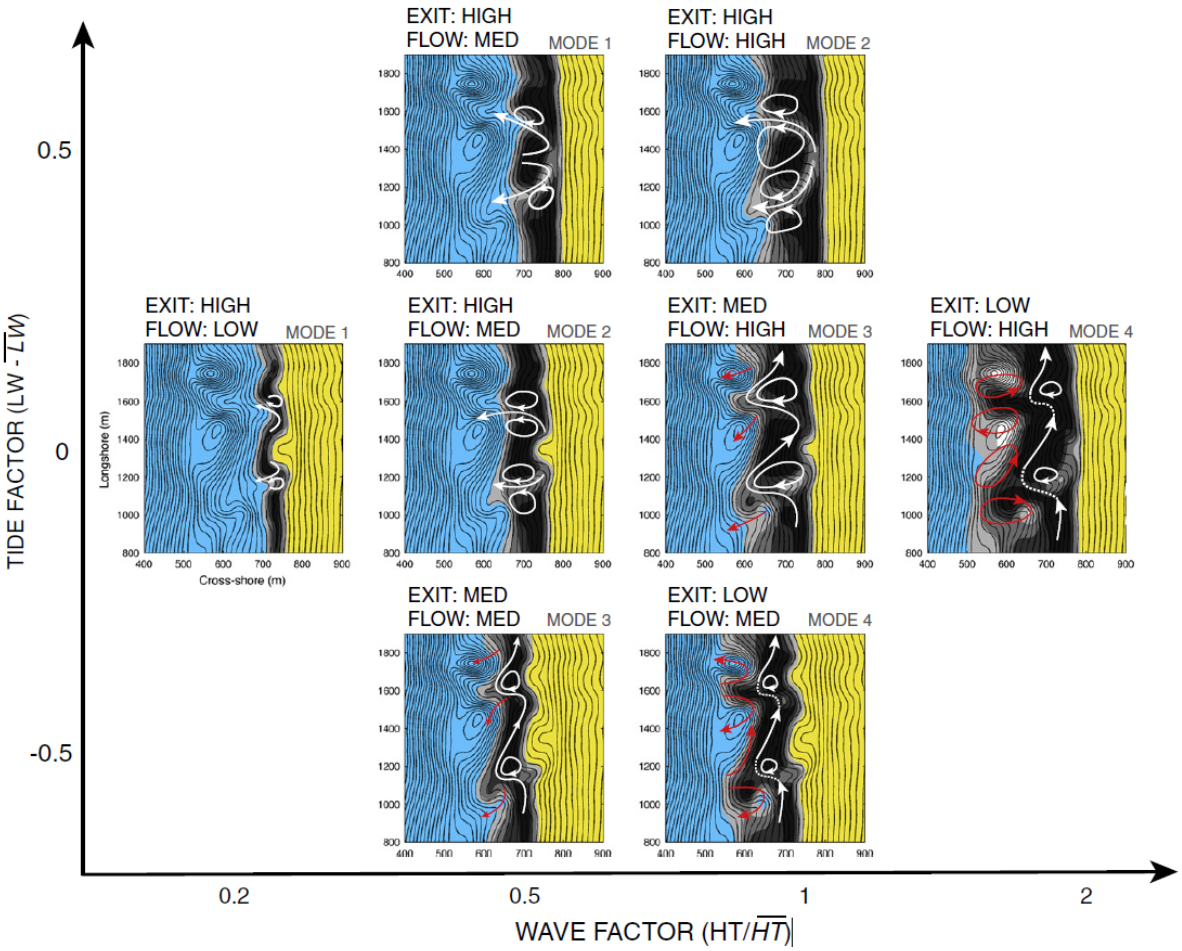

Figure 2.7: Conceptual representation of rip behaviour as a function of wave and tidal controls. LW refers to the height of the corresponding low water as an absolute water depth (m above CD). The overbar is indicative of the long term mean values. Large positive values of tide factor are indicative of neap tide conditions and large negative values indicative of spring tides. HT refers to significant wave height × peak period, with the again overbar indicative of long term mean values. Taken from Scott et al. (2014).

2.3.3 Retention rates

The balance of surfzone exit versus recirculation is referred to as surfzone retention. Retention is generally quantified in terms of how many drifters exit the surfzone in a

given time period, with typical exit rates around 20 % per drifter entry (Reniers et al., 2009; MacMahan et al., 2010; Castelle et al., 2014). Aside from the factors outlined in Section 2.3.2, controlling primarily rip velocity, there are also important factors that control surfzone retention. Scott et al. (2014) proposed a conceptual model of retention and flow rates based on extensive measurement of open coast beaches in a macrotidal environment (Figure 2.7). They found that exits were maximised under lower wave factor ($H_sT_p/\overline{H_sT_p}$) and higher tide factor ($LW - \overline{LW}$) conditions, where LW refers to low water and the overline refers to the long term (multi-year) mean values. This assertion was subsequently corroborated at a contrasting microtidal embayed beach by McCarroll et al. (2014). Previous studies had loosely linked wave heights to rip exits, with intermediate wave heights proving favourable for high exits (MacMahan et al., 2010), but the concept of a wave factor explains more variation than wave height alone. In addition to wave height, the angle of incidence is also an important factor in determining retention rates. At highly oblique wave angles ($\theta > 20°$), offshore flow can be replaced by alongshore dominated currents, with most matter retained within the surfzone (Johnson and Pattiaratchi, 2004; Reniers et al., 2009; Winter et al., 2014; Spydell, 2016).

Reniers et al. (2009, 2010) identified the importance of Very Low Frequency (VLF) motions (O(10 mins)) as a dominant mechanism behind surfzone exits in rip currents. The presence of VLF motions was seen to extend the rip current beyond the surfzone, and resulting eddies would detach from the main current (Reniers et al., 2009; Castelle et al., 2016b). Castelle et al. (2014) noted that not all variability could be explained by VLFs, especially as many studies had reported far higher exits rates than VLF motion would predict. As a result, they investigated the concept of an additional bathymetric control on surfzone retention, and found that more variability was explained with the use of a ratio between surfzone width (X_s) and rip spacing (λ).

2.3.4 Wave breaking patterns as a control on retention

Previously, the effect of wave breaking patterns on circulation has been opportunistically and qualitatively discussed as a result of field measurements (Scott et al., 2014).

However, no quantitative link between breaking patterns and circulation type has been investigated. The hypothesis of this thesis is that an important control on circulation is whether the rip exhibits an open connection in terms of wave breaking to the region offshore of the surfzone (hereafter referred to as the offshore), or whether wave breaking acts to close the rip channel. A rip channel that is closed in terms of wave dissipation (i.e., waves are breaking at the seaward edge of the rip, across the rip channel and/or on the rip head bar) may be more likely to exhibit circulatory behaviour and surfzone retention, as alongshore variations in depth-induced breaking dissipation create corresponding variations in water surface elevation. Conversely, a rip channel that is open to the offshore region (i.e., no wave breaking at the seaward edge) may be unhindered by wave breaking processes, and therefore the current may exit the surfzone.

Observational changes in wave breaking have been documented by various researchers; Brander (1999) provided a conceptual model of rip activity based on the Wright and Short (1984) beach state model, and discussed changes in morphology that are inferred from changes in the breaking pattern. Brander (1999) describes downstate change in morphology as a result of decreasing wave conditions, and the associated changes in rip channel configuration. The shift in channel configurations is accompanied by different patterns of wave breaking over the reconfigured bar system. Of particular interest was the longshore bar-trough state proposed, which is akin to an open rip, and the transverse bar rip which exhibits a welded rip head bar, akin to a closed rip described above. Whereas Brander (1999) showed virtual state transitions as a result of wave conditions, the work of Austin et al. (2010) took a similar approach with tidal control. They highlight how lowered water levels produce behaviourally similar results to that of a wide-spread accretion (down-state transition) in the beach state model, maximising bar relief. Quartel (2009) later classified intertidal rip channels as either open or filled, in terms of sedimentation, rather than wave breaking patterns, which is the focus of the current thesis. Both types were defined as funnel-shaped, where open rip channels showed a shoreward narrow end, with a clear opening through the wave break point to deeper water, similar to the definition of open used here. In contrast, a filled rip channel was an inverse-funnel (wider end towards the shore). A filled rip is said to develop as a

result of sediment infilling, whereas a closed channel in terms of wave breaking is the result of lower water levels inducing wave breaking at the offshore extent of a rip channel. Channels were classified from low tide video images, using the visual contrast between dry sand and water or wet sand.

While Brander's (1999) model and the work of Quartel (2009) discussed variability over timescales of O(days-weeks), the control exerted by tidal modulation of wave breaking can produce similar transitions over a single tidal cycle (Austin et al., 2014), whereby low tide levels can mimic a down-state transition in beach state. Quantifying these wave breaking patterns using *in situ* measurements is difficult. However, such patterns can be relatively easily identified using coastal imaging systems, such as Argus (Holman and Stanley, 2007), Cam-Era (Gallop et al., 2011; Blossier et al., 2016), and WavePack (Gal et al., 2014). For a full discussion of these systems, refer to Section 2.1.1.

Many studies have measured rips *in situ* (Austin et al., 2009, 2010, 2014; MacMahan et al., 2010; McCarroll et al., 2014; Scott et al., 2014), or using video imagery (Ranasinghe et al., 1999; Bogle et al., 2000; Whyte et al., 2005; Holman et al., 2006; Turner et al., 2007; Gallop et al., 2009, 2011), but very little research has attempted to combine *in situ* measurement of rips with video images for quantitative means. One study addressing this previously was Austin et al. (2010), which quantified wave roller dissipation over the sand bar at Perranporth, U.K., and linked the intensity of breaking to rip pulsations. They determined how changes in the intensity of wave dissipation activated the rip, but not how patterns of dissipation influenced circulation pattern, i.e., if a rip is retained within, or exits the surfzone. A possible link between readily observable phenomena, such as wave breaking, and the danger level of prevailing rip currents could have practical benefits. For instance, an indication of whether rip currents are likely to be retained within, or exit, the surfzone based purely on real time video imagery could be very useful to beach safety practitioners, who may elect to increase coverage or patrols on days where rips appear more dangerous in imagery.

Therefore, objective 3 attempts to gain new insights regarding the influence of wave breaking patterns on rip current circulation. In this thesis a new parameter is defined to classify wave breaking patterns around rip currents.

2.4 Control on rip current hazard

This section discusses literature pertinent to objective four; the danger posed by rip currents worldwide, and factors influencing their hazard.

2.4.1 Coastal drownings

Rip currents are a major hazard on surf beaches worldwide (Brander and MacMahan, 2011; Brander and Scott, 2016). For countries with accurate reporting measures, they are the primary cause of drownings, near-drownings and lifeguard incidents, accounting for 68 % of incidents in the United Kingdom (Scott et al., 2008), 81 % in the United States (Brewster and Gould, 2014), and at least 57 % in Australia (Brighton et al., 2013; Brewster and Gould, 2014) for example. Increasingly there are also reports and records for countries where records are less complete, that equally highlight the global nature of the problem, for example; China (Li, 2016), Turkey (Barlas and Beji, 2016), Costa Rice (Arozarena et al., 2015), and India (Arun Kumar and Prasad, 2014).

There is widespread public misconception that the danger posed by rip currents is as a result of their ability to pull you under the water surface (Gallop et al., 2016b). In reality, the danger lies in the resultant panic and fatigue, which can lead to severe consequences (Brander et al., 2011; Drozdzewski et al., 2012). The risk of drowning could be linked to understanding of rip currents, for example to experienced swimmers, lifeguards and surfers, rip currents can be advantageous as a means to travel offshore and therefore pose very little danger (Short, 2007; Shaw et al., 2014).

Studies into rip current victim demographies show that there are high risk groups when it comes to rip current rescues. Males are disproportionately represented in the rescue data (66 % - Woodward et al., 2013; 85 % - SLSA, 2011). Studies have shown males to perceive certain actions as less risky, resulting in more dangerous behaviour - a trait that appears more so in adolescent males (Reniers et al., 2016). This trend is reflected in

rescue statistics, whereby the majority of people rescued were male teens (Woodward et al., 2013).

2.4.2 Hazard and risk

Hazard and risk are two terms with differing meanings; hazard refers to the degree of harm likely and risk refers to the probability of a given outcome (Singley, 2004). It is important to differentiate between the two when considering the danger posed by rip currents. Hazard refers to the physical properties of the rip current itself (e.g. current speed). Higher current speeds are more hazardous as they result in expedited offshore transport of anyone trapped in the current. Perhaps more important is the balance between exits and retention, with more exits creating more hazardous conditions as bathers are moved further offshore than in retention scenarios. Risk instead refers to the likelihood that a person is subjected to a hazard, or more correctly, the level of exposure to the hazard (Austin et al., 2013). For example, in countries with popular and accessible surf beaches, beach tourism during summer holidays is a large industry, massively bolstering the number of people on the beach (McKay et al., 2014; Shaw et al., 2014), and therefore, increasing the likelihood that someone may end up in a rip (i.e. increasing the risk). The hazard changes between beaches, beach types, and over the tidal cycle (Scott et al., 2009). Most hazardous conditions on open coast beaches typically occur at or below average wave heights, with lower water levels and light winds (Scott et al., 2014). Castelle et al. (2016a) also recently showed that rip spacing is important in determining hazard, as it subsequently effects how far an individual has to swim to reach safety.

2.4.3 Escape strategies

Although the balance of hazard and risk can be useful in predicting both the severity and likelihood of rip current incidents, one of the primary determinants of the actual outcome is a person's ability to escape the rip current. This is generally a combination of

two factors; a) their ability as a swimmer, and b) their ability to select an appropriate escape strategy. The 'typical' historic description of a rip current highlighted in Figure 1.1 was based on early observations (Shepard and Inman, 1950, 1951; Bowen, 1969) of rip currents whereby floating matter would flow offshore in a shore-normal direction to the inner shelf. The general acceptance of this flow regime, combined with a need to reduce rip current rescue incidents, resulted in a widespread campaign informing anyone caught in a current to 'swim parallel' to the beach in order to reach a sandbar or the onshore breaking waves and escape the current (Brander et al., 2011; Miloshis and Stephenson, 2011; McCarroll et al., 2013). However, recent Lagrangian measurement using GPS-tracked surfzone drifters (Schmidt et al., 2003; Austin et al., 2009, 2010, 2014; MacMahan et al., 2009, 2010; McCarroll et al., 2014; Scott et al., 2014) alluded to not only the existence of a circulatory regime, but in many cases a circulatory regime that persists for almost 80 % of the time, discussed here in Section 2.3.

The realisation of this new circulatory regime prompted the formation of a new escape strategy by MacMahan et al. (2010); that of 'stay afloat'. This strategy was designed to avoid situations whereby the bather may exhaust themself in efforts to escape the rip (Van Leeuwen et al., 2016), when in the majority of cases, staying afloat would allow them to take advantage of the circulatory behaviour of the rip and be brought naturally back onshore. In the view of contrasting public safety advice, McCarroll et al. (2015) modelled the efficacy of various escape strategies, and found neither of the two outlined here to be 100 % effective. The key finding was that slow and steady swimming may be more effective than purely staying afloat, although the optimal swim direction changed depending on start location. A subsequent modelling study by Castelle et al. (2016a) highlighted the alongshore success of escape strategies on the same beach, and found high variability. Of particular concern was the success rate of the same strategy in adjacent rips on the same beach, with a successful strategy in one often becoming dangerous if employed in the neighbouring rip.

Given the high variability in rip current occurrence and circulation, it is vitally important to understand the drivers behind differing circulation patterns. This thesis investigates the link between wave breaking patterns and rip rescue events in order to

better inform coastal practitioners about high risk rip scenarios, that can be detected with relative ease and at low cost, using video imaging systems.

2.5 Summary & knowledge gaps

The hazard presented by rip currents is a prominent concern on beaches worldwide, and is the result of the interplay between a number of different factors, such as wave heights, tidal levels, wind speeds and rip spacing. Of key importance in determining the hazard is an understanding of the circulatory regime in terms of surfzone retention. One relatively easy and cost effective method of quantifying the overall state of the beach is through the use of video imagery, which highlights phenomena such as wave breaking through pixel intensity values. Therefore, the overall aim of this study is to use video imagery to determine how patterns of wave breaking can influence the hazard presented by rip currents on beaches worldwide.

In terms of measuring channel rips, timex imagery shows distinct darker areas that are indicative of rip channels. Extraneous noise in the image has resulted in a number of studies having to resort to either manual identification of rips in imagery, or manual cleaning post-processing. Despite the noise inherent in imagery, there has been very little investigation as to the effects of cleaning and filtering images prior to analysis or processing. Therefore, the first objective of this thesis is to investigate the progress made in automated rip detection, and consider means by which to improve the reliability of such detections.

There are obvious benefits to coastal classification schemes, such as the ability to communicate the main characteristics of a particular site succinctly, or the ability to make inferences about specific behaviours based on relatively small amounts of information. Rip current classification schemes fail to provide explanation of temporal change in rip currents. One such way to investigate temporal change is through the characterisation of channel shape. Therefore, the second objective of this study is to develop a classification of rip channel morphology based on wave breaking patterns.

Having identified the dominant patterns of wave breaking observed around rip channels, it is possible to investigate the possible links between channel shape and retention.

Therefore, the third objective of this study is to assess the control exerted by differing wave breaking patterns on rip current flow regimes.

The danger posed by rip currents is a combination of the hazard (how dangerous the rip current itself is), and the risk (the likelihood of exposure to that hazard). It is generally accepted that the two most hazardous conditions for a rip current are that of: a) high current speeds, and b) surfzone exits. Rip incidents worldwide have shown that there are high risk groups (e.g., young males, bodyboarders), but beyond the demographics, it is possible that wave breaking patterns may influence rip rescue events. Therefore, the fourth objective in this study is to determine which wave breaking patterns produce the most hazardous rip currents for bathers.

Chapter 3

Study sites

This thesis references imagery from three sites: Perranporth Beach, located in Southwest England, Tairua Beach, and Ngarunui Beach in New Zealand. These sites were selected as they all represent different morphological regimes (outlined below) and have long term ($>$ 10 years) camera monitoring programmes. Each of the beaches is a different tidal classification, ranging from micro-, to meso- to macrotidal. Tairua is a microtidal, intermediate embayed beach that receives medium energy swell. *In situ* data were collected from a macrotidal, intermediate, low tide bar/rip beach at Perranporth, and a contrasting mesotidal, double barred high energy beach at Ngarunui. In terms of the Masselink and Short (1993) beach state model, the transition from Perranporth to Ngarunui represents an increase in dimensionless fall velocity (increase in dissipation) and a decrease in relative tide range.

3.1 Tairua Beach, Coromandel, New Zealand

Tairua is an embayed beach located on the Coromandel Peninsula of New Zealands North Island (Figure 3.1), constrained at the northern end by a promontory and the southern tip by an extinct volcano. The 1200 m-long beach is easterly orientated and

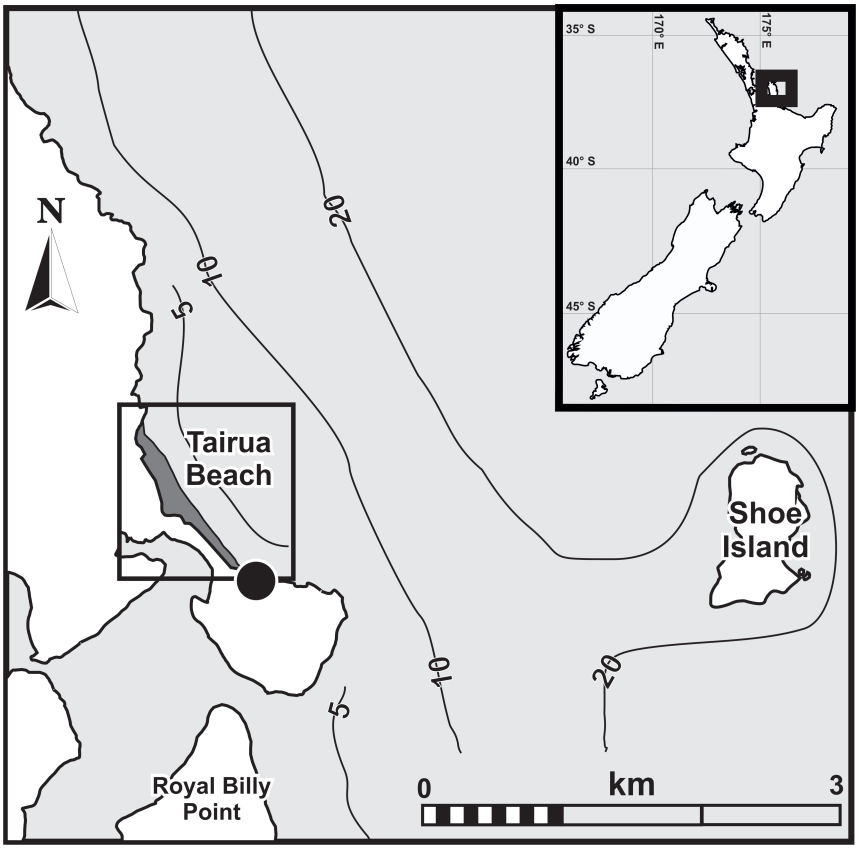

Figure 3.1: Map of Tairua Beach, New Zealand, with the field study location enclosed by a black box. The Cam-Era camera station is located on cliffs to the south (black circle).

Figure 3.2: Image of Tairua Beach. Photo credit: backpack-newzealand.com.

subject to medium energy (H_s 1.5 m, T_m 10 s) South Pacific Ocean waves (Almar et al., 2008). Tairua is an intermediate beach comprised of medium-coarse ($D_{50} \approx 0.6$ mm) sands. The beach is microtidal, with tide range varying between 1.2 m (neaps) and 2.0 m (springs) (van de Lageweg et al., 2013).

Tairua is a popular surf and swim beach, with lifeguard patrols operating between the start of December and the end of February. The patrol is operated by Surf Lifesaving Australia, and focusses on the use of zoned bathing areas. There is a dedicated swimming area, demarcated by red and yellow flags; outside of this zone, surfing is permitted and swimming is discouraged. No rip incident statistics are available for Tairua.

Research at Tairua has made use of a long video imagery record (since 1999). Many studies at Tairua have therefore used images to quantify other phenomena, including beach cusp morphodynamics (Almar et al., 2008), shoreline-sandbar coupling (van de Lageweg et al., 2013), and rip currents (Gallop et al., 2009, 2011). For the purpose of this thesis, Tairua is used only for development of imaging algorithms in Chapter 5, as imagery was freely accessible at the onset of the project.

3.2 Perranporth Beach, Devon, U.K.

Perranporth Beach, located in the southwest of England (Figure 3.3), is a 3500 m-long beach comprised of medium ($D_{50} \approx 0.3$ mm) sand (Austin et al., 2014). The beach has a wide (500 m) intertidal area at the southern end, which narrows into a 250 m wide intertidal area in the northern part. At high tide, the beach can become separated into two distinct beaches by a rocky cliff outcrop half way along. The site is macrotidal, with a mean spring tidal range typically around 6.3 m (Austin et al., 2014). The beach faces west-north-west towards the Atlantic and is subject to medium wave energy conditions with mean significant wave heights (H_s) and peak periods (T_p) of 1.6 m and 10.5 s, respectively (Austin et al., 2013). The beach often exhibits multiple rip currents, typically spaced O(200 m) alongshore (Figure 3.4).

Perranporth is a popular swimming and surf beach, and holiday destination. The beach is patrolled by the RNLI during summer, and some public holiday weekends throughout the year. The beach patrols are conducted by the RNLI, who also provide static signage at entry points to the beach and flags as a means of segmenting activities in the surfzone. The signs at likely entry points to the beach outline the patrol information as well as the likely hazards at that location, such as rip currents or strong tidal currents. In addition, the signs outline any prohibited activities, such as kite surfing. The RNLI also use red and yellow flags to indicate bathing areas, and set up their patrol lookout station between these flags. In addition, black and white flags are used to indicate craft zones, red flags are used to indicate dangerous conditions whereby people should not enter the water, and orange flags are used to indicate the prohibition of inflatables. In addition, mobile hazard-specific warning signs are used on the beach in locations where strong rip currents have been identified. Over a five year period between 2009 and 2013, there were 250 rip related rescues at Perranporth (approx. 65% of total rescues). Of these rip rescue events, the RNLI estimate that without their intervention, 16 events would have resulted in loss of life.

Research on surfzone currents at Perranporth is well established, through a number of field deployments (Austin et al., 2009, 2010, 2013, 2014; Scott et al., 2014). In particular, the dynamics of rip currents have been studied intensely at this site, as have the demographies of those rescued from rip currents (Woodward et al., 2013). To a lesser extent, research has also focussed on suspended sediment transport and swash processes (Masselink et al., 2005; Masselink and Russell, 2006; Thorpe et al., 2013). There is also a nucleus of research focussing on nearshore bathymetric estimation using video imagery (Bergsma et al., 2014, 2016). In this thesis, Perranporth is used as the primary site for the development of synoptic typing methods in Chapter 6. Field data was collected here, and it forms a substantial part of Chapter 7, where flow regimes are compared to wave breaking patterns. Finally, rip incident data from the RNLI for Perranporth was used to inform hazard estimation in Chapter 8.

3.3 Ngarunui Beach, Raglan, New Zealand

Ngarunui Beach, located on the west coast of New Zealands North Island (Figure 3.5), is a 2000 m-long, double-barred dissipative beach comprised of medium ($D_{50} \approx 0.3$ mm) black (iron) sand (Sherwood and Nelson, 1979). The beach fronts a steep, well-established dune ridge, and is laterally confined by a rocky headland at the southern tip and a tidal inlet at the northern edge (Huisman et al., 2011). The predominantly

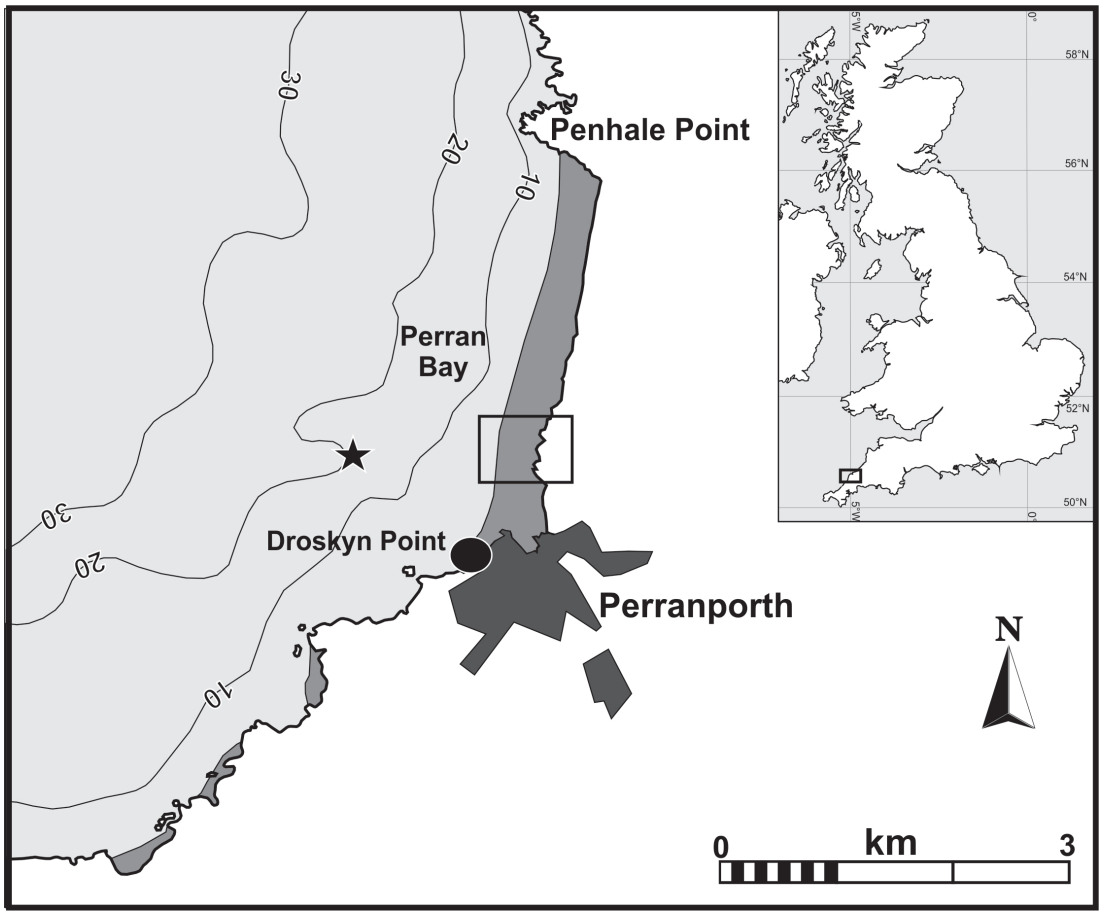

Figure 3.3: Map of Perranporth, U.K., with the field study location enclosed by a black box. The black circle shows the position of the Argus camera station, and the star the directional Waverider wave buoy.

Figure 3.4: Image of Perranporth Beach, with multiple clearly identifiable rip channels alongshore [dark, shore-normal streaks intersecting the breaking waves]. Photo credit: S. Pitman.

mesotidal beach (tide range $\approx$ 1.8 m neap, $\approx$ 2.5 m spring) faces northwest into the Tasman Sea and is routinely subject to energetic wave conditions ($H_s = 1.8$ m, $T_m = 8$ s) (Gorman et al., 2003). The headland at the southern end refracts the dominant wave field (propagating from the south west) into a slightly more shore–normal approach at the beach itself.

Ngarunui is a popular beach for swimming, surfing and fishing, and has lifeguard cover between October and March. The patrol is operated by Surf Lifesaving Australia, and focusses on the use of zoned bathing areas. There is a dedicated swimming area, demarcated by red and yellow flags; outside of this zone, surfing is permitted and swimming is discouraged. There are also static signs at entry points to the beach outlining the main hazards at that particular site, such as large shorebreaks, rip currents

and submerged rocks. Of 258 rescues over a five season period (2010-2015), 212 (82%) were attributed, at least in part, to rip current activity.

The selection of Ngarunui as a study site offers the novel opportunity to study rip hazard on a high energy beach. In addition, video monitoring has been in place at Ngarunui for a comparatively short amount of time (established 2007), meaning Ngarunui has received less attention by researchers than Perranporth. The introduction of the monitoring system has underwritten a number of studies into swash oscillations, shoreline dynamics, groundwater seepage and wave energy transformations at the site (Huisman et al., 2011; Guedes et al., 2013). There has been much recent interest in infragravity swash and resultant current pulsations at infragravity frequencies at the site (Guedes et al., 2013). Unlike Perranporth, no studies have attempted to quantify which hydrodynamic conditions are conducive to hazardous rip formation, nor the demographies of rip victims at Ngarunui. In this thesis, field data was collected for Ngarunui, and it forms a substantial part of Chapter 7, where flow regimes are compared to wave breaking patterns. Furthermore, rip incident data from SLSNZ for Ngarunui was used to inform hazard estimation in Chapter 8.

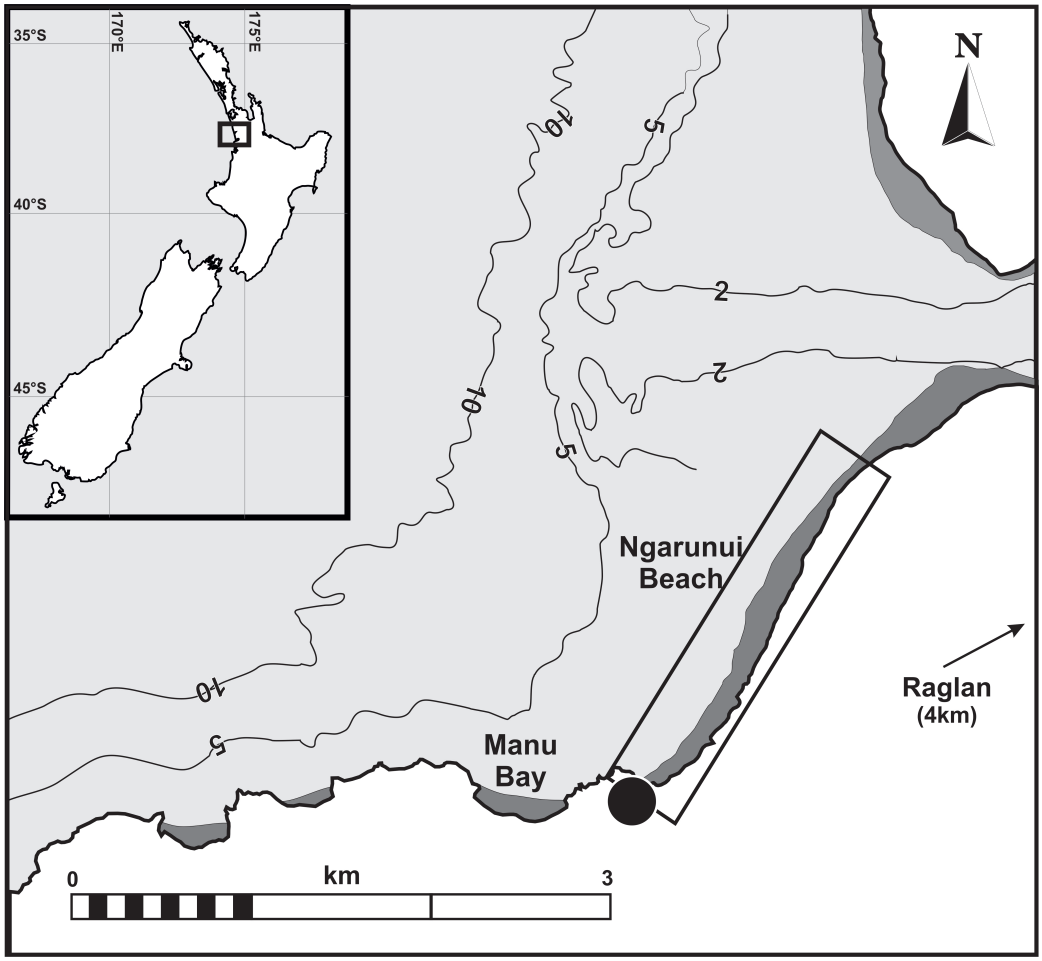

Figure 3.5: Map of Ngarunui Beach, New Zealand, with the field study location enclosed by a black box. The black circle shows the position of the Cam-era video monitoring station.

Figure 3.6: Image of Ngarunui Beach. Photo credit: aa.co.nz.

Chapter 4

Data & methods

This chapter details how Lagrangian, hydrodynamic, remote sensing and rip incident data were compiled and processed for the thesis. The methods discussed herein are standard processing techniques that were used, whereas new methodologies pioneered during this thesis are discussed separately in the relevant results chapters that follow.

4.1 Data

Two field campaigns were carried out in the course of this research at Perranporth from 16—19 May 2014, coinciding with spring tide; and Ngarunui between 10—11 Feb 2015, midway between spring and neap tides.

4.1.1 Lagrangian rip current data

Rip currents can be highly mobile, with channels often shifting laterally over $O(5$ m) in relatively short (tidal) timescales (Quartel, 2009), but equally, they can persist over long (seasonal) timescales (Holman et al., 2006). As a result of the channel mobility, when using Eulerian measurement (the deployment of fixed rigs), it is difficult to ensure that

the rig is positioned centrally in the rip channel. There is also a high chance that the rip channel may move during the course of measurement. Furthermore, a fixed rig by nature can only measure at one point. All these factors combine to hinder accurate measurement of rip channel flow velocities. For these reasons, there is a growing body of literature on rip currents whereby the primary means of data collection is Lagrangian (MacMahan et al., 2010; Austin et al., 2010, 2014; McCarroll et al., 2014). Indeed, Castelle et al. (2016b) note that this shift to Lagrangian measures is reminiscent of early rip studies (e.g., Shepard et al., 1941; Shepard and Inman, 1950), where observations were made of floating objects.

The Lagrangian approach that currently dominates the literature is the use of GPS-tracked surfzone drifters. Schmidt et al. (2003) designed a drifter from watertight PVC tubing, that promoted a low (submerged) centre of gravity, and therefore was quickly self-righting in the surfzone. The drifter had internal GPS components, and an external GPS antenna. It also incorporated a PVC plate on the bottom, to dampen vertical motions. The design was modified by MacMahan et al. (2009) with the addition of three vertical stabilising fins, and the externalisation of the GPS equipment. This revised design used small off-the-shelf handheld GPS devices, contained within a waterproof box, mounted on the mast. The addition of external fins improved the drifters ability to track the currents (MacMahan et al., 2009). A number of studies have since used variations of the modified design (MacMahan et al., 2010; Austin et al., 2013; Scott et al., 2014; Gallop et al., 2015, 2016a; McCarroll et al., 2014).

Perranporth

The drifters used at Perranporth were a combination of both designs, including vertical fins but internalised GPS components (Figure 4.1). The main body was made from 120 mm diameter PVC pipe cut to lengths of 400 mm, with three PVC vertical fins (85 mm $\times$ 300 mm) attached to the outside. A 400 mm vertical damping plate was affixed to the bottom. The top of the main PVC pipe had a removable bung lid, upon which the mast was affixed. The lid was sealed with o-rings and three screws into the main body. The

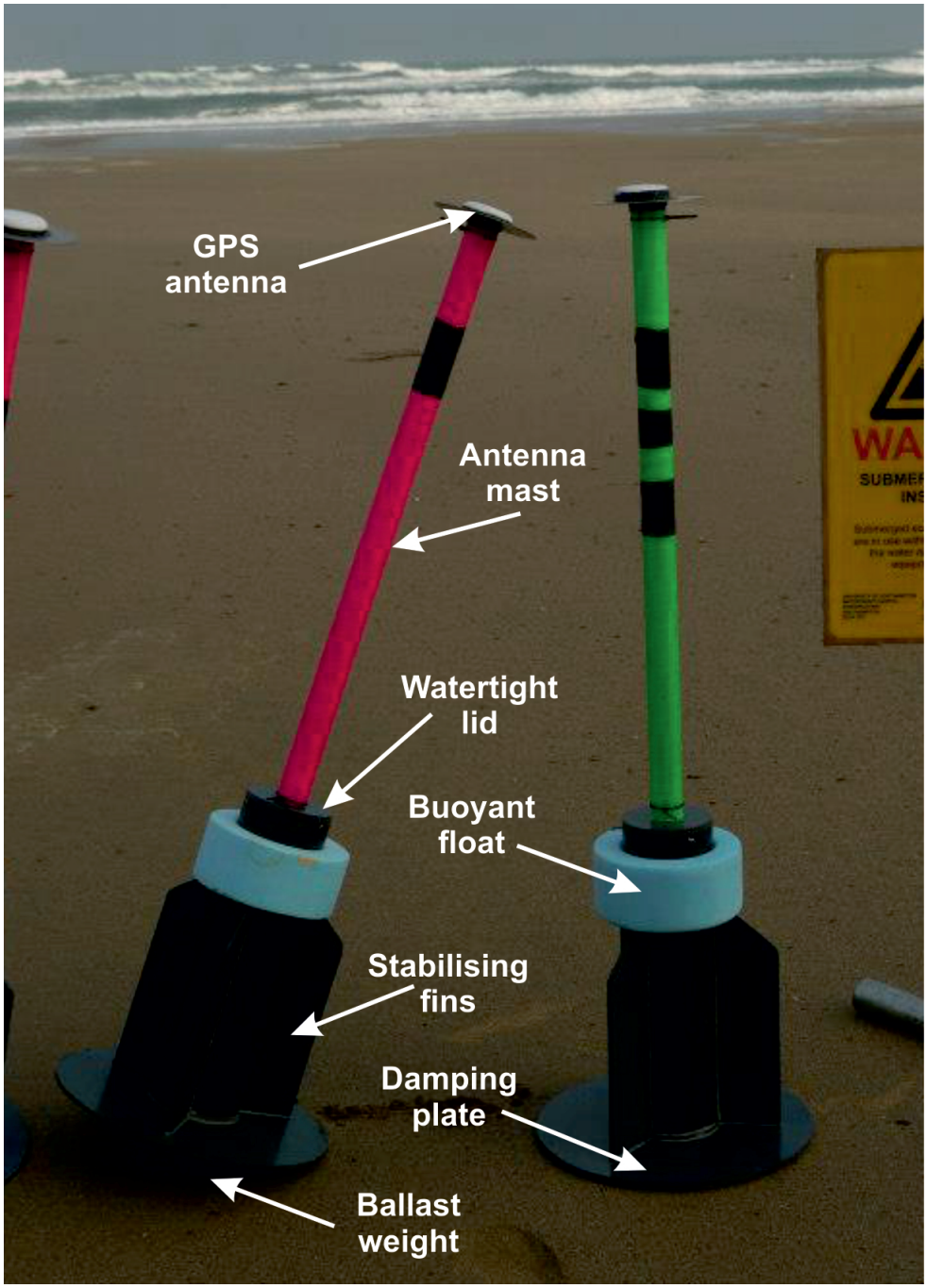

Figure 4.1: Photograph of the GPS drifters during fieldwork at Perranporth. Without ballast, the drifters stand 1200 mm in height. The design is modified from Schmidt et al. (2003) and MacMahan et al. (2009). Photo credit: S. Pitman.

mast was a hollow tube 45 mm in diameter and 750 mm in length, atop of which sits a 140 mm aluminium disc and the GPS antenna. The disc reduces the amount of GPS backscatter from the ocean that is able to reach the GPS antenna itself. From the antenna, a cable runs through the interior of the mast to the GPS components in the main body. A ballast weight was fixed to the bottom of the blanking plate, and a buoyant float affixed to the main body, to achieve the correct buoyancy and floating depth. When deployed in seawater, the waterline on the drifter was level with the lid of the main compartment.

The OEMStar low cost single frequency GNSS receiver was used to collect raw L1 GPS carrier phase signals, which were logged at 1 Hz on an Antilog serial data logger. The raw signal was post processed using the RTKLIB programme, against data from a static Trimble base station located on Droskyn Point (Figure 3.3), reducing the positional error from 1.5 m to < 0.3 m. MacMahan et al. (2009) demonstrated the method to be appropriate in resolution of flows on $O(0.05\ \mathrm{ms}^{-1})$.

At Perranporth, five drifters were used resulting in a total of 195 deployments over the four days, during 4-hour periods centred on low tide (Figure 4.3). The initial deployment each day consisted of simultaneous deployment with approximately 30 m spacing between individual drifters, in order to identify the main location of the offshore current. From that point forward, drifters were predominantly deployed individually by field assistants into the rip channel and feeder areas, in water depths of up to 1 m; with entry times recorded by an observer on the beach. Drifters were also deployed on sand bars either side of the main channel in order to maximise coverage of the entire circulatory system. Occasionally, water depth hindered these deployments, and subsequently some drifters were deployed by an Inflatable Rescue Boat (IRB) seaward of the bars. Drifters were retrieved (by assistants or IRB) when they entered water too shallow to allow free-floating, or when they washed along- or offshore to such an extent that it exited the study area or entered the area preferentially marked by the lifeguards for bathing. Retrieved drifters were immediately redeployed.

Ngarunui

The drifters used at Ngarunui were provided by the University of Waikato, and mirrored the MacMahan et al. (2009) design (Figure 4.2). The GPS unit sat in a waterproof box, affixed to a platform on top of the mast. Rather than a GPS chip and separate aerial, these drifters used handheld, off-the-shelf GPS units, with internal powerpack, receiver and logging capabilities. The GPS unit used here was the QStarz BT-Q100eX, which was used to measure latitude and longitude (as opposed to raw L1 carrier phase signals) at 1 Hz. MacMahan et al. (2009) showed that such handhelds exhibit positional errors of $O(2\text{ m})$ when stationary, and a test on a stationary drifter confirmed this with mean horizontal error and standard deviation of 3.78 ± 1.20 m. The stated manufacturer velocity accuracy for the units is 0.1 ms^{-1}.

Ten drifters were used at Ngarunui, and a total of 38 deployments were made over two days, during 3-hour periods centred around both falling and rising mid-tides (Figure 4.5). Here, drifters were also initially deployed simultaneously in one alongshore array. Thereafter, they were again primarily deployed individually after retrieval by field assistants into the rip channel and feeder areas, in water depths up to 1 m. Drifters were retrieved (by assistants on foot or jet-ski) when they entered water too shallow to allow free-floating, or when they washed along- or offshore to such an extent that it exited the study area or entered the area preferentially marked by the lifeguards for surfing. Retrieved drifters were immediately redeployed.

Drift classification

Each individual deployment was classified visually into one of four categories: 1) linear exit; 2) circulation then exit; 3) circulation with no exit; or 4) other. These classifications are similar to those used in other studies (MacMahan et al., 2010; Austin et al., 2013; Scott et al., 2014; Gallop et al., 2015, 2016a; McCarroll et al., 2014). A linear exit was defined as the drifter moving offshore immediately from the time of deployment, to beyond the edge of the surfzone. Circulation then exit was when drifters had a

Figure 4.2: Photograph of the GPS drifters during fieldwork at Ngarunui. Photo credit: S. Gallop.

significant portion of onshore movement before moving offshore, or when the drifter made at least one complete re-circulation before moving offshore beyond the edge of the surfzone. Circulation with no exit was defined as movement contained within the surfzone. Under this condition drifters would typically rotate 3 or 4 times over periods

O(15 mins) before washing alongshore or onshore. In an extreme case at Perranporth, one drifter recirculated 13 times over 80 mins before washing alongshore. Other was defined as occasions when the drifter washed ashore, or travelled significantly alongshore within the surfzone, without circulation in or around the rip channel.

4.1.2 Hydrodynamics and bathymetry

Perranporth

Sea-level data from the Port Isaac tide gauge (36 km north east of Perranporth) were obtained from the Channel Coastal Observatory (CCO) online repository (www.channelcoast.org). Wind and wave data were also obtained from the CCO, with waves measured using a directional wave rider buoy approximately 1 km offshore of Perranporth in 14 m water depth. All data was collected at 30 minute intervals.

The hydrodynamic conditions during the study were typical of Perranporth and during the deployments, H_s reached 1.5 m on the final day, with lower energy conditions (0.5 m $< H_s <$ 1.25 m) during the other days. Breaking wave heights were unavailable, but qualitatively estimated to be in the region of 0.5-1 m during the study. Maximum T_p coincided with the highest waves on the final day, with fluctuations between 8 and 12.5 s over the 4-day data collection period (Figure 4.3c). The spring tide range was 6.4 m. The incident wave field propagated approximately shore-normal throughout (Figure 4.3d). Wind was onshore over the first three days, with a low wind speed ($U =$ 2.5 m s^{-1}) on the first two days and high larger wind speeds ($U = 8.8$ m s^{-1}) on third day. On the final day of the experiment, a weak ($U \approx 1$ m s^{-1}) offshore wind prevailed (Figure 4.3e—f). The beach exhibited a typically double bar state (Masselink et al., 2014) with the inshore and outer bars at $c.$ 500 and 800 m offshore of the mean high water springs shoreline, respectively.

The bathymetry was measured on 17 May 2014 using an IRB, fitted with a single-beam echosounder. Bathymetry was collected in cross-shore profiles spaced 25 m apart over the nearshore bar, and 50 m offshore of the outer bar. Subaerial beach topography was

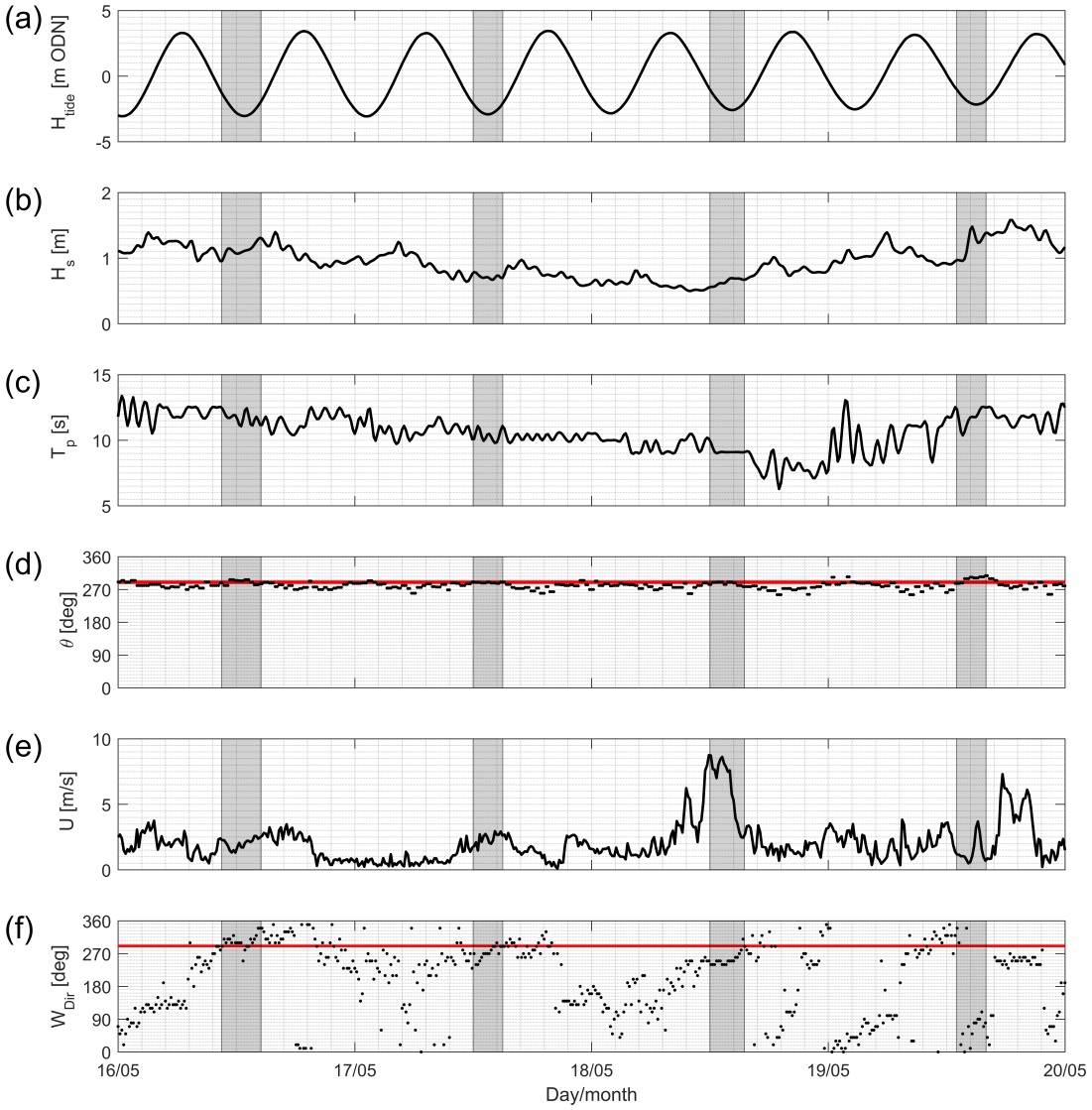

Figure 4.3: Summary of field conditions from 16 to 20 May 2014 at Perranporth Beach, with vertical grey bars indicating drifter deployments: a) water level H_{tide}; b) significant wave height H_s; c) peak wave period T_p; d) incident wave direction θ; e) wind speed U; and f) wind direction W_{Dir}. Red lines indicate the shore-normal direction. ODN refers to Ordnance Datum Newlyn, which is approximate Mean Sea Level in the UK.

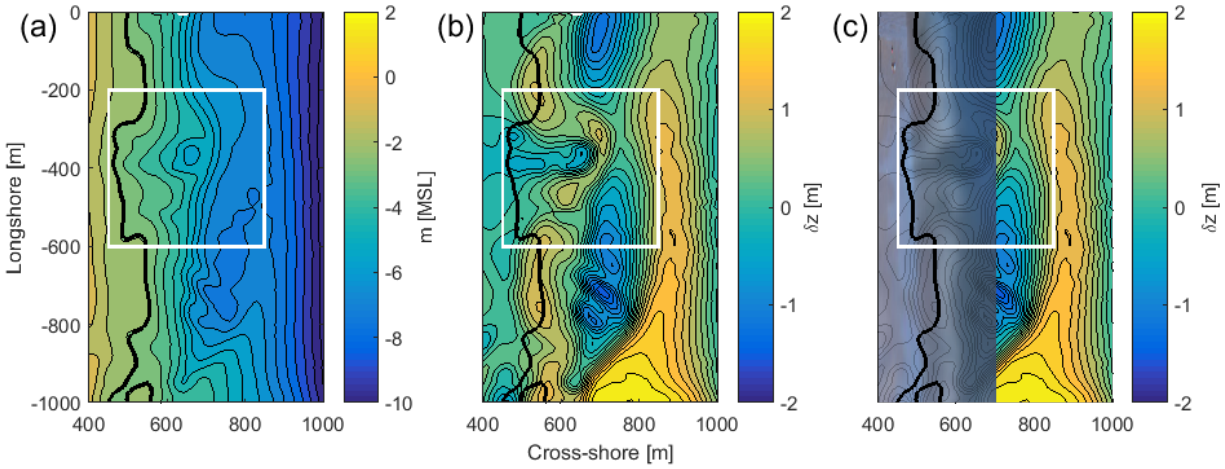

Figure 4.4: Bathymetry and drifter data for the field experiment with white boxes indicative of study area and solid black line is 0 m ODN. (a) The merged bathymetric and topographic data, measured on 17 May 2014. (b) The residual morphology. (c) The overlay of merged, rectified images from the Argus camera onto the bathymetry.

measured using an All-Terrain Vehicle (ATV) fitted with RTK-GPS, in alongshore lines spaced 10 m apart (Figure 4.4).

Ngarunui

Sea-level data from the Kawhia Wharf tide gauge (32 km south of Ngarunui) was obtained from Waikato Regional Council. The Kawhia record is more complete than the Raglan record, and tidal heights are comparable (typically within 0.2 m). Offshore wind and wave conditions were obtained from the nzwave_12 wave forecast using WAVEWATCHv3.14, run by NIWA. At the grid point closest to Ngarunui, hourly data are available from longitude –37.777834 and latitude 174.66760, at 53 m water depth.

The Ngarunui study also encapsulated average wave/tide conditions. H_s ranged between 1.4 m and 1.9 m during deployments (Figure 4.5b), slightly below the annual average ($H_s = 2.2$ m). Breaking wave heights were unavailable, but qualitatively estimated to be in the region of 1-1.5 m during the study. T_p during deployments ranged from 12 to 15 secs, with the shortest period waves occurring on 11^{th} Feb, and the longest period on the

10^{th} Feb (Figure 4.5c). Wave propagation estimated by the hindcast was predominantly from the south–west (Figure 4.5d), however, the headland at the southern end of the beach (Figure 3.5) acts to refract waves around to a slightly more shore–normal approach at the beach itself. Wind speed (Figure 4.5e) fluctuated between 7 and 9 m s^{-1} during deployments, with direction offshore for both days (Figure 4.5f).

The intertidal beach bathymetry was surveyed on 5 Feb using RTK-GPS, in alongshore transects. This intertidal bathymetry covers the cross-shore extent between -700 m and -450 m (Figure 4.6), which approximately covers the area above the MLW mark. Further offshore, the subtidal bathymetry used for Ngarunui can be considered as a general overview, rather than specific to the study. Data were collected via various methods on dates between 2008—2013, and combined with Chart data from 1977 by Harrison and Hunt (2014), and it will therefore have changed by the time of the study. As a result, bathymetry cannot be used as indicative of channel location, and is presented purely to give an overview of general slope. The composite subtidal bathymetry comprises elements of boat-mounted multibeam echosounder surveys, LiDAR surveys, jetski-mounted single beam echosounder surveys, in addition to the digitisation of navigational charts and orthophotos. Measurements were exported to a 1 m grid. The two datasets have been merged and used to present subtidal bathymetry in this thesis (Figure 4.6).

4.1.3 Video imagery

Tairua

Tairua has been monitored since 1999 by the NIWA Cam–Era scheme, located on Paku Hill at the southern end of the beach (Figure 3.1). The camera is located at 70 m above chart datum (van de Lageweg et al., 2013), affording good coverage of the dune, beachface and nearshore zone for the entirety of the beach, excepting the first 50 m which is hidden by outcrops of Paku Hill (Almar et al., 2008).

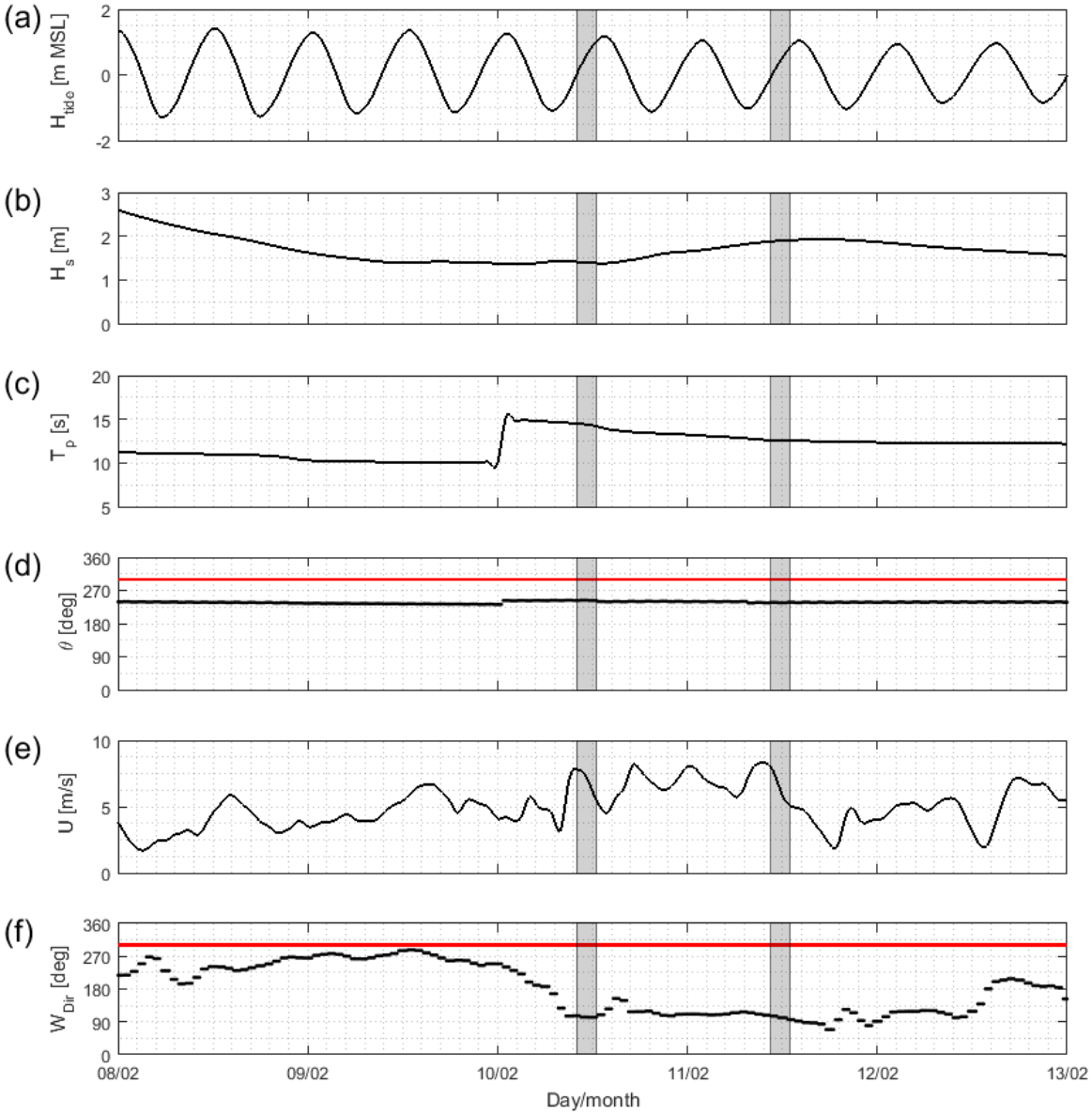

Figure 4.5: Summary of field conditions from 8 to 13 Feb 2015 at Ngarunui Beach, with vertical grey bars indicating drifter deployments: a) water level H_{tide}; b) significant wave height H_s; c) peak wave period T_p; d) incident wave direction θ; e) wind speed U; and f) wind direction W_{Dir}. Red lines indicate the shore-normal direction. Tidal heights are reference to MSL.

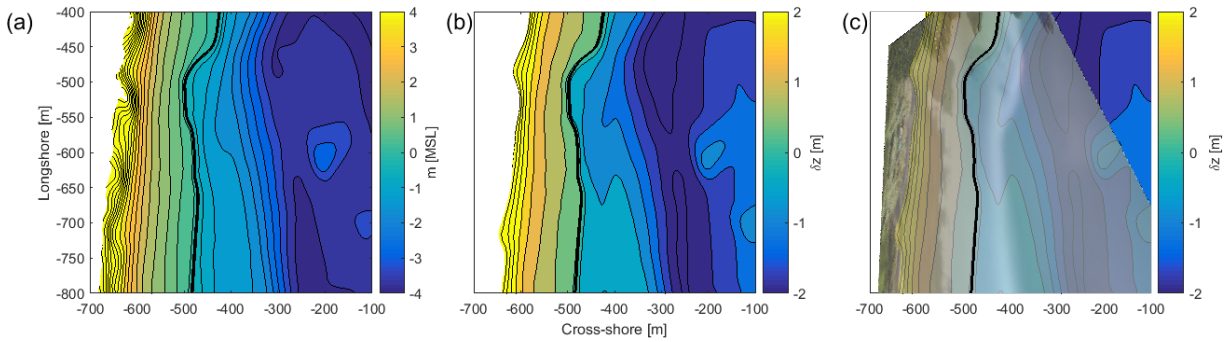

Figure 4.6: Bathymetry data for Ngarunui. The solid black line represents MSL. (a) The general bathymetric data merged with topographic data measured on 8 Feb 2015. (b) The residual morphology. (c) The overlay of merged, rectified images from the Cam-Era station onto the residual morphology.

Perranporth

Perranporth is monitored by a set of three Argus cameras located on Droskyn Point at the southern extreme of the beach (Figure 3.3), 48 m above mean sea level (Huntley et al., 2009). The first two cameras were installed in 1996, with the third installed in 2010 (Scott et al., 2014). This study uses half-hourly, geo-rectified 10-minute time exposure (timex) images (Figure 2.3) in the local Argus co-ordinate system.

It is unfortunate that the Argus camera was unserviceable for the period 20—23 Jul and also 6—22 Aug 2013, when a large number of incidents occurred. However, investigation of the images captured immediately prior to and following these outages showed the presence of numerous and prominent open rip channels. Furthermore, the wave conditions between 23 Jul and 23 Aug 2013 were low energy (mean $Hs = 1.02$ m), with no storms and therefore it is likely that the prominent open rip channels persisted throughout the period.

Ngarunui

Ngarunui is monitored by a set of two NIWA Cam–Era video cameras located at the southern end of the beach (Figure 3.5) at a height of 95 m above mean sea level (Guedes

et al., 2013). One camera provides coverage of the outer bar and offshore, with one focussed on the inner bar, swash zone and subaerial beach. The merged, rectified image gives coverage of the entire 2 km beach to the boundary with the tidal inlet.

One of the two cameras was unserviceable for the latter half of 2015, and therefore images from this period are omitted from further analysis within this thesis.

4.1.4 Rip incident data

Perranporth

Rip incident data were supplied for Perranporth by the RNLI for 2009—2013, during which time RNLI patrols were active between April and October. The RNLI record an incident every time they intervene. They record time and location, demographic data, qualitative observations of meteorological and hydrodynamic conditions and, crucially, information on the cause of the incident (e.g., inexperience, rip currents, tidal cut off, etc.).

Ngarunui

Rescue, first aid and search data at Ngarunui was supplied by Surf Life Saving New Zealand (SLSNZ) for 2010—2015 (SLSNZ, 2016), during which time the beach was patrolled between October and March. This database is compiled by surf lifeguards after any incident whereby some intervention physical (as opposed to verbal) response is required. They record the time and location, demographic data, qualitative data on strength of wind and surf, and a narrative on the activity a person was involved in, as well as any compounding factors (e.g., poor swimmer, rip currents, etc.).

4.2 Methods

4.2.1 Drifter GPS data

The drifter data collected at 1 Hz was initially filtered by location into a 0.1 Hz signal, to remove noise inherent in the GPS signal that is not representative of the true drifter path. Velocity was calculated between the new filtered 0.1 Hz dataset, and the velocity signal was subject to a zero phase, fifth order Butterworth lowpass filter, as in the case of previous drifter studies (Johnson and Pattiaratchi, 2004; McCarroll et al., 2014), with a cut off of 0.05 Hz. The positional data is now linearly interpolated back into observations at 1 Hz, representing the original sample frequency. At this point, the bearing of the drifter is calculated and recorded at 1 Hz. Then all values are converted into the Argus co-ordinate system, resulting in latitudes and longitudes converted into a co-ordinate system based on metres distance from a nominal Argus origin.

The spatial domain in which the drifters circulated was divided into 10 $\times$ 10 m cells (Figure 4.7a; 4.8a) and all drifter data for subsequent discrete time periods were calculated within these cells. This cell size is appropriate to quantify the circulation pattern, given that typical scales of rip circulation are O(100 m), and is comparable to previous studies (MacMahan et al., 2010; McCarroll et al., 2014). Following the work of Spydell et al. (2007) and MacMahan et al. (2010), observations in the same grid square were grouped into one independent observation. If the drifter later re-entered the grid square, it would be considered a new independent observation if it had travelled a significant distance (defined as the length of the grid square) before doing so. A re-entering drifter was independent when $t > lg/U$ (MacMahan et al., 2010), where t is elapsed time, lg is the grid square size and U is the average drifter speed whilst in transit outside of the gridsquare. Velocity and direction measurements were then calculated for bins with at least 5 independent observations (Figure 4.7a; 4.8a), following Spydell et al. (2007) and MacMahan et al. (2010). Velocity calculations (Figure 4.7b; 4.8b) were based on the mean of independent observations in each grid square ($\overline{U'}$). Following (McCarroll et al., 2014), the overbar is herein used as a denotation for a value based on a grid

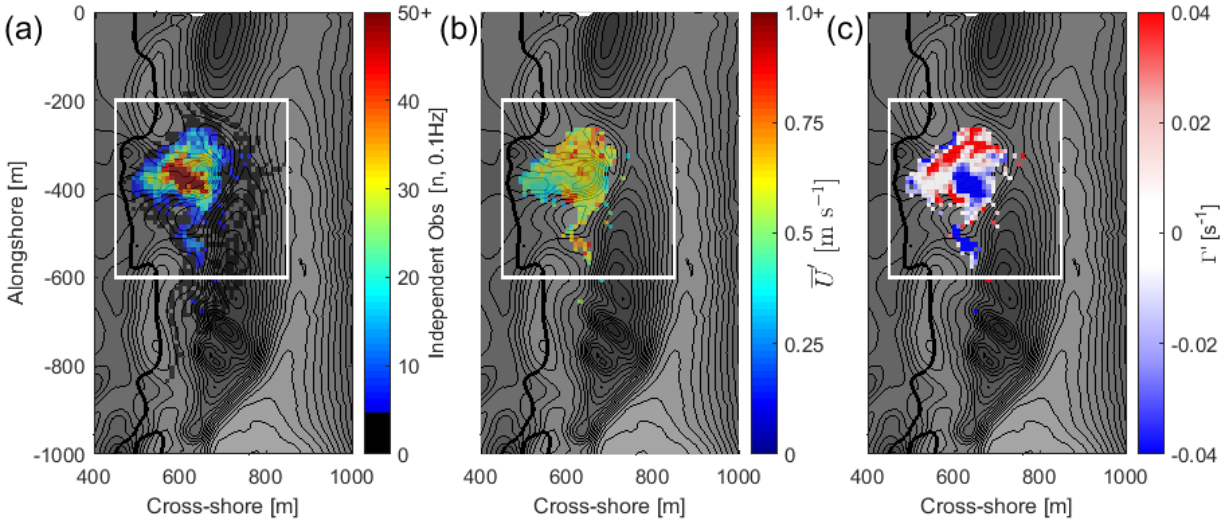

Figure 4.7: Bathymetry and drifter data for the Perranporth field experiment with white boxes indicative of study area and solid black line is 0 m ODN. (a) Number of independent observations recorded at 0.1 Hz over the study period, binned into 10 × 10 m grid squares. Grid squares with < 5 observations appear as grey and are not considered further in the thesis. (b) Mean drifter velocities recorded during the experiment. (c) Overall surfzone vorticity over the experiment, with red values indicative of an anti-clockwise horizontal rotation, and blue values indicative of clockwise rotation.

square mean, and the prime symbol denotes the use of independent observations. The 10 s window was used because the maximum drifter speeds from previous Perranporth experiments (Austin et al., 2009; Scott et al., 2014) were typically around 1 m s^{-1}, equating to up to 10 m horizontal displacement over a 0.1 Hz window, coinciding to the initial filtered frequency of drifter positions. This is comparable to the 10 × 10 m cells that were used to construct the spatial domain for processing. These processing steps are summarised along with examples of each stage at Appendix A.

The circulation of rip currents is of paramount importance in this study and therefore a measure of vorticity (Γ) is presented throughout (Figure 4.7c; 4.8c). Vorticity is defined as the change in orientation of a parcel of water, without change in area or shape (Molinari and Kirwan, 1975; MacMahan et al., 2010) and is a parameterisation of the local rotational motion of a fluid, or velocity shear (McCarroll et al., 2014). Vorticity

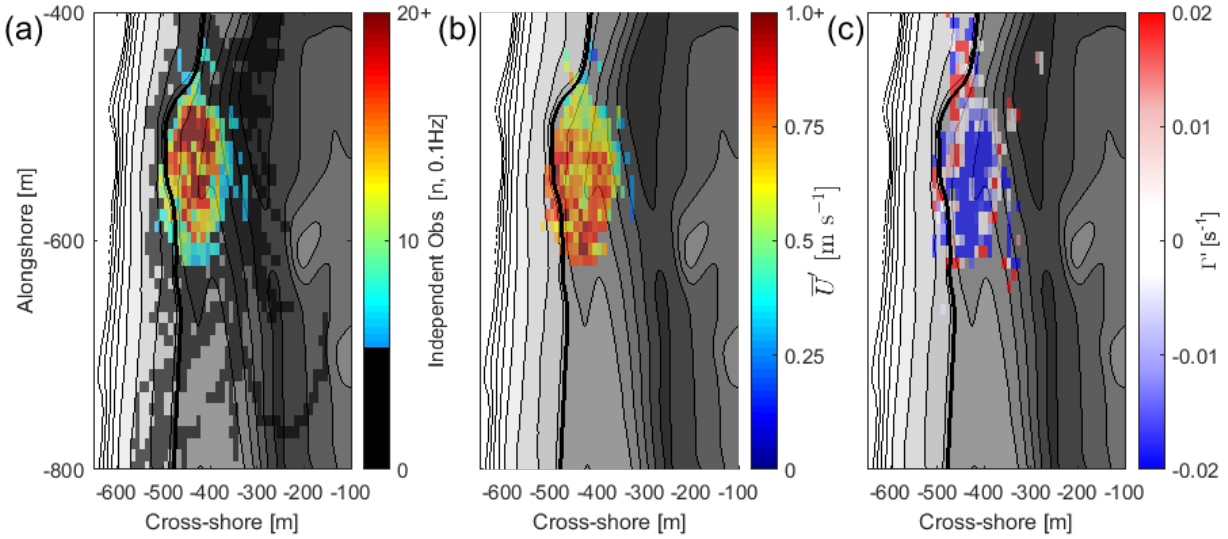

Figure 4.8: Bathymetry and drifter data for the Ngarunui field experiment with solid black line is MSL. (a) Number of independent observations recorded at 0.1 Hz over the study period, binned into 10 × 10 m grid squares. Grid squares with < 5 observations appear as grey and are not considered further in the thesis. (b) Mean drifter velocities recorded during the experiment. (c) Overall surfzone vorticity over the experiment, with red values indicative of an anti-clockwise horizontal rotation, and blue values indicative of clockwise rotation.

was calculated using the weighted central difference method (MacMahan et al., 2010), as follows;

$$\Gamma = \frac{dv}{dx} - \frac{du}{dy} \tag{4.1}$$

where u and v are the vector components of $\overline{U'}$ at point x,y.

4.2.2 Bathymetry

The subaerial topography and submerged bathymetry were merged with significant overlap for quality control (Figure 4.4a). The bathymetry presented here is the residual morphology (Figure 4.4b), following the approach of Austin et al. (2010). The residual bathymetry is obtained by subtracting the cross-shore linear trend surface over the entire intertidal area from the measured bathymetry at that same cross-shore transect. Waves breaking over a linear surface would be expected to break in a uniform manner, and therefore the deviations from this linear surface obtained by subtracting from the real profile act to highlight areas where increased (positive values) and decreased (negative values) wave breaking would be expected. No post-processing was conducted on Ngarunui bathymetry, as it was supplied in complete form.

4.2.3 Video imagery

The use of video imagery for quantitative analysis requires an understanding and application of the various technical transformations to yield results in terms of real world (x, y and z) location. All imagery for this study was converted from oblique imagery, to rectified, merged, plan view images. This process was discussed in Section 2.1.1, and a full technical overview of the process was provided by Holland et al. (1997).

In general, there is potential that the imagery at this frequency aliases the wave group frequency, which has before been postulated as an important process in controlling rip current velocity pulses (Shepard et al., 1941; Sonu, 1972; Aagaard et al., 1997). However, Scott et al. (2014) estimate wave group frequency at Perranporth to be between 25—250 secs, and the chosen image sampling frequency of 600 secs ensures that at least one wave group is captured per timex image. Furthermore, the nature of the timex image ensures that the maximum extent of wave breaking is captured, and therefore aliasing effects do not present a significant problem for later analysis.

Chapter 5

Synthetic imagery for rip channel detection

This chapter discusses progress in the development of an automated approach to rip detection from video imagery and the creation of synthetic images to facilitate this. It is adapted from the following publication:

> Pitman, S.J.; Gallop, S.L.; Haigh, I.D.; Mahmoodi, S.; Masselink, G., and Ranasinghe, R., 2016. Synthetic imagery for the automated detection of rip currents. **In:** Vila-Concejo, A.; Bruce, E.; Kennedy, D.M., and McCarroll, R.J. (eds.), Proceedings of the 14th International Coastal Symposium (Sydney, Australia). Journal of Coastal Research, Special Issue, No. 75, pp. 912-916. Coconut Creek (Florida), ISSN 0749-0208.

5.1 Introduction

The development of coastal imaging systems over the past 30 years has provided huge opportunity for investigation of the coastal zone through remote sensing. Such systems

are an attractive prospect as they are comparatively cheap and are constantly recording data, under all manner of meteorological and oceanographic conditions. Their use as a means to detect rip currents was first proposed by Ranasinghe et al. (1999), who noted alongshore pixel intensity minima locations were coincident with rip channels. Since then, there have been numerous attempts to automate the detection of rip currents. Automation is a goal for researchers because video imaging systems, constantly recording data generate datasets that are too large to manually sift. That said, to date, the complexity of surfzone imagery has prevented the development of automated detection methods. Here, the background to video imaging the coastal zone, attempts to automate rip current detection, and the steps that can be taken to simplify surfzone imagery in an attempt to make automation possible are all considered.

An overview of past literature dealing with automated rip detection was presented in Section 2.1, and a brief summary follows here. After the discovery of Lippmann and Holman (1989) that video imagery provided a useful means of quantifying nearshore processes using light intensity in time exposure images, numerous studies have linked the intensity minima to rip detection. A simple alongshore-orientated intensity profile was first found to work well for simple rip detection scenarios, but failed to cope for more complex or energetic scenarios (Ranasinghe et al., 1999). The method also suffered a degree of subjectivity in the selection of analytical thresholds (Holman et al., 2006). These complications in automated detection meant that many rip detection studies have instead favoured subjective manual means of rip detection in imagery (e.g. Bogle et al., 2000; Whyte et al., 2005; Holman et al., 2006; Turner et al., 2007; Quartel, 2009; Orzech et al., 2010; Murray et al., 2013). The most recent attempt to develop an automated means of detection was that of Gallop et al. (2009, 2011), but this too ultimately needed manual cleaning as a result of the complex trends evident in the imagery. With image complexity being a recurring theme, it is of interest to investigate how pre-processing of an image may affect its subsequent utility for rip detection. The dominant image type used for analysis, the timex, is already considered to be filtered as it represents the time-mean pixel intensity over (typically) a ten minute period, however, there are still

large amounts of noise in the imagery (e.g. fouling by dirt or rain on the lens during acquisition).

Therefore, the overall objective of this chapter is to develop pre-processing image techniques to improve the reliability of automated rip channel detection in video imagery. Here, two case study sites are used; the macrotidal, intermediate, low tide bar/rip beach at Perranporth and the microtidal, intermediate embayed beach at Tairua. In order to address the objective, there are a number of sub-objectives: (1) To assess the utility of image filtering as a method of removing noise and image fouling in video imagery; (2) To develop a (semi)automated approach to rip detection, and (3) To explore the use of synthetic imagery as an aid to automated rip detection. The contents of this chapter are heavily weighted towards methodology, as unless stated, the methodology was developed as part of this work, and is not simply the employment of established methodologies. This chapter focuses on imagery from Tairua and Perranporth.

5.2 Methodology

This section will first outline the novel method for pre-filtering surfzone imagery, before outlining the methods employed to create a synthetic image of the surfzone for subsequent processing. Subsequently, a new means of automating detection on the synthetic imagery is explored.

5.2.1 Image rectification

The first stage in rip detection is generally to rectify the images, using standard photogrammetric transformations between ground and image co-ordinates (Holland et al., 1997), as discussed in Section 2.1.2 and this is the approach applied here. The image is subsequently cropped to minimise peripheral noise and re-orientated so that the shoreline runs parallel to the x-axis (Figure 5.2a). It is important that the image

includes not only the breaking zone, but also a portion of the offshore environment, so that the breaking region can be delineated later (Section 5.2.4).

Pixel resolution of the original imagery has an important bearing on the ability to make quantitative measurements from the resultant rectified image. A typical coastal imaging camera will image in an array of 1024 $\times$ 768 pixels, with spatial resolution a function of the projection from a pinhole lens, through the pixel and onto the ground footprint of that pixel (Holman and Stanley, 2007). The result of this transformation is that near-camera features are imaged with high spatial resolution (pixel = $\approx$ 0.05 m), but resolution decreases linearly with range such that alongshore resolution 1,500 m from the camera is of the order 30 m (Aarninkhof et al., 2003). Cross shore resolution is much better conserved at range, likely to be $<$ 5 m at a distance of 1,500 m (Aarninkhof et al., 2003). Generally, long-shore features have much smaller spatial gradients than those in the cross-shore, requiring less resolution to resolve. In this study, all features are typically within 500 m of the camera, and the resolutions quoted are more than sufficient to resolve rip currents with length and width scales typically around 100 m and 30 m, respectively.

5.2.2 Image filtering

Simple single-image filtering of nearshore images has not been widely used before, because the prevalent image type used for analysis is the so called timex image, which represents the time-mean of intensity in all frames collected at 2 Hz over a 10-minute period (Holman and Stanley, 2007). This constitutes a form of average filtering during the image acquisition stage; however, the resultant image may still include background noise or erroneous data. One such example is raindrops on the lens covering, which would appear in the rectified image, giving a false intensity signature for the pixel(s) concerned. Studies using video images tend to reject imagery where raindrops are visible on the lens for this reason. Holman et al. (2013) described how consecutive images in a time series can be used to create a running-average estimate (cBathy). cBathy uses wave celerity to estimate bathymetry, and the use of this running-average filter was successful

in removing fouling from subsequent images, such as rain drops or sun glare. Despite the assumption that a timex image is already prefiltered, it still contains noisy signals, representative of a very dynamic surfzone. Furthermore, inclement weather still appears as fouling in the imagery. Therefore, there is a need to pre-filter the image before processing, rather than relying on filtering the signal that is extracted as a result of processing.

The first stage to create a synthetic image is filtering the parent image. A common approach to filtering is the use of high- and low-pass filters. These operate in the frequency domain of the image, akin to Fourier transforms. High frequency noise is introduced to imagery by sharp intensity transitions, such as edges observed at the shoreline. These high frequency signals can be smoothed using a lowpass filter (Tomasi and Manduchi, 1998), attenuating the high frequency components and therefore blurring the image (Gonzalez and Woods, 2008).

In simple cases, where only a few raindrops have fouled the image, spatial filtering can remove the effect of this noise. When the fouled image is rectified, the previously small element of noise (the rain drop), is projected across a wide area (e.g. Figure 5.1a), as a result of the transformation between image co-ordinates [u, v] and real-world co-ordinates [x, y, z]. A Gaussian lowpass filter (Tomasi and Manduchi, 1998) is applied (mask = 15×15, $\sigma = 10$) to the rectified image (Figure 5.1b). Subsequently, pixel intensities from the same transect of pixels in each image are extracted (Figure 5.1c). The maximum gradient in intensity profile is used as an estimation of the onset of wave breaking. In the unfiltered image, large errors are evident in the detected location of wave breaking (Figure 5.1d) wherever rain fouls the lens. In contrast, the errors are much reduced in the profile extracted from filtered imagery.

This example highlights the benefits to be gained from image manipulation prior to processing, such as the removal of small patches of lens fouling. As these sharp intensity transitions are often expected to represent the very feature we wish to investigate, such as the edge of a rip channel, filtering can smooth these features yielding more accurate results.

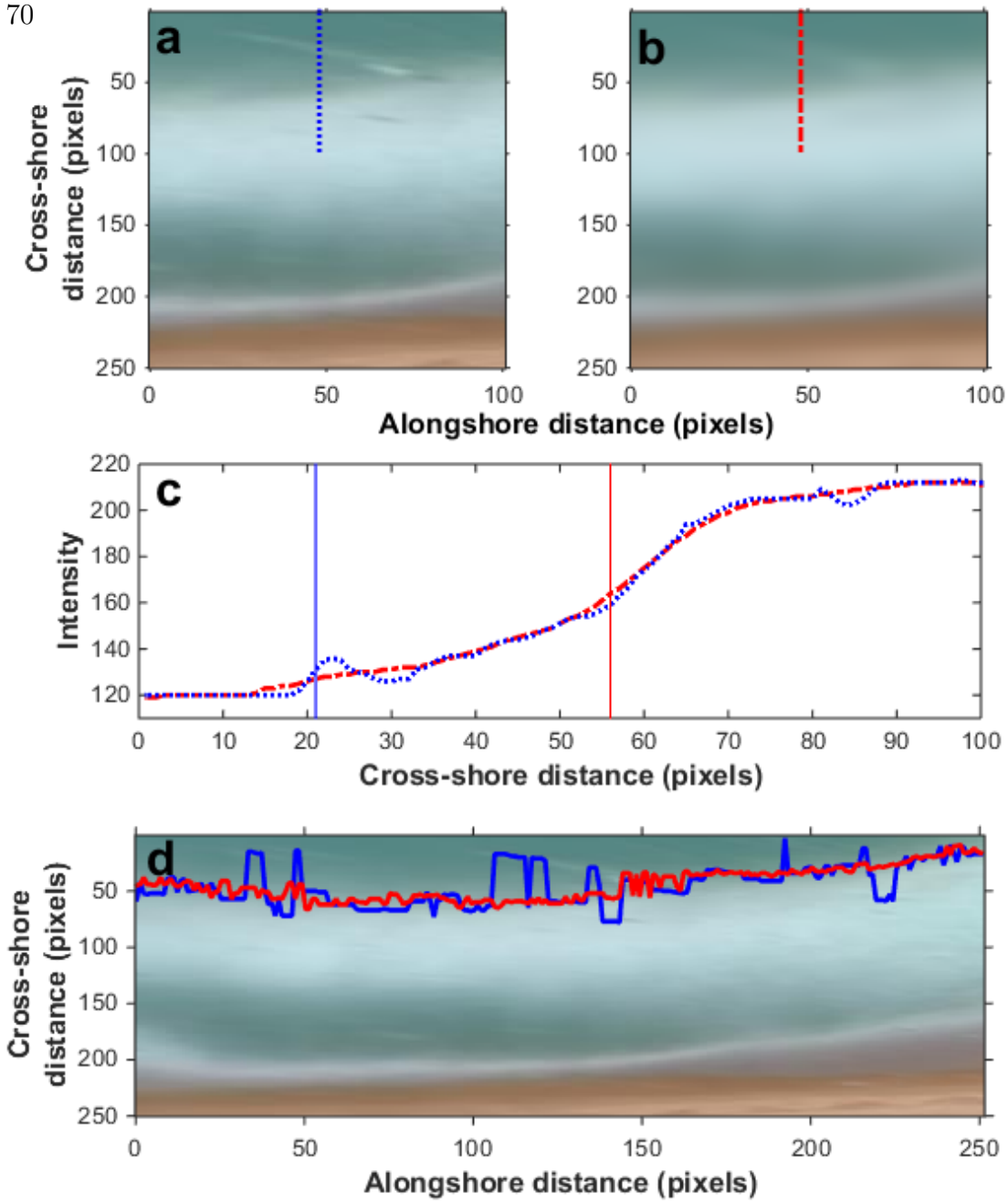

Figure 5.1: (a) Rectified timex image of Tairua Beach, New Zealand. Rain drop fouling is evident in the region of the blue transect line. (b) Filtered version of (a) with red transect line. (c) Intensity profiles for both transect lines, with the maxima marked by horizontal lines. (d) Onset of wave breaking detected alongshore using intensity maxima transects, as per (c).

5.2.3 Shoreline detection

Before proceeding any further, it is important to isolate the surfzone in the imagery. The surfzone is bounded by the shoreline on one side, and the maximum intensity of wave breaking (henceforth referred to as the barline) on the other. The shoreline and barline are used here to mask the outer areas of the image, as rips will not occur outside of the breakers or on the beach. Colour is a useful way to segregate objects and is used here as a means of detecting the shoreline. However, the absolute colour recorded in an image is susceptible to a number of conditions (e.g. illumination, shading, and reflectivity) that may result in depicted colour being different to actual colour (Gevers and Stokman, 2003). In contrast, normalised colour (the difference between percentage of red, green and blue hues in each pixel) was almost invariant to changes in lighting and camera positions (Gevers and Smeulders, 1999). Therefore, rather than using absolute colour, this approach uses colour histograms derived from all available pixels in the imagery.

The image is segmented into 3 broad clusters using k-means clustering (Wang and Adelson, 1994). This method assigns each pixel a location in space, and then partitions the image into 3 clusters, based on the signature of the RGB value of pixels (Figure 5.2b). The cluster with a dominance of red pixels is invariably associated with the darker colours of the beach, and contrasts against the blues and greens associated with swash and breaking waves. The boundary between the red cluster and its nearest neighbour is therefore used as an estimate of shoreline position for the remainder of the algorithm steps (Figure 5.2c).

5.2.4 Barline position

When attempting to detect the barline (i.e. the offshore extent of wave breaking), colour images are less useful. In graycale imagery the sand bars show as white pixels in images as waves break over the shallower sea bed (Lippmann and Holman, 1989), making an obvious contrast against a darker, offshore area. If colour imagery is used, assessment of

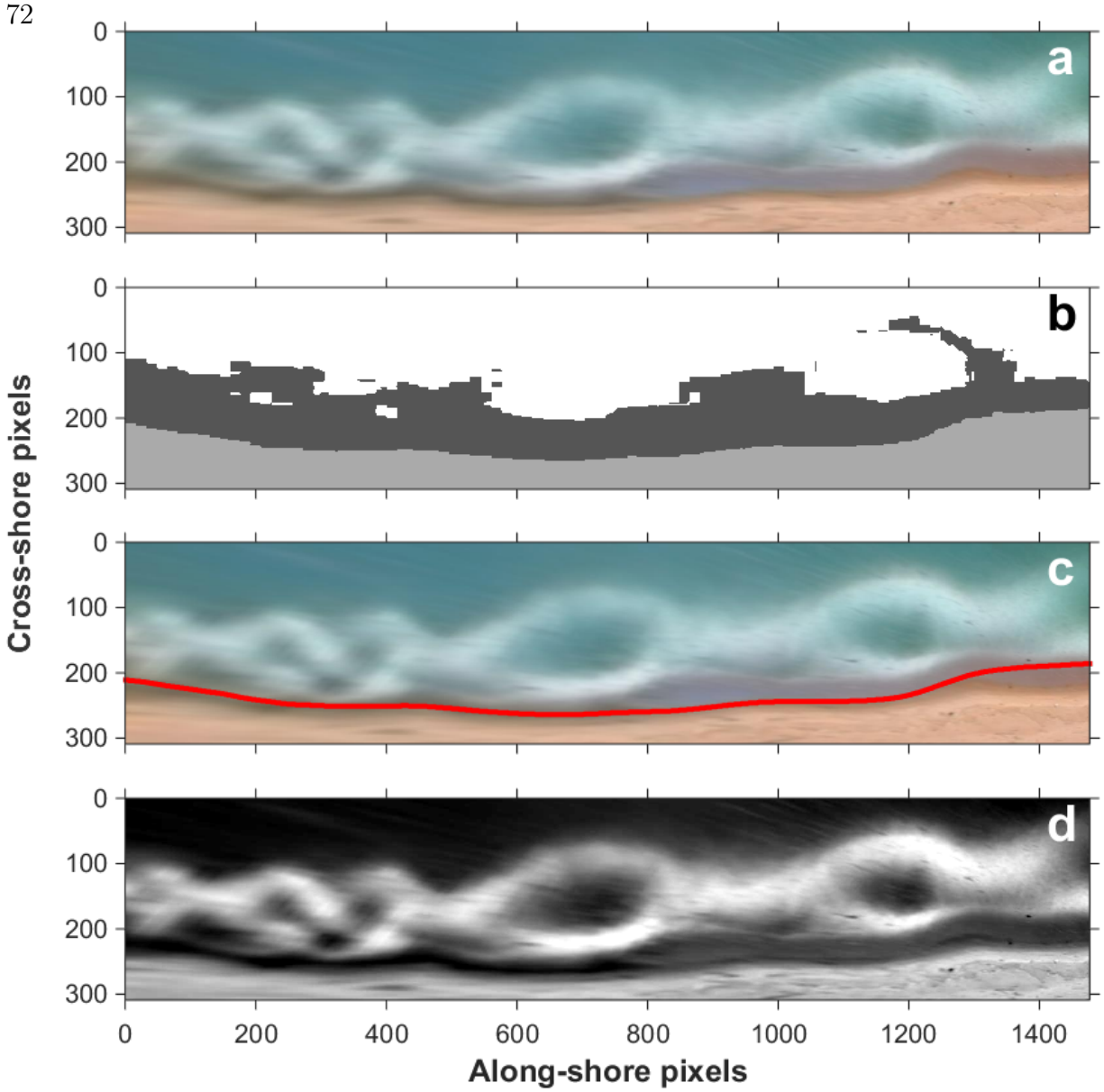

Figure 5.2: (a) Original rectified timex image from Tairua Beach, New Zealand (NIWA). The image is orientated so that shoreline runs along the x-axis. (b) The image is first segregated into three groups, corresponding to the dominant red, green, and blue pixel clusters. The boundary between beach and breaking zone is depicted well by this method, and is therefore used (c) as an approximation of shoreline. (d) The image is then converted to grayscale for further processing.

the absolute colour is required, detracting from the algorithms ability to work at multiple sites without calibration.

Although it is possible to detect a change from the aquamarine colours of the offshore area to the lighter areas of wave breaking, this study has found it to more accurate to make use of grayscale imagery for the reasons stated (Figure 5.2d). The image is therefore converted to grayscale, and the dynamic range (the contrast between dark and light intensities) is stretched. The intensity profile of each column of pixels is then measured (Figure 5.3a), with the onset of wave breaking identified as the first peak above a significant threshold in the intensity profile. That is to say, the algorithm looks for the first sharp change between darker offshore areas and lighter pixel intensities. This threshold needs a sensitivity analysis within and between sites, but is currently set at 0.2, on a normalised intensity scale between 0 and 1. This intensity threshold is to ensure that the detected signal is above any offshore generated noise in the intensity profile, and represents a significant feature (the onset of depth-induced wave breaking). This is henceforth simply referred to as the barline. The location of this significant peak is calculated for every column of pixels in the image, and the resulting indexed locations are lowpass filtered to give a coherent barline (Figure 5.3b). This increase in pixel intensities has previously been deemed an appropriate indication of bar position (Bogle et al., 2000), however, the threshold chosen will vary according to site.

The accuracy of the methods outlined above for bar- and shoreline detection were tested against expert-user digitised datasets of positions. The employment of an expert-user allows for 'ground truth' positions to be ascertained, using a trained person to digitise the features of interest directly. In this case, the author acted as the expert-user. Both methods outlined above show good correlation with manual detections (Figure 5.4). Comparison between manual and automated shoreline detections were correlated at $r^2 = 0.87$, with a slightly lower correlation ($r^2 = 0.81$) in barline detection. Both methods were deemed to be of a suitable level of accuracy for surfzone delineation as a stage on the automated detection algorithm.

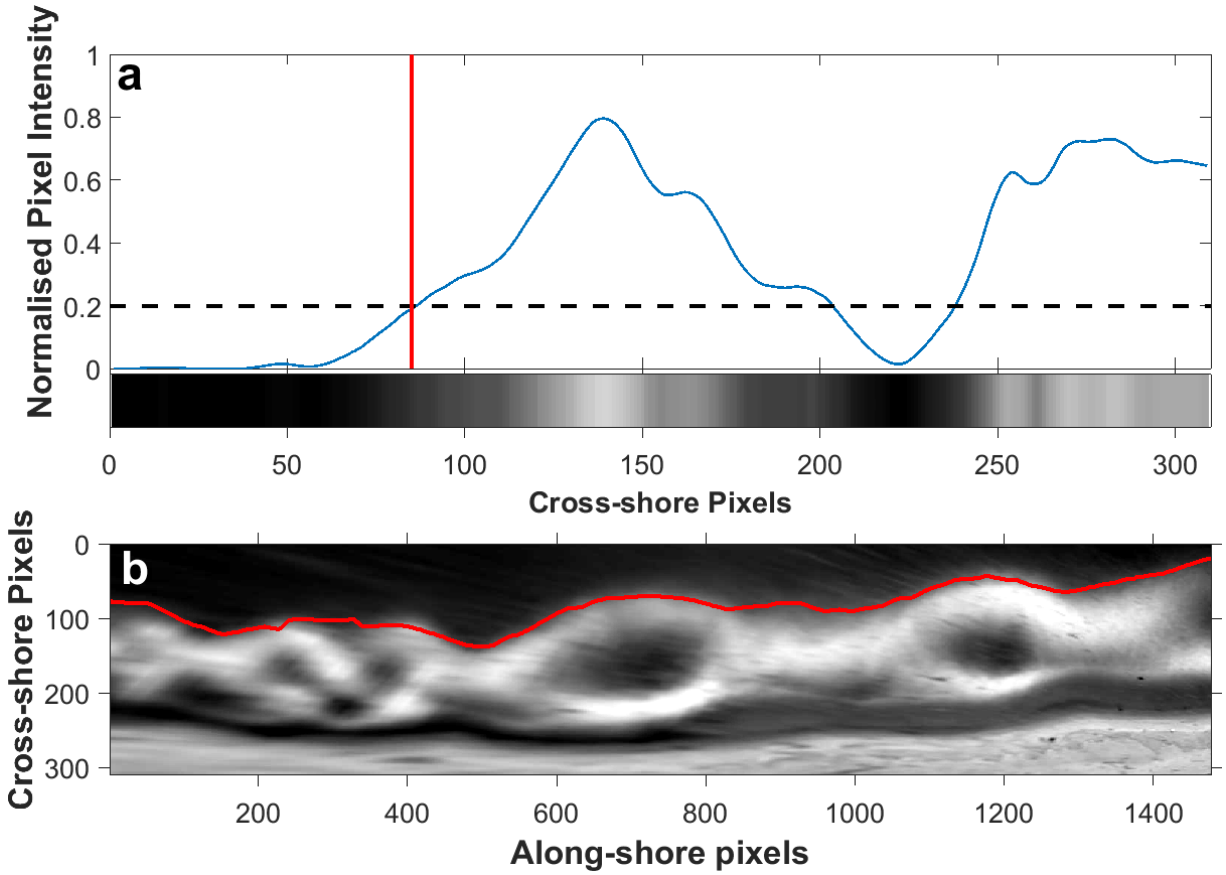

Figure 5.3: (a) Derivation of barline for one individual column of pixels. The pixels are shown in the bar below the figure, with the respective normalised pixel intensity along that bar shown above by the blue line. The 0.2 threshold is marked (dashed line) and the first peak in intensity above that threshold (red line) is stored as the barline location. (b) Repetition of this method for every column of pixels in the image gives an estimate of the longshore variable barline.

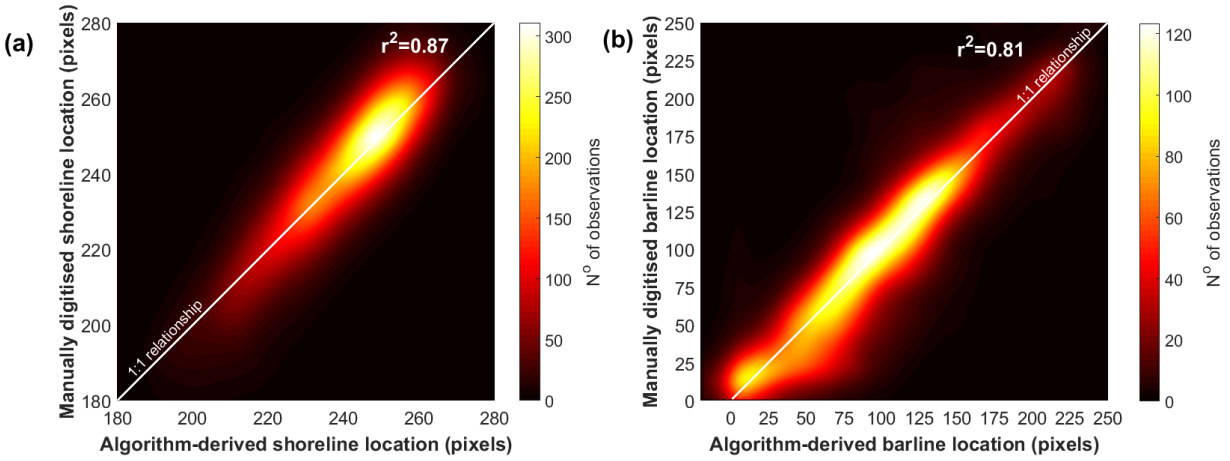

Figure 5.4: Scatter intensity plot of algorithm and (a) manually derived shoreline and (b) barline locations, with white line representing 1:1 correlation. The colour is indicative of the number of observations at that location.

5.2.5 Creation of a synthetic image

Having isolated the surfzone, the creation of a synthetic image requires the segmentation of the surfzone into two categories that identify areas of wave breaking and non-breaking (rip channels). This ultimately creates 4 distinct zones in the image as a whole: beach, rip channels, breaking waves, and offshore. The offshore boundary of the surfzone is the limit of wave breaking which is defined by the first significant increase in the pixel intensity gradient (Bogle et al., 2000). The landward boundary of the surfzone is determine by the shoreline. This is detected using segmentation based on 3-banded k-means clustering (Wang and Adelson, 1994). This method identifies the beach by the dominance of the red pigmentation in the RGB signature. The surfzone must then be separated into rip channels and wave breaking regions. This is done by thresholding the extreme intensity values of the remaining zone (between the detected bar- and shoreline), and using the mid-point as a cut-off to separate into two distinct zones.

The image is now composed of 4 distinct zones (Figure 5.5b). Subsequently, it is important to return the now zoned image into something that visually represents a normal image, so that existing surfzone imaging algorithms can be applied to it. These

algorithms would fail on the segmented image, as a result of the lack of colour and the sharp transitions between zones. In order to return the image to a visually correct state, the outline of the zones are overlaid onto the original image, and the RGB values for each pixel within the various zones are recorded. This allows the creation of a pixel colour historgram that is epresentative of the colours observed in each zone (Figure 5.5c—f). For each zone in turn, it is then possible to reconstruct the dominant colour using the normal distribution of red, green and blue pixels in the histogram. In order to avoid uniform colours for each zone, the algorithm randomly selects a red, green and blue value from the normal distribution, weighted towards the higher probability occurrences on the normal distribution. It is then able to replace all pixels in the zoned map with an appropriate colour, representative of the real image (Figure 5.5g). The final result is that all original pixels are replaced with visually similar, but less noisy synthetic pixel zones.

5.2.6 Minima detection

Minima detection focusses on the area between the shoreline and barline. The pixel intensities in the grayscale version of the original image are first lowpass filtered to remove localised noise (Figure 5.6a).

Energetic wave breaking on the edge of channels creates very high intensity areas. As a result of this, sometimes the area along the bar can appear as a localised intensity minima between these high intensity areas, despite the fact that it is light in colour and does not correspond with a channel. Therefore, the lightest 50 % of pixels are removed (Figure 5.6b). This has the effect of removing areas of wave breaking, and thus the localised minima over bars.

The algorithm then detects minima in 4 directions across the image: gradient is assessed across each of the 8 neighbouring pixels (Figure 5.6c). If the algorithm detects a local minimum in any direction, then the observation is stored, as long as it falls within the thresholded image (Figure 5.6d).

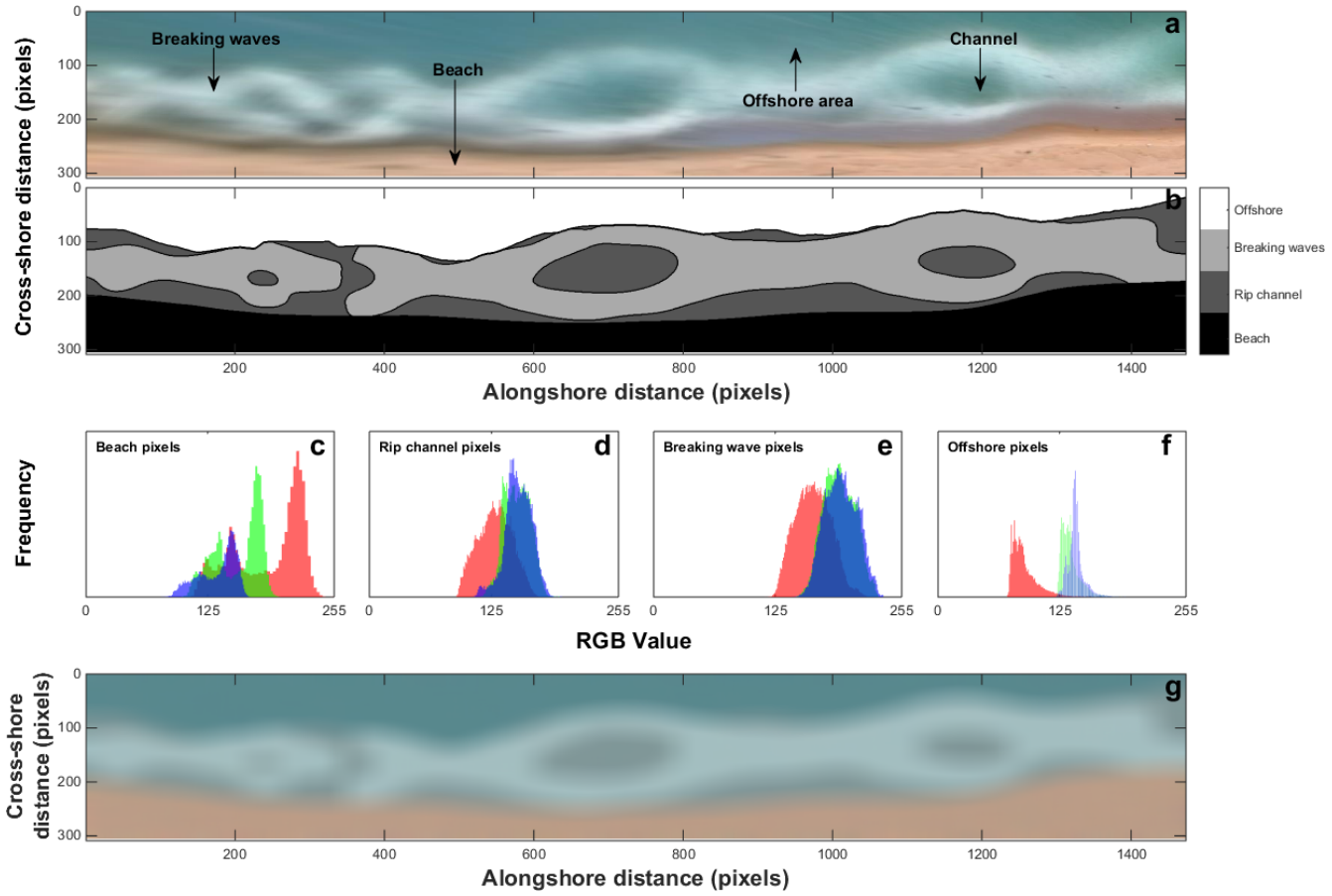

Figure 5.5: (a) An original rectified image from Tairua Beach. (b) The parent image (a) was segmented into the offshore region, the beach, and then within the surfzone into areas of wave breaking, and deeper channeled areas. (c—e) The pixel values from the original image (a) for each zone identified in (b) have been extracted, and presented in terms of their red, green, and blue pixel values. The zones in (b) are then filled with pixels randomly selected from the corresponding pixel value distribution curve in (c—f). The resulting image is the synthetic image, with each zone now exhibiting the dominant colour trend observed in the parent image.

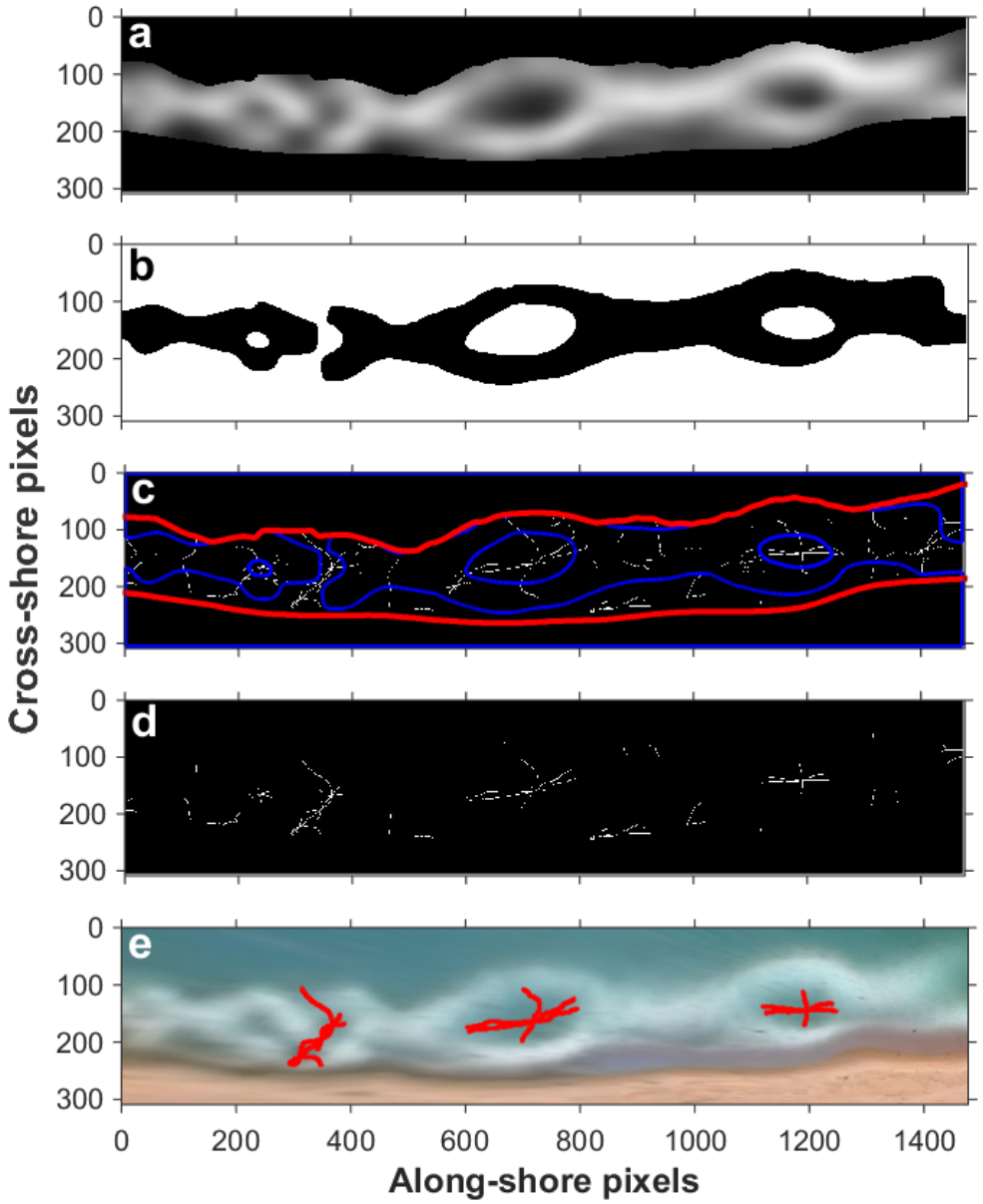

Figure 5.6: (a) The detected barline and shoreline are used to create a masked image, depicting only the surfzone. The image has also been lowpass filtered. (b) The remaining image is thresholded so that areas of wave breaking (black section) can be removed from the search area. (c) Minima are then located in the remaining areas. Red lines depict the shore- and bar-line, with blue lines highlighting the search areas. Detected minima are shown as white lines. (d) This search returns the minima contained within the darker parts of the image. (e) Significant features detected in the algorithm are stored as coherent rip currents (red features).

5.2.7 Rip grouping

Once individual minima have been detected, the algorithm groups observations into coherent features. In order to do this, it segregates the image into a grid, with typical grid sizes being around 2-3 pixels wide, enabling clusters of minima to be grouped into defined features. Neighbouring grid squares that contain minima observations are recorded as the same feature (potentially a rip). The process is repeated until no more distinct features are found. The algorithm then makes an assessment as to whether any of the detected features are significant. To do this, it looks at their along- and cross-shore extent. Features which extend over a cross-shore distance greater than 30 % of the surfzone width at that point are classed as significant. Likewise, features that extend alongshore over a distance greater than twice the width of the surfzone would be saved (Figure 5.6e). The cross-shore threshold was particularly important at Perranporth to remove small features in the intertidal that appeared as a result of the shallow beach slope.

5.2.8 Application of method

The method was first applied to imagery from Tairua Beach, described in Section 3.1. The beach is microtidal with a comparatively steep gradient, which made rip features often appear prominently in the imagery. It also meant the tidal translation over the image was minimal, meaning the same crop area was applicable over the entire tidal cycle. The method was secondly applied to imagery from Perranporth Beach, described fully in Section 3.2. Perranporth is a macrotidal environment, with large tidal translation rates over a large intertidal area. As a result, analysis was confined to images centred around low tide, in the field of view of the camera.

In both cases, the algorithm was applied to the original rectified image and the corresponding synthetic image, created using methods outlined above. The standard against which these detections were applied is an expert digitisation, which were user

digitised images of the rip current, outlining the features the digitiser deemed to be rip channels, and of interest.

5.3 Results

5.3.1 Automation of rip detection

On occasion at Tairua, the rip currents were too subtle for the algorithm to detect them (e.g. Figure 5.7a). In the majority of cases, the algorithm was able to detect the minima related to the rip currents, but there was a bias for over-detection (i.e. far more detected than was desirable), compared to the expert digitisations. For example, Figure 5.7b shows four small distinct features considered of interest by expert digitisations, but in the automated detections on the original image, the algorithm has detected one large alongshore feature on the left, and one smaller feature on the right. This is a result of over-detection of minima in the image, and was a trend echoed throughout the dataset. Qualitatively, the problem is reduced when using synthetic imagery, where detections are reduced and mirror more accurately the expert digitisations. Despite the improvement as a result of synthetic imagery, the majority of detections still required a degree of manual post-processing in order to remove unwanted detections. This was a trend echoed throughout the majority (>70 %) of the dataset, with the automation alone not being sufficient. In the majority of cases, the time required to correct inaccuracies far exceeded the amount of time required to digitise the imagery from scratch.

At Perranporth, the effect of a sweeping tidal zone and shallower beach slope was to obscure the rip channels somewhat. In order to achieve similar results as for Tairua detections, the threshold by which the surfzone is turned to a black and white image (Section 5.2.6) required calibration to a new site. The propensity to over-detect was magnified at Perranporth (Figure 5.8), increasing the amount of manual cleaning required. In the majority of cases, individual rip currents were classified by the algorithm as interconnected along almost the entirety of the alongshore zone in the image. There is

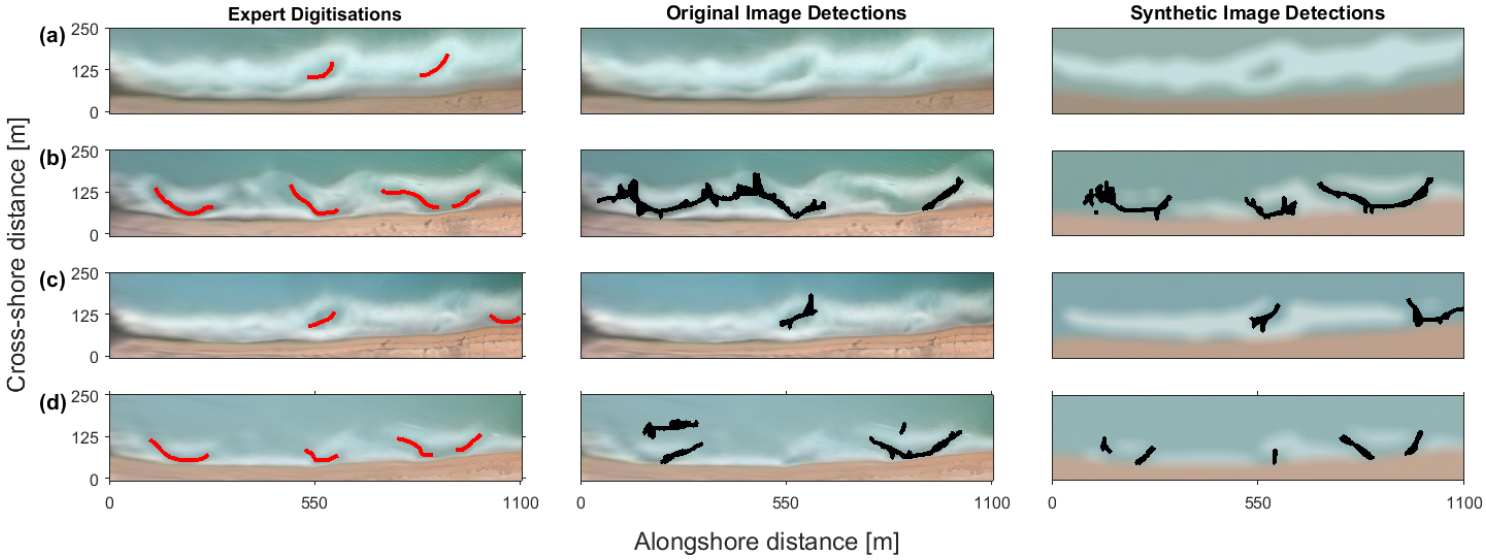

Figure 5.7: Test automated detections from Tairua Beach. The left column shows expert digitisations, and provide the standard against which the automated detections should be judged. The middle column shows detections made on the original imagery. The right column shows detections made on the synthetic imagery. Each row (a—d) shows images from a different time.

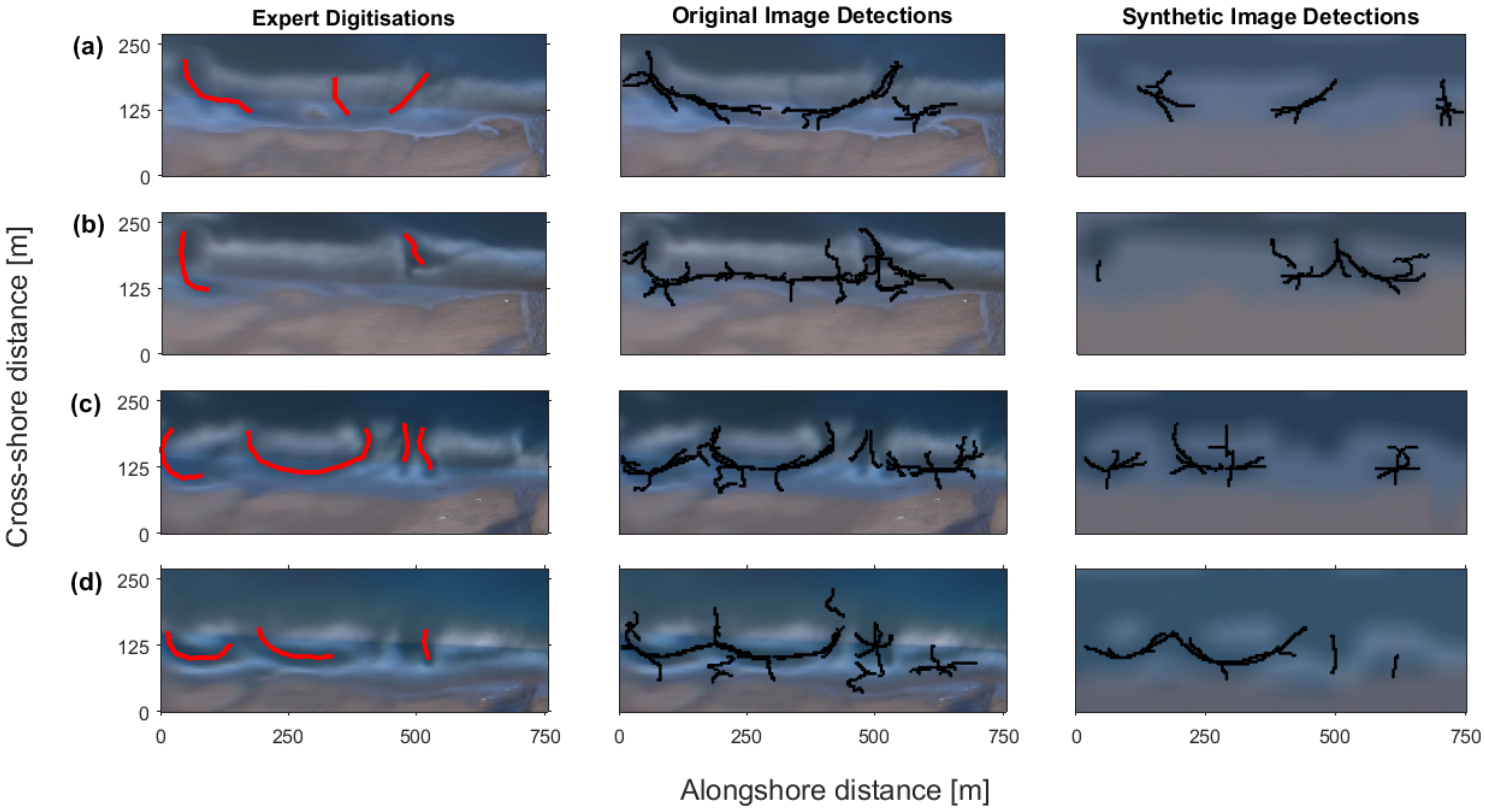

Figure 5.8: Test automated detections from Perranporth Beach. The left column shows expert digitisations, and provide the standard against which the automated detections should be judged. The middle column shows detections made on the original imagery. The right column shows detections made on the synthetic imagery. Each row (a—d) shows images from a different time..

an image seam between two cameras present in Perranporth imagery that may have contributed to this. More important, however, was the shallow nature of the beach that resulted in an unclear definition between dry sand, wet sand, and surfzone. The algorithm became highly sensitive to the detected shorelines and barlines when applied to the Perranporth dataset. The result was an even higher proportion of images in the Perranporth dataset requiring manual post-processing to be of quantitative value.

The selection of thresholds is the dominant factor behind the inability of the method to cope with inter- and intra-site conditions. Despite it being the main factor in the algorithms inability to be deployed at any site, the inclusion of thresholds appears to be a necessary step in the extraction of quantitative data from imagery (Ranasinghe et al., 1999; Alexander and Holman, 2004). One major step forwards would be in the inclusion of some means empirically derive the threshold for a particular site based on a sample set of images, yet this appears to be some way off, not least because of the number of different thresholds currently required to extract quantitative data. One such threshold is the value chosen to isolate darker areas in the surfzone. A sensitivity analysis of this method is presented as Figure 5.9. This thresholding is required as part of the process to avoid detections of localised minimas over areas of wave breaking, when the area actually of interest is localised minima in channels. Figure 5.9 shows an original image and the threshold used at each stage. In the middle column, the threshold is applied to the surfzone (delineated by the bar- and shorelines), to convert the image into black and white areas. Black areas are constructed from areas lighter than the given threshold, and white areas are constructed from areas darker than the threshold, and are therefore the areas of interest. In the middle column, white areas have been made transparent to show the minima detected in those areas. At low thresholds ($\tau \approx 0.3$; Figure 5.9a), the majority of the surfzone is blacked out, even some of the darker channels, meaning the area left for rip detection is minimal. Conversely, at high thresholds ($\tau \approx 0.7$; Figure 5.9e) the majority of the surfzone is included in the analysis, which results in minima detected across areas of wave breaking (e.g. Figure 5.9e [$x = 650$m, $y = 100$m]). Therefore, both the number and extent of rips detected increases with increasing values

of τ, but the ideal threshold changes depending on inter-, and even intra-site variations, such as wave height, tidal range, etc.

5.3.2 Utility of synthetic imagery for rip detection

Analysing the performance of the automated detection method showed that the synthetic imagery performed better than the original imagery. In order to objectively estimate the utility of synthetic imagery for improved methods of automated rip detection, this study applies the rip detection method proposed by Ranasinghe et al. (1999) to both the original rectified imagery, and the corresponding synthetic image. The original image is manually digitized in a similar method to that described by Whyte et al. (2005) as a benchmark to assess the accuracy of the rip detection algorithm. One expert digitiser was used, and this was sufficient based on the errors of such digitisation as documented in Holman et al. (2006). They report that two users digitising rips on average recorded the same number of rips in the imagery per day, but the recorded location of rips was more variable between digitizers. For the purposes of this study, the more consistent rip number parameter is used. The images selected are a random selection of 80 images from the archive.

Both image types produce a statistically significant (at 95 %) correlation in the quantity of rips. Correlation in the original imagery ($R = 0.28, P = 0.013$) is poorer than that in the synthetic detections ($R = 0.47, P = 1.2 \times 10^{-5}$). The correlation in synthetic imagery was statistically significant at 99 %. Correlation alone is not a good measure of agreement; therefore, the error in each method has been presented here.

The user-digitized number of rips in each image varies between 1 and 4 (Figure 5.10). A nominal 'acceptable error' threshold of ± 1 detected rip is plotted onto Figure 5.10. In total, the original imagery produces correct detections 34 % of the time, compared to 41 % in the synthetic imagery. The detections lay inside of the ± 1 error threshold 81 % of the time in the original imagery, compared to 92 % of the time in the synthetic imagery, resulting in total error ($> \pm 1$) in 19 % of the original image detections, and 8 % of the synthetic detections.

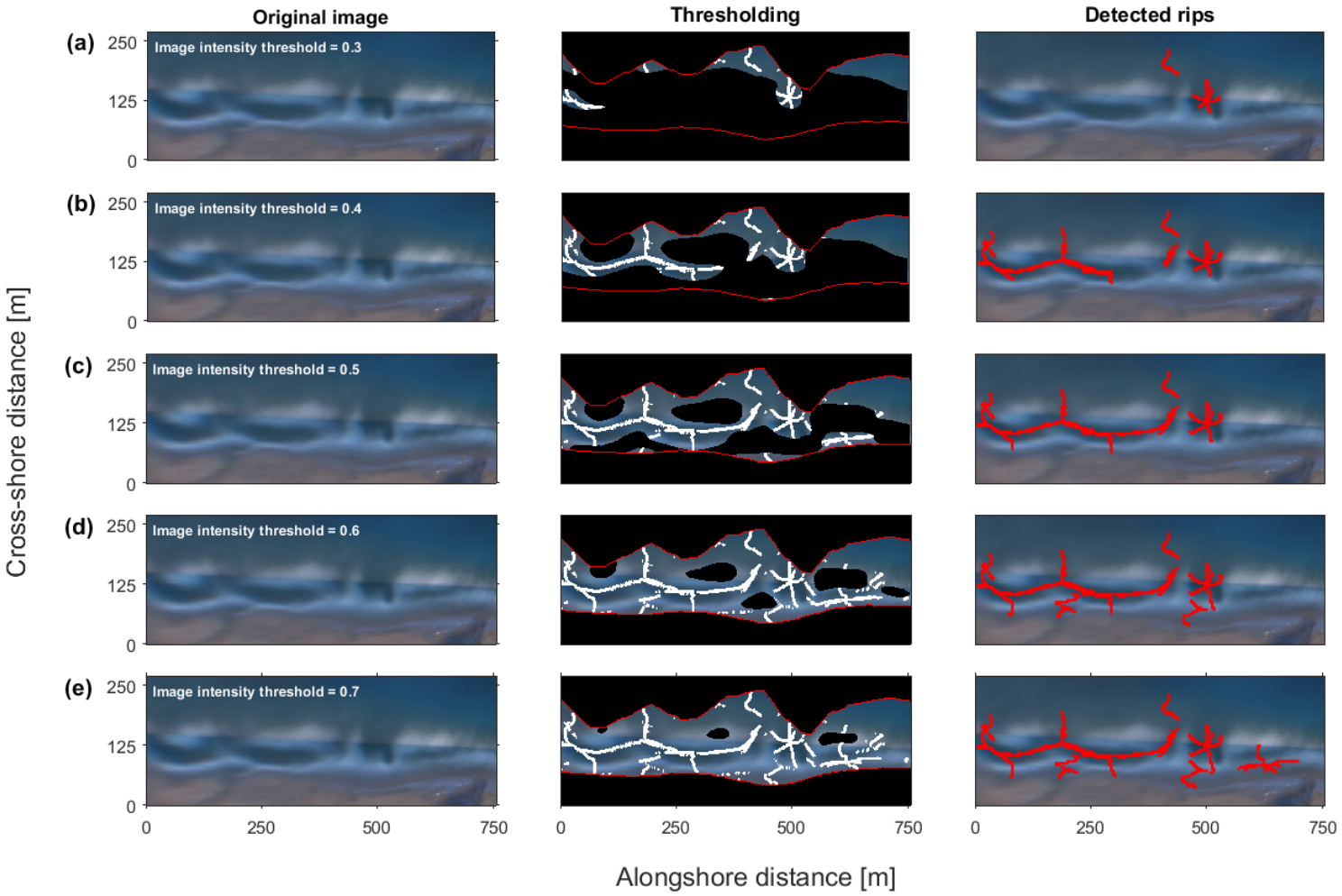

Figure 5.9: Sensitivity analysis of surfzone thresholding intensities. Left column shows the original Perranporth image, and an annotation of the threshold used for subsequent analysis. Middle column shows detected bar and shorelines (red lines), as well as the masking applied after the various intensity thresholds have been applied to the surfzone. White lines are indicative of local minima detected. Right hand column shows the resulting rips detected in the imagery. Each row (a—e) shows an image from a different time.

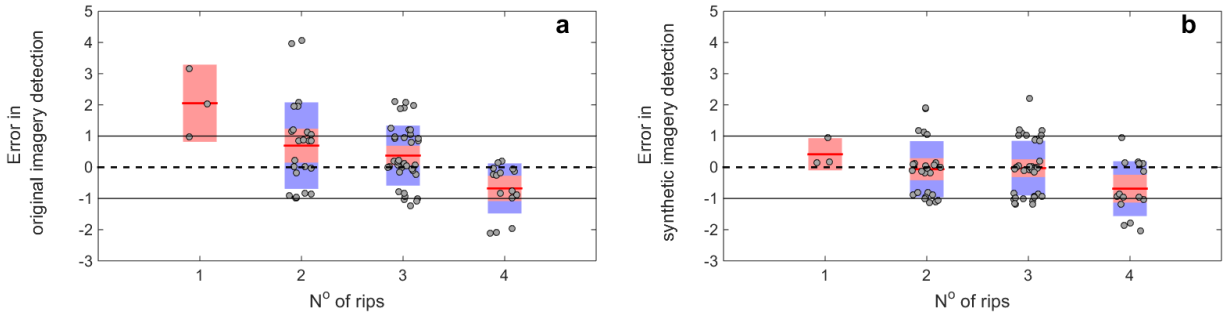

Figure 5.10: The user-digitized number of rips in each image obtained by digitization compared to the error in the number of rips detected in (a) the corresponding original image and (b) synthetic image. Positive and negative numbers represent over- and under-predictions, respectively. Each prediction is represented as a scatter point. The data is binned by the user-digitized number of rips, with the mean (red line), the 1.96 standard error of the mean for each class (red bar), and the standard deviation (blue bar).

Of the detections that were incorrect in the original imagery (66 %), 38 % were under-predictions, compared to 62 % over-predictions. The opposite is true of the synthetic imagery (59 % incorrect), whereby 64 % of erroneous detections were under-predictions and 36 % were over-predictions.

In the original imagery, in all 4 scenarios (1—4 digitized rips), the standard deviations in the detection lie outside of the ±1 error threshold (Figure 5.10a), whereas only one scenario (4 rips) contains standard deviations outside this threshold in the synthetic imagery (Figure 5.10b). Interestingly, both methods produce an under-estimation of comparable magnitude in the 4 rip scenario.

5.4 Discussion

5.4.1 Progress in automated detection

Here, a number of new methods were developed to aid the pursuit of automated detection of rip currents, although this research stopped short of successfully achieving

automation itself. Of particular use was the development of dynamic shore- and barline detection. As part of this new methodology, the shoreline was individually detected in each image by means of k-means clustering. This k-means cluster extracts the beach as an entire feature in the imagery, based on the dominance of red colours in the video imagery. The process provides a good approximation of shoreline position when compared to expert digitisations (Figure 5.4a). This method of shoreline detection appears superior to previous attempts to detect the feature in rip current studies. Ranasinghe et al. (1999) defined a log spiral that matched the average shoreline, and this then became a static shoreline approximation, despite any changes in morphology or tide. A number of studies following the initial Ranasinghe et al. (1999) study were based around manual rip detection and therefore no shoreline detection was applied. More recently, the work of Gallop et al. (2009, 2011) applied a method developed by Smith and Bryan (2007), which relies on the transition of RGB values along a cross-shore transect. This method relies on a subjective user-defined threshold to identify the point at which RGB variance becomes significant, and correlates with the shoreline. Conversely, the use of k-means clustering alleviates any user subjectivity in terms of thresholds. The only aspect that is subjective is the user selection of how many clusters the algorithm should detect. For the purposes of shoreline detection, three was deemed ample as there are specific signatures associated with the beach, wave breaking and offshore regions. Therefore, it is unlikely that there would be a requirement to change this cluster number between differing field sites, and indeed it was applied with equal success at two contrasting sites as part of this study.

In terms of delineating the surfzone, the offshore extent of wave breaking was isolated, which provided a good estimate of the surfzone. This was achieved by monitoring a change in pixel intensity over cross-shore transects. Here, a threshold in intensity was identified above which all offshore noise was ignored. The effect of this is that the detected barline is positioned further offshore than in previous studies. For example, in the studies of Ranasinghe et al. (1999) and Gallop et al. (2009, 2011), the barline was delineated by the intensity maxima, which is the position of most intense wave breaking. Although their method is robust, objective and repeatable, it has the effect of onshore

displacement of the edge of the surfzone. This is demonstrated well by Figure 5.3a, whereby the cross-shore detected barline is located at ≈ 80 pixels, whereas the intensity maxima is located at ≈ 140 pixels, representing a real-world cross-shore displacement of ≈ 40 m, or roughly 20 % of the surfzone excluded from further analysis. Despite the use of a subjective threshold in order to achieve this greater coverage, the same threshold (intensity > 0.2) appeared to apply equally well to both sites. More robust sensitivity analysis of this threshold is required in the future, taking into account more study sites and a wider range of conditions.

Before attempting minima detection for rip channel position, the surfzone is first thresholded into a binary image. This approach has not been used before, but proved extremely useful as a quick and easy way of isolating regions not of interest to a rip channel study, namely, areas of wave breaking. Although the threshold selection here was important (Figure 5.9), it was relatively easy to calibrate for each of the individual sites. The time taken to perform a calibration is minimal in contrast to time needed to manually clean data from areas of wave breaking. For the first time, this study has considered the detection of intensity minima in all image directions. In order to achieve this, profiles are made between individual pixels and all eight neighbouring pixels, which gives complete coverage across the surfzone, and ensures the channels will be detected irrespective of their orientation relative to the shoreline. Hitherto, minima have either been detected on alongshore orientated transects (Ranasinghe et al., 1999), or both along- and cross-shore orientated transects by Gallop et al. (2009, 2011). The multidirectional approach employed here maximises the amount of information about the rip channels that can be extracted through pixel intensity minima, as it detects information on feeder channels and any rips at oblique angles to the shoreline.

Finally, this study introduced the concept of a rip length to surfzone width ratio. This proved useful in excluding features not considered of interest. Although this is another parameter that was found to be largely site specific, the ratio proved most worth at the shallow gradient Perranporth, where there were many features extending offshore for a small portion ($< 30\%$) of the surfzone, that were not rip currents. The inclusion of this threshold provided easy, automated removal of small scale features. It is worthy of note

that at the steeper, microtidal Tairua Beach, most rip channels were found to extend for in excess of 75 % of the surfzone width.

5.4.2 Value of filtering and synthetic imagery

It was found that simple image filtering is effective in reducing small-scale fouling and noise in imagery. Previously, the signal extracted from the raw image would generally be filtered, as opposed to filtering the image first. This is important as the extracted signal through a set of pixels is generally 1-directional and does not take account of neighbouring pixels and trends. The filtering of an image, rather than extracted signal, uses 2-dimensional filters and local pixel statistics to remove noise (Lee, 1980). This filtered image is then ready for quantitative analysis, or here, the creation of a synthetic image. The use of synthetic imagery as opposed to original images improves rip detection using the method outlined by Ranasinghe et al. (1999). The total error in detections with synthetics is halved when compared to original imagery.

The reported limitations of the Ranasinghe et al. (1999) method (Holman et al., 2006; Turner et al., 2007) were clear in the results, as detections on both the original and synthetic images produced considerable scatter. This is likely the result of the complex rip channel morphologies at Tairua, where rips orientated shore-normally are a minority occurrence. That said, there are significantly fewer rips detected in the synthetic imagery ($n = 203$), compared to the original imagery ($n = 242$), which infers that the synthetic images provide a dataset with much less unrelated extraneous noise.

The method used for rip detection oversimplifies the morphology qualitatively observed in the imagery, and therefore, it is expected that any results obtained via this method would under predict the occurrence of rip channels. Despite the oversimplification inherent in the method, detections based on the original imagery still produces over-estimation of rip number 41 % of the time, which is perhaps indicative of the amount of noise the original image contains. In comparison, the synthetic imagery produces under-estimation (as would be expected using this method) on 38 % of detections.

The work of Bogle et al. (2000) used the same approach as Ranasinghe et al. (1999) on Tairua, but ultimately resorted to visual selection of intensity minima. This is presumably because the complex patterns observed in imagery made automation via the use of thresholds (such as in the approach using original imagery outlined here) unviable. The use of a simplified synthetic-type image may aid steps towards an automated approach to rip detection. For the same study site, the simplification of the imagery via the creation of a synthetic images increases the number of correct detections, and also the number of predictions correct to within $\pm$ 1 rip. This new intermediate step may help overcome the documented limitations of current attempts to automatically detect rip channels in imagery.

5.4.3 Thresholding imagery

In the process of constructing synthetic imagery, thresholding of the surfzone was able to supply information about the shape of rip channels. It is widely reported that areas of wave breaking appear as white bands of high pixel intensity (Lippmann and Holman, 1989), and that rip channels appear as darker regions (Ranasinghe et al., 1999). This is a result of waves breaking over raised areas such as bars, and areas of no wave breaking indicative of deeper areas, such as channels. It became apparent that when the rip channel was manually isolated in the image (Figure 5.11a), and then thresholded into a binary image (Figure 5.11b), that this preferential breaking over shallower areas could give information about the shape of the rip channel.

Such information (shape) is very rarely reported in the literature. Most previous studies describe rips in terms of their spacing (Holman et al., 2006), persistence and mobility (Turner et al., 2007), or more generally, by their generation mechanism (Castelle et al., 2016b). Each of these descriptors offers little information about the way the rip current itself is behaving at any given time (i.e. surfzone exits or surfzone retention). If we assume that the areas of wave breaking around a rip channel act as a boundary to the rip current itself, then the variations in patterns of wave breaking could effect the flow patterns within. Such knowledge is commonplace within the field of fluid physics,

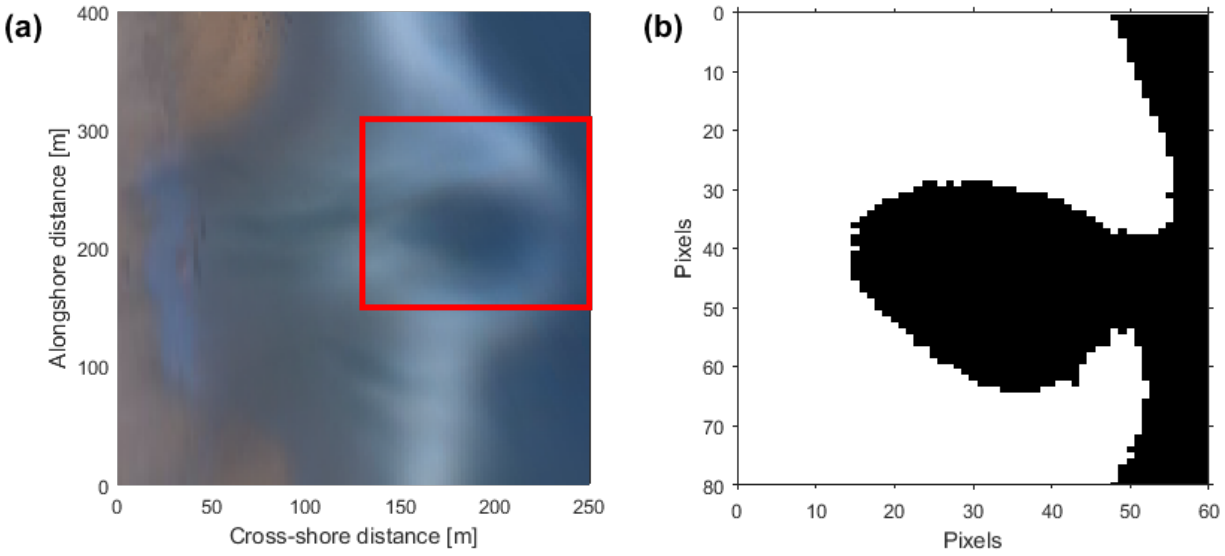

Figure 5.11: Adaptation of the process used to create a synthetic image. (a) The original, rectified image, with a rip channel of interest manually selected (red box). (b) After thresholding, information about the pattern of wave breaking is evident, with white areas indicative of wave breaking and black areas indicative of the offshore or rip channel.

whereby flows experiencing constriction exhibit increased shear stresses, flow separation, and varying velocities (Chow and Soda, 1972). This may have an important effect on rip channel velocities, vorticity, and exit rate. The concept of rip channel shape, detected through patterns of wave breaking, will be explored further in Chapter 6.

5.5 Conclusions

This study has successfully defined a new objective method of detecting shorelines in video imagery that was equally applicable at two contrasting sites. Further work should be conducted on the viability of k-means clustering as a means to detect shorelines on a range of study sites worldwide, as it could be useful in replacing subjective methods that necessitate the use of user-derived thresholds. Furthermore, in the pursuit of automated rip channel detection, a new means of detecting the edge of the surfzone has been proposed, which increased the detected surfzone width by 20 % in some cases. The

method relies on the selection of a threshold and therefore needs more experimentation to ascertain the sensitivity of this threshold on sites beyond the two to which it was applied here. Also useful in the pursuit of automated rip detection are the inclusion of a rip current length:surfzone width parameter, which has the effect of removing small features that would not be considered of interest. This was most applicable at a site with shallower beach gradient and a large swash zone. Equally, the thresholding of the surfzone into a binary image proved useful in narrowing the search area to only the darkest areas of the surfzone, associated with rip channels.

This research investigated the effect of image manipulation, in the form of image filtering and synthetic image creation, on automated rip channel detection in surfzone imagery. Simple filtering methods were able to reduce the effects of small scale fouling and noise on image intensity signals. The use of synthetic imagery increased rip detections within the acceptable error threshold from 81 % correct to 92 %. Rip channel detection using synthetic imagery reduced the total number of detections by 16 %, showing a reduction of extraneous noise inherent with the original image. A systematic underprediction was observed in the detection of rips using synthetic imagery, which is consistent with the detection method selected. This paper provides proof of concept for image manipulation prior to processing, in order to aid automated surfzone feature detection.

Finally, it was discovered that the thresholding of imagery containing rip channels is a useful means of providing information about rip channel shape. This information is an inferred morphology, as it relies on patterns of wave breaking and areas of no breaking. It is postulated here that rip channel shape may exert some control on the dynamics of the rip current itself; a concept that will be explored further in Chapter 6 and tested in Chapter 7.

Chapter 6

Classification of rip channel morphologies

6.1 Introduction

Coastal classification schemes are an important means of communicating vast amounts of information about a phenomena or site succinctly. It is particularly important that any classification scheme can be applied in an objective manner. For this reason, classification schemes should ideally be based upon objective parameters, rather than subjective observation. Video imagery allows for the quantification of numerous beach (e.g. shoreline), surfzone (e.g. width) and inner-shelf parameters, through pixel intensity values in just one image.

A brief summary of past literature dealing with this topic was presented in Section 2.2. This section concluded that much work has been done on morphodynamic beach state classification (Wright and Short, 1984; Masselink and Short, 1993), but comparatively little work has focussed on the classification of rip currents. Some approaches have used terms such as open-coast or embayed rip currents (McCarroll et al., 2014; Scott et al., 2014), fixed or transient (Vos, 1976; Johnson and Pattiaratchi, 2004), or accretive and

erosive (Short, 1979, 1985). A recent scheme proposed by Castelle et al. (2016b) classified rips based on their primary forcing mechanisms. All these schemes confer different information about the channel behaviour (such as infilling, or widening), but none of them have been able to quantify the change in hazard of a particular rip over time. Rip channel circulation is of critical importance in determining this hazard (Section 2.4), and therefore should form a keystone of any classification scheme. The discussion in Section 5.4.3 introduced the likely control of morphological shape on circulation, therefore, it is possible that quantifying the plan view form of a rip channel could provide information on rip current circulation, and therefore, hazard.

The overall objective of this chapter is to develop a classification of rip channel morphology based on wave breaking patterns using the macrotidal, intermediate, low tide bar/rip beach at Perranporth as a case study. To this end, the sub-objectives are: (1) To investigate the utility of synoptic typing to ascertain differences in wave breaking patterns derived from video imagery; (2) To identify the range of wave breaking patterns observable in video imagery; (3) To examine the degree to which hydrodynamic parameters control the observed patterns of wave breaking; and (4) To establish the controls on temporal change in wave breaking patterns.

6.2 Methodology

In order to assess pattern similarity between images, this study uses an adapted Kirchofer (1974) method of synoptic typing. Synoptic typing identifies statistically similar environmental variables (Hemer et al., 2008). It was originally developed to compare meteorological phenomena, such as the change in 500 millibar isoline patterns over Europe (Kirchofer, 1974), and has since been used to investigate airborne pollutants (McGregor and Bamzelis, 1995), cloud cover (Barry et al., 1981) and wave characteristics (Hemer et al., 2008). To the author's knowledge, the method has not previously been applied to coastal processes or video imagery.

Here, the method is applied to assess the visual similarity of rip channel morphology, as expressed through wave breaking in timex images. Timex imagery is an appropriate means of measuring persistent processes such as wave breaking (Lippmann and Holman, 1989). The effect of continuous wave breaking in an area over the sample period is the creation of a high intensity return in video imagery pixel intensity (Holman and Stanley, 2007). The interspersed rip channels are deeper and do not generally induce wave breaking, appearing in the resultant image as darker areas (Ranasinghe et al., 1999). The resultant rectified image provides a good spatial map of wave breaking patterns, making it an appropriate data source for synoptic typing. For the application of this methodology, imagery from Perranporth (Section 3.2) is used. Here, a Kirchofer sum-of-squares technique(Kirchofer, 1974; Yarnal, 1992) adapted by Hemer et al. (2008) is applied to categorise rip imagery. The original Kirchofer (1974) method was successful in quantifying overall similarity in grids, however, it was unable to differentiate significant sub-grid level differences (Blair, 1998). The Hemer et al. (2008) method accounts for this by assigning a similarity rating for each row and each column within the grid, and checking that it passes a given threshold.

In order to implement this method, rip channels were first manually selected in imagery using a simple Matlab Graphical User Interface (GUI). The user first selects a rip channel, and the algorithm automatically selects the nearest pixel intensity minima, as a proxy for the mid-channel location. The user is then presented with a preview of a grid, showing an image centred on this minima location. The user then assesses if the grid image accurately and sufficiently represents the rip channel, and can choose to save this image to the database, attempt to recentre the image on a new location, or disregard the image entirely. For the Kirchofer analysis to work, the grids must all be the same size, thus selection of grid size is important. There is a trade-off between being large enough to encapsulate the rip channel, but not so large as to encroach on the edge of the image (as the algorithm relies on the rip current being centralised in the grid), nor encapsulating too much of the subaerial beach (as the algorithm could interpret the darker intensities of the sand as rip channel). Here, a grid size of 120 $\times$ 120 pixels was selected, which represents a 120 $\times$ 120 m^2 area of the beach/nearshore at Perranporth.

The selection of grid size was based on typical rip channel length scales. Rip channel length is a function of surfzone width, and generally appears to be on the order of 100 m, with widths on the order of 30 m. The important aspect to capture in the image was the offshore extent of the rip channel, which was certainly achievable with a grid size such as this. Each new image in the database is transformed into grayscale form, and normalised between 0 and 1 so that features in different images are comparable, regardless of the lighting conditions during image capture. With regard to rip channels, the orientation of the rip channel in respect of the shoreline is an important differentiating factor (i.e. the absolute angle of the rip channel is important, not whether it is orientated towards or away from the incident wave field). Therefore, each image is duplicated and mirrored in the alongshore direction, so that rips of the same absolute orientation relative to shore normal were considered similar. There are a total of 1873 original images (3746 including mirrored images), however, when an image is selected by the Kirchofer method, the corresponding mirrored/original image is removed from the dataset, such that only a total of 1873 images are analysed.

The analysis then looks to assign a Kirchofer score of similarity, S, to each possible pairing of image grids within the database (Figure 6.1), calculated as follows;

$$S = \sum_{i-1}^{n} (Z_{ai} - Z_{bi})^2 \tag{6.1}$$

where a and b are the two grids, Z_{ai} is the normalised intensity of pixel i in grid a, Z_{bi} is the normalised intensity of pixel i in grid b and n is the number of pixels in each image. Hemer et al. (2008) discuss that a low value of S may be achieved, indicating overall statistical similarity, by two grids with prominent sub-grid level differences. In order to ensure sub-grid similarity, they propose the resolution of subscore values based on each row and column of the grid as a key part of the process. Additionally, a measure of offshore connectivity in the image is included, which ensures that rip channels must span comparable cross-shore extents to be considered similar. Grids are therefore considered

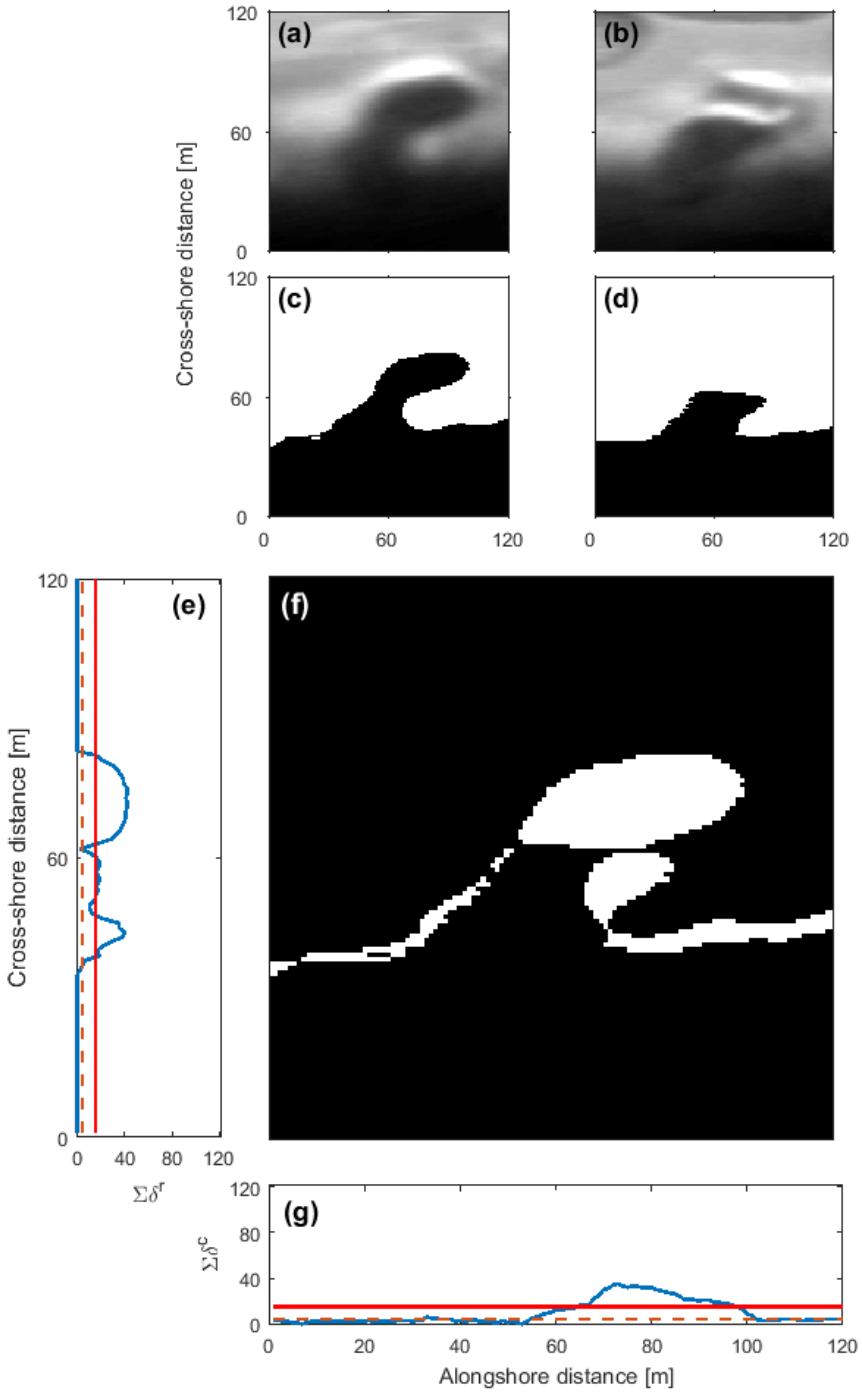

Figure 6.1: The original grayscale images (a and b), and the corresponding black and white images (c and d). These are two images that the Kirchofer analysis deems similar. The overall difference (S) is shown with black indicative of areas that are the same and white indicative of difference (f). Row scores (SR) and column scores (SC) are shown as a blue line (e and g, respectively), the solid red line indicates the median score threshold applied here, and the dashed orange line shows the scores achieved.

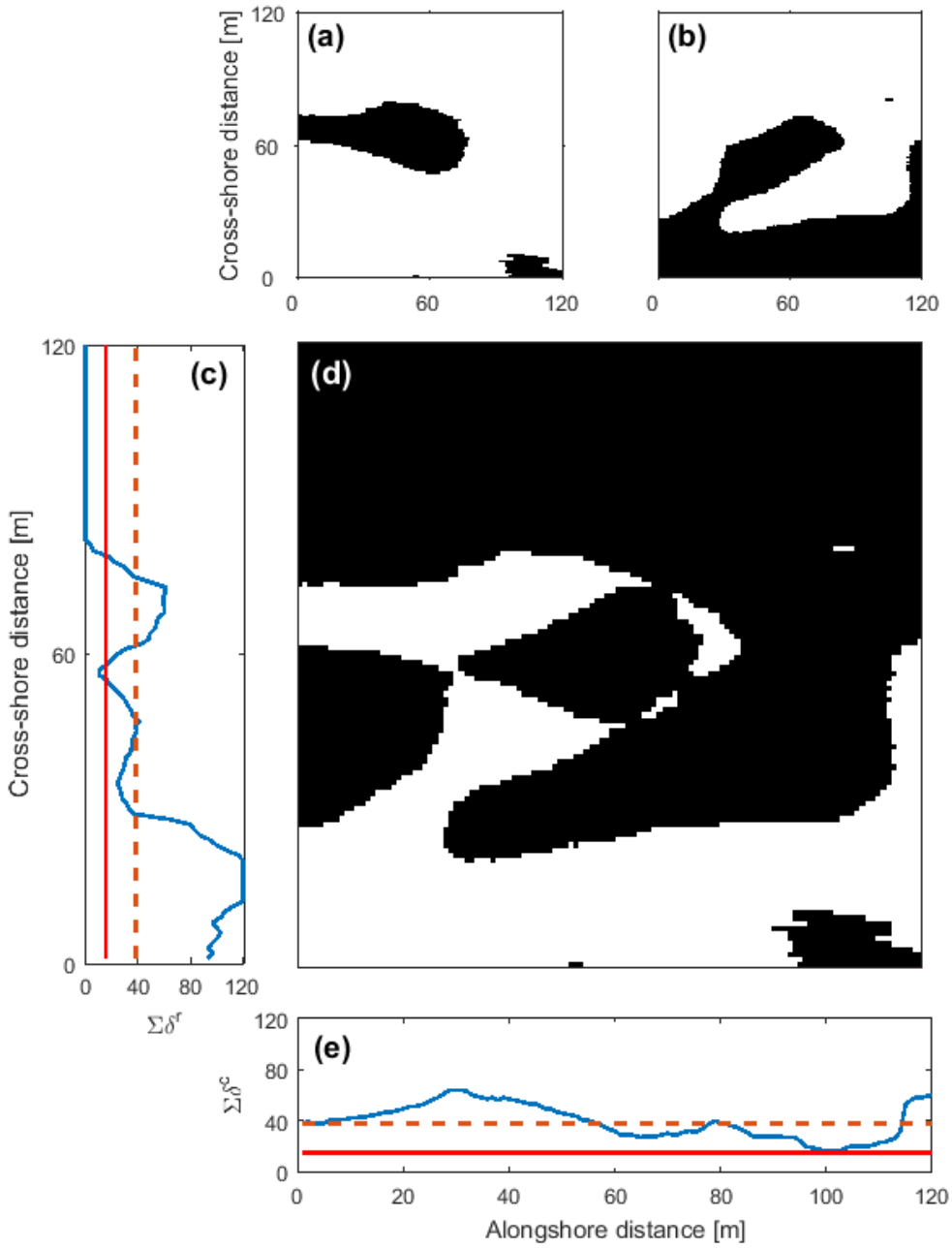

Figure 6.2: Two rip channels extracted from the dataset (a and b) that the Kirchofer analysis deems different. (d) The overall difference (S) is shown with black indicative of areas that are the same and white indicative of difference. (c) Row scores (SR) and (e) column scores (SC) are shown as a blue line, the solid red line indicates the median score threshold applied here, and the dashed orange line shows the scores achieved.

similar (Figure 6.1) when $S < 2000$, $(S_{R_50} + S_{C_50}) < 30$, and $SE < 20$, where S_{R_50} and S_{C_50} are the median Kirchofer scores for rows and columns in the grid, respectively and SE is a measure of the difference in cross-shore extent between two images. Images are considered different (Figure 6.2) if any of the scores exceed the given threshold. Scores are determined for each pair of images in the database and a cross-reference table populated with binary values indicating whether or not a pairing is considered similar or not. The individual grid that has the most matches is then designated as a 'keygrid' (Hemer et al., 2008). The keygrid and its matching grids are then stored separately, after which it is deleted from the cross-reference table, along with all the grids with which it was paired. The analysis is repeated, with more keygrids and groups being identified, until all grids in the sample are classified into m groups of five grids or more. Any groupings left at the end of analysis that have less than 5 similar grids are termed unclassified.

6.3 Results

6.3.1 Synoptic typing

Synoptic typing reveals that 91 % of the variance in the image archive can be explained by four distinct rip channel configurations (Figure 6.3), with 70 % of the overall variance explained by only two types. *Type A* is a wide, shore-normal channel with an open connection to the offshore through the sand bar (Table 6.1). The channel is typically around 40 m in length and width, and is typical of 38 % of the dataset (718 images). *Type B* is an isolated 'hole-like' region, whereby wave breaking totally encompasses the offshore perimeter of the channel, meaning there is no connection to the offshore. The hole typically has a diameter of 20 m (Table 6.1). Type B makes up 32 % of the dataset (602 images). After the first two main types of channel (Type A and B), the percentage of the dataset to which each keygrid applies reduces by half into Type C and half again into Type D. *Type C* is another hole-like region, totally encompassed by wave breaking, but a significant difference is the proximity of the channel to the offshore region, which

has now reduced from >50 m in Type B to nearer 30 m here (Table 6.1). This may be indicative of a transition phase between an isolated hole and a channel with an open connection to the offshore, and the size of the hole has not altered between Type B and C. This type of channel accounts for 14 % of the variation in the dataset (264 images). *Type D* is similar to Type A, in that it shows an open connection to the offshore. However, Type D displays a much reduced channel width (20m), and is no longer shore-normal in orientation (Table 6.1). This type of channel can explain 7 % of the variance in the data (139 images). The four dominant types and a selection of images classified as similar are presented as Figure 6.4. Images similar to Type A channels show a degree of variability, but are all characterised by a large mass of black (channel) area extending towards the top (inshore) of the image, with a wide open connection to the offshore (Figure 6.4a). The defining characteristic of images similar to Type B channels is the isolation in which the rip channel exists, with only small amounts of offshore zone visible, if at all (Figure 6.4b). This is in contrast to the images presented as similar to Type C channels, whereby despite still being closed, they appear in much closer proximity to the offshore, with a solid black layer visible in the bottom of each (Figure 6.4c). Type D channels vary considerably, but are all characterised by a channel that extends at oblique angles inshore. In some cases this channel has a connection to feeder channels, evident as shore-parallel dark areas in the imagery (Figure 6.4d). The length and width scales quoted here are specific to Perranporth, but do broadly compare with rips observed at other sites.

These four distinct types of channel can also be categorised broadly based on their connection to the offshore. Types A and D can both be considered open in terms of this offshore connectivity, and Types B and C can both be considered as closed. Categorising this connectivity to the offshore is important because the influence of wave breaking across the channel in closed conditions is likely to influence the circulation of the offshore directed rip current as it interacts with the band of wave breaking.

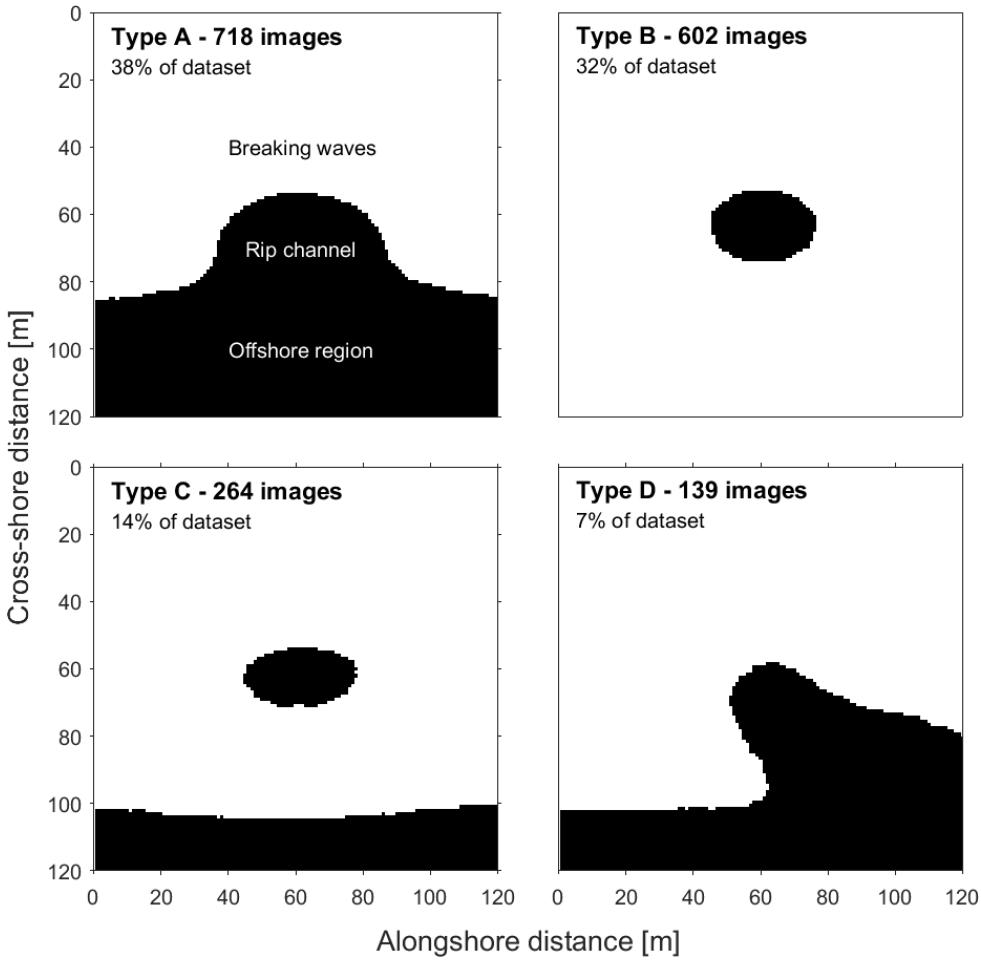

Figure 6.3: The four dominant rip channel configurations at Perranporth, classified using synoptic typing. Black is indicative of rip channels and the offshore region, white depicts wave breaking over sand bars or subaerial beach.

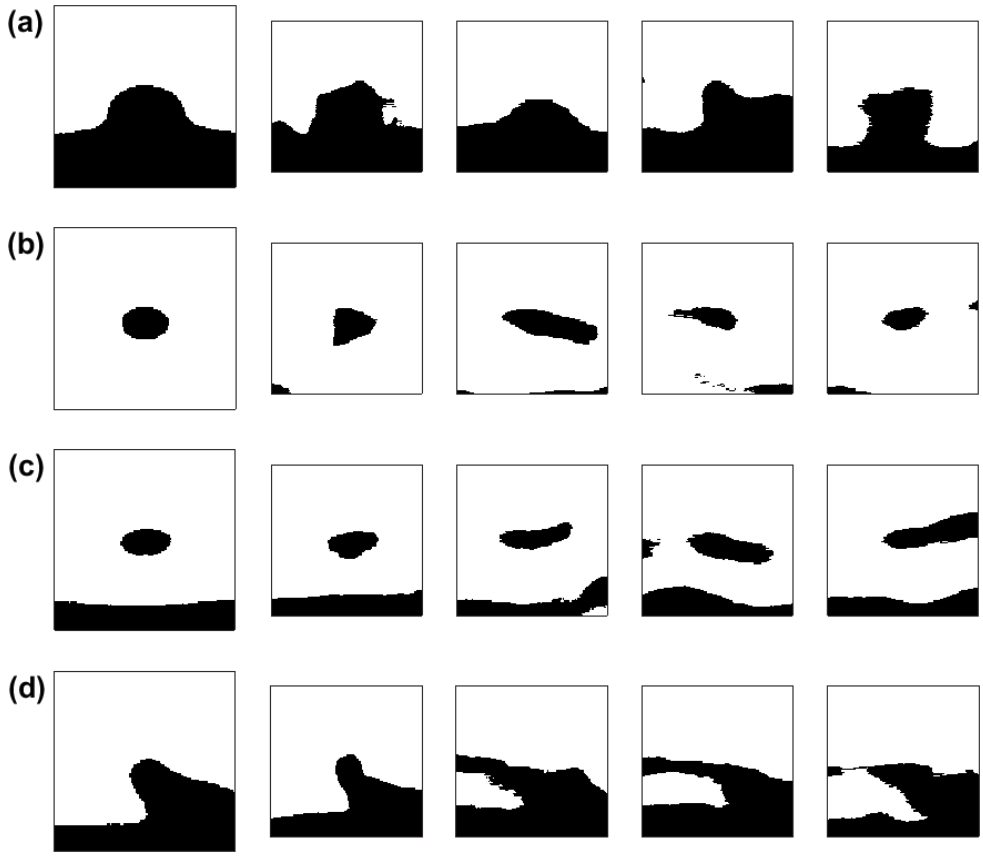

Figure 6.4: The four dominant rip channel keygrids (a—d) at Perranporth, and a selection of imagery from the database considered to be similar to the keygrids.

6.3.2 Hydrodynamic controls

Scott et al. (2014) identified hydrodynamic controls on rip circulation through the use of wave and tide factors, discussed in Section 2.3.3. Following this method, the output imagery from the synoptic typing was plotted as a function of wave ($H_sT_p/\overline{H_sT_p}$) and tide ($LW - \overline{LW}$) factors, where LW refers to low water and the overline refers to the long term (multi-year) mean values. In order to achieve this, all imagery that fell within the requisite categories (Figure 6.5) was averaged and thresholded ($\tau = 0.5$, where τ represents the normalised intensity cut-off), to produce one image representative of each class. Here, a hydrodynamic trend was far more apparent (Figure 6.5). Under higher

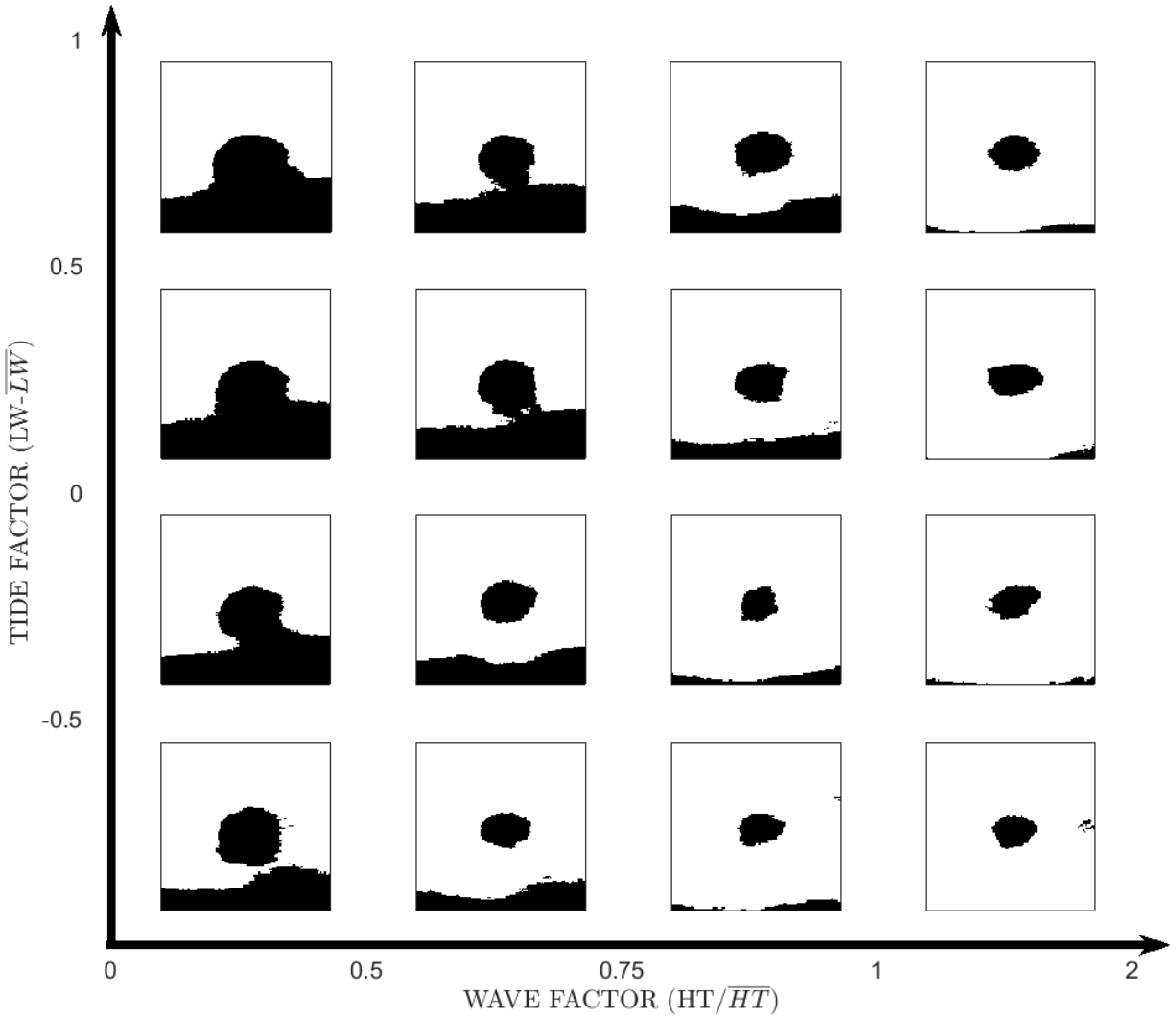

Figure 6.5: A compartmentalisation of the dataset based on wave and tide factors. All images within the requisite wave and tide conditions have been averaged, and then thresholded to form a black and white representation.

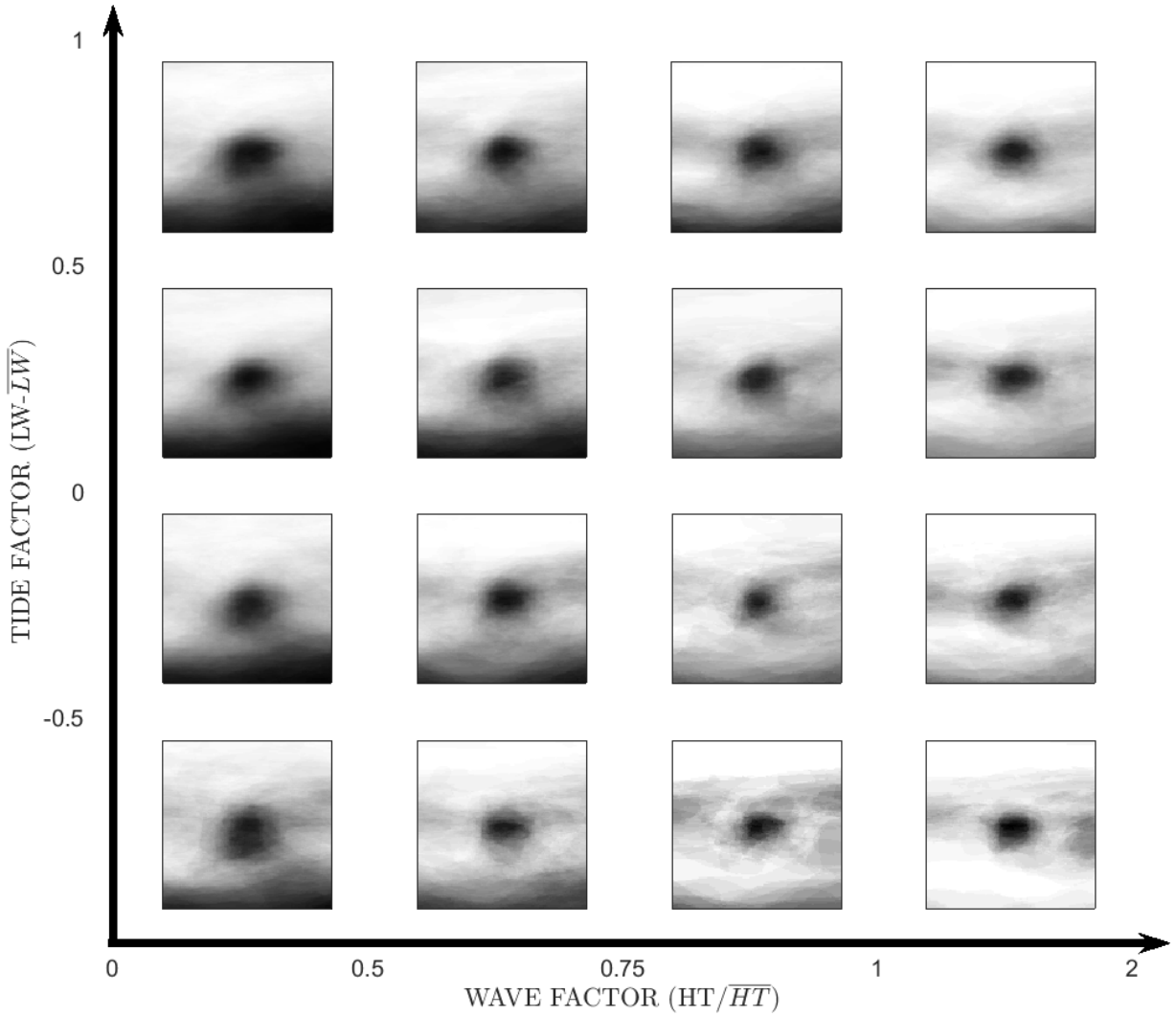

Figure 6.6: A compartmentalisation of the dataset based on wave and tide factors. Here, all variation from the averaging process was presented to reconstruct exemplar greyscale imagery.

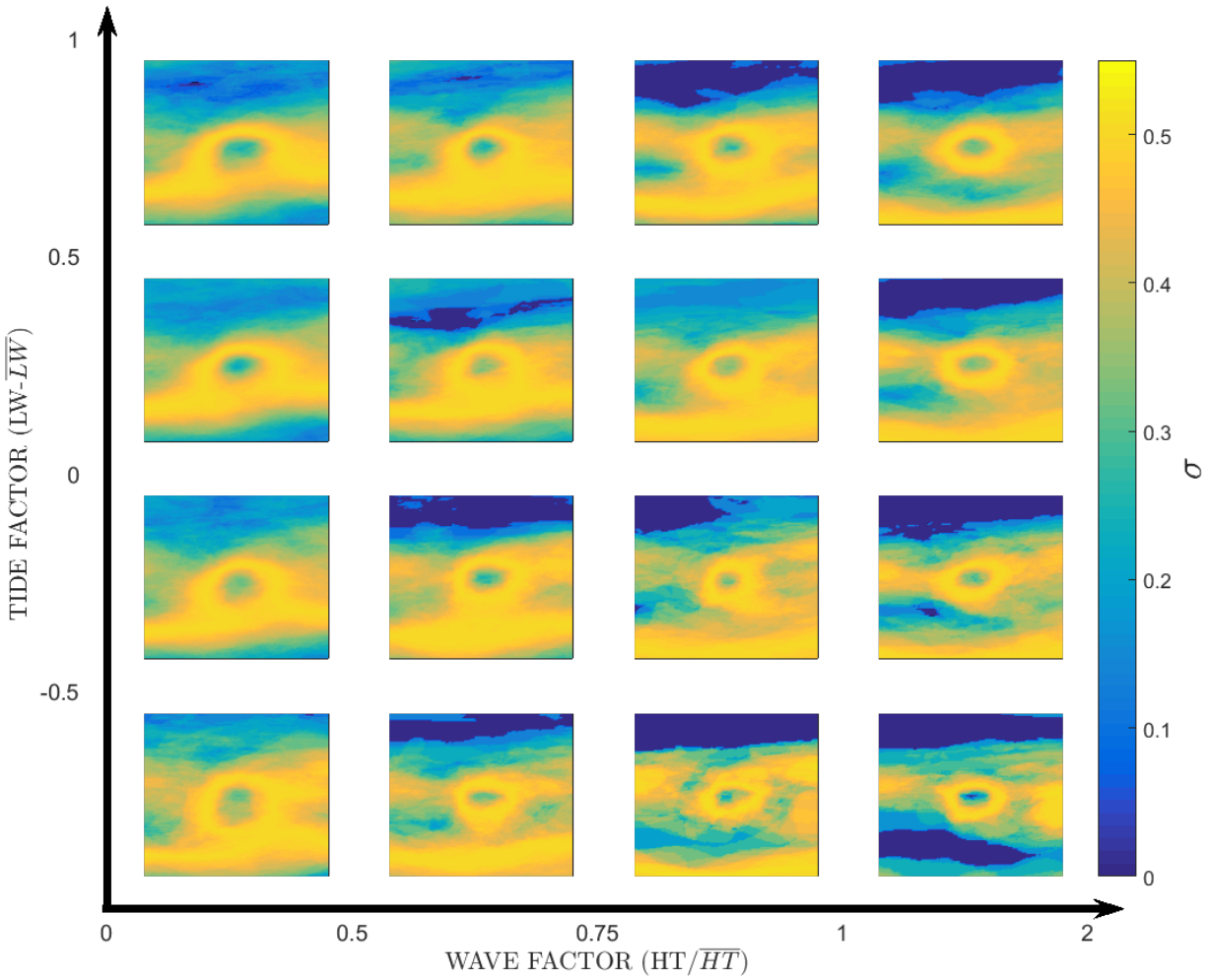

Figure 6.7: Standard deviations (σ) in compartmentalised imagery.

Table 6.1: Summary of characteristics for each of the four dominant morphology types identified at Perranporth after synoptic typing. Distance to the offshore is only relevant in closed channels, and refers to the width of the wave breaking band separating the rip channel from the edge of the surfzone.

Synoptic type	Offshore connectivity	Shape	Distance to offshore [m]	Length (cross-shore) [m]	Width (alongshore) [m]
Type A	Open	Bell	N/A	40	40
Type B	Closed	Oval	>50	20	20
Type C	Closed	Oval	<30	20	20
Type D	Open	Linear	N/A	40	20

tide and lower wave conditions (top left of plot), there is a dominance of open-type rip channels, with a connection to the offshore. Under lower tidal conditions and higher waves, the rip channel was much more likely to present as an isolated hole, i.e., a closed channel. Figure 6.5 also illustrates the transition between the two dominant types, with various conditions under which the isolated hole is seen to be in the process of connecting with the offshore.

It is possible to reconstruct an exemplar greyscale image for each of the 16 wave/tide classes using the averaged data, without the application of a threshold, which gives slightly more information about each of the 16 conditions (Figure 6.6). The effect of the greyscale imagery is to better represent the degree of connectivity each channel shares with the offshore. However, when the imagery is presented as a function of the standard deviation of each pixel location in all images (Figure 6.7), for the majority of outputs there is a high degree of variability ($\sigma > 0.4$). This acts to blur the interesting trends evident in Figure 6.5. Thus, the inclusion of all images in each discrete wave/tide factor bracket is inappropriate as a means to assess the dominant trends. Therefore, this thesis re-applies the synoptic typing method, this time to each sub-group (wave/tide factor bracket) in order to elicit the dominant wave breaking patterns.

The standard deviation was calculated on a subset of synoptically typed data within the wave/tide brackets (Figure 6.8). This significantly reduced the standard deviations

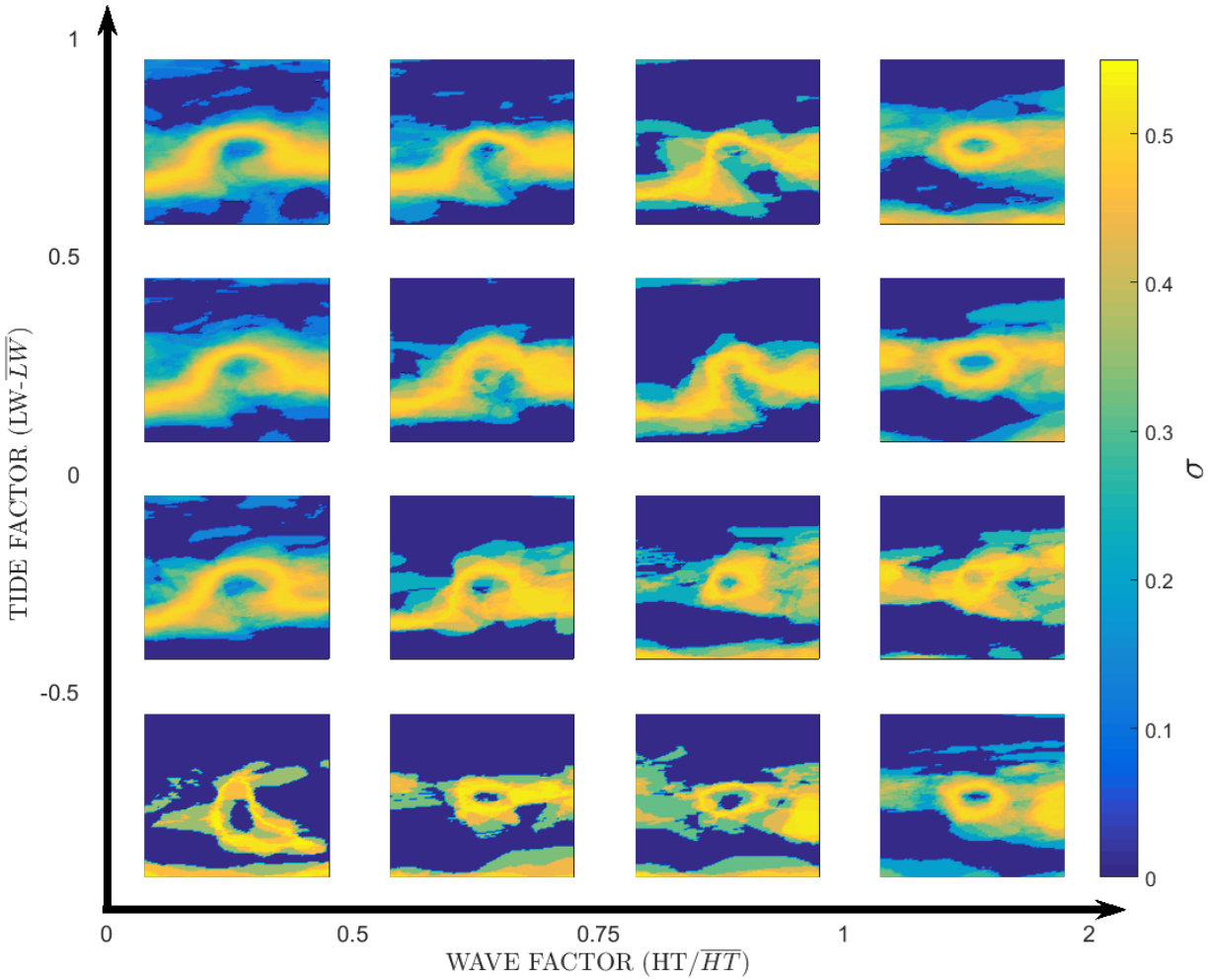

Figure 6.8: Standard deviations (σ) in the top Kirchofer group for each wave/tide threshold.

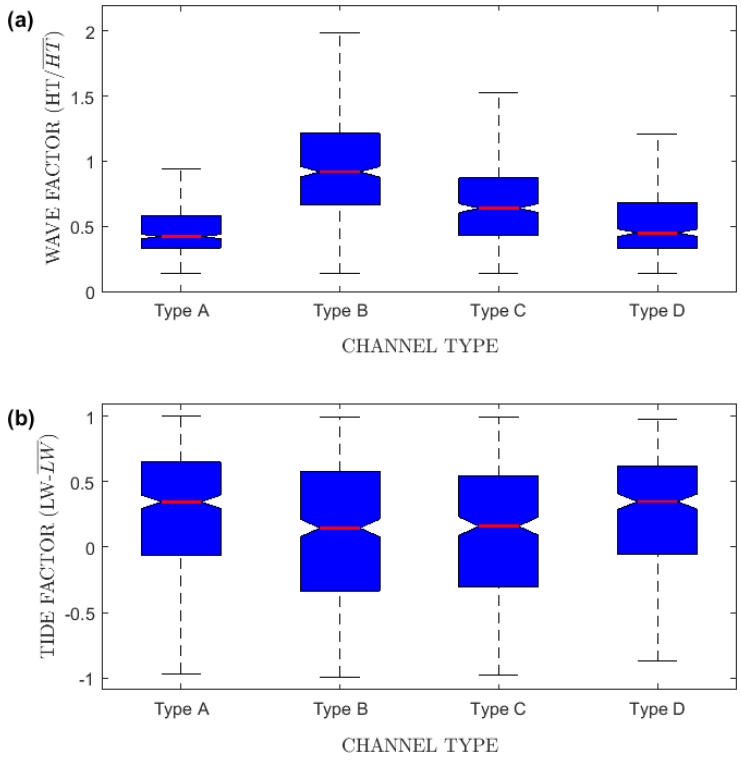

Figure 6.9: Distribution of (a) wave factor and (b) tide factor data points for each of the four synoptic channel types. Red bars are indicative of median values, and notches show the 95 % confidence interval of the mean.

around the channel when compared to earlier analysis on the full range of images (Figure 6.7). Of particular note is the large swathes of area where σ is zero in each of the images, which was not evident in the earlier iteration (Figure 6.7). There are still bands of high variance, although these bands of variance appear much narrower. In the open channel scenarios, the variance is low across the opening with the offshore. This low variance increases the confidence in the fact that under low wave and high tide conditions, the most dominant trend is that of open connectivity to the offshore.

It is also possible to use the wave and tide factor results above to investigate the distribution of wave/tide conditions for each of the original four types of channel (Figure 6.9). As may be expected, the two open channel types (Type A and D) and the two closed types (Type B and C) occupy similar domains in both wave and tide factors.

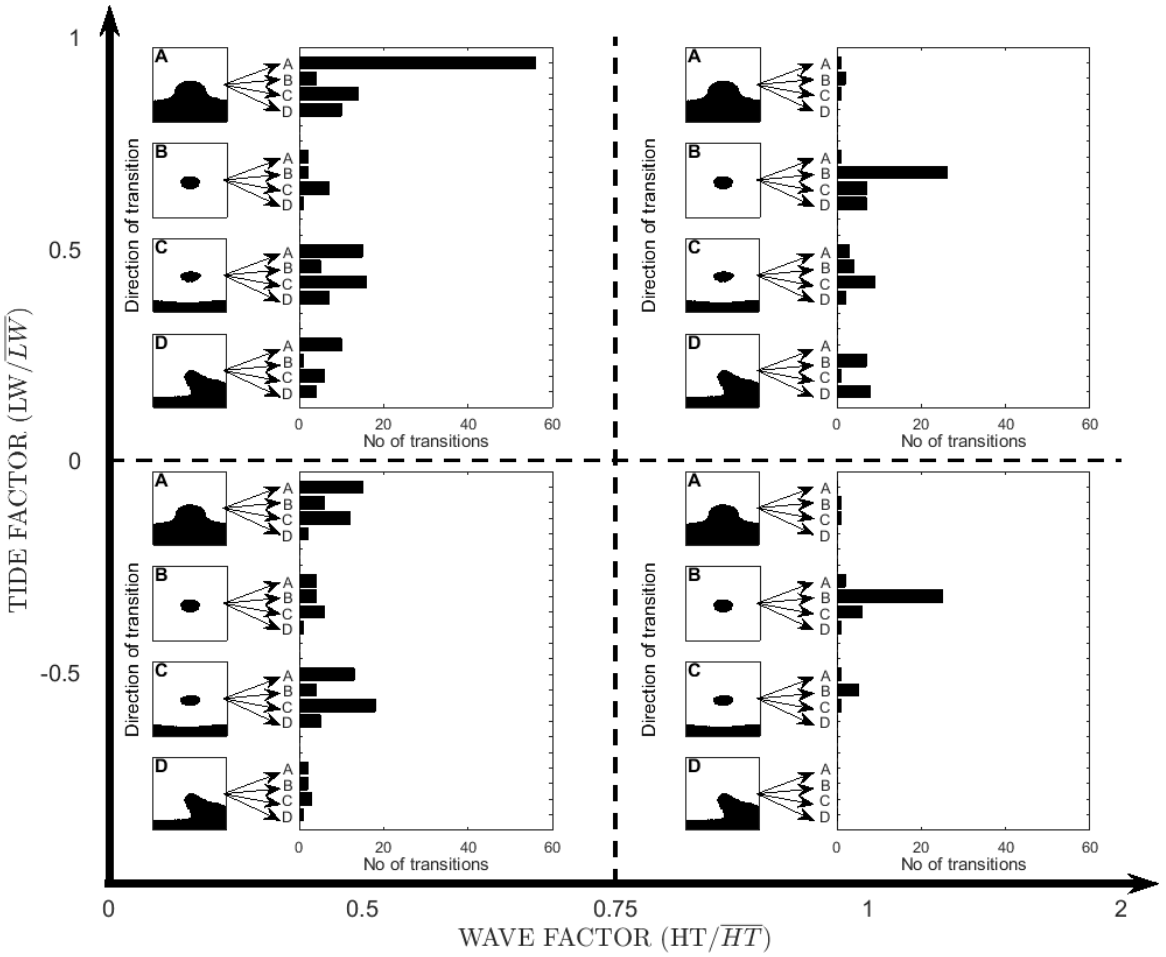

Figure 6.10: Rip channel types as a function of wave and tide factors. For each quadrant of the wave-tide factor grid, the prevalence of each of the four channel types is shown by the barcharts. The direction of transitions observed at each of the wave/tide conditions is shown by the arrows, with a transition being defined as the difference in synoptic type between one image and the next one sampled at that same location (which may in fact be no change).

Type A and D occupy low wave factor (Figure 6.9a) domains. There is some overlap with wave conditions for Type C channels, but total separation between the interquartile range of Type A/D channels and that of Type B. There was much less separation in terms of tide factors (Figure 6.9b). There were similarities again between Type A and D

channels; there was a lower interquartile range and a higher overall median tide factor than compared to Type B and C channels. Type B and C channels exhibit a similar median tide factor, and it therefore appears that the primary mechanism controlling the transition between one or the other is a decrease in wave conditions between Type B and Type C.

6.3.3 Temporal controls

In order to investigate temporal transitions in the type of rip channels observed at Perranporth, one rip channel, known to be persistent in location over O(years, was isolated and its development tracked over an 18 month period. At each sample point in time (1873 useable images in total) the rip was classified using synoptic typing into one of the four types identified in Figure 6.3. Following the findings in Section 6.3.2, each rip channel was subsequently compartmentalised based on wave and tide factors (Figure 6.10). In Figure 6.10, the image type on the left is indicative of the starting image type, and the arrows represent the transition between that sampled image (at time t), and the next image in the dataset ($t + 1$). In many cases, there was no transition at all, such as the top left quadrant, where most Type A images are shown to remain as Type A.

Under higher water level, lower wave conditions, Type A (open, bell-shaped) are most dominant, which is consistent with the findings demonstrated in Figure 6.10 that Type A channels are highly likely to remain as Type A, with a small chance of transition to Type C (closed, in close proximity to offshore). This is further evidenced by the fact that overall, Type C is the second most prevalent channel type under these conditions. Once a channel becomes a Type C, it is equally as likely to transition back to Type A or to persist as a Type C.

A similar trend is evident under lower wave, lower water level conditions where Type A and C channels dominate, and there is regular transition between the two types. As wave factor increases, there is very little occurrence of Type A and C channels. Under higher wave, higher tide conditions, the dominant channel is Type B (closed, in isolation from offshore). Again, the dominant behaviour is one of no change, although there is evidence

of transitions to Type C and D channels. Under higher wave, lower water level conditions Type B channels still dominate, with very little occurrence of any other channel types.

6.4 Discussion

This section first considers the utility of the new synoptic typing method itself, before discussing the dominant types of wave breaking patterns and subsequently the hydrodynamic controls and temporal changes in breaking patterns.

6.4.1 Synoptic typing of surfzone imagery

The synoptic typing method is normally applied to continuous meteorological data such as isobar maps (Kirchofer, 1974), or discrete data with a wide range of variables, such as percentage cloud cover (Barry et al., 1981). However, here it was applied to discrete data with only two possible data values (one or zero). Despite the much reduced range of values, the method still works successfully. In particular, it was able to identify the dominant channel types observed in video imagery, accounting for 91 % of the variability in only four categories of image. This output was subsequently useful in informing a first order classification scheme based on the overall dominant observable trends. It again provided an objective means to remove outliers in the dataset when attempting to explain the opening and closing of the rip channel in terms of wave and tide factors (Figure 6.8), where it was able to reduce much of the background standard deviation to near zero values.

The method shows promise for tracking changes in broader coastal phenomena measured through video imagery than have been discussed here. Indeed, there are a number of processing regimes that assign video imagery pixels a nominal value based on the process of interest, such as wet vs. dry pixels (Quartel et al., 2006). In that study, wet and dry pixels are used to identify intertidal morphology, such as bars, troughs and rips, but the paper presents no means to quantify change between images. The application of synoptic

typing to data such as maps of wet and dry pixels may be able to identify periods when morphological configuration was similar, and subsequently allow identification of forcing mechanisms responsible for the creation of certain morphological configurations. In order for the method to be applied to video image datasets such as this, it is likely that some degree of pre-processing will be required on any video imagery prior to synoptic typing, in order to isolate the trend of interest. Although it could be applied to a complete grayscale image, and give an overall similarity score, there will always be a high degree of variability as the score would account for all changes on the beach, changes in patterns of wave breaking, the width of the surfzone, cloud cover on the day, etc.

The use of video imagery as a means to extract information from the coastal zone provides a basis from which objective conclusions can be drawn. The use of imagery quantifies every aspect in the field of view, through allocation of a discrete pixel [RGB] value. Although some of the thresholds used in synoptic typing can be considered subjective, sensitivity testing goes a long way to reducing the degree of subjectivity involved. Synoptic typing is thus an effective means of using all this quantitative information available to inform a largely objective classification.

6.4.2 Classification and hydrodynamic control

The use of synoptic typing in combination with hydrodynamic thresholds reduced the standard deviation in video images, to elicit hydrodynamic controls on rip channel shape. Four main channel types were identified (Figure 6.3), and when the images are broken down by hydrodynamic thresholds, at a given point in time any particular rip will exist in a state on a spectrum from the most closed and isolated (Type B) channel, through to the most open bell-shaped channel (Type A), and/or all stages in between. Therefore, moving forwards, this thesis will take the two extremes of offshore connectivity on this spectrum as a means to classify channel type, resulting in two types of rip channel; ‘open’, or ‘closed’.

Open channels are characterised by free connectivity to the offshore, in that there is insignificant/no wave breaking over the seaward end of the channel. Open channels

occur predominantly under low wave conditions. The effect of low waves is that there is no breaking in the deeper regions of the nearshore (Lippmann and Holman, 1989; Ranasinghe et al., 1999; Holman and Stanley, 2007), such as the seaward extent of the channel. Tidal levels seem to have less effect on the opening and closing of the channel, however, extreme elevation of water levels (e.g. spring high tide) mean that waves have to travel further inshore, past the rip channel before they enter water of breaking depth. A conceptualisation of some commonly observed open channel types is shown as Figure 6.11a—d. The two types of open channel identified by synoptic typing are shown as Figure 6.11a& b. The most common type is given as Figure 6.11a, and shows a channel widest at the mouth, progressively thinning onshore. Synoptic typing identified 38 % of the dataset as being similar to this type of channel (Figure 6.3). Although no information exists as to how the hydrodynamics of a channel like this would operate, the channel starts narrow and widens towards the offshore, and it could be postulated that this may result in a weakening in the strength of the current as the channel moves offshore. Figure 6.11b shows a channel at an oblique angle. Unlike the first symmetrically forced channel, these channels appear to be fed predominantly from one side, and the onshore extent of the channel at times merges directly into a feeder channel. Also included in the conceptual figure are two channel types qualitatively observed in the dataset, but not elicited in the synoptic analysis. They are included as they may feature more frequently at other sites not included here, and their shape is likely to induce significantly different flow regimes to the two channels identified here. In Figure 6.11c, the open channel has a constant width as it moves through the surfzone. Unlike the bell-shaped channel in Figure 6.11a which widens at the end, a channel that maintains a constant width is less likely to experience a weakening of the current speed as it moves offshore. The final type of open channel presented is that of an inverse funnel shape (Figure 6.11d), whereby the channel narrows offshore. Currents may be strongest in these channels at the most offshore extent, where a wide swath of channel is constricted through a comparatively narrow connection to the offshore. Open channels were seen to occur primarily at low wave, high tide factor conditions (Figure 6.8), which is the domain in which Scott et al. (2014) described increased surfzone exits (Figure 2.7). Therefore, the explicit link between surfzone exit and open channels will be explored in the next Chapter.

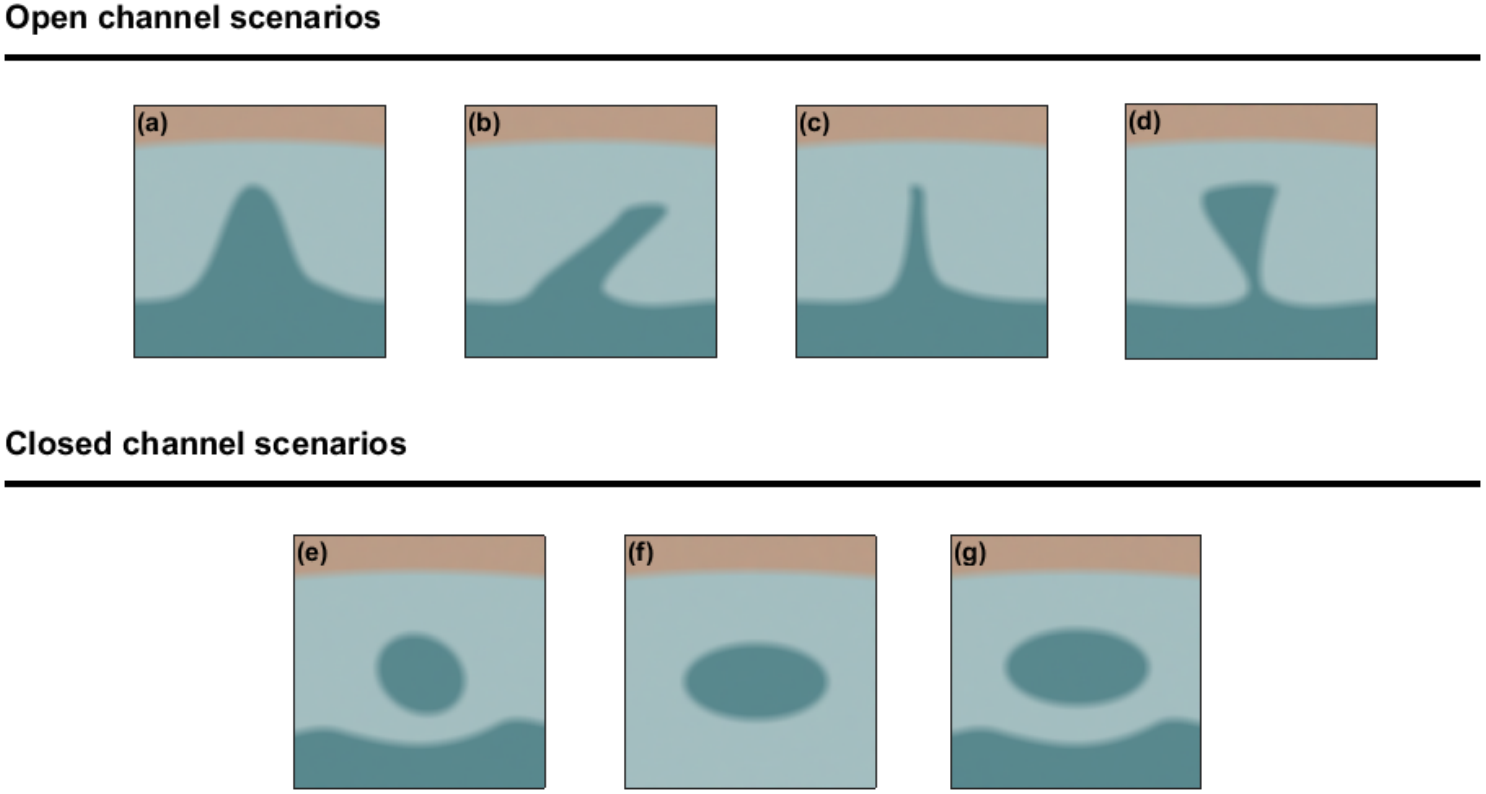

Figure 6.11: Conceptualisation of different rip channel types. First order classification is determined by whether the channel is deemed 'open' or 'closed' to the offshore region. Second order exemplar channels for each type are shown.

In contrast, closed channels are characterised by a deeper channel existing in isolation from the offshore. These channels are 'hole-like' regions, that are enclosed on all sides by wave breaking processes. They are most prevalent under higher wave conditions as there is more wave breaking in the vicinity of the channel, including around the offshore extent. Closed channels are also controlled to a lesser extent by tidal level, with low levels allowing comparatively smaller waves to interact with the seabed and break, creating a closed channel. A subjective review of the image archive reveals much less variability in the form of closed channels, and the three main types observed have been conceptualised in Figure 6.11e—g. The first type (Figure 6.11e) is characterised by an almost circular region, disconnected from, but in close proximity to, the offshore region. Figure 6.11f is characterised by a more dominant isolation from the offshore, where there is at least one rip channel width of wave breaking separating the channel from the offshore. In the example given, there is no discernible offshore area evident at all in the imagery, as the surfzone is widened to such an extent that the area outside the breaking zone is excluded from the imagery field of view. It follows that these sorts of channel occur under the highest wave conditions, where breaking is induced over a large area, creating a large surfzone. This is evidenced in Figure 6.5, where the proximity to the offshore area is seen to decrease under increasing wave conditions, with almost total isolation from the offshore appearing evident in the right hand column (maximum wave conditions). In order for these channels to persist, the actual morphology must be well developed and deep, in order to prevent wave breaking through the channel. Figure 6.11g shows an elongated channel, less circular in form. Although the synoptic typing did not discriminate based on channel width-to-length ratios, the wider channel may produce a hydrodynamically different response to more circular channels (e.g. Figure 6.11e). These channels can at times appear more oblate, or even linear. They may run at parallel or oblique angles to the shore, and at times can be hard to distinguish from feeder channels. In general, these channels still run in close proximity to the offshore area, and the effect of widening the channel may be that offshore directed velocities are weakened as there is no constriction to channel the flow offshore. Closed channels were seen to occur primarily at high wave, low tide factor conditions (Figure 6.8), which is the domain in which Scott

et al. (2014) described increased surfzone retention (Figure 2.7). Therefore, the explicit link between surfzone retention and closed channels will be explored in the next Chapter.

Rip channel shapes have not received attention directly in the literature, yet this research suggests that wave breaking-derived channel shape is one of the most highly dynamic aspects of a rip system (changing on O(minutes)), especially when compared to parameters such as migration rates (O(days)) or persistence (O(weeks)). Previous research details how circulation patterns can change drastically over periods of O(mins), aligned with incident wave group frequencies (Sonu, 1972; Fowler and Dalrymple, 1990; MacMahan et al., 2004), and more broadly, linked to morphological change over both tidal (Austin et al., 2010) and seasonal (Masselink and Pattiaratchi, 2001) cycles. Over these same (O(mins)) timescales the underlying morphology and rip spacing is unable to significantly change, yet circulation patterns do. Circulation type (as well as rip current speed) exerts a primary control on rip current hazard. Therefore, it is of interest to investigate the role of changing channel shape on rip circulation in order to differentiate between times when an individual rip current is more- or less-hazardous than others.

Although no direct measurement of the effects of open and closed channels on circulation has been made, there is some evidence that supports the assertion that the pattern of wave breaking may exert control on surfzone retention. Scott et al. (2016) showed that under low wave and high tide conditions, exit rates were high (Figure 2.7), which mirrors the conditions under which rip channels typically present as open. Likewise, they report low exit rates under high wave, low tide conditions, similar to those at which closed channels persist. Brander (1999) presented a conceptualisation of how changes in rip channel appearance under decreasing wave energy conditions can appear visually similar to actual downstate transitions in morphology. Of interest, his schematic (although not applying the same terminology) detailed rip currents that under the current description could be considered as open or closed, and he showed that the transition between each is accompanied by changing rip channel speeds; another factor in quantifying rip current hazard. Research has also shown that wave-current interaction has an important role in regulating the offshore extent to which a rip current can flow (Yu and Slinn, 2003). Here, the presence (or otherwise) of a band of wave breaking at the seaward extent of the rip

channel is likely to interact with the rip current, and modulate it's ability to continue flowing offshore, thus also controlling the hazard.

6.4.3 Temporal controls

Wave height appears to be the primary control on the occurrence of Type A (open, bell shaped) channels, as Type A is common at both high and low tide conditions, but rarely occurs under high wave conditions. This shows that the dominant process controlling the closing of a Type A channel is an increase in wave heights that induce breaking over the end of the channel and wider surfzones (Figure 6.10; Figure 6.9a). Similarly, Type B channels (closed, in isolation) occur infrequently under low wave conditions, requiring bigger waves and a wider surfzone to prevail. Type C channels (closed, in close proximity to offshore) can occur at all combinations of wave and tide factor, but are most prominent under low wave conditions. This shows that as wave heights increase, the isolation from the offshore increases until the channel would overall be classed as a Type B channel.

Wave heights have been shown here as a primary driver of change between open and closed channels. The effect of higher waves is to increase surfzone width by the initiation of breaking further offshore. This in turn promotes breaking around the end of the channel, which acts to close the channel. Although not observed here to a great extent, tidal controls are also potentially important. The work of Austin et al. (2010) at Perranporth showed the effect of changing tidal levels on the form of the rip channel, using maps of wave roller dissipation. Under uniform wave conditions, a drop in tidal elevation was seen to close the rip channel at its offshore extent, effectively mirroring a transition from a Type A or D channel to a Type C. This is a result of the lower water levels allowing comparatively smaller waves to break further offshore as water depth is reduced, also promoting the formation of closed channels.

6.5 Conclusions

For the first time, video imagery was used as the primary means to objectively classify rip channel morphology. Synoptic typing, hitherto primarily used on meteorological data, was effective in identifying and distinguishing the dominant wave breaking patterns evident in video imagery. This method enabled the identification and removal of anomalous images, thus reducing background variation and identifying the dominant trends. Of particular note is the ability of synoptic typing to act as one of the first means to objectively classify video imagery. Moving forwards, synoptic typing could be more widely applied to identify shoreline change, beach rotation, changing widths of the surfzone and other coastal indices tracked through video imagery.

The method applied here resulted in a new means of classifying rip channels. Firstly, four main types were identified and differentiated by the rip channel's shape, size, and connectivity to the offshore. These types could be broadly classified into one of two classes; (1) open; or (2) closed, in terms of their connectivity to the offshore region. Unlike previous classification schemes, typically focussed around the controlling mechanisms on a rip current, this classification scheme can be used to differentiate between the state of an individual rip channel over time.

The connectivity to the offshore discussed above may have implications for how the rip current is behaving. An increase in wave-current interactions at the offshore extent of closed channels may hamper the rip current's ability to continue offshore, ultimately reducing the hazard. This was evidenced by comparison to earlier work that showed high rates of exit at Perranporth during the conditions under which this thesis has found open channel states to persist. This investigation provides an interesting insight to the possibility that rip hazard can be estimated using video imagery. Future work should focus on coincident *in situ* measurements and video imagery, to measure the flow regime of rip currents during times when rip currents can be classified as open and closed in video imagery. Furthermore, it may be possible to link rescue events in the rip rescue

databases of surf lifesaving organisations to the occurrence of open and closed channel conditions.

It is important to note that the findings of this Chapter are currently only site specific, as there is no similar (wave/tide factor) measure of exit rate and open/closed channels at any other site. The main factor that makes this finding site specific are the values of wave and tide factor that are seen to bring about change between open and closed conditions (i.e. what threshold of wave conditions marks the transition from open to closed channels). The broad findings should be applicable to channelled rips on any beach worldwide, as the morphodynamic controls on such rips are comparable. It is reasonable to assume that increased wave breaking will act to close channels, and that to a lesser extent, tidal levels will modulate the spatial location of wave breaking with similar results on the transition between open and closed. On that basis, the remainder of this thesis will assume the results are applicable for any channel rips, as the process controlling formation is the same across sites.

Chapter 7

Wave dissipation as an indicator of nearshore circulation

This chapter discusses Lagrangian and remote sensing data from two field studies in order to understand how wave breaking patterns influence rip circulation. Analysis on Ngarunui data is as yet unpublished, however, discussion of Perranporth data is adapted from the following publication:

> Pitman, S.J.; Gallop, S.L.; Haigh, I.D.; Masselink, G., and Ranasinghe, R., 2016. Wave breaking patterns control rip current flow regimes and surfzone retention. *Marine Geology* 382: 176—190.

7.1 Introduction

There is a longstanding view of rip currents whereby the current always extends far offshore, a behaviour termed a *rip exit* (Shepard et al., 1941). However, Lagrangian measurement has identified a wide variety of circulation patterns, including recirculation that promotes *surfzone retention*, rather than exit (MacMahan et al., 2010). Although

there is good agreement in the literature about the activation of rip currents (i.e. the establishment of rip current flow through rip channels (Austin et al., 2010)), there is not yet consensus on what conditions promote surfzone retention over rip exit, or vice versa.

A brief summary of past literature dealing with this topic was presented in Section 2.3, and is summarised below. For activation of channel rips to occur, it is widely accepted that there needs to be an alongshore gradient in radiation stress from the breaking waves (Longuet-Higgins, 1970), and variations in the alongshore bathymetry inducing spatially variable patterns of wave breaking (Bowen and Inman, 1969). Attempts have been made to explain surfzone retention rates through VLF motions (Reniers et al., 2009, 2010), and combinations of wave and tide factors (Scott et al., 2014), but neither approach has successfully explained all variability. Previously, the role of wave breaking patterns in controlling surfzone circulation was opportunistically and qualitatively discussed (Scott et al., 2014), however, no quantitative link was investigated.

Therefore, the overall objective of this chapter is to assess the control exerted by differing wave breaking patterns on rip current flow regimes at two sites; the macrotidal, intermediate, low tide bar/rip beach at Perranporth, and a contrasting mesotidal, double barred high energy beach at Ngarunui. In order to address this, there are two sub-objectives: (1)To investigate rip current flow regimes through the use of Lagrangian drifters at two contrasting sites; and (2) To identify the occurrence of open and closed rip channels during the field studies, in order to classify drifter behaviour in terms wave breaking patterns.

7.2 Methodology

Much of the methodology pertinent to this Chapter has been outlined in Chapter 4, however, a few further processing steps for video imagery and Lagrangian data are outlined below.

7.2.1 Video imagery

Timex images for tidal levels less than 3m ODN from 2009 - 2013 were classified using the segmentation method developed by Pitman et al. (2016) and described in Chapter 6, into open or closed rips. This classification involves thresholding images based on greyscale intensities into a binary image, where white values show wave breaking and black pixels show deeper channels. The binary image allows for a simple, objective visual classification of either open or closed channels. A threshold from 0 to 1 is selected in order to produce the black and white pixels required for the binary image. The threshold (τ) used here was 0.5, and sensitivity analysis showed that for $0.3 < \tau < 0.7$, the technique was robust, with 95 % of images being classified correctly by all values of τ within this range . It is unfortunate that the Argus camera was unserviceable for the period 20 - 23 Jul 2013 and also 6 - 22 Aug 2013, when a large number of incidents occurred. However, investigation of the images captured immediately prior to and following these outages showed the presence of numerous and prominent open rip channels. Furthermore, the wave conditions between 23 Jul and 23 Aug were low energy (mean $H_s = 1.02$ m), with no storms and therefore it is likely that the prominent open rip channels persisted throughout the period.

7.2.2 Lagrangian drifter data

Each individual deployment was classified visually into one of four categories: 1) linear exit; 2) circulation then exit; 3) circulation with no exit; or 4) other. These classifications are similar to those used in other studies (MacMahan et al., 2010; Austin et al., 2013; Scott et al., 2014; Gallop et al., 2015). A linear exit was defined as the drifter moving offshore immediately from the time of deployment, to beyond the edge of the surfzone. Circulation then exit was when drifters had a significant portion of onshore movement before moving offshore, or when the drifter made at least one complete re-circulation before moving offshore beyond the edge of the surfzone. Circulation with no exit was defined as movement contained within the surfzone. Under this condition drifters would

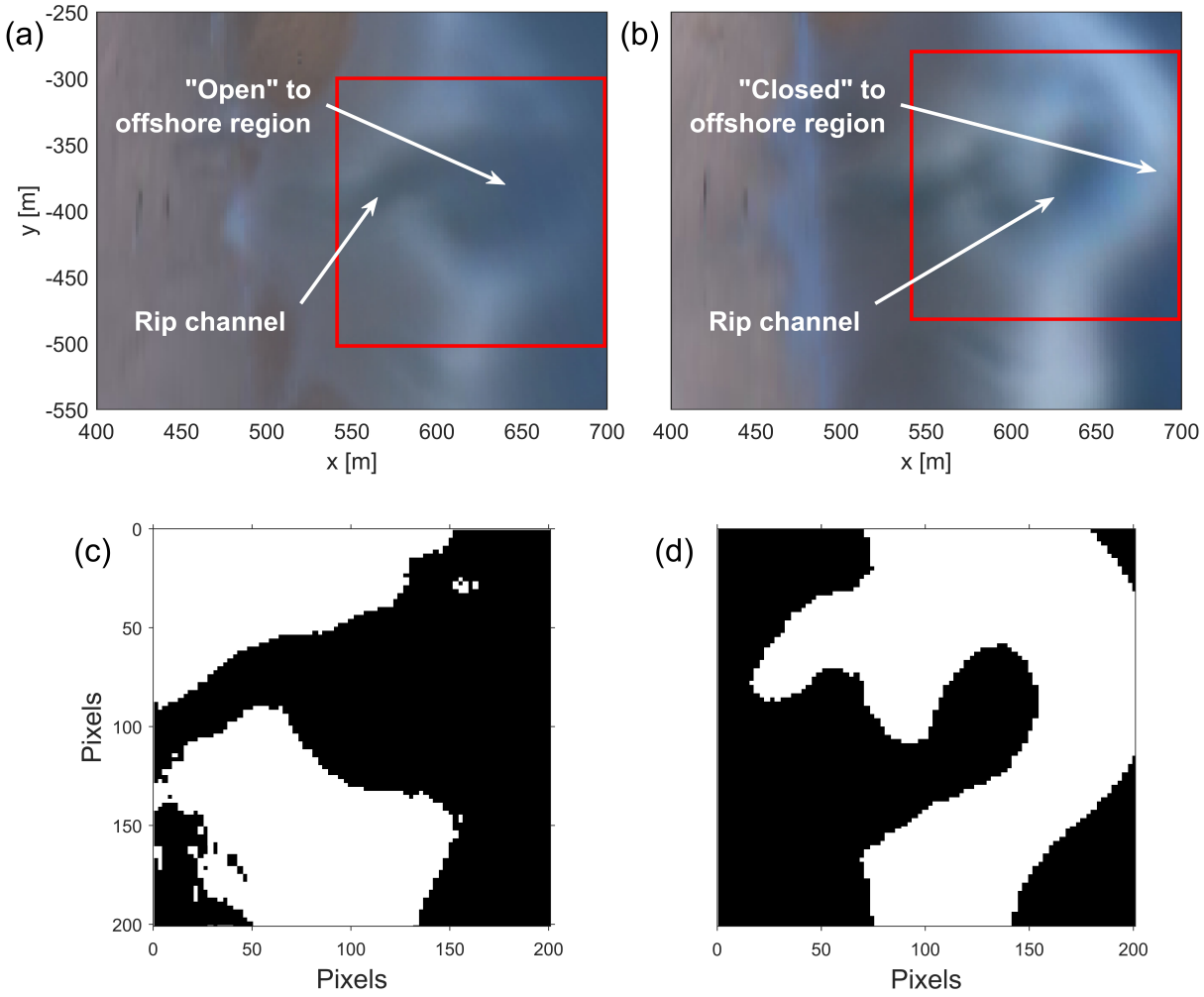

Figure 7.1: Examples of rip currents from Perranporth Beach, U.K. The examples here are classified as (a) open; and (b) closed to the offshore region, by wave breaking. The classification is achieved through thresholding. (c) Open channels extend as black pixels from the extreme left of the area and have an open connection to the offshore area. (d) Closed channels are segregated from the offshore region by a distinct band of white pixels, indicative of wave breaking.

typically rotate 3 or 4 times over periods $O(15$ mins) before washing alongshore or onshore. In extreme cases, one drifter circulated for 80 mins, recirculating 13 times before washing alongshore. Other was defined as occasions when the drifter washed

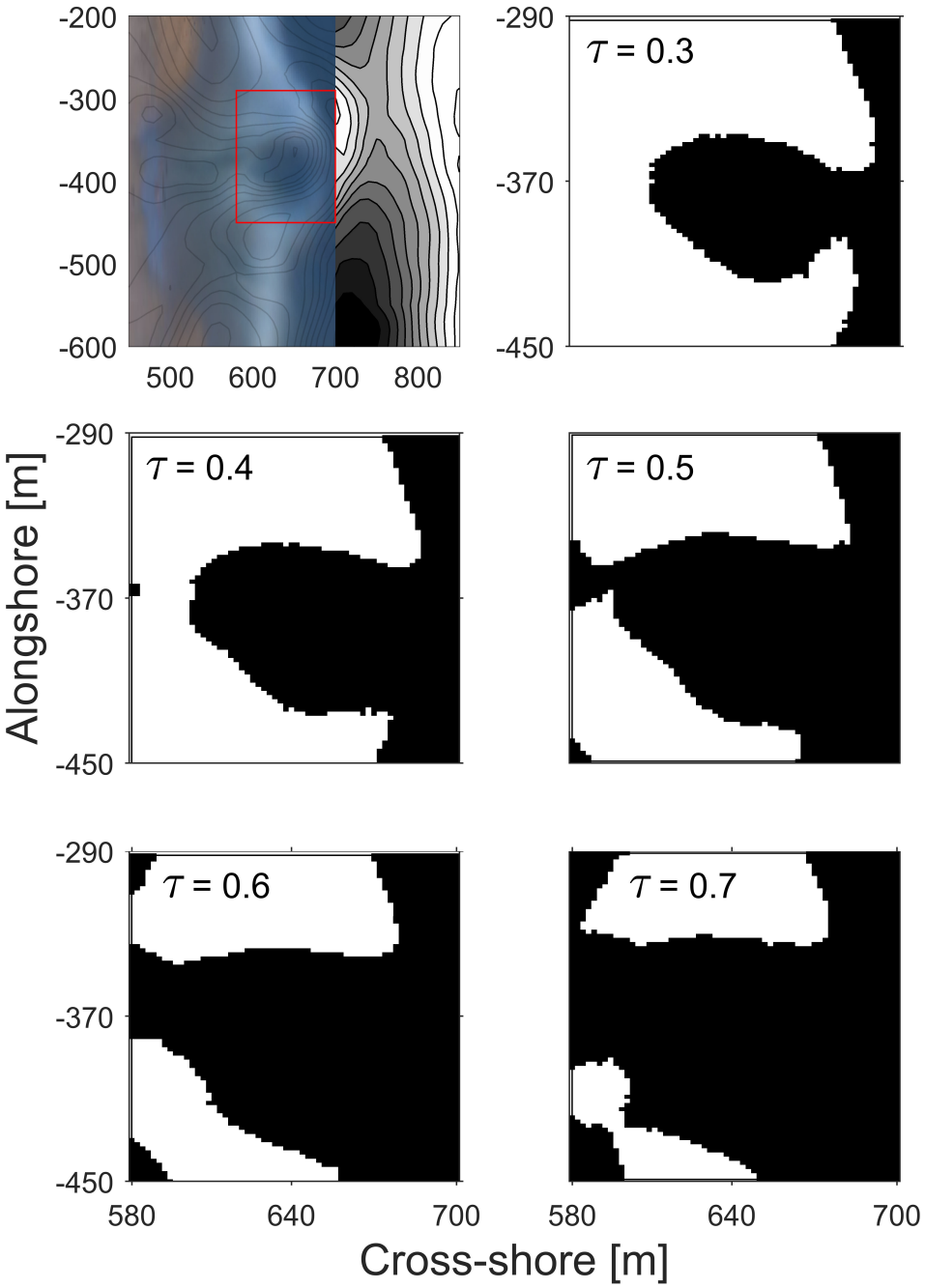

Figure 7.2: Sensitivity analysis for the application of the Pitman et al., (2016) method. An original, rectified, timex image from Perranporth (top left) with area of the surfzone incorporating a rip channel used for thresholding (red box). Thresholds (τ) from 0.3 0.7 were tested, and in all the cases shown in the figure, the rip current was classified as open, irrespective of the selected threshold within that range.

ashore, or travelled significantly alongshore within the surfzone, without circulation in or around the rip channel.

7.3 Results

In this section the general hydrodynamics at each site are first considered for the course of the field experiments, followed by a comparison with video imagery to elicit wave dissipation controls.

7.3.1 Hydrodynamics

The first objective of this study is to quantify how hydrodynamics at each site changed over the field experiments, so that a later comparison with wave breaking patterns can be made.

Perranporth

During the Perranporth experiment, two dominant flow regimes were observed: 1) circulation confined within the surfzone; and 2) surfzone exits. On 16 May, the incident wave field was near shore-normal, with weak ($U \approx 2.2$ m s^{-1}) onshore winds (Figure 4.3). The wave conditions were some of the most energetic observed during the study ($Hs \approx 1.25$ m, $Tp \approx 12$ s), but waves were still less steep than the summer average ($Hs \approx 1.1$ m, $Tp \approx 8.3$ s). Breaking wave heights were visually estimated to be around 1 m. Figure 7.3 shows the overall circulation patterns each day. Mean and max speeds were calculated over each 4-hour deployment. The combination of these factors drove a symmetric (MacMahan et al., 2010) rip, with the main channel extending perpendicular to the shore at $y = 350$ m (Figure 7.3a) and recirculations on either side of the rip neck in opposing gyres. The larger of the two cells is the clockwise circulation with the peak onshore return flow from this cell at $y = 420$ m. A counter-clockwise

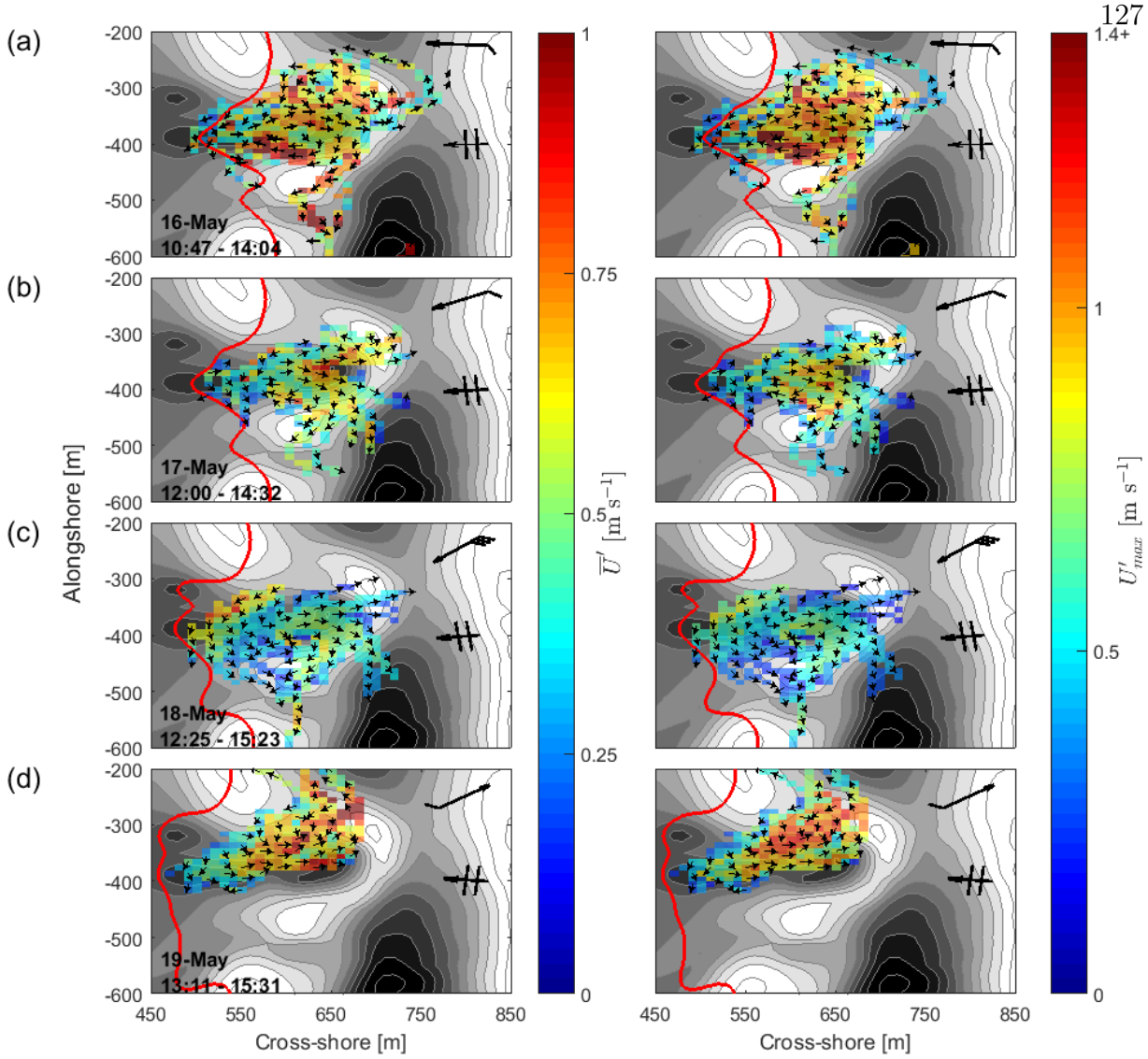

Figure 7.3: Daily observations from Perranporth drifter deployments. Mean (left column) and maximum (right column) observed velocity is presented as the underlying colour on grid with cells of 10 x 10 m for the (a) 16th, (b) 17th, (c) 18th, and (d) 19th May 2014 deployments. The overlaid arrows indicate the dominant direction of flow in each grid square. Wind direction is indicated in the top right, with each barb indicating increments of 2.5 m s^{-1} in the average wind speed. Dominant direction of wave propagation is given by the symbol at mid height on the right hand side of each panel, and the lowest still water elevation for each day is given as a solid red line.

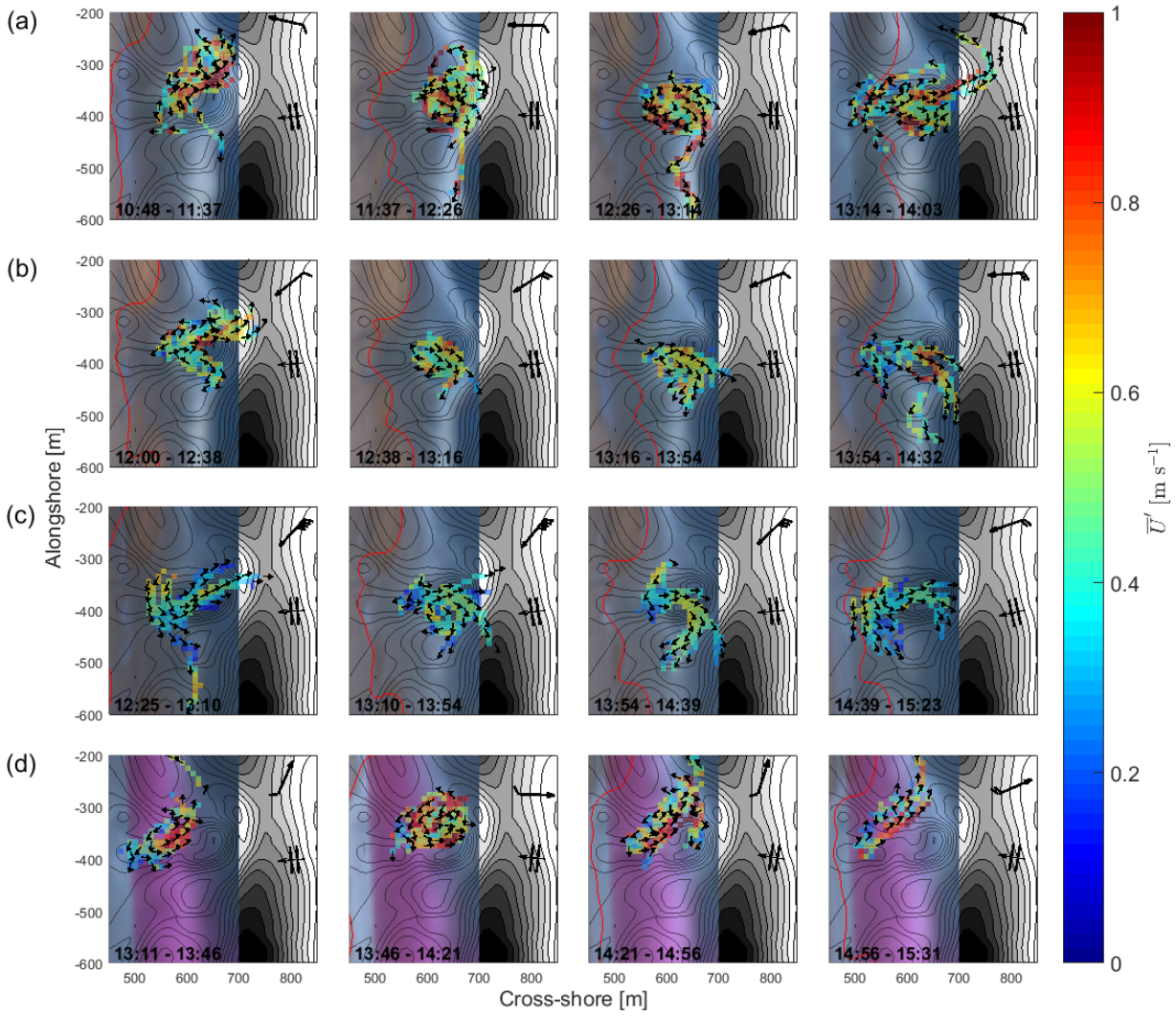

Figure 7.4: Drifter observations binned into approximately 45 minute periods throughout the Perranporth experiment, with (a) 16 May, (b) 17 May, (c) 18 May, and (d) 19 May presented on individual rows. Timing of the observations is given in each panel. Mean observed velocity is presented as the underlying colour on grid with cells of 10 x 10 m. The overlaid arrows indicate the dominant direction of flow in each grid square. Wind direction is indicated in the top right, with each barb indicating increments of 2.5 m s^{-1} in the average wind speed. Dominant direction of wave propagation is given by the symbol at mid height on the right hand side of each panel, and the lowest still water elevation for each period is given as a solid red line.

circulation is also observed, although the circulation cell is much weaker and less established. Mean offshore-directed flow through the centre of the channel was ≈ 0.8 m s^{-1} throughout the course of the day, with peak flows reaching ≈ 1.1 m s^{-1}. Mean onshore flows ranged from 1 m s^{-1} in the clockwise circulation to 0.5 m s^{-1} in the counter-clockwise flow (Figure 7.3a). These two circulation regimes existed in temporal isolation from each other (Figure 7.4a). Between the first deployment at 10:47 and 11:37 flows were predominantly confined to the counter-clockwise circulation cell, with recirculation dominating and few surfzone exits. Throughout the course of the day, the counter-clockwise circulation cell became less prominent as a clockwise circulation developed. Recirculations continued to dominate flow patterns until after 13:15 when surfzone exits became the primary form of flow pattern.

The clockwise circulation persisted into 17 May, with the counter-clockwise cell decaying into a purely offshore component (Figure 7.3b). Winds persisted in the onshore direction and increased in speed ($U \approx 3$ m s^{-1}), but wave conditions ($Hs \approx 0.75$ m, $Tp \approx 10$ s) were comparable to the previous day (Figure 4.3). Mean offshore rip flows were comparable to the previous day; however, there was a slight reduction in peak offshore flows to 1 m s^{-1}. Mean onshore flows reduced to around 0.7 m s^{-1}. Early afternoon showed, again, a split circulation between both clockwise and counter-clockwise cells (Figure 7.4b); however, as the day progressed the counter-clockwise circulation ceased. This day was predominantly characterised by surfzone exits as the dominant flow regime.

Circulation on 18 May was dominated by an alongshore component to the flow. Strong onshore winds with an alongshore element dominated this day ($U \approx 8.5$ m s^{-1}), with wave conditions largely unchanged from the previous day ($Hs \approx 0.65$ m, $Tp \approx 9$ s). Breaking wave heights were visually estimated to be around 0.5 m. The rip was fed alongshore by the strong prevailing wind and wave direction, before sharply turning offshore through the rip neck (Figure 7.3c). Rather than a typical rip head dispersion, whereby the current disperses in all directions, there was a further strong change in direction alongshore toward in the direction of the prevailing wind and wave fields. This alongshore dispersion was only evident later in the day (Figure 7.4c), whereas drifters in the first deployment (12:25—13:10) exited the surfzone almost directly into the

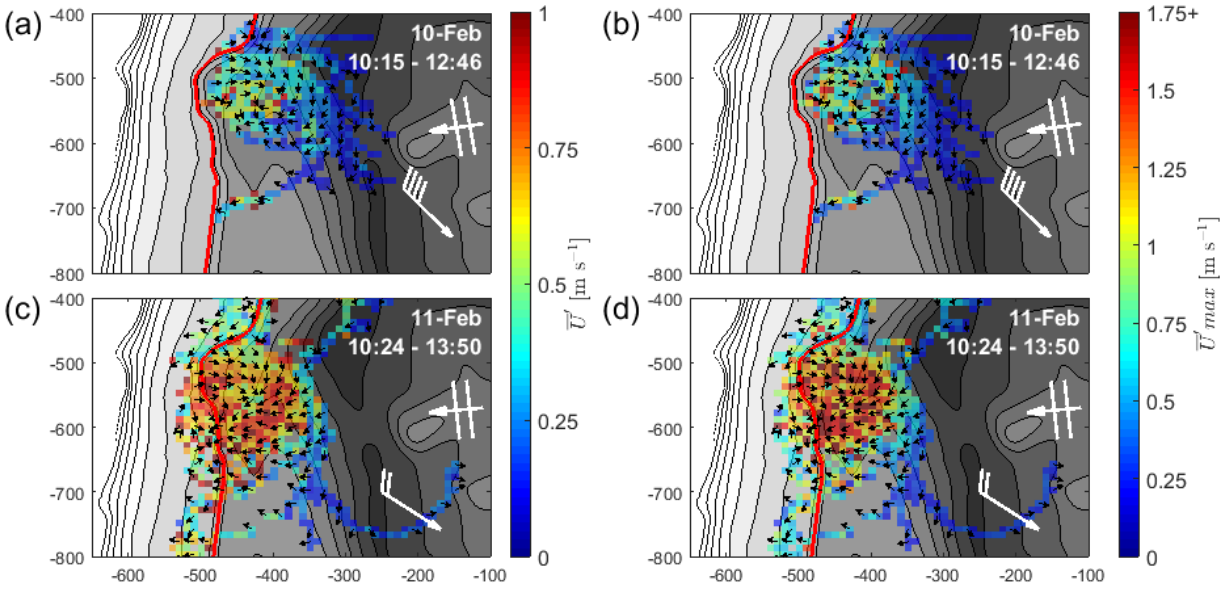

Figure 7.5: Daily observations from Ngarunui drifter deployments. Mean (left column) and maximum (right column) observed velocity is presented as the underlying colour on grid with cells of 10 x 10 m for the (a) 10th and (b) 11th Feb 2015 deployments. The overlaid arrows indicate the dominant direction of flow in each grid square. Wind direction is indicated in the top right, with each barb indicating increments of 2.5 m s^{-1} in the average wind speed. Dominant direction of wave propagation is given by the symbol at mid height on the right hand side of each panel, and the lowest still water elevation for each day is given as a solid red line.

prevailing wind direction. Mean offshore flow speeds on this day were the lowest of the experiment, peaking around 0.4 m s^{-1}.

Circulation on 19 May was confined almost entirely within a well-established counter-clockwise cell (Figure 7.3d), aligned with the direction of a weak ($U \approx 2$ m s^{-1}) offshore wind (Figure 4.3). Wave conditions were most energetic during this period ($Hs \approx 1.5$ m, $Tp \approx 13$ s). Offshore current speeds throughout the day were consistently the highest observed during the experiment, often in excess of 1 m s^{-1} (Figure 7.4d).

Ngarunui

At Ngarunui, the same two dominant flow regimes (circulation, and exit) were observed to persist. On 10 Feb the incident wave field was near shore-normal, with strong ($U \approx 8$ m s^{-1}) offshore winds (Figure 4.5). Wave heights were average ($Hs \approx 1.5$ m), although periods were longer than average ($Tp \approx 15$ s), resulting in waves of low steepness. Breaking wave heights were visually estimated to be around 1 m. Figure 7.5a—b shows the overall circulation patterns on the day. Mean and max speeds quoted were calculated over the length of the deployment. On 10 Feb a slight clockwise rotations persisted, although drifter exit was the dominant trend. The main channel of the rip extended offshore at y = -500 m, and after approximately 80 m of offshore movement as the current reaches the edge of the surfzone, a large proportion would continue to meander offshore, with a smaller percentage recirculating back onshore. Mean offshore current speeds in the mid-channel were typically 0.35 m s^{-1}, slowing to $<$ 0.25 m s^{-1} as the current meanders offshore. For the recirculating current, speeds were slightly higher onshore ($\approx$ 0.6 m s^{-1}). Maximum offshore speeds mid-channel were $\approx$ 1 m s^{-1}, comparable to maximum onshore flow of $\approx$ 1.15 m s^{-1}. When considering how the flow changed throughout the course of the day, rotation and recirculation was highest early in the deployment (10:32—11:18) when tidal levels were lowest (Figure 7.6a). During this low water phase of circulation, rip current speeds were generally at their greatest over the course of the day both onshore and offshore. As water levels increased into the afternoon, all evidence of circulation ceased and the current comprised solely an offshore meander.

On the 11 Feb, a pattern of recirculation dominated. Offshore wind speeds were lower than the previous day ($U \approx 6$ m s^{-1}), the incident wave angle remained unchanged although wave heights increased ($Hs \approx 2$ m) and period decreased ($Tp \approx 12$ s), resulting in steeper waves (Figure 4.5). Breaking wave heights were visually estimated to be around 1.5 m. The entire circulation cell spanned a 200 m^2 area, with offshore flows at y = -550 m and an onshore return flow centred around y = -620 m (Figure 7.5c—d). Mean offshore speeds mid-channel were double that of the previous day (0.53 m s^{-1}), and mean onshore speeds were similarly elevated ($\approx$ 1 m s^{-1}). Maximum onshore and

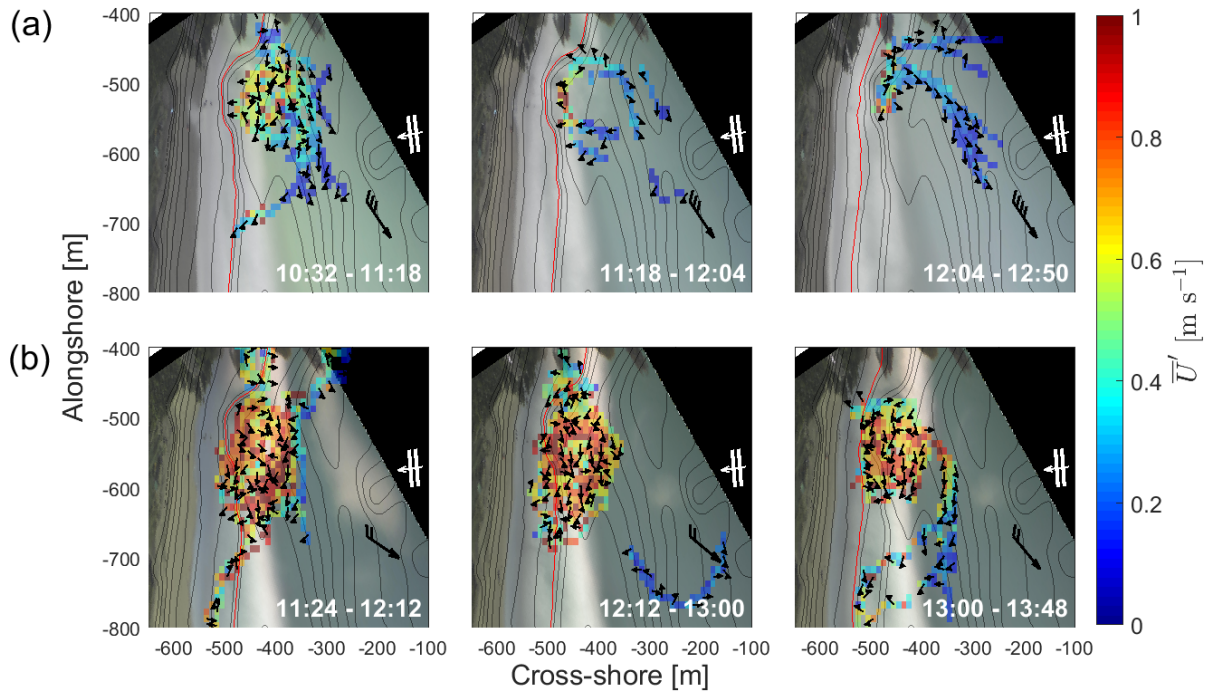

Figure 7.6: Drifter observations binned into approximately 45 minute periods throughout the Ngarunui experiment, with (a) 10 Feb and (b) 11 Feb presented on individual rows. Timing of the observations is given in each panel. Mean observed velocity is presented as the underlying colour on grid with cells of 10 x 10 m. The overlaid arrows indicate the dominant direction of flow in each grid square. Wind direction is indicated in the top right, with each barb indicating increments of 2.5 m s^{-1} in the average wind speed. Dominant direction of wave propagation is given by the symbol at mid height on the right hand side of each panel, and the lowest still water elevation for each period is given as a solid red line.

offshore speeds were also significantly higher ($\approx$ 1.7 m s^{-1}) than the previous day (Figure 7.5c—d). As the day progressed, the alongshore extent of the circulation decreased from $>$ 200 m (Figure 7.6b; [11:24—12:12]) to $\approx$ 120 m (Figure 7.6b; [13:00—13:48]). This accompanied a slight decrease in mean offshore speeds from 0.8 m s^{-1} to 0.6 m s^{-1}. This transition occurred during a rising tide, with the total increase in water level over the deployment $\approx$ 1 m (Figure 4.5).

7.3.2 Wave breaking controls

The main objective of this Chapter was to compare the hydrodynamic behaviours identified in the previous section with the occurrence of open or closed rip channels. Here, an analysis has been done for both sites. The occurrence of open and closed channels at Perranporth was variable within each day (Figure 7.7), whereas at Ngarunui open channels occurred on 10 Feb, and closed on 11 Feb (Figure 7.8).

At Perranporth, in closed scenarios (Figure 7.7a—d) there were 6 occurrences when drifters exited the surfzone, but the dominant circulatory regime was circulation with no exits ($n = 55$). There is a clear demarcation at the offshore extent of wave breaking that coincides with the offshore extent of the majority of drifter tracks during closed conditions. This subsample is comparable to the entire dataset, where there were 23 exits compared to 113 circulations (Figure 7.9), with no exits during conditions when wave breaking enclosed the rip channel (Figure 7.7). Of the 4 closed scenarios, Figure 7.7a had a high number of exits ($24\%, n = 4$) compared to the other periods when the channel was classified as closed. Three of these exits subsequently re-circulated back through the breaking waves after periods between 50—140 s. For most of the deployment, drifters were retained within the surfzone and only one drifter exited and did not return.

A similar trend is evident at Ngarunui (Figure 7.8a—c), where recirculation and retention dominated the closed conditions. The balance was more mixed than at Perranporth (e.g. Figure 7.8c), where there were more exits (36 %), despite the dominance of retention. This is representative of conditions over the entire day, where under closed conditions 59 % ($n = 10$) of drifter entries resulted in retention, compared to 41 % ($n = 7$) exits (Figure 7.10). At times, under closed conditions, surfzone retention was as high as 80 % (Figure 7.8b). In the most extreme scenario, two drifters were seen to continue circulating within the surfzone for 2 hours, each making 6—8 full circulations without exiting.

When considering the open rip scenarios at Perranporth (Figure 7.7e—h), there is a marked shift towards the dominance of surfzone exits or circulation resulting in an exit. Most of these exits occurred through the middle of the channel. Typically, drifters that

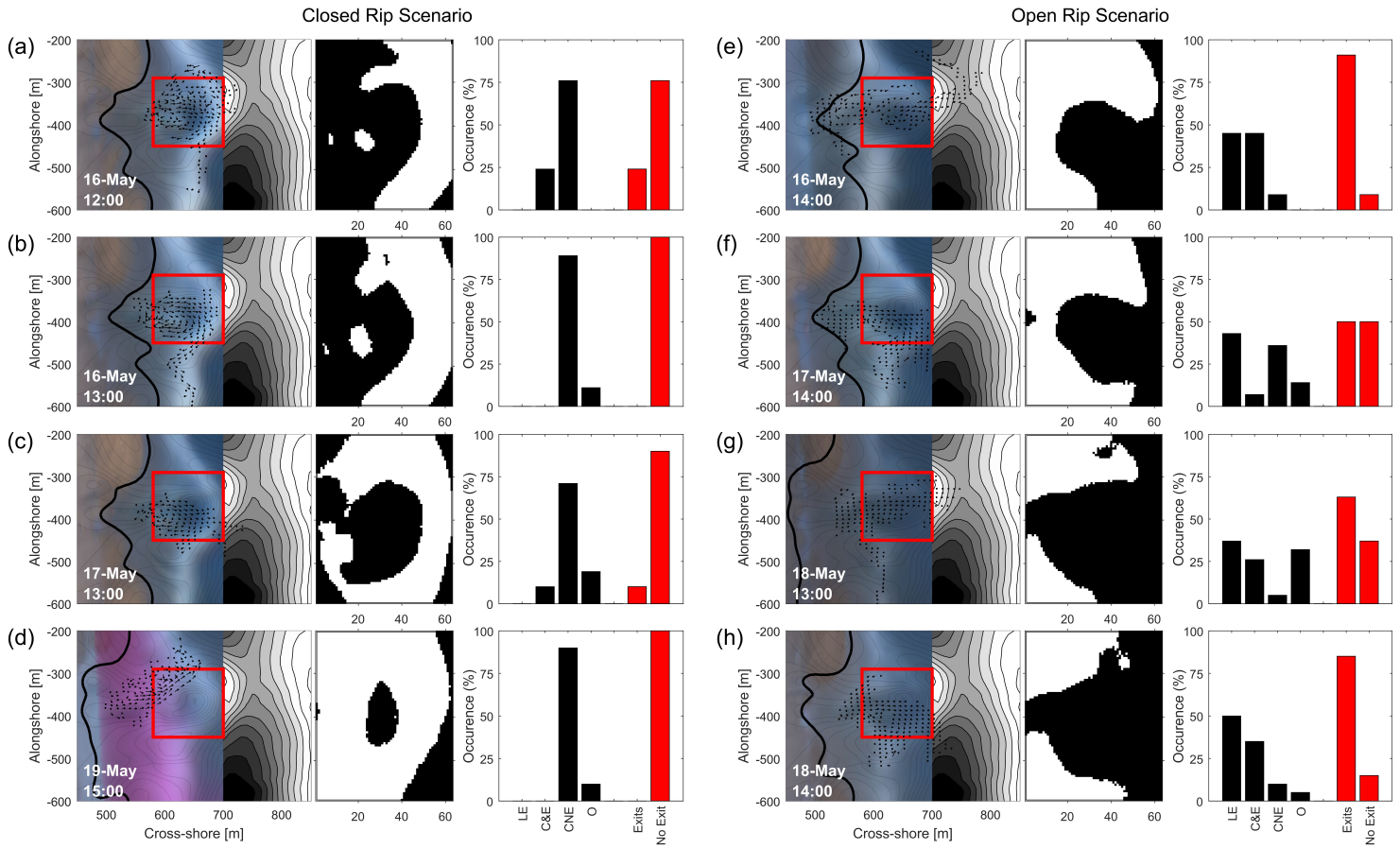

Figure 7.7: Rip current flow regimes under open and closed channel conditions at Perranporth. (a—d) Closed and (e—h) open channel scenarios observed during the field experiment. The left hand panel shows the drifter plots for that individual hour of observation, binned into a 10 x 10 m grid, with black arrows indicative of flow direction, with a solid black line indicative of the lowest still water elevation during that period. The red box indicates the part of the channel the classification algorithm was applied to, with the results presented in the middle panel. Black pixels are indicative of both channels and the offshore area, with white pixels representative of wave breaking. The various behaviours observed (right panel) are presented, with each drift classified as either a linear exit (LE), circulation followed by an exit (C&E), circulation with no exit (CNE), or other (O). The right hand two bars represent overall behaviour, with Exit constituting the sum of LE and C&E behaviours, and No Exit the product of CNE and O behaviours.

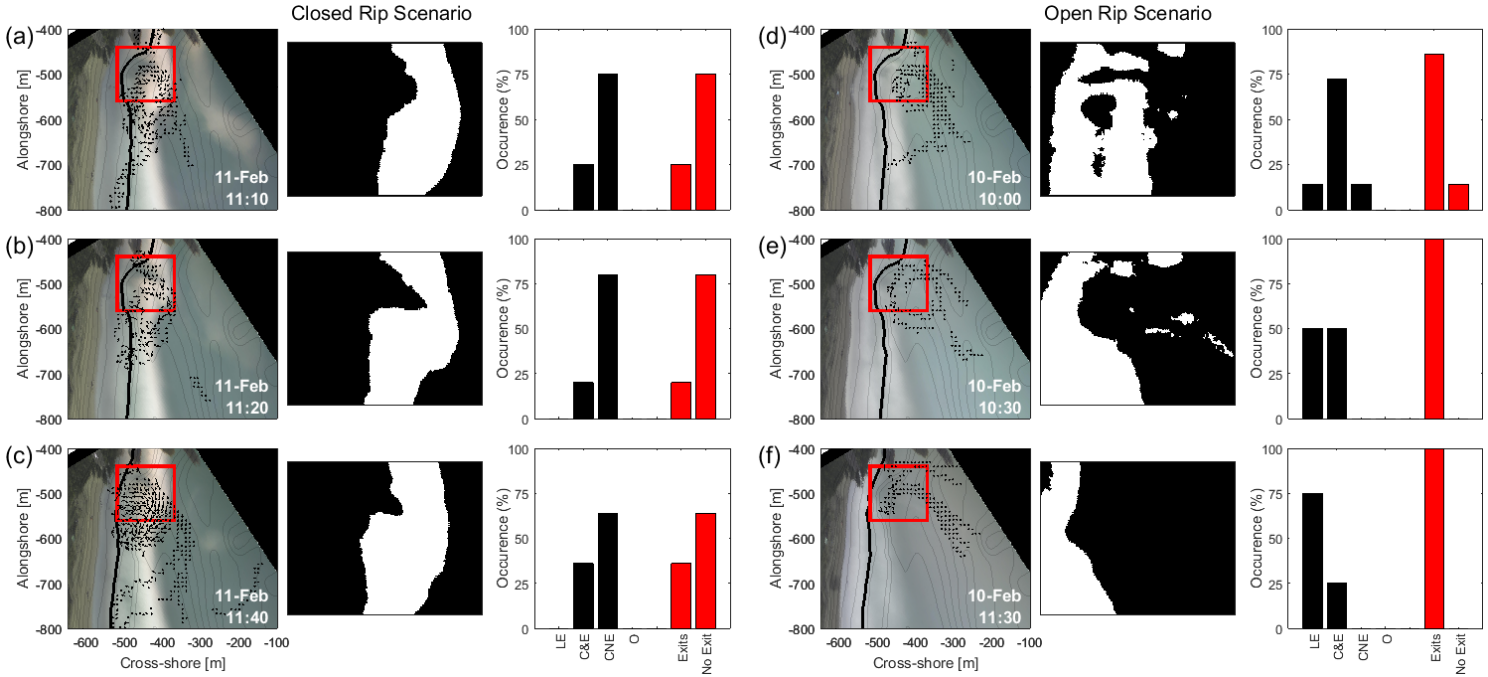

Figure 7.8: Rip current flow regimes under open and closed channel conditions at Ngarunui. (a—c) Closed and (d—f) open channel scenarios observed during the field experiment. The left hand panel shows the drifter plots for that individual hour of observation, binned into a 10 x 10 m grid, with black arrows indicative of flow direction, with a solid black line indicative of the lowest still water elevation during that period. The red box indicates the part of the channel the classification algorithm was applied to, with the results presented in the middle panel. Black pixels are indicative of both channels and the offshore area, with white pixels representative of wave breaking. The various behaviours observed (right panel) are presented, with each drift classified as either a linear exit (LE), circulation followed by an exit (C&E), circulation with no exit (CNE), or other (O). The right hand two bars represent overall behaviour, with Exit constituting the sum of LE and C&E behaviours, and No Exit the product of CNE and O behaviours.

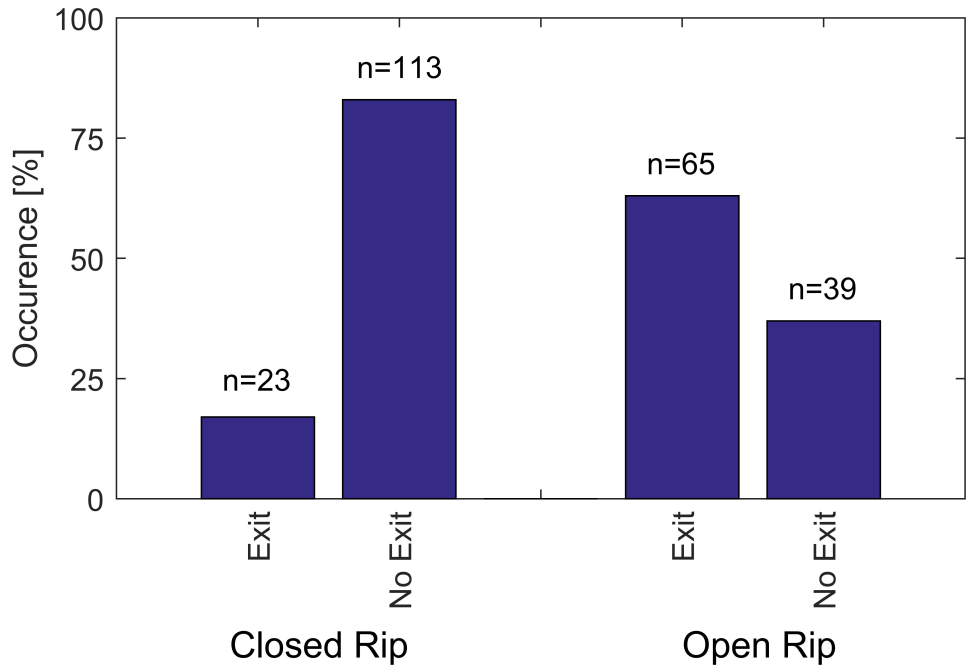

Figure 7.9: A summary of all behaviours observed during the 4-day field campaign at Perranporth, split into (left) closed and (right) open scenarios. Exits were defined as the sum of Linear exit and Circulation then exit scenarios, whereas the No Exit total was the sum of Circulation, no exit and Other scenarios. In total, there are 240 individual drifts classified.

flowed offshore in regions of wave breaking either side of the channel failed to exit the surfzone and instead recirculated onshore. In the closed rips, there was a consistent dominance of recirculation in the drifter behaviour. Conversely it may be expected to see a dominance of exits in the open channels; however, the opening of the channel appears only to increase the chance of an exit, rather than making surfzone exits the dominant form of circulation. For example, at times, despite the open channel, there were equal numbers of exits and recirculations (Figure 7.7f). Over the course of the experiment, the exit rate per drifter entry in open rip channels was 63 % (Figure 7.9), compared to 17 % in closed channels. Chi Squared analysis of the two channel conditions shows the difference in flow regimes to be statistically significant at 99.9 % confidence ($p < 0.001$).

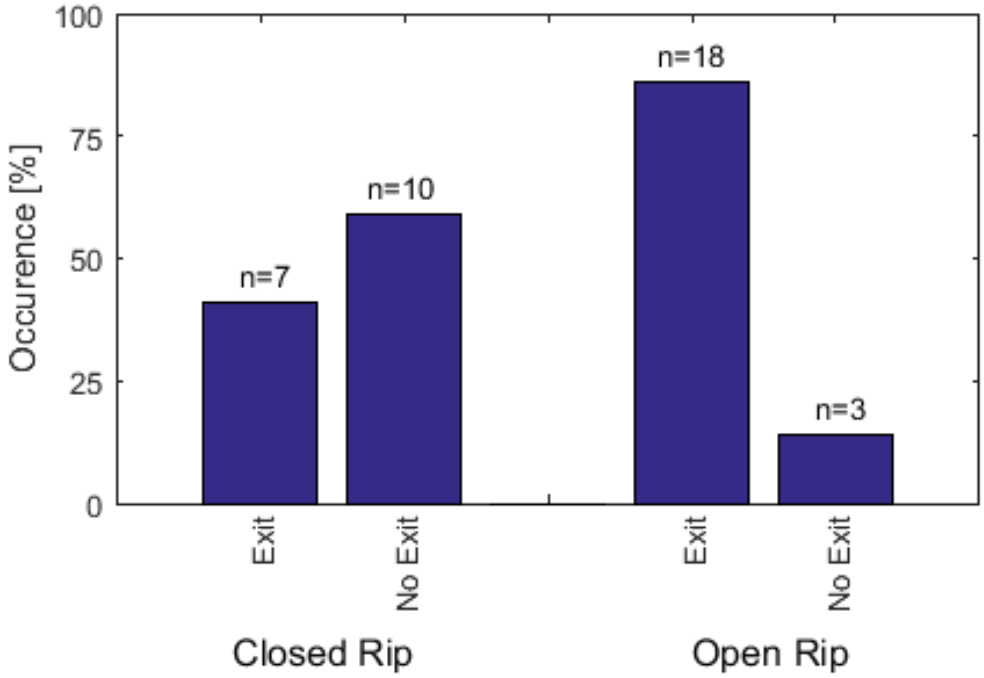

Figure 7.10: A summary of all behaviours observed during the 2-day field campaign at Ngarunui, split into (left) closed and (right) open scenarios. Exits were defined as the sum of Linear exit and Circulation then exit scenarios, whereas the No Exit total was the sum of Circulation, no exit and Other scenarios. In total, there are 38 individual drifts classified.

Open conditions at Ngarunui produced similar results (Figure 7.8d—f). At times, surfzone exit under open conditions reached 100 % per drifter entry (Figure 7.8e & f). Over the entire day, where open conditions persisted, rip exits were seen in 84 % of deployments (Figure 7.10), compared to retention in 16 % of cases. A repeat Chi Square analysis for Ngarunui data also shows the difference in responses under the two channel conditions to be significant at 99.9 % confidence ($p < 0.001$).

The dominance of surfzone retention under closed conditions coincides with higher current speeds and increased vorticity at Perranporth (Figure 7.11) and Ngarunui (Figure 7.12). The average offshore-directed drifter velocity under closed conditions at Perranporth was 0.59 $\pm$ 0.15 m s^{-1} (Figure 7.11a), which is a 31 % increase over open conditions, where average speeds were 0.45 $\pm$ 0.17 m s^{-1} (Figure 7.11b). A two tailed

t-test found the difference to be significant at 99.9 %. At Ngarunui, offshore directed drifter velocities under closed conditions was 0.53 ± 0.34 m s^{-1} (Figure 7.12a), an 83 % increase over open conditions where mean velocity was 0.29 ± 0.19 m s^{-1} (Figure 7.12b). The higher values in Perranporth closed rips ($\bar{U}' \approx 0.8$ m s^{-1}) were observed mid channel (Figure 7.11a), showing an increase in speed from the peripheral feeder zones to the rip channel itself. The trend was echoed at Ngarunui where $\bar{U}' \approx 0.85$ m s^{-1} in the mid-channel compared to $\bar{U}' \approx 0.4$ m s^{-1} in the feeder regions (Figure 7.12a). In open rips at Perranporth the lowest offshore-directed velocities ($\bar{U}' \approx 0.3$ m s^{-1}) were located at the onshore extent of the channel (Figure 7.11b), with velocities doubling as the current extends to the edge of the surfzone. Despite this increase in velocity offshore, the mean speeds at the edge of the surfzone are still lower than the average mid channel speeds of a closed current. Velocities at Ngarunui were seen to progressively decrease offshore in open conditions from $\bar{U}' \approx 0.4$ m s^{-1} to $\bar{U}' \approx 0.2$ m s^{-1} (Figure 7.12b).

Vorticity was also maximum in the closed rips at both sites. This was less pronounced at Perranporth where mean absolute vorticity in closed channels was 0.027, 8 % greater than open channels (0.025) (Figure 7.11c). At Ngarunui, there was a much more defined and coherent band of high vorticity under closed conditions (Figure 7.12c), with a mean absolute vorticity 0.02, 66 % higher than open conditions where mean absolute vorticity was 0.012. Standard deviations were high (± 0.018 and ± 0.014 respectively), with a t-test confirming the two populations were separate at 99.8 % confidence. A large band of strong ($\Gamma > 0.04$) anticlockwise circulation was evident in the feeder region (Figure 7.11c, $x = 550$ m, $y = -350$ m) of closed channels at Perranporth, whereas the coinciding region in open channels had a much more smaller band of anticlockwise circulation, albeit of comparable magnitude. This was also true of closed conditions at Ngarunui, where a strong anticlockwise rotation was observed to feed the main channel (Figure 7.12c, $y = 470$ m). In closed channels, there is a non rotational offshore flow through the middle which is coincident with the rip flow, but a large proportion of surfzone is characterised by strong rotational flow. Conversely, comparatively small areas of rotational flow exist in the open current, with a higher proportion of flow being linearly offshore. The effect of this strong rotation in closed channels is to promote

surfzone retention as drifters are deflected alongshore in the breaking waves. For Ngarunui, the absolute minimum vorticity is after drifters have exited the surfzone as they meander offshore.

At Perranporth, the patterns of wave breaking showed the propensity to change between open and closed channel scenarios on short (hourly) timescales, as a result of tidal modulation over the morphological template. This was well demonstrated on 17th May 2014 which was initially dominated by an open rip (Figure 7.4b), and a high proportion of drifters exiting the surfzone and minimal recirculation (Figure 7.4b: 1200—1238 hrs). However, by low tide (Figure 7.4b: 12:38—13:16 hrs), there was a well-defined closed channel, coinciding with the flow pattern changing to nearshore circulation without exits. As the tide level increased, the expression of the morphology produced an open channel (Figure 7.4b: 13:16—14:32 hrs) and the number of exits increased. For Ngarunui, the change was less tidally controlled and seems more linked to wave height. Open conditions persisted throughout the entirety of 10 Feb, and closed conditions persisted on the 11 Feb. Hydrodynamics remained largely unchanged, apart from an increase in wave heights from 1.5 to 2 m, which accompanied the transition from open to closed channels.

7.4 Discussion

The primary objective of this research was to quantify the effect of open and closed rip channels on surfzone exit rate. A rip that is visually classified as closed is likely to exhibit recirculatory behaviour. Wave breaking around the channel closes the rip, which increases the vorticity and the current speed resulting in the formation of a circulatory current which encourages surfzone retention. In open rips, the absence of wave breaking at the offshore extent of the rip channel decouples the offshore morphology from the rip channel circulatory system. A slower current then persists that extends offshore of the surfzone and increases the exit rate per drifter entry. Thus the likelihood of being ejected from the surfzone by an open rip channel is greater than that in a closed channel.

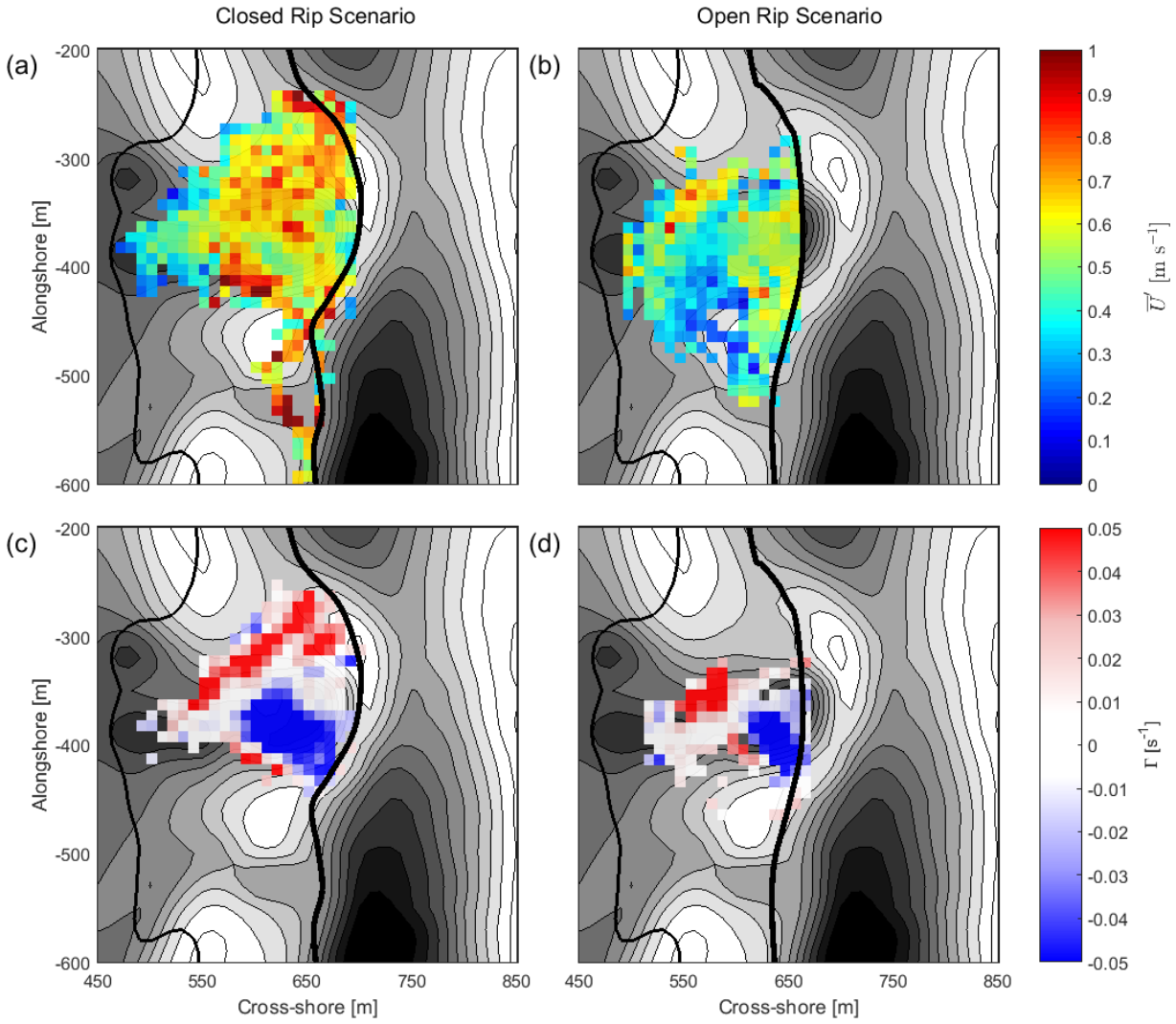

Figure 7.11: Offshore-directed current speeds (top) and vorticities (bottom), derived from surfzone measurements in closed (left) and open (right) rip channels at Perranporth. The thin black line is indicative of the mean shoreline position during deployments, with the thick black line indicative of typical surfzone limits in closed (a and c) and open (b and d) rip channels. In the vorticity plots, positive/red values show an anticlockwise horizontal rotation in the fluid, whereas negative/blue is indicative of clockwise rotation.

Patterns of wave breaking exhibited large differences over a single tidal cycle at Perranporth. At low tide, wave breaking is more likely to occur on the seaward edge of

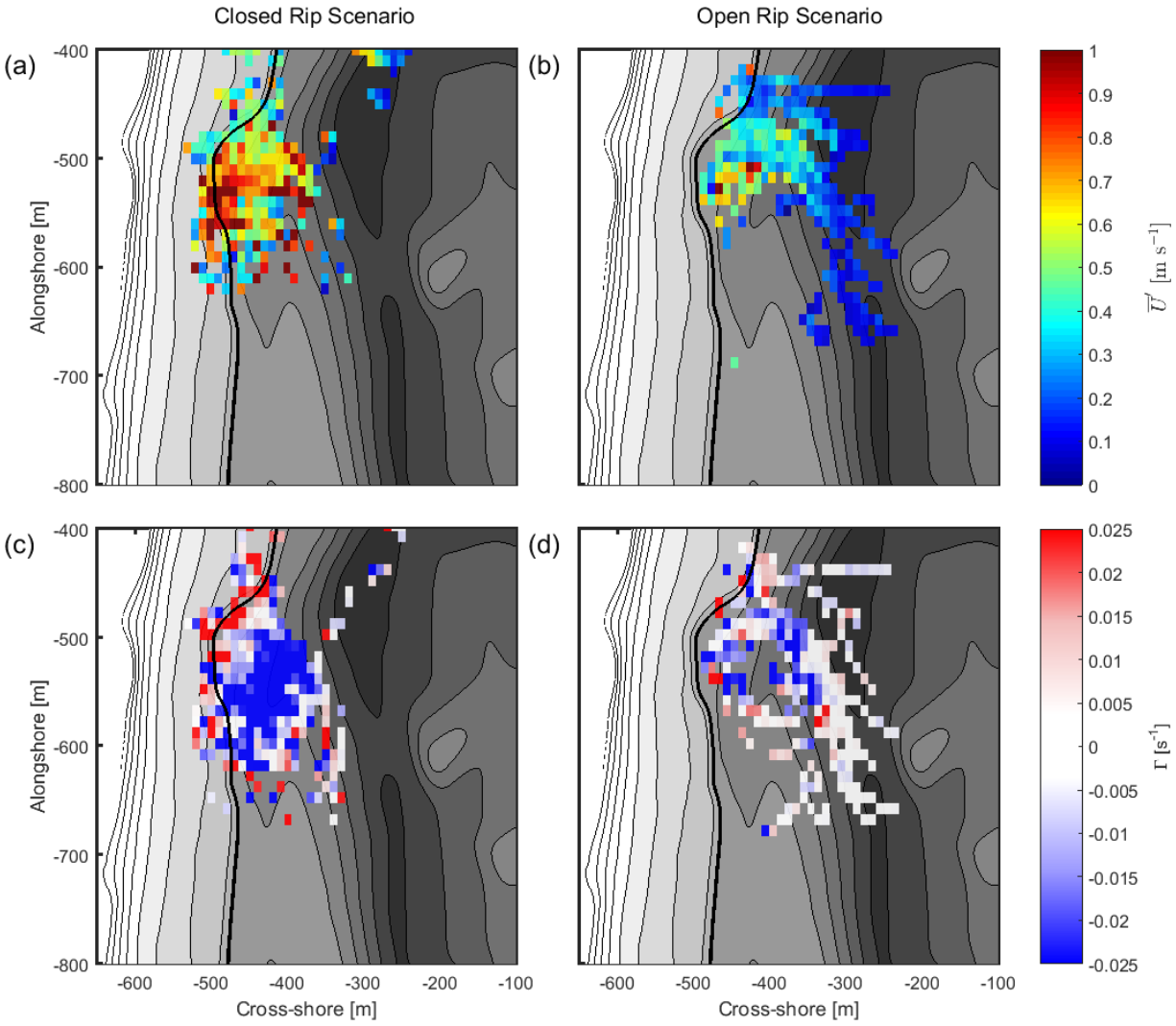

Figure 7.12: Offshore-directed current speeds (top) and vorticities (bottom), derived from surfzone measurements in closed (left) and open (right) rip channels at Ngarunui. The thin black line is indicative of the mean shoreline position during deployments. In the vorticity plots, positive/red values show an anticlockwise horizontal rotation in the fluid, whereas negative/blue is indicative of clockwise rotation.

the channel resulting in a visual classification as a closed rip, increasing the likelihood that the rip will form eddies and drifters will be retained in the surfzone. As water level increases towards mid - high tide, the water depth over the rip head bar is generally too

great to induce wave breaking, resulting in a system whereby the rip can be visually classified as open. Under closed conditions, there is also an increase in wave breaking on the adjacent bars in addition to the rip head bar feature, which ultimately reduced the extent of the channel through lateral constriction, whereas the decrease in breaking in open channels lowers wave-current interaction and increases the offshore extent of the rip (Yu and Slinn, 2003). In open channels, the offshore directed current speeds were seen to be 31 % lower, consistent with work by Brander and Short (2000), linking lower intensity breaking to lower velocities through morphodynamic scaling. Another control on this transition is that of wave heights, which appeared to be the primary driver of transition between open and closed conditions at Ngarunui. An increase in wave heights also had the effect of inducing wave breaking further offshore and increasing the width of the surfzone. This meant wave breaking extended beyond the end of the rip channel, resulting in a closed rip. The nett result was the same as invoked by lower tide levels at Perranporth, where breaking across the end of the rip channel created a strong rotational circulation, and subsequently retained most drifters within the surfzone. At lower wave heights, the surfzone width narrowed and wave breaking was not induced offshore of the rip channel, allowing the current to flow freely out of the surfzone. This results in reduced vorticity through reduced wave-current interaction, and a flow regime that promotes surfzone exit.

The observed circulation patterns in this study are consistent with those of Brander (1999) who placed rip dynamics into the context of the Wright and Short (1984) beach state model. They use the underlying morphology over timescales of days to months, whereas this study has discussed the expression of the morphology in terms of patterns of wave dissipation over a single tidal cycle. They describe the transition from longshore bar-trough morphology (LBT), through a rhythmic bar beach (RBB), a transverse bar rip beach (TBR), to a low tide terraced beach (LTT). The LBT-RBB scenario is akin to the open channel described here, with an open connection beyond the surfzone. The feeder channels described for LBT are less obvious or established in the imagery used in the current study, but the gap in the bar is obvious (Figure 7.7e—f; Figure 7.8d—e). The TBR/TBR-LTT states are akin to closed channels observed in imagery (Figure

7.7a—d; Figure 7.7a—c). The state is characterised by a complete welding of the rip head bar to the adjacent longshore bars. They also note a constriction and increased flow during the transition from LBT [open] towards TBR-LTT [closed]. As progression through the beach states is made, one feeder channel reduces in strength with the opposite channel becoming the dominant feeder for the rip. This mirrors observations at both sites where the rip channel was predominantly fed from one side (Figure 7.3c). Austin et al. (2010) discuss similar transitions as a result of tidal fluctuations, whereby lowering water levels result in the constriction of the channel. Unlike the present study, they show that conditions here described as closed exist without the presence of a rip head bar and suggest that wave-current interactions are an important process at the seaward end of the channel under these conditions.

An increase in vorticity has been demonstrated through the channel under closed conditions, with vorticity maxima towards the outer edge of the surfzone (Figure 7.11c and 7.12c). Austin et al. (2014) demonstrated that around low tide, when conditions could be considered closed, that water surface gradients were greatest around the rip neck and over the end of the longshore bars. This difference in water surface gradients ($O(0.1$ m)) could be a factor controlling the much increased vorticity through the neck of the rip and over bars observed in Figures 7.11c and 7.12c. Overall, velocities in the closed rips were much greater (Perranporth - 31 %; Ngarunui - 83 %) than open channels (Figure 7.11a, Figure 7.12a, and Figure 7.13a). This is in contrast to the findings of Austin et al. (2014), whereby rip flows were maximised either side of low water. In their study they describe the drying of the feeder and bars, which was not observed here. Therefore, it is likely that the absolute water levels of closed rips in this thesis and the Austin et al. (2014) conditions of maximum flow were similar. Alongshore-averaged cross-shore velocities are fairly consistent across the surfzone at Perranporth, with a slight tail off at the offshore extent (Figure 7.13a). This decreasing velocity was coincident with the location of maximum negative (clockwise) vorticity, potentially explained by wave-current interaction at the offshore extent. Yu and Slinn (2003) demonstrated that in narrower [closed] channels interaction at the offshore extent of the current with the incident wave field was greatest, reducing the strength and extent of currents. This

shows agreement with the results of this thesis, that showed a reduction in exits (Figure 7.9) and current speed at the offshore extent (Figure 7.13a). The association between increased wave breaking and increased vorticity was observed before (Houser et al., 2013), where higher intensity breaking narrowed the available area for the rip channel, which has previously been linked to increased flow speeds (MacMahan et al., 2006). In terms of circulatory patterns, a closed rip here behaves in a similar fashion to the low tide factor rips in the study of Scott et al. (2014), where currents were fed predominantly by one alongshore direction. Here, the current was directed offshore (positive vorticity band in Figure 7.11c and 7.12c), and as it reached the edge of the surfzone it was again directed alongshore in its original direction (negative vorticity in Figure 7.11c and 7.12c).

The variation in current speeds and vorticity between open and closed channels may have important implications for sediment transport in the nearshore. Recent research has shown that the dominant driver of sediment suspension and transport in rips is as a result of mean offshore flows (Orzech et al., 2011; Thorpe et al., 2013), with very low frequency (VLF) motions also playing an important role in entrainment and transport of sediment in rips (Aagaard and Greenwood, 1995). Results of this study show increased mean offshore flows under closed channel conditions, and based on these previous studies it is possible to infer that more sediment was suspended under these conditions. However, the vorticity in closed channels was much increased and the dominant circulation pattern was that of surfzone retention. Therefore, under closed conditions, it may be possible that despite the entrainment of greater masses of sediment, the net cross-shore exchange between the surfzone and nearshore is reduced than when compared to open channels. In an open channel, although the flow velocity is reduced (yet not insignificant), the dominant circulatory behaviour is that of surfzone exit, which may be responsible for a greater net offshore mass transport of sediment. This area is certainly worth investigation as part of future studies, as no quantitative measure of sediment transport was made here.

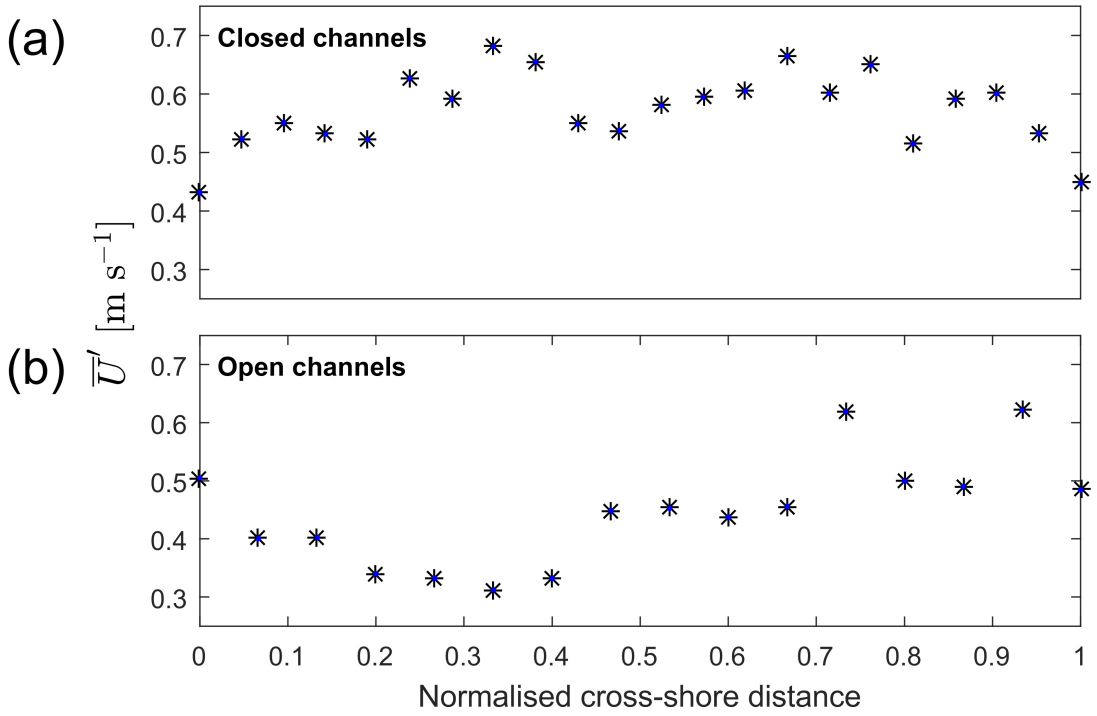

Figure 7.13: Alongshore-averaged, cross-shore velocity profiles for closed (top) and open (bottom) rips at Perranporth. All alongshore observations have been accounted for at each cross-shore location. The cross-shore location is normalised between minimum and maximum extents of the surfzone in closed and open channels respectively. Normalisation was necessary as typically, the surfzone under open conditions was approximately 25 % narrower.

7.5 Conclusions

The effect of wave breaking on rip current circulation was investigated using a novel wave breaking parameter defined from video imagery at two hydrodynamically diverse study sites. The study was complemented by Lagrangian drifter data that showed closed channel conditions increased the intensity of wave breaking, narrowed the effective channel width and increased both current speed and vorticity in the channel. This promoted surfzone retention and a low exit rate per drifter entry (0—40 %). Under open

channel conditions, the offshore extent of drifter tracks extended beyond the surfzone under a steady, slower current with much reduced vorticity. The likelihood of surfzone exits increased, with a maximum exit rate during one period reaching 100 %. In the closed channel scenario surfzone retention dominates the nearshore flow regime. However, when the rip channel configuration is open it increases the likelihood of exits, albeit with no guarantee that surfzone exits will be the dominant flow regime. A Chi Squared analysis showed that open channels were statistically more likely to result in rip exits, compared to closed channels. Furthermore, this thesis hypothesises that increased flow conditions under closed conditions may entrain more sediment, but the circulatory nature of the flows may ensure that any subsequent transport is more confined to the surfzone than would be the case in open circulations.

Chapter 8

Quantifying rip current hazard

8.1 Introduction

Rip currents are a coastal hazard on beaches worldwide (Brander and Scott, 2016), and have been heralded as the greatest hazard to beach bathers (Brander and MacMahan, 2011). Rips are attributed to the majority of incidents attended by beach lifesaving organisations around the world, with 68 % of incidents in the United Kingdom (Scott et al., 2008), 81 % in the United States (Brewster and Gould, 2014), and at least 57 % in Australia (Brighton et al., 2013; Brewster and Gould, 2014) occurring as a result of rip currents. Given the large loss of life attributed to rip currents, and the burden on the resource of surf lifesaving organisations, understanding and predicting rip current hazard is of paramount importance.

A brief summary of past literature dealing with this topic was presented in Section 2.4, summarised below. Education is seen as a key requirement in reducing the number of people caught in rip currents each year (Leatherman, 2011), as there is a lot of misinformation surrounding the dangers. For example, there is widespread misconception that rip currents will pull you under the water (Gallop et al., 2016b), which could induce panic in someone caught in a rip. Demographics of beach users can

also be a factor in considering risk. Young males are reported to be at high risk of rip rescue at Perranporth (Woodward et al., 2013), and worldwide (Gensini and Ashley, 2010; Brighton et al., 2013). This is typically attributed to young males undertaking more high risk behaviour. Despite quantifications of hazard and risk, one of the most important survival factors in rip current incidents is the victim's selected escape strategy, which links back to education. The historic advice for escaping a rip was to swim parallel to the shore (Brander et al., 2011; Miloshis and Stephenson, 2011), but recent Lagrangian experiments have shown that rip currents can at times recirculate back to shore or propagate at oblique angles to the shoreline (Schmidt et al., 2003; Austin et al., 2009, 2010, 2014; MacMahan et al., 2009, 2010; McCarroll et al., 2014; Scott et al., 2014), and therefore, a more effective escape strategy may just simply be to tread water and stay afloat (MacMahan et al., 2010). Hydrodynamic analysis, in terms of quantifying wind/wave/tide conditions, surrounding rip incidents is a useful first order predictor of rip current hazard. For surf beaches in SW England (including Perranporth), Scott et al. (2014) showed that incidents predominantly occurred around MLW, under low (< 1 m) wave heights, with shore normal waves and low wind speeds. No such analysis has been done for Ngarunui (or New Zealand beaches in general), and therefore the conditions resulting in most rip rescues here remain unknown. Despite the ability of hydrodynamic indices to partly explain occurrence of rip incidents, they are unable to make any inference about flow conditions (i.e. exiting or recirculatory flow). Following the finding in Chapter 7 that wave breaking patterns can be related to rip current flow regimes, it may be possible to associate documented rip rescue events with these same observed wave breaking patterns.

Therefore, the overall objective of this chapter is to identify the wave breaking conditions most conducive to formation of hazardous rip currents at two sites; the macrotidal, intermediate, low tide bar/rip beach at Perranporth, and a contrasting mesotidal, double barred high energy beach at Ngarunui. No previous research has been done at Ngarunui on rip hazard or rescues, and therefore in order to ensure rip rescue events at both sites are comparable, the first two sub-objectives are: (1) To compare victim demographies between Perranporth and Ngarunui; and (2) To investigate the high-hazard

hydrodynamic conditions at Ngarunui for comparison to Perranporth, in order to ascertain overall similarity of high risk scenarios. Finally, having ascertained that the two sites are suitable for comparison, the final sub-objective is as follows: (3) To investigate the link between open and closed rip channel conditions and rip current rescue statistics.

8.2 Methodology

Here, rip incident data from both Ngarunui and Perranporth is considered for further analysis. The two sites were selected as they both have long (> 5 years) records of rip rescues events, recorded by beach lifeguards. They also represent hydrodynamically different study sites; Perranporth is a macrotidal, low tide bar/rip beach whereas Ngarunui is a mesotidal, double barred high energy beach.

8.2.1 Rip incident data

Ngarunui

Rip incident date were supplied for Ngarunui by SLSNZ for Oct 2010—Apr 2015. The data is recorded by lifeguards for all beach interventions they are involved with (e.g. rescue, advice, etc.) and is stored centrally on SLSNZ's Patrol and Membership's Database. For each incident, lifeguards report on confounding factors to the rescue (rip currents, strong surf, strong winds, weak swimmer, etc.), as well as demographic data (age, sex, area of residence). The Ngarunui record refers to rescues of swimmers, defined as people in the water without any form of craft (i.e. bodyboard), or bodyboarders/surfers, grouped together to mean anyone in the water using some form of flotation device or craft (i.e. surfboard). Of particular use in the SLSNZ record is a narrative that is complete for ≈ 90 % of rescues, offering some background to the incident. Of 258 rescue events during the period, 212 (82 %) were attributed, at least in part, to rip currents. Of these 212 rip-related rescues, video imagery was available for

196. Each of the images for the 196 rescues was classified as open or closed, in the same manner as for Perranporth. Unlike Perranporth, no published data on Ngarunui deals with tidal heights for rip activation and therefore all tidal levels were considered. The primary bathing zone at Ngarunui is located in front of the SLSNZ surf shack (Figure 4.6c; x = -550 m), with the most temporally persistent rip located south of the bathing zone by approx. 100 m (Figure 4.6c; x = -450 m). This rip was usually visible in the imagery, with an occasional well-developed rip presenting at x = -650 m (approx. 100 m north of the bathing zone).

Perranporth

Rip incident data were supplied for Perranporth by the RNLI for 2009—2013. The RNLI record an incident every time they intervene. They record time and location, demographic data, qualitative observations of meteorological and hydrodynamic conditions and, crucially, information on the cause of the incident (e.g., inexperience, rip currents, tidal cut off, etc.). The RNLI also record the victim activity in terms of swimmers, but they split bodyboarders and surfers into two separate categories. Of all recorded incidents at Perranporth, 250 (some of which were for multiple persons) were attributed at least in part, to rip currents. During these incidents, there were 400 people rescued and assistance was given to a further 215 people. The RNLI estimates that without intervention, 16 lives would have been lost over the 5-year period at Perranporth. For each incident, the rip channel was classified as open or closed from timex images (if images were available). Of the 250 incidents, 185 were used for image classification and 65 incidents were disregarded as a result of either fouled images or their occurrence at mid- to high-tide. Austin et al. (2014) showed that rips on Perranporth are inactive when water depths are above 3 m, and thus, incidents during these periods have been omitted from further analysis. Of the remaining 185 images, 82 were classified as closed and 103 as open. A limitation of the RNLI dataset is that the exact location of rescues in relation to the surfzone morphology is not recorded. For each incident, the lifeguards report an approximate alongshore zone (generally 50 m-wide) of the incident relative to their primary position. Rip spacing at Perranporth is typically

O(400m), which means the approximate rescue location supplied by the lifeguards is sufficient to estimate rescue location, in relation to a specific rip channel. The rip channel chosen for the field experiment is one of the most persistent topographic rip channels at Perranporth, present over a number of years in the imagery with a total alongshore oscillation over an area no greater than 400 m. The RNLI dedicated bathing area is generally located $\approx$ 250 m alongshore from this prominent rip.

8.2.2 Hydrodynamic analysis

Analysis on the frequency distribution of rescue events was compared to the frequency distribution of background hydrodynamic parameters, following Scott et al. (2014). All frequency distributions were normalised, such that the sum of all values in the distribution is equal to one. The hydrodynamic parameters that have been compared are the low water height (LW), significant wave height (H_s), peak wave period (T_p), wave direction (θ), and wind speed (U). For each comparison, the background normalised frequency distribution (F_N) has been calculated from the entire 5 year time series co-incident with the rip incident database. Thereafter, a new F_N is calculated, using only the subset of data taken from each of the rip incidents. Subtraction of the background F_N from the subset F_N offers an indication of any control exerted by that particular hydrodynamic parameter on rip rescue events. If the two distributions were even (i.e. rip rescues were normally distributed), the resulting number would be zero. When a positive number is returned, this is indicative of more rip rescues occurring for that given threshold than would be suggested by the frequency distribution of the background data, and conversely, a negative value reflects less rescue occurring than would be expected.

8.3 Results

This section presents analysis of rip current rescue demographics and hydrodynamics at Ngarunui, followed by application of the wave breaking pattern parameter to both

Ngarunui and Perranporth. The hydrodynamic high risk/hazard scenarios for Perranporth have been categorised in previous research(Scott et al., 2014), and therefore the research does not feature in this Results section, but will be introduced as part of the Discussion.

8.3.1 Demographics

RNLI rip incident data between 2009—2013 shows bodyboarders to be the most at risk from rip currents, accounting for 76 % (n = 183) of rescues (Figure 8.1a). Swimmer and surfer rescues account for 12 % (n = 29) of rescues each. At Ngarunui, investigation of demographic data within the SLSNZ database for 2010—2015 showed the most at risk group to be swimmers, whom were associated with 63 % of rescues from rip currents (Figure 8.1b). All remaining rescues (37 %) involved surfers or bodyboarders. From the lifeguard's qualitative remarks on rescues, one such observation shows the majority of rescues (56 %) involve people rated as either good or strong swimmers, and exhaustion was seen to be a factor in 35 % of rescues.

In terms of rescues by age and sex, 74 % (n = 572) of people rescued at Perranporth were male (Figure 8.2a). Male adults were the most populous group, accounting for 37 % of all rescues, followed by male teens (23 %), male children (14 %), female teens (10 %), female adults (9 %), and finally female children (7 %). At Ngarunui, the majority of rescue victims were male (67 %), with the most at risk age group being that of 16—30 yrs old (Figure 8.2b). Males in this age bracket account for 39 % of all rescues, whereas the combination of male and female rescues in this age group account for 60 % of all rescues.

8.3.2 Hindcast hydrodynamics - Ngarunui

A comparison of all rip incidents, and a subset of mass rescues (> 3 people rescued simultaneously) has been presented for all hydrodynamic parameters. This analysis is first applied to LW level (Figure 8.3). In both the complete and mass rescue datasets, there is a dominant occurrence of rip rescue when LW ≈ -1.5 m, between MLW and

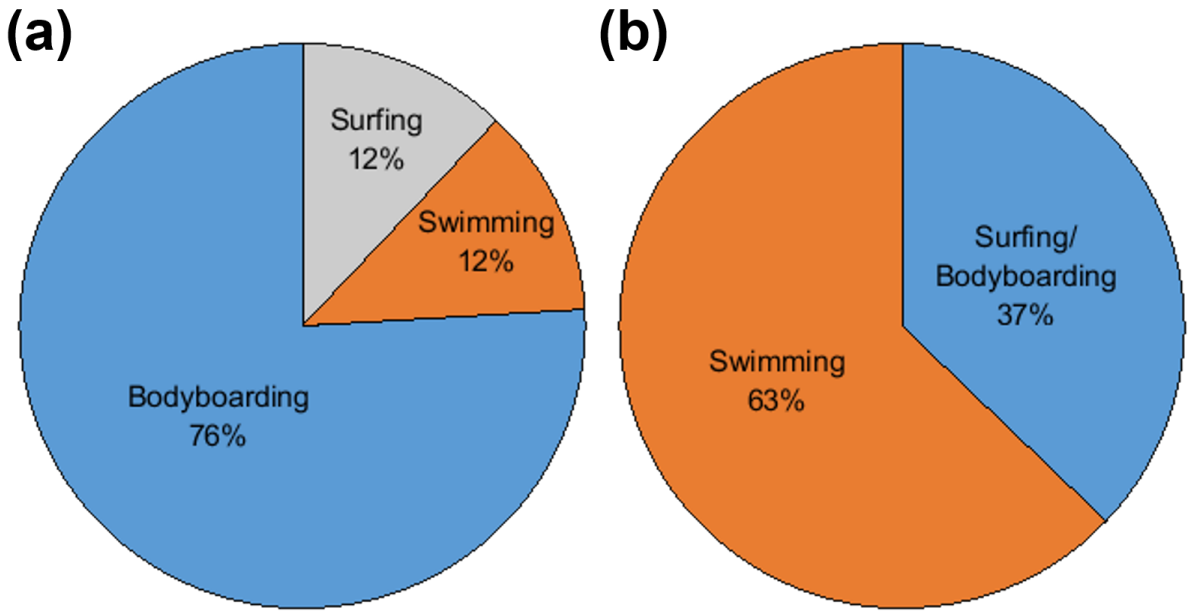

Figure 8.1: Victim activity for rip rescues at (a) Perranporth (2009—2013); and (b) Ngarunui (2010—2015). Rescue events involving surfers or bodyboarders at Ngarunui are amalgamated into one category by the lifeguards, hence the difference in the two charts.

MLWS. For MLWS and MLWN, rip incident occurrence is similar to the background frequency, indicating no increased likelihood of rip rescue under these conditions. There is a notable lack of rip rescues for times when LW is at or around MLW (i.e. the middle of the spring - neap cycle).

A significant proportion of rescues occur under average wave conditions ($H_s \approx 1.5$ m), with very few occurring when wave heights exceed 3 m (Figure 8.4a). For mass rescues, wave conditions between 1.5 m and 2 m are most conducive to the initiation of a rescue event (Figure 8.4b). More rescues occur under lower than average (≈ 10 s) period waves (Figure 8.4c—d), which in combination with H_s findings likely indicates that small, steep waves are responsible for hazardous rip formation at Ngarunui.

Incident wave data for offshore of Ngarunui show that waves predominantly approach at oblique angles, promulgating north along the coastline. The headland at the southern end refracts waves back to a near shore-normal orientation as they approach Ngarunui

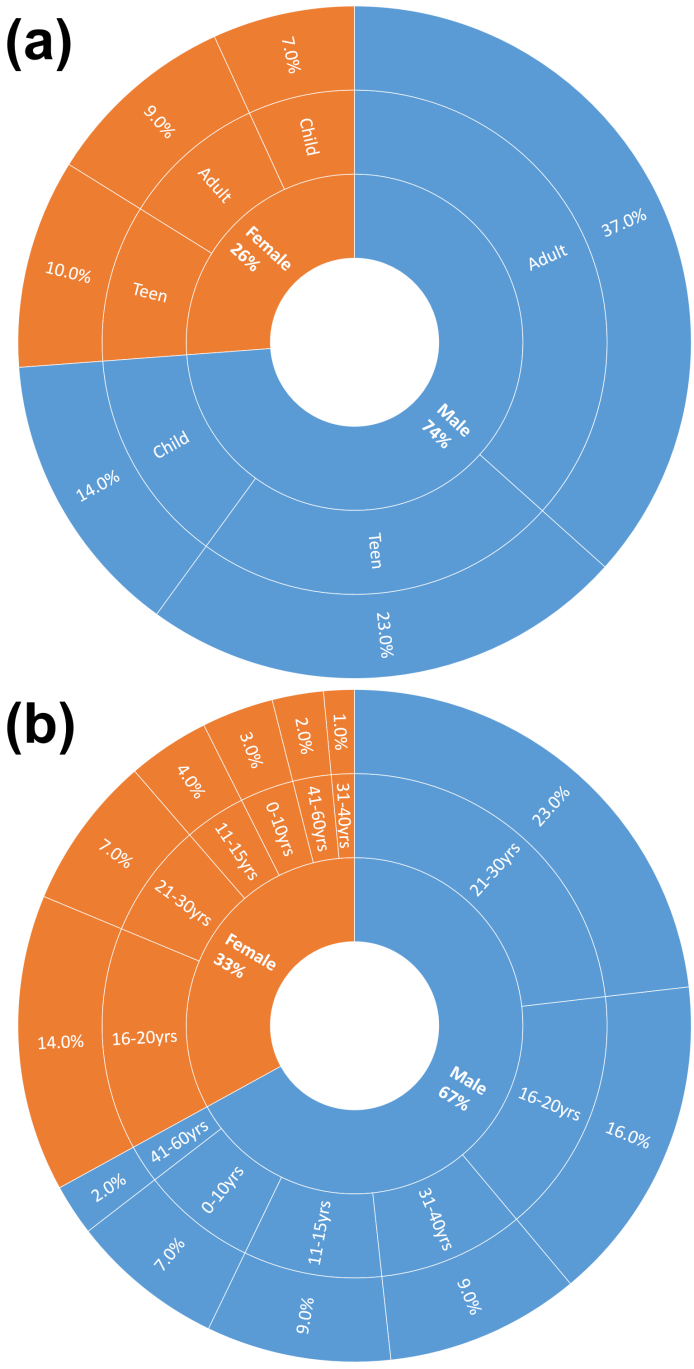

Figure 8.2: Distribution of rescue events at Perranporth (a) for the period 2009—2013; and (b) Ngarunui for the period 2010—2015, broken down by gender and age.

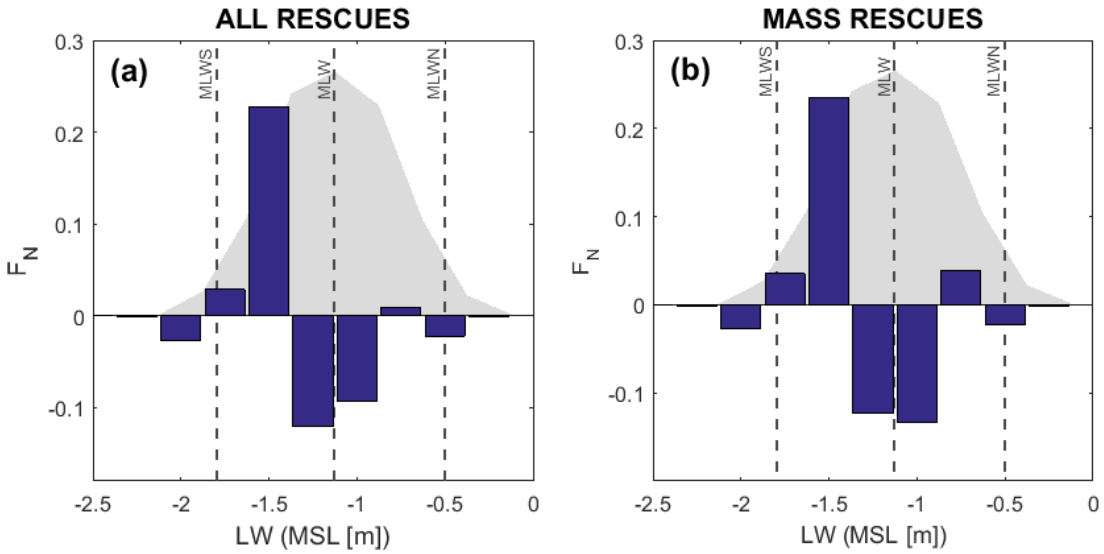

Figure 8.3: Normalised frequency distribution F_N of LW heights over a 5 year period (grey area). Blue bars indicate the difference between incident LW F_N (the distribution of LW heights on days when rip rescues occurred) and background F_N. Positive values indicate a greater proportion of rescues occurred at that LW level than would be expected when compared to background F_N, and negative values represent less rescues than expected for a given LW. All rip incidents are presented (a), as are a subset based on mass rescues where 3 or more people were rescued at once (b). Dashed lines show Mean Low Water Springs (MLWS), Mean Low Water (MLW), and Mean Low Water Neaps (MLWN).

itself (Section 3.3). As a result, modelled offshore wave data is less useful at giving an indication of wave conditions on this beach. However, it does appear that greater angles of wave incidence result in more rip rescues (Figure 8.4e—f), with more shore-normal approaches under represented in the rip incident record.

Overall, rescues occur predominantly under low wind speed conditions ($U < 5$ m s^{-1}) (Figure 8.4g). However, for mass rescue events, there is a marked dominance of rip rescues at wind speeds of less than 2 m s^{-1} (Figure 8.4h).

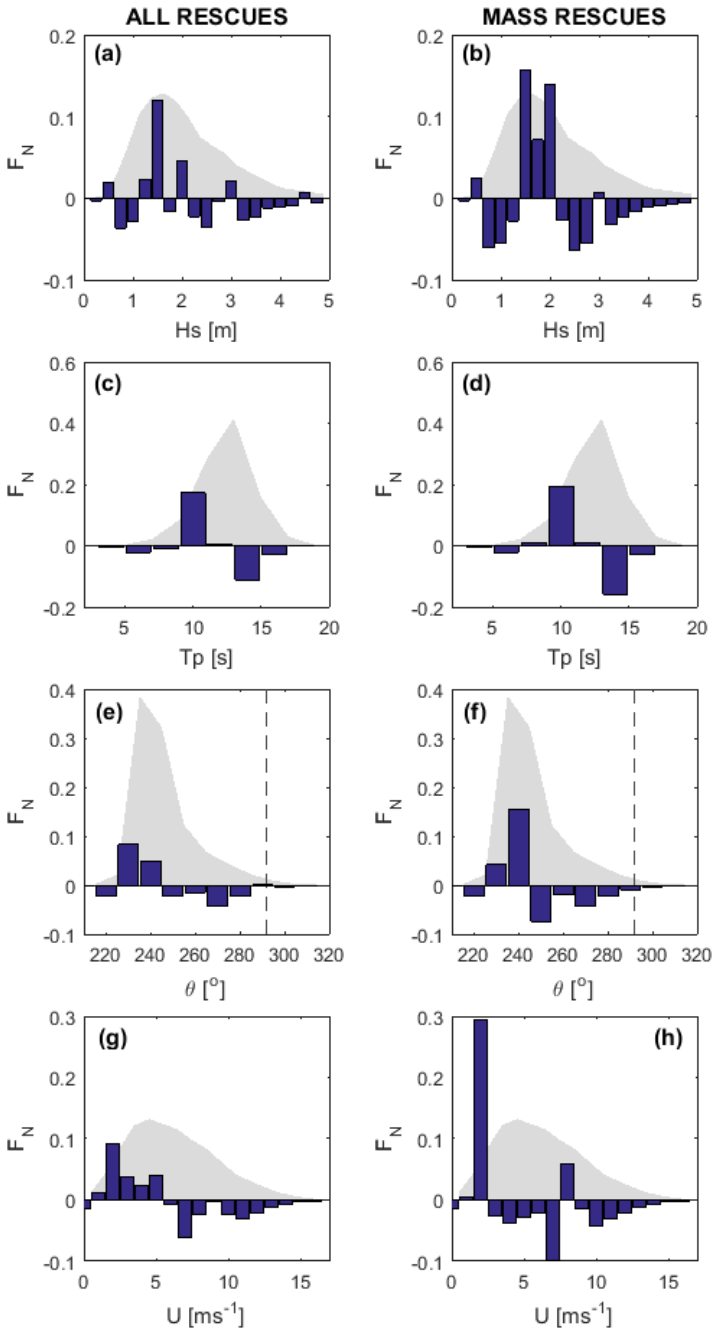

Figure 8.4: Normalised frequency distribution F_N of: (a & b) H_s; (c & d) T_p; (e & f) wave direction θ; and (g & h) wind speed U over a 5 year period (grey area). Blue bars indicate the difference between incident F_N (the distribution on days when rip rescues occurred) and background F_N. Positive values indicate a greater proportion of rescues occurred at that value than would be expected when compared to background F_N, and negative values represent less rescues than expected for a given value. All rip incidents are presented, as are a subset based on mass rescues where 3 or more people were rescued at once. Dashed line (e & f) show shore normal wave direction.

8.3.3 Wave breaking patterns

Ngarunui

Lifeguard rescue data from Ngarunui, over the 2010—2014 lifeguarding seasons identified 199 rescues for which video imagery was available. Twenty-two usable mass rescue events were identified at Ngarunui; one mass rescue was omitted from further analysis as the lifeguard narrative stated that it was the result of a flash rip, and it would not therefore be appropriate to attempt to classify the wave breaking pattern as the rip was not morphologically controlled. Open channel morphologies were identified for 62 % (13) of these events, whereas closed channel morphologies occurred in 38 % (8) of the events. In terms of the total number of people rescued during mass rescues, 56 % (55) were rescued from open channels, and 44 % (43) were rescued from closed channels.

The trend is mirrored in the overall dataset, although the number of rescues overall is much closer (Table 8.1). There were a total of 100 rescues (53 %) from open channels, and 89 (47 %) from closed channels. The balance of activity being undertaken by each rescued person is fairly even between both open and closed rip channels, with slightly more swimmers (53 %) rescued from closed rips but slightly more surfers (59 %) rescued from open channels (Table 8.1). Of note is that in 63 % of closed channel rescues, strong surf was a factor, which fits with closed channels forming under larger wave conditions. The balance of exhaustion and victims rated as poor swimmers was fairly even balanced between both open and closed channel rescues.

When considering the prevalence of open and closed channels at Ngarunui, images from guarded hours (1100—1600hrs) in a single lifeguard season (1 Oct 2014—31 Mar 15) were classified. Of 1,905 images classified, rip channels were visible in 1,712 images. Closed channels persisted 63 % of the time (1087 images), compared to 37 % (625 images) occurrence of open channels. Using this as an overall estimate of the prevalence of open and closed rip channels, the data can be normalised as per equation 8.1:

Table 8.1: Analysis of rip incident data for Ngarunui Beach between the 2010 and 2014 seasons. For each reported incident, the contemporaneous image was located and the rip channel classified as open or closed. Below is a summary of the type of rescues, activity and the narrative of confounding factors recorded by lifeguards.

		Activity		Confounding Factors		
Channel classification	Rescues	Swimming	Surfing	Strong Surf	Exhaustion	Poor Swimmer
Open	100	54	41	30	30	42
Closed	89	61	28	50	38	46

$$\frac{{}^{B_o}/_{B_r}}{{}^{A_o}/_{A_r}} \tag{8.1}$$

where B and A represent closed and open rip channel conditions respectively, o is the occurrence of each condition and r is the number of rescues in each condition. When Equation 8.1 is applied to the Ngarunui dataset, based on occurrence and rescues in each channel type, open channels are found to be twice as dangerous (1.95) when considering the likelihood of inducing a rip rescue event.

Perranporth

RNLI rescue data for the period 2009—2013 showed 25 incidents when 5 or more people were rescued, or where the RNLI predicted there would have been loss of life without intervention. The threshold is higher at this site to achieve a comparable number of large scale rescue events. Of the 25 major incidents, 18 were analysed. Of the seven discarded, three high tide incidents were outside the scope of the study based on the rip activation threshold at Perranporth following Austin et al. (2014), two major incidents occurred > 1000 m from the lifeguards and an additional two incidents occurred during a time when the camera lens was fouled. Incidents predominantly occurred during British school summer holidays (Jul—Aug), with most incidents occurring between 23 Jul and 23 Aug

Table 8.2: Analysis of rip incident data for Perranporth Beach between 2009 and 2013. For each reported incident, the contemporaneous image was located and the rip channel classified as open or closed. Below is a summary of the type of incident, and the narrative of confounding factors recorded by the lifeguard.

	Type of incident			Involving		
Channel classification	Lives saved	Rescue	Assistance	Body boarder	Swimmer	Inexperience
Open	10	169	81	97	18	35
Closed	3	122	104	30	2	16

2013. In this time, there were 6 major incidents, with a total of 49 people rescued and 5 lives saved.

Open channel morphologies were observed in 78 % (14) of the major incidents, compared to 22 % (4) incidents occurring under closed channel configurations. Of these 14 open rip major incidents, the RNLI rescued 85 people and saved the lives of 10, in comparison to 32 rescues and 3 lives saved under closed conditions. This trend in major incidents is echoed in the incident record as a whole (Table 8.2), where there were a total of 169 (58 %) rescues from open rip channels during the 5 years, compared to 42 % from closed channels. Of all the lives saved, 77 % were from open channels. When considering incidents involving body boarders, 76 % of rescues occurred in open channels. Rescues involving swimmers echo a similar trend, with 90 % (18 incidents) of swimmer rescues occurring in open channels. The RNLI cited inexperience as a factor in 35 incidents in open channels, compared to only 16 in closed channel scenarios (Table 8.2). An analysis of one lifeguarding season's worth of data (May—Sep 2013) showed that open rips occurred in 109 (40 %) of images, whereas closed rips occurred in 163 (60 %) of images. Using Eq 8.1 it is possible to quantify that open rips are twice (2.08) as dangerous as closed rips. Here, no information was available on the number of beach users at each time, and therefore exposure to the hazard was assumed to be uniform throughout.

8.4 Discussion

8.4.1 Demographics - Ngarunui

Analysis of victim demographics for both sites showed that in excess of two-thirds of rescues were attributable to males. This is similar to results from the UK as a whole [63 % were male victims] (Woodward et al., 2013), Australia [65 % of cases where gender reported] (Brighton et al., 2013), and America [84 % of all rip related fatalities] (Gensini and Ashley, 2010). Most likely to be involved in a rescue at Perranporth were male adults. At Ngarunui, the most at risk were young males, with the two most populous age groups being males aged 21—30 yrs (23 %), and 16—20 yrs (16 %). The Ngarunui finding is comparable with previous studies such as Woodward et al. (2013) who found that teenage males were most at risk in the UK. At Ngarunui, young people (16—30yrs) of both genders in total accounted for 60 % of all rescues. The finding that adults at Perranporth were most at risk is likely a result of the classification of adult, taken to mean anyone over 18 years, which would encompass most of the 'young people' (16—30 years) group quoted by SLSNZ. The primary activity that resulted in rip current rescue at Ngarunui was swimming (63 %), which is in agreement with analysis from Australia (83 %) (Brighton et al., 2013). It was in contrast to findings for Perranporth, where 76 % of rescues were bodyboarders. Perranporth appears representative of UK-wide data that showed bodyboarding incidents (52 %) to account for double the number of swimming related rescues (Woodward et al., 2013).

8.4.2 Hydrodynamics - Ngarunui

In terms of hydrodynamics, there was over-representation of rip rescues either side of spring tides, which decreased sharply towards the middle of spring-neap cycle (MLW) and also at the spring tides themselves (Figure 8.3). This increase in the proportion of rip rescues under the lowest water levels is likely a result of the sub-tidal, rather than inter-tidal, nature of the rip morphologies. The lower water levels increase the interplay

of breaking waves with the morphology, and likely correspond with maximum wave dissipation over the rip channelled area, resulting in increased flows. Austin et al. (2014) found similar results at Perranporth, where maximum flows were observed either side of the lowest water levels. They also reported that at the lowest observed levels, the bar/rip region intermittently dried, closing down rip circulation, which may go some way to explaining the under-representation of rip rescues at the lowest observed low water levels here. There was no discernible difference in the occurrence of mass rescues and all rescues with regard to LW conditions at Ngarunui. The findings in this thesis contrast those of Scott et al. (2014), where a maximum rip occurrence was reported directly on MLW, in the middle of the spring-neap cycle. A likely explanation for this difference is the contrasting tidal regimes. At spring tide, Perranporth has a tidal range of > 6 m, and a wide 500 m intertidal zone. Scott et al. (2014) cites surfzone stationarity in the transition period between spring and neap tides as a reason behind the increased rip activity. The effect is a much reduced intertidal zone, and therefore exposure to the nearshore rip morphology is prolonged. At mesotidal Ngarunui, the intertidal is typically < 150 m and therefore the tidal translation rate is much reduced. This reduction in tidal translation increases exposure time to all cross-shore locations when compared against Perranporth. Typical bar/rip channel configurations at Ngarunui are around -2.5 m MSL, and the high frequency rip rescue events are occurring when LW are around -1.5 m MSL. This in effect places the rip channel morphology right at the typical bathing/swimming depth ($\approx$ 1—1.5 m), and maximises exposure to it, resulting in more rescues.

The majority of rescues occur during mean wave height conditions ($H_s \approx 1.5$ m) (Figure 8.4a). Research suggests that rip velocities increase with increasing wave heights (MacMahan et al., 2010), but crucially, that there is a requirement for a certain magnitude of breaking to induce the radiation stresses (Longuet-Higgins and Stewart, 1964) required for the establishment of a rip current circulation. The under representation of rip rescues for values less than 1.5 m may be indicative of the radiation stresses being too minimal to induce dangerous rip circulation. Where wave heights are large enough to establish strong rip flow (conceptually ≥ 1.5 m), they are also deemed

suitable for both swimming and surfing, and so attract a larger number of people to the beach. Scott et al. (2014) therefore explained similar relationships between mean wave heights and high rescue numbers as high risk, high exposure scenarios. The same applies here, the waves are strong enough to establish rip circulation, but low enough that most people would feel comfortable entering the water, which explains the high number of rescues around this wave height.

Increased exits were observed here at lower peak wave periods (typically $T_p \approx 10$ s) (Figure 8.4b), which is contrary to the suggestion in many studies that longer wave periods typically force increased velocities and exits in rip systems (Castelle et al., 2006; MacMahan et al., 2010; McCarroll et al., 2014; Castelle et al., 2016b). However, the longer wave periods quoted are typically on the order of 12 s, so remain comparable to this finding. Furthermore, a T_p of 10 s is significantly greater than the mean spectral period (7 s) at Ngarunui (Guedes et al., 2013). The only study to correlate drifter exits with decreased wave periods was that of Reniers et al. (2009), but the application of his predictive parameter significantly underpredicts exits observed in field data (McCarroll et al., 2014). It is possible that the shorter period (steeper) waves result in higher energy (plunging) breakers, which would increase wave set up, radiation stresses and drive a stronger and more hazardous circulation, although further investigation into rip dynamics under high steepness waves would be required. Most rip current rescues were triggered when incident wave angle was most oblique to the shoreline (Figure 8.4c), which is unusual as this often drives longshore currents (Scott et al., 2014). This infers that wave refraction around the headland at the south of the beach would have been greatest for these rescue events. This concurs with previous research that identified increased wave refraction or diffraction as a driving mechanism of rip currents (Dalrymple, 1975; Dalrymple and Lozano, 1978; Dalrymple and Martin, 1990). The majority of rip rescues at Ngarunui occur under low wind speeds (Figure 8.4d). In the wider (all event) dataset, rescues are over represented at all speeds < 5 m s^{-1}, whereas there appears to be one dominant speed (2 m s^{-1}) in the mass rescue record. Generally, light onshore winds are conducive to rip current formation (Scott et al., 2014), which concurs with results here.

8.4.3 Wave breaking patterns: Open vs. closed rips

The results from both sites are comparable and show that a greater number, and more serious incidents occur when rips were classified as open. The prevalence of open rips was similar for both sites: Ngarunui 37 %; and Perranporth 40 %. Despite the prevalence of open channels being around 20 % lower than closed channels, they account for the majority of rescues (Ngarunui 53 %; Perranporth 60 %). The measure of incident and occurrence allows for the data to be normalised (Equation 8.1), which shows open rip channels to be twice as hazardous as closed channels (Figure 8.5). Bathymetric channel rips are generally described as patches of darker, calmer water between areas of whitewater induced by wave breaking (Brander and MacMahan, 2011). In this area the deeper channel is moving water offshore, whereas the breaking waves on either flank are indicative of shoreward mass transport, thus making the channel a more hazardous area to swim (Hatfield et al., 2012). The calmer appearance of the surface of rips is cited as a key factor in an inexperienced beach users decision on where to swim, with the mistaken belief that the seemingly calmer waters away from breaking waves are safer (Sherker et al., 2010; Gallop et al., 2016b). This visual description applies well to the scenario of an open rip channel, where the absence of wave breaking typically extends from the shore to seaward of the surfzone. As a result, casual bathers are more likely to select an open rip channel as a safe area to swim and ultimately increase the risk of ending up in the current. This is in contrast to the closed scenario where a darker patch of clear water would be visible, but would exhibit a defined band of wave breaking at the seaward edge, which makes it a less appealing choice to bathers than the open rip. The open channel is hydrodynamically more dangerous for bathers and now in addition, the visual signature of an open channel may also increase the likelihood that it is selected by beach users as a place for bathing.

At both sites, bodyboarding (classified under surfing for Ngarunui) was a more prevalent confounding factor in open rips rather than closed. Of the bodyboard incidents investigated here, at Perranporth 73 % occurred under open rip conditions. When normalised by prevalence, it can be said that bodyboarders are 5 times more likely to be

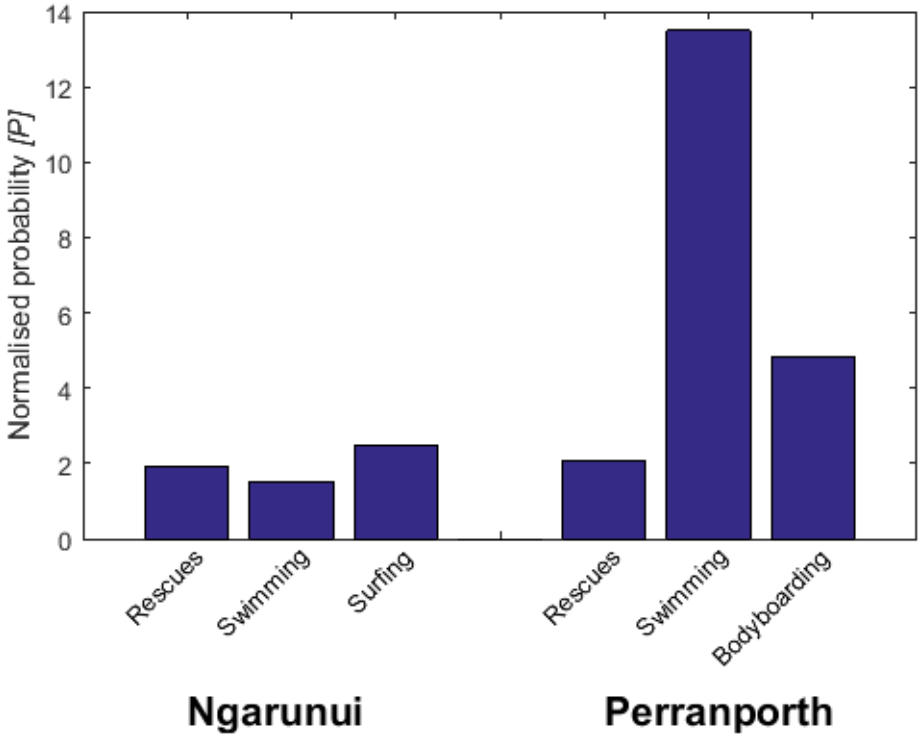

Figure 8.5: Normalised probability of rescue events and confounding factors under open conditions compared to closed conditions. Values of one indicate that the occurrence of rescues matches the prevalence of open rip channels. Values greater than one indicate how much more likely to occur an event is when compared to the same variable in closed conditions (i.e. value of two shows twice as likely). All values calculated using Equation 8.1.

involved in an open rip rescue at Perranporth (Figure 8.5). At Ngarunui, 60 % of bodyboarder and surfer rescues were from open rips, showing a rescue from open currents to be 2.5 times more likely (Figure 8.5). Bodyboards are often used primarily as floats, with users not maintaining contact with the floor, increasing their susceptibility to rips as they float out on the current (Woodward et al., 2013). Open rip hydrodynamics mean that any floating matter is more likely to move offshore into deeper water. Drozdzewski et al. (2012) surveyed people that had been caught in rip currents, and identified their first feeling when caught in the rip as one of being out of their depth or out of control. Bodyboarders trying to put their feet to ground after being transported

in a rip are likely to experience the same feeling when they realise they are now out of their depth. The same survey showed that the dominant emotional response was panic at realisation they were caught in a rip. Therefore, the combination of this out of depth feeling, and resultant panic response may be more likely to result in the initiation of a rescue event. In comparison, during closed channel scenarios, bodyboarders are much more likely to float around the surfzone and therefore more likely to stay in an appropriate depth of water. Conceivably, they are therefore much less likely to panic or initiate a rescue event. A large proportion of swimmer rescues at Perranporth (88 %) were from open channels, and the same logic may apply. This 88 % showed swimmers were 13 times more likely (when normalised by occurrence) to be rescued from open rips than closed (Figure 8.5). Conversely, swimmer rescues at Ngarunui were more mixed (47 % occur in open channels). However, when compared with the prevalence of open channels (37 %), the normalised value for Ngarunui shows that swimmers could be considered 1.5 times more likely to be rescued from an open channel (Figure 8.5).

8.5 Conclusions

This study was the first to quantify the effect of wave breaking patterns on rip rescue events. Demographics of rip rescue victims at Ngarunui mirrored those of Perranporth, and wider worldwide statistics, showing young males to be most at risk. There was divergence in the most at risk activity for both sites, with bodyboarding being the most prominent rip victim activity at Perranporth, whereas swimming was the most prevalent activity at Ngarunui. The most hazardous hydrodynamic conditions for rip rescues at Ngarunui were seen to occur either side of spring tides. At these times, water levels result in rip channel submergence of around 1—1.5 m, making it an ideal bathing depth. Therefore, this study concludes that rip rescues are over represented at these times as a result of increased exposure to the hazard. Mean wave heights ($\approx$ 1.5 m) result in the majority of rip rescues at Ngarunui, confirming previous findings that rips persist under relative calm. Rip rescues could be under-represented for lower wave heights as a result of insufficient radiation stresses to drive strong currents. Comparatively short wave

periods at Ngarunui increased rip rescues, which was in contrast to much research elsewhere indicating that long wave periods were normally responsible. It is possible that short period waves increased wave steepness, resulting in more energetic breaking and increased wave set up, ultimately driving more hazardous rips but more information is needed to draw substantive conclusions. In common with previous studies, increased refraction and low winds speeds also created an increase in rip rescue events.

The most novel aspect of this study was the application of a new wave breaking parameter to the rip current rescue databases. The occurrence of 'open' rip channels was around 40 %, yet they were responsible for the majority of rescues over a 5 year period. When rescues were normalised against occurrence of each channel type, open rip channels were twice as hazardous. Bodyboarders or surfers were most at risk, with most rescues occurring under open conditions. Eighty-eight percent of swimmer rescues at Perranporth were from open rips (13 times more likely than a rescue occurring under closed conditions), and after normalising by occurrence, swimmers at Ngarunui were also seen to be 1.5 times more likely to be rescued from an open rip. Open rip configuration are characterised by less wave breaking and therefore appear calmer and safer for bathing, which may increase the likelihood of their selection as a safe place for bathing. In turn, the flow regime associated with an open rip is notably more dangerous, with the likelihood of surfzone exit increased.

Chapter 9

Conclusions and implications

The overall aim of this thesis was to determine how patterns of wave breaking influence rip channel hazards on beaches. To achieve this, this research first investigated new approaches to the automation of rip detection, using image archives from two contrasting sites. Although automation was ultimately unsuccessful, both pre-filtering and the construction of synthetic imagery was a beneficial pre-cursor to further work with images of the surfzone. These processing steps ultimately identified a new parameter that can be measured in rip currents, concerning the shape and patterns of wave breaking around channels. Throughout the thesis, the pattern of wave breaking has been linked to the hazard posed by the rip current at that time.

This chapter will first summarise the key findings of each of the four results chapters, before considering the holistic implications of this research as a whole, including any implications it may have for future work.

9.1 Automation of rip detection & the use of synthetics

The first objective of the thesis was to develop pre-processing image techniques to improve the reliability of automated rip channel detection in video imagery. The utility of coastal imagery for quantitative means was first recognised over 30 years ago, with the discovery that timex images provide a view of persistent nearshore processes. Channel rip currents are an example of one such process, visible in the imagery. Previous attempts to automate channel rip current detection have always fallen short of the required accuracy, and often necessitated subsequent manual cleaning of data. Little attention was given to the pre-filtering of coastal video imagery, prior to subsequent processing. The image therefore still contains extraneous noise, such as lens fouling, which may later affect the rip detection algorithm. Therefore, here this research explores a new means to filter imagery, attempts to code an automated approach for rip detection, and latterly explores a new method of creating simplified imagery for later processing.

The introduction of pre-processing of coastal video imagery proved to be effective at noise reduction, without obscuring the dominant features in the imagery. A simple lowpass filter was able to increase the accuracy of shoreline detection in an image fouled by rain drops on the lens. In the example shown, the detected shoreline was displaced by 30 pixels ($\approx$ 27 m) by rain fouling on the lens. An oft-quoted limitation to the use of video imagery is the number of images that have to be discarded as a result of environmental fouling, which ultimately results in a loss of data, and can be responsible for prominent data gaps in a timeseries of an event. There is a palpable advantage to pre-filtering of imagery. Although it is not necessarily appropriate to the most heavily fouled of images, more investigation would be able to ascertain the range of conditions (and degree of fouling) under which it is appropriate. Furthermore, investigation should aim to identify the foremost filtering method to apply to achieve results. Ultimately, this new approach will result in fuller datasets and a more complete overview of events that occur under slightly adverse conditions.

This research was unable to escape from the pitfall identified in previous attempts to automate rip detection, whereby site specific, subjective thresholds are required to achieve results. Even with the inclusion of such thresholds, the vast majority of the algorithm's detections ($> 70\%$) required manual cleaning as a means of post-processing the results. Automated detection is likely to enjoy more success in the future at microtidal sites, with steep beach gradients, as the net effect of these conditions is the spatial constraint of rip channels, making their features more prominent in video imagery.

The utility of synthetic imagery as a means of providing simplified coastal images was also explored. The use of synthetic imagery increased acceptable detections from 81 % to 92 % compared to using the original image. When considering erroneous detections, in original imagery, the fouling resulted in an over-prediction of rip features in 62 % of cases where the rip number was incorrectly identified. The use of synthetic imagery (and thus the removal of the fouling) lowered over-predictions in erroneous detections to 36 %. It may, therefore, be of use to convert imagery to a synthetic version for future attempts to automate rip detection, or even to quantify other nearshore processes. In the process of creating a synthetic image, a novel rip thresholding method was applied, whereby manually selected rips are converted to a binary image. The effect of the threshold is to outline the patterns of wave breaking, which ultimately delineates the outline of the rip channel itself (albeit an approximation of actual bathymetry). Rip channel shape has not been investigated previously, and therefore this formed the basis of the next chapters of the thesis, whereby the variability in shape, and the control it exerts on surfzone circulation was measured.

9.2 Morphological classification of rip currents

The second objective of the thesis was to develop a classification of rip channel morphology based on wave breaking patterns. Previous rip current classification schemes almost entirely focus on the process controlling the formation of a rip current to guide their classification. Although such schemes offer much information on morphology, they

provide little in the way of indication on how the rip current circulation may vary over time. Therefore, for this component the thresholded imagery identified in the last chapter is used as a means by which to classify rip currents, with the novel application of synoptic typing to coastal imagery.

Synoptic typing identified 4 distinct broad types of channel that could account for 91 % of the variance in the video imagery. The dominant channel configuration (38 %) was a wide channel with an open connection to the offshore, and the second most prominent (32 %) was a closed, isolated hole-like region, far from the offshore. The third and fourth conditions were variations on the first two. The third most prominent (14 %) was again an isolated hole, but this time it occurred in much closer proximity to the offshore. Finally, the fourth type (7 %) was a narrow channel with an open connection to the offshore, often occurring at an oblique angle.

An initial assessment of temporal changes between patterns showed no evidence that a particular type of channel was most likely to have evolved from, or into another specific type. The main temporal change was that, predominantly, a channel was most likely to retain its current form in the subsequent image. The reason behind this lack of a trend was largely a result of the way in which the rip is sensed. The use of wave breaking is only a surrogate for morphology, and therefore there is no actual measured morphological change, just changing water levels and wave conditions, creating different wave breaking patterns. Therefore, the hydrodynamic controls on channel type are isolated through the use of wave and tide factors. Under low wave and high tide conditions, channels with an open connection to the offshore were most likely to persist, whereas under high wave and low tide factors, isolated channels were more common. Previous studies suggest that the conditions under which open channels were observed generally produce more exiting rip flows, and under the conditions whereby isolated and closed currents persist, there was a tendency for surfzone retention.

The original synoptic typing identified 4 main channel types, however, the analysis of wave and tide factors showed that there appears to be a spectrum between entirely open and entirely closed channels, with this connectivity to the offshore being the defining factor. Therefore, from this point forward, two simple channel types are used; open, or

closed. The channel type was defined by whether, after thresholding, there was a solid connection between the rip channel itself and the offshore area. This approach is a new classification of rip currents. Importantly, unlike other classification schemes, this one is dynamic in that it can account for changes in a rip current over a tidal cycle, whereas previous schemes have looked predominantly at formation mechanisms which never change for a particular rip channel.

9.3 Wave dissipation as a control on surfzone retention

The third objective of the thesis was to assess the control exerted by differing wave breaking patterns on rip current flow regimes. Although rip current formation mechanisms are well understood, much less is known about the controlling processes affecting surfzone retention. Researchers have found some success through the use of VLF motion analysis, and also through the combination of wave and tide factors, but neither approach was able to successfully explain all variability in surfzone retention rates. Hitherto, the pattern of wave breaking and it's effect on surfzone circulation had been opportunistically and qualitatively discussed, but found no quantitative conclusions to suggest a control was indeed exerted on retention.

Here, a field experiment was conducted to ascertain *in situ* rip current flow, and surfzone circulation. Each deployment had the drifter track classified as either linear exit, circulation then exit, no exit, or other. This assessment was made by overlaying the drifter track onto the video imagery, to delineate the edge of the surfzone, and allowed a classification of wave breaking patterns to be made.

During closed channel conditions, wave breaking across the end of the channel was seen to increase vorticity and current speed in the rip channel, ultimately promoting re-circulatory currents and surfzone retention. Previous research has shown that under similar conditions to those defined here as closed, water surface gradients are highest, which may exert control on the increased vorticity observed. Furthermore, it is

postulated that under closed conditions, the current interaction with the offshore wave field is greatest, reducing the strength and extent of the offshore rip current flow at that location, consistent with results here that showed velocity tailed off at the edge of the surfzone under closed conditions. Under open channel conditions, the absence of wave breaking across the channel results in a slow steady current that meanders offshore. The offshore directed current speeds were seen to be considerably lower (Perranporth 31 %; Ngarunui 83 %), consistent with previous work that linked lower intensity breaking to lower velocities through morphodynamic scaling. The net result was that surfzone exits much increased under open conditions, at times reaching 100 % exits. A Chi Squared analysis showed that open channels were statistically more likely to result in rip exits, compared to closed channels.

9.4 Rip current hazard signature

The fourth objective of the thesis was to identify the hydrodynamic and morphologic conditions most conducive to formation of hazardous rip currents. Hazard refers to how dangerous a particular rip current is at a specific time. It is widely accepted that the most hazardous rips have a combination of fast flow velocities, and a circulatory regime that means they predominantly exit the surfzone, rather than recirculate. Given that in the previous objective, open rip currents were responsible for surfzone exits, here a link between wave breaking patterns and rip current rescue events is explored, to see if open rip currents proved to be more hazardous.

Rip incident data for a 5 year period at both sites was compared against the image archive for the same period, enabling rescue events from the rip incident database to be compared against patterns of wave breaking. Open rips were over-represented in the rip rescue record at both sites, with major rescues at Perranporth accountable to open rips in 78 % of cases. The majority of bodyboarder and/or surfer rescues at both sites were from open rips. At Perranporth, 90 % of swimmer rescues were from open rips. Open rip hydrodynamics show that the current often extends further offshore and greatly increases

the likelihood of rip exits, which is used to explain the over-representation of open rip channels in the rip rescue record observed here.

Having identified that open rips are more hazardous, it is important to quantify the level of risk of exposure to the hazard. Estimations of people using the beach at the time of each rescue were not available, so as a proxy, the prevalence of open and closed rips was used to estimate risk. An analysis of one lifesaving season's worth of data showed that open rips occurred only 40 % of the time, compared to 60 % prevalence of closed rips at both sites. Using a combination of the prevalence of open and closed rips, and the number of rescues each is responsible for, it was possible to normalise the data and calculate that open rips can be considered to be twice as dangerous as closed rips to the bather.

9.5 Summary

The overall aim of this thesis was to determine how patterns of wave breaking influence rip channel hazards on beaches. The main motivation for this work was a desire to quantify the most hazardous conditions for bathers on beaches. Rip incidents account for a large drain on beach lifeguarding resources each year, and despite knowing when rips are most likely, there was very little information to predict how hazardous a particular rip current may be. Furthermore, there is little information concerning how circulation within a single rip current changes over time. Understanding of the controls behind changing rip current circulations is of vital importance for coastal managers and beach lifeguards in deciding how best to ensure beach safety at a given site. Patterns of wave breaking had previously been qualitatively considered as a control on rip current circulation, but had not been the focus of any research effort. Before being able to address the scientific question, it was necessary to develop a number of methodologies to enable quantification of wave breaking patterns. Having developed appropriate methodology for quantification of wave breaking patterns, this study then employed the use of a typing algorithm to inform a classification of types of wave breaking patterns.

From this classification, two broad types of wave breaking pattern were identified, and postulated as hydrodynamically different. With the combination of *in situ* data, rip incident reports, and imagery classified using this new scheme, this study was able to apportion an indication of hazard to a rip, based on the exhibited patterns of wave breaking in imagery.

The first methodological challenge was in the development of a means to automatically detect rip channels in video imagery. Many previous attempts have been made to automatically detect rips, but ultimately, most researchers revert to manual digitisation as a result of attempts to automate requiring subjective thresholds, and lacking inter-site operability. One reason behind the inability of other algorithms to be automated centres around the degree of noise evident in coastal imagery, whether by fouling, or complex processes. In previous attempts, images have been used without any means of filtering (aside from image rectification) prior to processing. The first objective, therefore, was to develop pre-processing image techniques to improve the reliability of automated rip channel detection in video imagery. Although complete automation was not possible, the use of filtered imagery improved feature detection in video imagery, with the example in this report being that of barline detection. Such filtering is commonplace in the signal processing world, but has not been employed by coastal researchers using video imagery hitherto. This finding presents a step change to the approach that should be taken by coastal researchers moving forwards. Taking the technique a stage further, this research was able to for the first time, develop novel synthetic imagery of the surfzone for analysis. Synthetics create an image of the nearshore entirely devoid of noise, for secondary processing. In this study, a simple rip detection algorithm was applied and the results for detections on synthetic imagery removed the tendency for over-detection (a function of noise), and increased the overall accuracies of detections. Of particular interest with this new approach, is that as part of the construction of the synthetic, the thresholding of the surfzone reveals information about the patterns of wave breaking. The ability to capture information on rip channel shape, through this expression of wave breaking, is entirely novel.

The second objective was to develop a classification of rip channel morphology based on wave breaking patterns. The change in shape of a rip channel over short (tidal) timescales had not previously been studied. There have been observational studies that noted changing wave roller dissipation produces visually similar results to actual up/downstate beach morphological transitions, but never before has this shape been quantified. The first approach employed here was another method not previously employed in the coastal science discipline; that of synoptic typing. More commonly used to identify patterns in weather maps, the method looks to assign overall similarity to a pair of images, and was engineered here to also assess sub-image similarity by means of row and column comparisons. This method was able to isolate four types of rip channel, that accounted for 91 % of the variance observed in the image database. In broad terms, the algorithm identified two types of channel whereby the rip channel itself shared an open connection to the offshore area, and two types where the rip channel was isolated from the offshore by wave breaking processes. The four types of channel identified in synoptic typing were simplified into two types based on their connectivity with the offshore; open, or closed. A comparison of image types with hydrodynamic forcing revealed a prevalence for the open types of channel to occur under lower wave conditions or increased water levels, as a result of reduced wave breaking (either through smaller waves or higher absolute water levels) at the offshore extent of the channel. Conversely, higher wave heights and lower water levels promoted the formation of closed channels, where bigger waves and lower water levels induced breaking at the seaward extent. The hydrodynamic analysis could be linked to previous work that suggested lower wave and higher water level conditions were conducive to rip current exits, and higher wave, lower water level conditions were conducive to surfzone retention. The suggestion that wave breaking patterns may be able to provide information on surfzone circulation is both novel, and important. It is important because coastal imaging systems can be purchased and operated at a much reduced cost compared to *in situ* equipment, such as wave buoys or rigs. Such systems are also highly mobile, and therefore, can be deployed to a totally new site and combined with this algorithm to provide information about rip behaviour. At this point, this link between wave breaking and circulation was speculative, and so

the next piece of work focussed on obtaining contemporaneous imagery and *in situ* rip current measurements to test the hypothesis.

The third objective was to assess the control exerted by differing wave breaking patterns on rip current flow regimes. Very little previous work was done to combine the use of video imagery and *in situ* measurement of rips for anything other than qualitative means. Typically, studies have measured the rip current *in situ*, and drawn qualitative conclusions about conditions based on the video imagery. This research presents one of the first efforts to use Lagrangian measurement, and explain it using quantitative information from the video imagery, in terms of the wave breaking pattern. This research provided new insight as to what may control surfzone circulation in rip currents. The discovery of increased vorticity in closed channels, promoting retention is a key finding. It is likely that the increase in wave breaking around the offshore extent of a closed channel creates localised variations in absolute water level, with pressure gradients driving the increased vorticity. Although absolute control on surfzone circulation was not established, the much increased tendency for a surfzone exit under open channel conditions is an important discovery. In the closed condition, however, surfzone retention appeared as a very dominant trend. The conclusion to draw from this is that under closed conditions, the rip current is highly unlikely to result in surfzone exit (0—35 %), whereas under open conditions there is a much increased chance of exit.

Having now made a physical link between wave breaking and rip circulation, the fourth objective of this study was to identify the hydrodynamic and morphologic conditions most conducive to formation of hazardous rip currents. Hydrodynamic analysis of rip incident data at Perranporth has been completed before, and this study was able to confirm that similar hydrodynamic conditions drive rip rescues at the high energy Ngarunui beach. Furthermore, this study was able to assess whether a novel wave breaking parameter could explain the occurrence of reported rip incidents. It was possible to account for 62 % and 75 % of the most serious incidents at Ngarunui and Perranporth, respectively, through the occurrence of an open channel promoting surfzone exit. In rescues involving swimmers and bodyboards, open channels were disproportionately represented. The implications of this finding are primarily concerned

with beach safety practitioners. Although this method does not provide a predictive capability, per se, it does provide an easy means to categorise the risk factors at a particular beach using just video imagery. For a totally unstudied beach, the deployment of a mobile video camera for a field period would allow capture of wave breaking patterns, and the opening/closing of the rip channel could be compared to wave conditions, whether by wave buoy data or modelling, to make assessment of high risk surf scenarios (i.e. the hydrodynamics under which the rip was open).

During the course of this investigation, a novel approach to both processing and classification of surfzone imagery was proposed. Moving forwards, it is clear that some outputs from coastal imaging systems should not be directly processed until they have undergone pre-processing to remove noise, in line with work done in the field of signal processing. Synoptic typing has proved to be a useful post-processing technique to assess similarity in extracted features from surfzone imagery and should be considered in any coastal classification scheme centred around morphological shapes. A new means of classifying rip channels by morphological shape has proved effective in explaining rip current circulation, offering remote insight as to whether a rip current is likely to exit the surfzone or not. Furthermore, the application of this technique to a dataset of rip rescues at two sites shows that the open rip currents described in the classification can be considered as twice as dangerous for bathers when compared to closed channels. This new technique will likely provide a quick an easy way to assess high risk surf conditions at rip beaches worldwide, with just the deployment of a mobile coastal imaging system.

9.6 Outlook for further work

This research has raised a number of further research questions, and avenues of investigation for future work. Although discussed in the main body, they have been summarised below.

Shoreline detection

There are many approaches to shoreline detection in video imagery, and a comprehensive review was provided 10 years ago in Plant et al. (2007), where the Shore Line Intensity Maximum Model (SLIM), Pixel Intensity Clustering Model (PIC), the Artificial Neural Network Model (ANN), and the Colour Change Divergence Model (CCD) were tested. The results of their work showed an over-prediction of shoreline (higher up the beach) in the PIC, ANN, and CCD approaches, and under-prediction in the SLIM model. The SLIM model, although the most objective measure, was showed to be primarily applicable at reflective beaches where there is a sharp transition in pixel intensity. The research presented here used a novel k-means clustering approach, without the selection of any thresholds. It was seen to be effective at both contrasting studies sites here ($r^2 = 0.87$), and is certainly worthy of further investigation across a multitude of sites to estimate it's overall performance.

Synthetic imagery

This research proposed the use of synthetic imagery as a means for simplifying surfzone imagery, and isolating the dominant trends. It was shown here to be effective in reducing the error of rip detections when the Ranasinghe et al. (1999) method was applied to the dataset, however, its applicability reaches beyond rips. It provides, for example, a useful means to quantify changes in bar configuration over time. Furthermore, it acts as a useful testing ground for development of automated models. The creation of the synthetic image involves zonation of the features of interest, therefore, the application of automation models to synthetics gives you an actual error indication against the ground truth, which you are unable to get from real imagery. Therefore, investigation can commence on reasons for automated models not detecting the selected feature, whether it be feature size, orientation, or shape.

Automated rip detection

Although this research was unsuccessful in developing a completely automated means of rip detection, there is still promise for development in this field. The complex nature of the surfzone, and the features of interest therein will necessitate advanced processing techniques to delineate. Hitherto, all work in this area has been conducted by coastal researchers employing signal processing and image analysis techniques borrowed from other fields. A complex problem such as this likely requires someone who's sole field is signal processing, to come and work in coastal imaging. With them, they would bring a whole range of techniques, such as region growing algorithms, advanced shape detection, etc, that would be of most use in the pursuit of automated detection.

Synoptic typing

This, to the author's knowledge, was the first application of synoptic typing to video imagery. The assessment of similarity proved not only useful in the classification of rip current morphologies (Figure 6.3), but also in identifying anomalous results and significantly reducing standard deviation between image pairs (Figure 6.8). Synoptic typing is a powerful tool to map changes in patterns, its uses for the coastal zone could well extend beyond rip studies. For example, it could be applied to unrectified images of the beach to quantify beach change, and the switch between swell and storm profiles. As part of this study, it was applied to thresholded (black/white) imagery, however, future studies should investigate its utility as a means of classifying RGB imagery.

Wave breaking patterns

The discovery of a link between wave breaking patterns and rip current circulation is entirely novel, and as yet needs testing across a number of sites and conditions. It is likely to be applicable to any of the bathymetrically controlled rips (Section 2.2.2) defined by Castelle et al. (2016b) by nature of the processes that control being inherently linked to spatial variation in wave breaking. Although it may apply to hydrodynamically

controlled rips, it is likely that such rip types (e.g. flash rip) would be unlikely to persist long enough to appear as a feature in timex imagery. Future work should also focus on measuring *in situ* processes when the rip is open or closed, such as localised water levels, vorticity, etc, in order to help explain why spatially different wave breaking patterns exert differing controls. One shortcoming of this thesis was that the categorisation of wave dissipation was theoretical. Future work should focus on replicating the results of this study with the *in situ* measurement of wave dissipation patterns to confirm these findings. Perhaps the most important outcome here is that wave breaking patterns are explicitly linked to surfzone hazard. Therefore, future work should focus on how this information can be used to aid surf lifesaving groups and beach practitioners. In particular, investigation on the possibility of using this information to inform realtime beach hazard state reports would be beneficial. It would be interesting to test these ideas with the use of numerical modelling. In particular, it would be beneficial to investigate whether different open and closed rip configurations (as outlined in Figure 6.11) produce different flow regimes or flow velocities.

Appendices

Appendix A: GPS drifter data processing steps
Appendix B: Rip perception paper
Appendix C: Rip current observations paper
Appendix D: Pulsations in surfzone currents paper

Appendix A: GPS drifter data processing steps

This Appendix sets out, with examples, the processing steps taken to convert raw GPS drifter data sampled at 1 Hz into the sets of independent observations used throughout this thesis.

1. The raw GPS tracks, collected at 1 Hz, are first filtered to remove the noise inherent in the drifter movement (Figure 9.1). This noise is generally caused by the tilt of the drifter as it moves in the surf, and also surface reflection of GPS signals. The data is filtered into 0.1 Hz observations. This is achieved by averaging all latitudes and longitudes in each 0.1 Hz window. The result of the filtering is shown below.

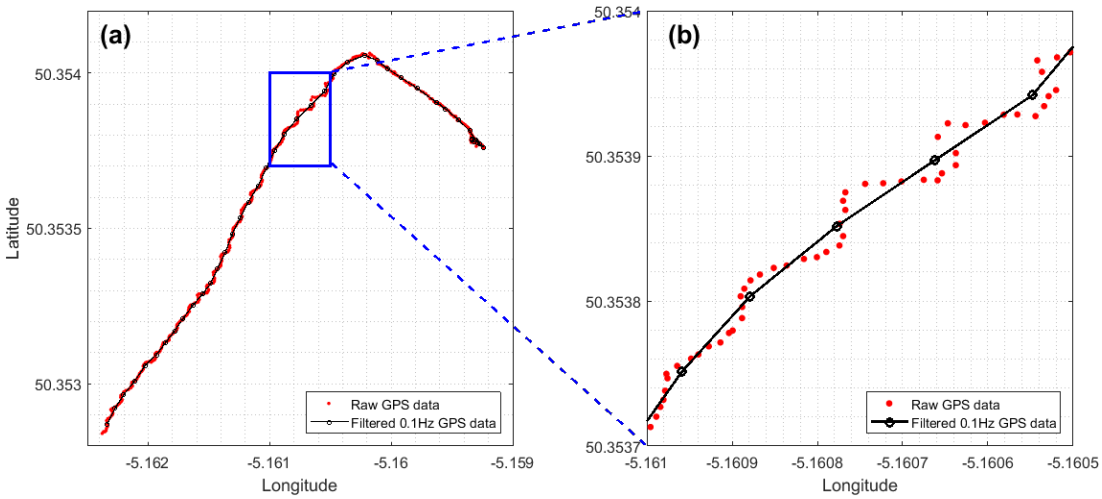

Figure 9.1: Processing of GPS drifter positions. (a) shows the entire track with red data points indicative of raw data, and black data points indicative of the filtered data. (b) An enlarged segment of the data is presented, indicated by the blue box in (a).

2. Once the data is organised into filtered 0.1 Hz observations, it is possible to calculate the drifter velocity based on the filtered positions. The raw velocity data is noisy, and has been filtered using a zero-phase, fifth order Butterworth lowpass filter, as in the case of previous drifter studies (Johnson and Pattiaratchi, 2004; McCarroll et al., 2014), with a cut off of 0.05 Hz (Figure 9.2).

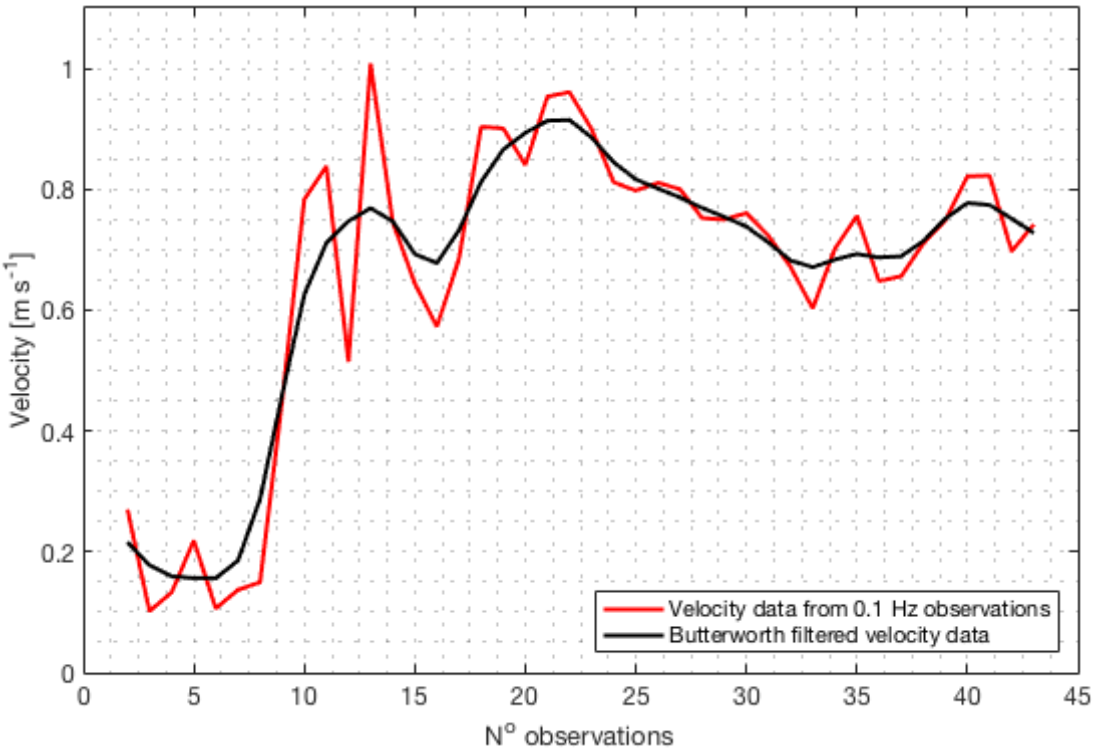

Figure 9.2: Velocity data, derived from 0.1 Hz filtered positional data (red line), is filtered using a Butterworth lowpass filter to reduce error (black line).

3. The positional data is now linearly interpolated back into observations at 1 Hz, representing the original sample frequency (Figure 9.3). At this point, the bearing of the drifter is calculated and recorded at 1 Hz. Then all values are converted into the Argus co-ordinate system, resulting in latitudes and longitudes converted into a co-ordinate system based on metres distance from a nominal Argus origin.

4. Finally, in line with previous studies (Scott et al., 2014; McCarroll et al., 2014), the 1 Hz observations are checked for independence. This is based on the user defined gridding of the surfzone. In this experiment, and others, grid size was 10 $\times$ 10 m (rationale discussed in Chapter 4). Following the work of Spydell et al. (2007) and MacMahan et al. (2010), observations in the same grid square were grouped into one independent observation (Figure 9.4). If the drifter later re-entered the grid square, it would be considered a new independent observation if it had travelled a

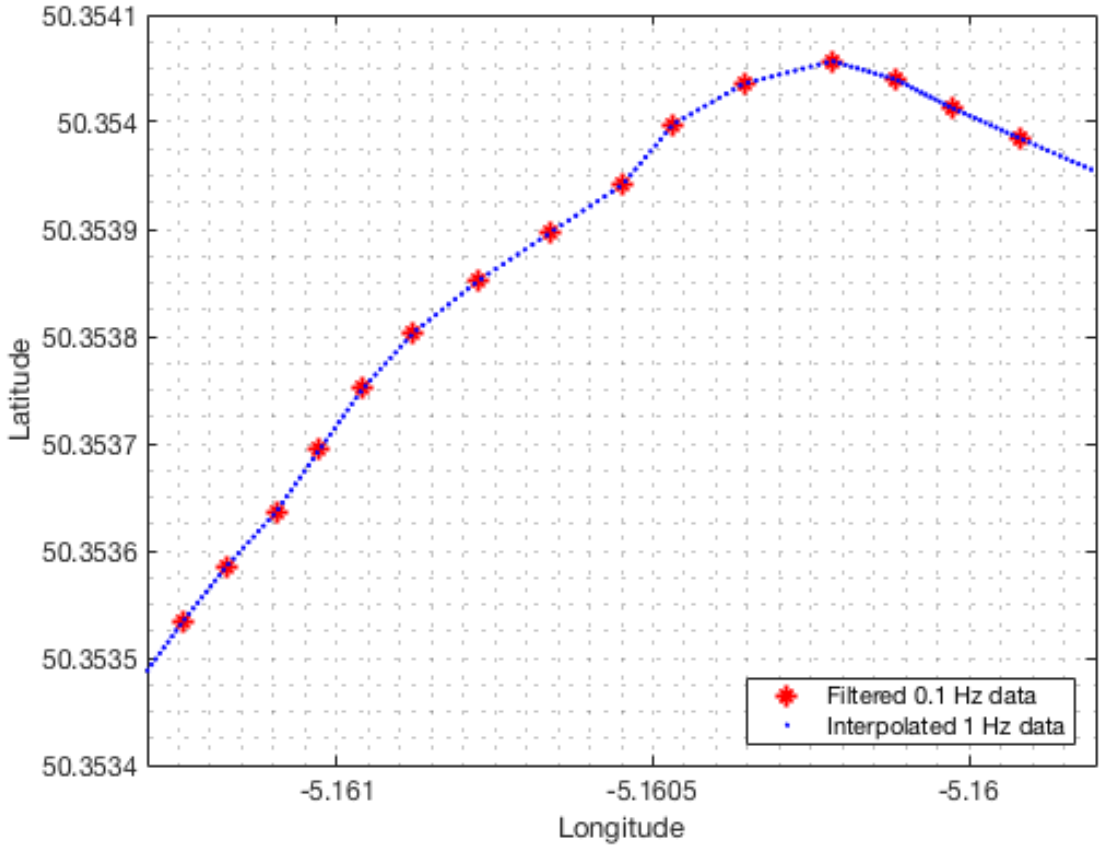

Figure 9.3: Filtered data (red star) is linearly interpolated back to the original 1 Hz sample frequency (blue dots).

significant distance (defined as the length of the grid square) before doing so. A re-entering drifter was independent when $t > lg/U$ (MacMahan et al., 2010), where t is elapsed time, lg is the grid square size and U is the average drifter speed whilst in transit outside of the gridsquare.

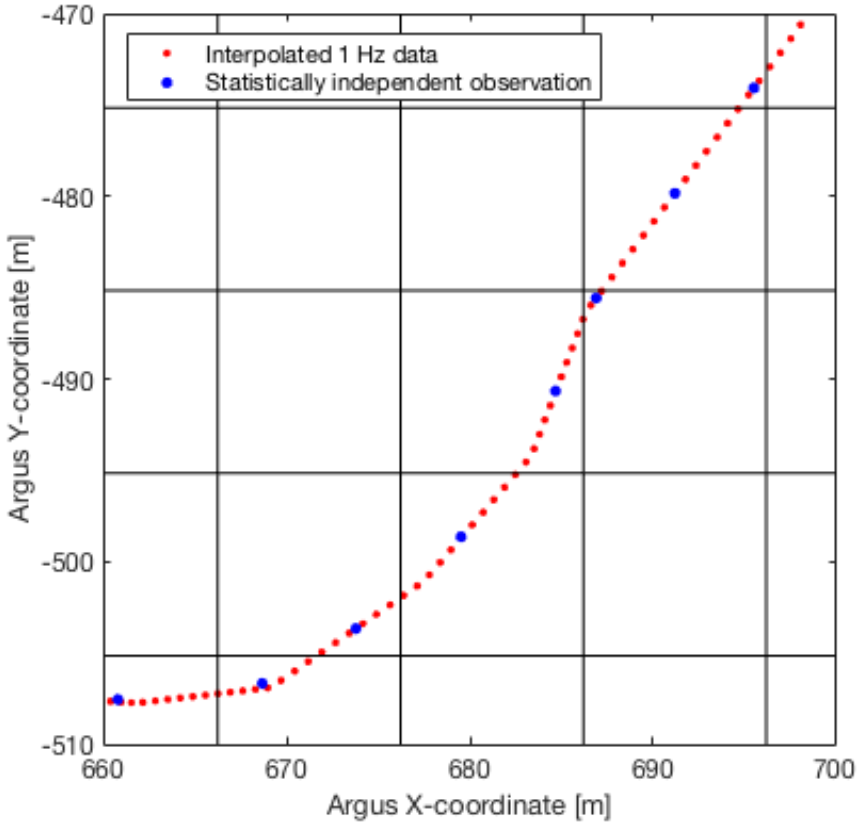

Figure 9.4: The selection of independent observations (blue dots), from the full 1 Hz filtered dataset (red dots), based on the user defined grid (black gridlines).

Appendix B: Rip perception paper

This paper was published on the back of the lit review conducted as part of this PhD.

Ocean & Coastal Management 119 (2016) 14–20

Contents lists available at ScienceDirect

Ocean & Coastal Management

journal homepage: www.elsevier.com/locate/ocecoaman

Perceptions of rip current myths from the central south coast of England

Shari L. Gallop [a, b, *], Eleanor Woodward [c], Robert W. Brander [d], Sebastian J. Pitman [b]

[a] Department of Environmental Sciences, Macquarie University, Level 2, The Australian Hearing Hub (AHH), NSW 2109, Australia
[b] Ocean and Earth Science, National Oceanography Centre, University of Southampton, European Way, Southampton, SO14 3ZH, UK
[c] School of Marine Science and Engineering, University of Plymouth, Plymouth, PL4 8AA, UK
[d] School of Biological, Earth and Environmental Sciences, UNSW Australia, NSW 2052, Australia

ARTICLE INFO

Article history:
Received 14 July 2015
Received in revised form
21 September 2015
Accepted 22 September 2015
Available online xxx

Keywords:
Rip currents
Coastal hazards
Drowning
Surf rescue
Beach safety management

ABSTRACT

Rip currents (rips) are the global leading cause of fatalities on surf beaches, yet numerous long-standing misconceptions exist. Evidence of the prevalence of these myths is largely anecdotal. This opportunistic, exploratory study presents perceptions on rip current hazards (n = 187), of members of the public attending an open day at the National Oceanography Centre, Southampton. The survey was undertaken as a fun but informative quiz, aimed at families attending the research-facility. It also explored using such events as a conduit to gain valuable knowledge on the understanding of rip currents and other hazards. While most respondents (81%) knew appropriate escape strategies (swim parallel and stay afloat), only 11% identified what makes rips dangerous (panic), with 44% incorrectly saying that rips suck you under. Rip identification is poor, and many are unaware of the meaning of beach safety flags. This study identifies that safety communication messaging needs to focus on debunking rip current myths, to improve understanding of safe swimming areas; and to reduce panic if caught in a rip.

1. Introduction

1.1. Introduction to rip currents

While beaches are important for social, recreational, cultural, ecological, and economic activities (Stronge, 2005; Martínez et al., 2007), they also represent a risky environment, particularly for bathers (Short and Hogan, 1994; Ballantyne et al., 2005; Matthews et al., 2014). Beach safety management (ILFE, 2005; Hatfield et al., 2012) relies on understanding potential hazards to bathers, swimmers and surfers (Short and Hogan, 1994; Scott et al., 2009). The main natural hazard for bathers on global surf beaches is rip currents, or rips (Klein et al., 2003; Hartmann, 2006; Scott et al., 2007; Short, 2007; Gensini and Ashley, 2010; Arun Kumar and Prasad, 2014; Arozarena et al., 2015). Rips occur inside the surf zone (Short, 2007), which is the area shoreward of the wave break point (MacMahan et al., 2011, Fig. 1). They occur as concentrated, seaward-directed flows (Fig. 1), with velocities on the order of 0.5–2 m s^{-1} (MacMahan et al., 2006; Brander, 2015). Rips are generated by radiation stress-gradients (Longuet-Higgins and Stewart, 1964), created by temporal and spatial patterns in breaking waves (MacMahan et al., 2011). They are often coupled to the bathymetry, where they occur in channels incised into sand bars (Fig. 1), which are visible as areas of wave breaking (Gallop et al., 2011) due to the shallower bathymetry (Fig. 1). These flows are easily capable of transporting bathers offshore into deeper water, often against their will. Current speed in rips varies with water level, wave conditions, and morphology. Rips generally flow fastest at low tide (Brander, 1999). They often circulate as eddies inside the surf zone, from which there may be occasional exits to offshore (Scott et al., 2014). The rate of these exits can be referred as the exit rate. The hazard of rips to swimmers is thought to increase with: (1) current speed inside the rip; and (2) the exit rate from the surf zone (McCarroll et al., 2014a).

* Corresponding author. Department of Environmental Sciences, Macquarie University, Level 2, The Australian Hearing Hub (AHH), University Avenue, NSW 2109, Australia.
E-mail addresses: shari.gallop@mq.edu.au (S.L. Gallop), eleanor.woodward@plymouth.ac.uk (E. Woodward), rwbrander@unsw.edu.au (R.W. Brander), S.J.Pitman@soton.ac.uk (S.J. Pitman).

1.2. Rip current rescue statistics

On beaches where they exist, rips are often the leading cause of

http://dx.doi.org/10.1016/j.ocecoaman.2015.09.010
0964-5691/

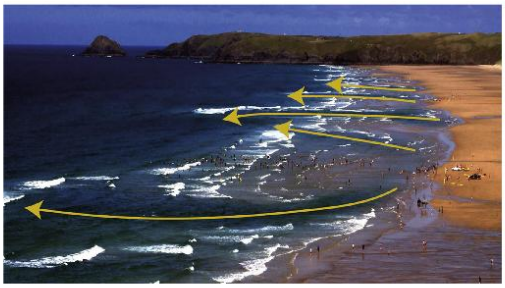

Fig. 1. Photo of Perranporth Beach, Cornwall, UK, showing breaking waves (white) with rip currents in between indicated by darker water. Direction of rip current flow is highlighted by arrows (photo courtesy of Tim Scott).

lifeguard rescues and drowning fatalities (Short, 1999; Scott et al., 2008; Brander and MacMahan, 2011; Woodward et al., 2015). They are a global problem, with annual deaths due to rips averaging 21 in Australia (Brighton et al., 2013), 35 in the U.S. (Gensini and Ashley, 2010), and 39 in India (Arun Kumar and Prasad, 2014). However, due to often incomplete incident reporting, these numbers are likely considerably higher (Brighton et al., 2013).

Of the 613 coastal drowning deaths recorded in Australia from 1 July 2004 to 30 June 2011, 293 (48%) were at a beach location. Of these beach drowning deaths, at least 44% were attributable to rip currents (Brighton et al., 2013). In the UK in 2013, of 381 reported water-related fatalities, 93 (24.4%) were classified as occurring at the coast/shore/beach, second only to 124 (32.5%) in rivers (National Water Safety Forum, 2014). In 2014, of 2507 total lifeguard rescues by the Royal National Lifeboat Institution, the largest proportion (1138, 45.4%) were attributed to rip currents as the environmental cause (RNLI, 2014). The leading activities which lead to rescues were body boarding (799) and swimming (660) (RNLI, 2014).

1.3. Rip current myths

While our understanding of the physical behaviour of rip currents is well established (Shepard et al., 1941; MacMahan et al., 2006; Gallop et al., 2011; Bruneau et al., 2013), significantly less is known about how the public understand this important and common hazard. There has traditionally been communicative information disconnects between rip current scientists, beach safety practitioners and beachgoers, leading to gaps in knowledge regarding the rip hazard (Brander and MacMahan, 2011). In response, a growing field of social science-based rip studies has emerged attempting to address this problem. Several recent studies examined the demographics, behaviour and rip and beach safety knowledge of beachgoers and the general public (Drozdzewski et al., 2012, 2015; Caldwell et al., 2013; Brannstrom et al., 2014; Woodward et al., 2015). However, very few studies have been able to assess the perceptions of infrequent beachgoers and, in particular, children (<18 years old), of the rip current hazard. Moreover, there are several misleading myths about rip currents that are at odds with rip current science, such as the notion that rips suck you under (Brander and MacMahan, 2011; Leatherman, 2013), or that breaking waves (white water) is a dangerous place to swim (Brannstrom et al., 2014). Just how persistent and prevalent these myths are in the public vernacular is largely anecdotal and yet to be quantified. This is important because overcoming rip current misconceptions remains a communication barrier for many beach safety organisations in their education efforts.

1.4. Project description

This contribution describes results from a survey questionnaire undertaken at the National Oceanography Centre, University of Southampton (NOCS), on the central south coast of the UK, on 25 April 2014, during the annual 'Ocean and Earth Day'. The main purpose of this family-orientated open day was for the public, and particularly children, to learn about research at NOCS and get hands-on experience. The survey was undertaken as a fun but educational quiz, aimed at improving understanding of the public perception of rip currents; and to provoke discussion about the misperceptions about rip currents. It was also an ideal opportunity to learn more about public knowledge on rip currents and beach safety. The aim of this study is therefore to gain an appreciation of the perception of adults and children members of the public on rip current myths and (potential) misunderstandings. Moreover, this study explored using such research facility open-days as a conduit to gain valuable knowledge on the understanding of rip currents and other hazards.

2. Methods

The survey method and questions received ethical approval by the University of Southampton Research Governance Office. The survey gained 187 respondents (10.8%) from a total number of 1731 visitors that attended the NOCS open day, which gives a margin of error of ±7% at the 95% confidence level. Of the 1731 visitors, 58% were adults and 42% children. People were recruited by advertising on a large screen, and posters that welcomed visitors to test their knowledge of beach safety with a rip current quiz. The goal was to recruit as many visitors as possible to take the survey, which therefore, had to be relatively short. Upon entering the open day, visitors were asked their postcodes. Eighty nine percent (n = 503) of 563 groups were from the south coast coastal cities of Southampton (79.5%, n = 447), Portsmouth (5.5%, n = 31), and Bournemouth (4.5%, n = 25). The remaining 8.5% (n = 48) were mostly from the inland areas of NW London, Salisbury, Reading, and Guildford, with 12 people (2.13%) from further afield in England. While the exact demographic breakdown of the survey respondents is not known, observations suggest that they represented an even mix of ages and genders.

The 187 respondents were asked a series of ten multiple choice questions that were displayed on a large screen. Each individual was provided with a handheld numeric keypad to select their answer, which was recorded electronically by a computer. As described in the following section, some of the questions had more than one correct answer. Participants could only select one answer, which may include 'all of the above' where specified. On occasion, individuals began the survey after it had already started and several left before it was completed. For each question, this is taken into account in percentages of responses. At the end of the survey, a graph of participant responses was displayed, followed by the correct answers. This primed follow up educational discussions about rip currents and associated myths and misunderstandings.

3. Results and discussion

Below, the survey questions are given, followed by the list of possible answers in italics, with the correct answer(s) underlined. A brief discussion of results for each question is provided. Percentages of answers are shown graphically in Fig. 3.

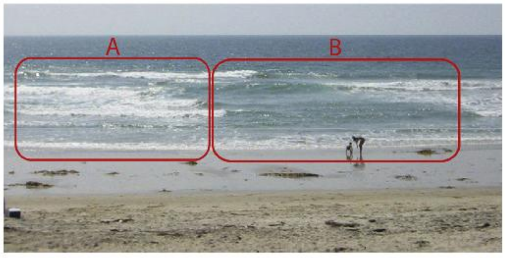

Fig. 2. Image shown to individuals asking which area is the safer place to swim. Location B denotes a rip current channel (image source: U.S. Coastguard).

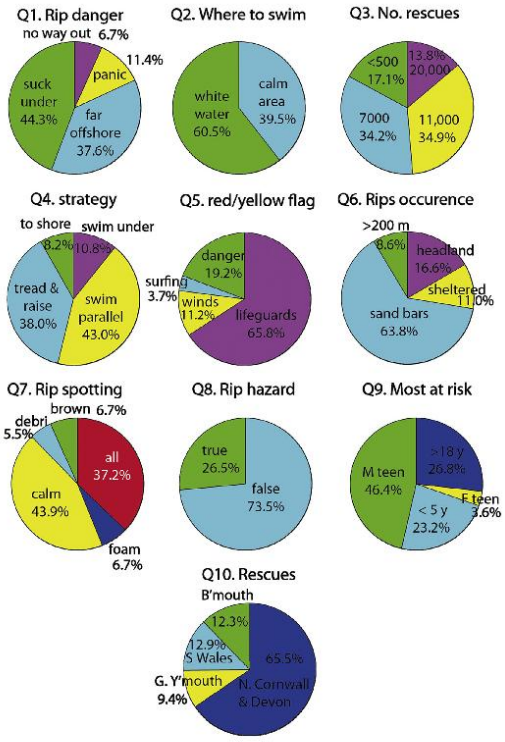

Fig. 3. Summary of results of survey questions with response percentages indicated.

Q1: What makes a rip current dangerous?

(a) It sucks you under the water; (b) It takes you really far offshore; (c) If you panic; (d) There is no way out

There are many misconceptions about rip currents. For example, as far back as the 1920's (Davis, 1925), rip currents have often been referred to as 'undertow', with the implication that bathers will be pulled or sucked under the water (Brander and MacMahan, 2011; Leatherman, 2013). This phenomena simply does not occur in rip currents, but the use of the term persists in the public vernacular (Brander, 2010; Leatherman, 2012, 2013). This is evident from the results of Q1, where 44% (n = 66) of respondents thought a rip current is dangerous because it 'sucks you under the water'.

Similarly, the traditional scientific understanding of rip current flow structure dates back to the 1940's (Shepard, 1941), and consists of a shore-perpendicular current that extends well seaward of the surf zone, where it then dissipates. This definition is still commonly found in modern scientific literature. However, recent studies have shown that rips are often dominated by recirculation within the surf zone (Austin et al., 2010; McCarroll et al., 2014a; Scott et al., 2014). The impact of the long standing paradigm is clearly evident from the survey results with 38% (n = 56) of respondents selecting that rips 'take you really far offshore' (Fig. 3). There are several escape action strategies that can be adopted to escape a rip, including swimming parallel to the beach, or just staying afloat (McCarroll et al., 2014a), yet 7% (n = 10) chose the response of 'no way out'. Only 11% (n = 17) of respondents chose the correct answer of 'if you panic', which is globally accepted as being the primary cause of rip related drowning and rescue (Short, 2007; Sherker et al., 2010; Brander et al., 2011; Drozdzewski et al., 2012, 2015).

After the survey, the explanation that rips actually do not suck you under was largely met with surprise, as was the notion that in general, rips will only take you as far as the offshore extent of the surf zone, and, in some cases, potentially recirculate back to shore. The implication here is that there is an on-going need for communicating that the danger of rips is not in 'sucking you under', but in panicking. If people caught in rips knew that they would not be sucked under, nor carried 'really far offshore', this may help reduce fatalities due to panic. A key enabler to this problem appears to be media reporting, with headlines and content such as: "*… a paediatric surgeon sucked under by rip currents after rescuing two children*" (Bradley, 2012); "*Rip current pulls girls under …*" (Harper, 2014); "*Family day out turned to horror as rip current pulled Plymouth swimmers underwater*" (Giodano, 2014), and '*Going under: Anne Hathaway was pulled under by a riptide*' (Daily Mail, 2014). In reality, rip currents do not suck under, or even out. Many field measurements of rip current flow, including those of vertical velocity structure, have been made (Brander and Short, 2001; MacMahan et al., 2006), and there is no evidence to support this notion. Indeed, writing on behalf of many experienced rip current scientists who frequently jump in rip currents in the name of science, MacMahan et al. (2011) stated that there is no feeling of suction or pulling, and when you float you move with the fluid like in a river.

Q2: Which is the safer place to swim?

(a); (b)

Rip currents often occupy deeper channels between shallow sand bars (Wright and Short, 1984; Short, 2007). Wave breaking is maximised over the shallow bars, appearing as white areas due to foam and bubbles (Figs. 1 and 2), whereas the deeper rip channels reduce the amount of wave breaking and hence appear as dark gaps of seemingly calmer water (Brander, 2010). Furthermore, white water associated with breaking waves is generally being transported towards the shoreline. Therefore, in terms of the rip current hazard, the area of relatively rougher, whiter water is actually the safer area to swim (Hatfield et al., 2012; Brannstrom et al., 2014).

Survey respondents were shown Fig. 2, and were asked which area they thought was the safer place to swim. Despite potential bias due to the survey being about rip currents, 40% (n = 60) of respondents incorrectly said that the apparent calm area 'B' (a rip channel) was the safer area to swim (Fig. 3). Other studies have used a similar method to assess the publics' ability to identify rip currents, with results ranging from <20% of respondents at Pensacola, Florida (Caldwell et al., 2013), to 40% in New South Wales (NSW), Australia (Sherker et al., 2010). Of concern, 52% and 61% of survey respondents in NSW (Sherker et al., 2010) and Queensland, Australia (Ballantyne et al., 2005) respectively selected rip channels as the safest place to swim. In Texas, U.S., 87% of survey respondents

either failed to locate rips in photos or incorrectly said that the photo with the heaviest surf represented the most hazardous area and is likely to contain rip currents (Brannstrom et al., 2014). In general, these studies found that the main reason(s) for choosing the rip as the safest place to swim was due to the (incorrect) ideas that calm water is safe (Ballantyne et al., 2005) and that rip currents are associated with areas of heavy surf (Caldwell et al., 2013; Brannstrom et al., 2014).

Q3: In the 5 years between 2009 and 2013, how many people did the Royal National Lifeboat Institution (RNLI) pull from rips?

(a) <500; (b) 7000; (c) 11000; (d) 20000

The purpose of this question was to: (a) get an understanding on the perspective of the public on how many people they think are rescued from rips; and (b) to stress how common it is for people to be caught in rips. There were 11275 people rescued and assisted by the RNLI in incidents involving rip currents between 2009 and 2013 (inclusive) (Woodward, 2015). The correct answer of 11000 was selected by 34% (n = 53), and 35% (n = 52) selected 7000. Less respondents chose the remaining two answers with 17% (n = 26) selecting <500 and 14% (n = 21) choosing 20000. The low number selecting <500 shows that in general, people are aware that rip current rescues are a relatively common occurrence, yet a third were specifically aware of how many people become victims of rip currents.

Q4: What should you do if you are caught in a rip?

(a) Swim directly back to shore; (b) Tread water and raise your arm; (c) Swim parallel to the shore; (d) Swim under the water to avoid the current

There is presently no agreement among beach safety practitioners on a single generic message to promote to bathers about how to react when caught in a rip current. As described by Brander and MacMahan (2011), the messages 'do not panic' and 'do not swim against the rip' are endorsed globally by beach safety organisations. However, there is considerable debate surrounding swimmer escape strategies — whether it is safer for those caught in rips to 'swim parallel to the beach' or 'stay afloat' (Brander et al., 2011; MacMahan et al., 2010; Bradstreet et al., 2014; McCarroll et al., 2014a; Drozdzewski et al., 2015).

'Swim parallel to the beach' is a long standing message communicated to the public, that is based on early scientific understanding of rip current flow behaviour (Bradstreet et al., 2014), which suggested that rips flow perpendicular to the beach at distances well seaward of the surf zone (Shepard et al., 1941; Brander and MacMahan, 2011; Brander, 2015). This idealised definition of a rip current is generally what is depicted on rip current warning signs and other media such as brochures. In this scenario, swimming parallel to escape the rip is an optimal strategy. However, in reality, rips often flow at extreme angles to the shoreline making the 'swim parallel' option very difficult, and could lead to exhaustion and panic. Moreover, it is problematic for weak or non-swimmers (Drozdzewski et al., 2015). The 'stay afloat' option is supported by recent field observations that show rip circulations to be largely contained within the surf zone (Austin et al., 2010; McCarroll et al., 2014a; Scott et al., 2014), with the implication that floating objects, such as bathers, will be returned to the relative safety of shallow shoals within minutes by currents (MacMahan et al., 2010). However, recent field research by McCarroll et al. (2014a) involving direct measurements of rip current escape strategies, suggested that neither option is viable in all situations, and is dependent on variables such as wave height, direction and rip current circulation patterns. These findings were supported by subsequent modelling studies involving simulated swimmers of all abilities (McCarroll et al., 2015). Based on these results, Surf Life Saving Australia has now incorporated the 'combined approach' to react to being caught in rip currents into their core educational material, while also suggesting that on a beach patrolled by lifeguards, staying afloat and signalling for help is certainly a preferred option (Bradstreet et al., 2014).

When interpreting the answers to Q4, it should be noted that there was no context provided, e.g. whether the swimmer was on a patrolled beach, alone, or with others. The impact of the long standing 'swim parallel to the shore' message is evident from the majority of respondents (43%; n = 68) choosing this answer (Fig. 3). This is remarkably similar to results of Brannstrom et al. (2014) in Texas, U.S., where 44% of survey respondents knew to swim shore parallel if stuck in a rip, but much less than the 76% in NSW, Australia who said they would swim across the rip (Sherker et al., 2010). It is also encouraging that 38% (n = 60) choose the passive response of 'treading water and raising their arm'. Nineteen percent answered incorrectly, with 11% (n = 17) selecting to swim under to avoid the current, and 8% (n = 13) to swim back to shore, which in a rip current would be against the flow. Both of these options could lead to fatigue and could increase the risk of drowning.

Q5: At a UK beach, what does a red and yellow flag mean?

(a) Danger — don't swim here; (b) Area for surfing; (c) Strong winds = no inflatables to be used; (d) Area patrolled by lifeguards

In the UK, as in other countries such as Australia, New Zealand, Thailand and South Africa, lifeguards designate areas that are safe for bathing using a pair of red and yellow flags, in accordance with International Life Saving Federation (ILSF) recommendations (Woodward et al., 2015). These flags are intended to be placed away from rip currents and other hazards. Research has proven internationally that bathers are safest in lifeguard patrolled areas (Fenner, 2000; Branche and Stewart, 2001; Hartmann, 2006; Sherker et al., 2010). In this survey, 66% (n = 106) of respondents knew that this flag means the area is patrolled by lifeguards (Fig. 3), just slightly lower than the figure of 77% obtained by Woodward et al. (2015) from people on UK beaches. However, 34% did not know what this means: 19% thought it meant 'danger — do not swim here' (n = 31), 11% 'strong winds — do not use inflatables here' (n = 18) and 4% thought it designated an area for surfing (n = 6). Ballantyne et al. (2005) found that almost all domestic Australian students surveyed recognised that these flags identify patrolled areas, compared to 60% of the international students, with 13% saying they indicated a dangerous area. Unfortunately, even when people know that such flags indicate safe bathing areas, some still choose to swim elsewhere (Ballantyne et al., 2005; Wilks et al., 2007; Sherker et al., 2010 White and Hyde, 2010). According to a survey conducted by Surf Life Saving Australia (SLSA, 2014), only 43% of people choose to swim between the flags (SLSA, 2014).

Q6: Where is a rip current likely to occur?

(a) In water deeper than 200 m; (b) Between sand bars; (c) On beaches sheltered from waves; (d) Along a headland

There are essentially 3 categories of rip currents (Brander, 2015): (1) beach rips that occupy distinct morphological channels between sand bars on open sections of beaches, and tend to be relatively fixed in place for periods of days/weeks/months (Short, 2007; Brander, 2010); (2) boundary rips, which also occupy deeper channels, but are located adjacent to physical structures such as headlands, rock platforms and groynes (Short, 1985, 2007; Gallop et al., 2011; McCarroll et al., 2014b); and (3) transient or 'flash' rips, which are spatially and temporally variable, and are not coupled to the underlying morphology, but are hydrodynamically controlled (Johnson and Pattiaratchi, 2004). It is well established that fixed beach rip currents and boundary rips are the most common and persistent (Short, 2007; Brander, 2010). Therefore, the two correct answers to Q6 are (b) and (d).

The majority (n = 104, 64%) of respondents selected 'between sand bars', and (n = 27, 16%) along headlands (Fig. 3). Twenty

percent (n = 32) of respondents provided incorrect answers with 11% answering 'on beaches sheltered from waves' (n = 18); and 9% 'in water deeper than 200 m' (n = 14; Fig. 3).

Q7: How do you spot a rip current?

(a) Discoloured, brown water; (b) Debris on the surface; (c) Calm area; (d) Foam on the surface; (e) All of the above

Just as there are different types of rip currents, there are also different visual identification characteristics associated with these types (Shepard et al., 1941; Brander, 2010) that are communicated to the public. In general, fixed beach and boundary rip currents appear as darker bands of water, due to the presence of a deeper channel that inhibits wave breaking (Lippmann and Holman, 1989; Ranasinghe et al., 2004). However, water carried seaward by the rip flow interacts with incoming water due to wave action, and the surface of the water in rip currents may often be disturbed and characterised by surface rippling, foam and bubbles (MacMahan et al., 2006). Similarly, rip flow can carry floating material such as seaweed, debris, and sand (Smith and Largier, 1995; Reniers et al., 2010). In the case of the latter, sand clouds are primarily visible once the rip current exits the surf zone (Fig. 1), particularly for transient rip currents. Therefore all of the answers to this question are correct. The purpose was to see what type of visual characteristics they associated most with rip currents.

Most respondents (44%; n = 72) said rips can be spotted as a calm area, 7% said foam on the water surface (n = 11), 7% as discoloured, brown water (n = 11), and 5% said debris on the surface (n = 9) (Fig. 3). Those indicating that rips can be spotted by all of these answers totalled 37% (n = 61). Due to the pre-defined responses to the question, it is likely that percentages represent an inflated representation of rip current identification understanding. For example, in the US, Brannstrom et al. (2014) found that only 13% of beach users were able to identify a rip current, Caldwell et al. (2013) noted that less than 20% of respondents were able to identify rip channels and currents, and in Australia, Williamson et al. (2008) found 40% of survey participants were able to identify a rip. There is evidence to suggest that people can be overconfident in what they know about rip currents. For example, Ballantyne et al. (2005) found that 62% thought they knew what a rip current was, but the majority could not actually recognise one; and Caldwell et al. (2013) found that 57% said they could identify a rip currents with high confidence, but in practice less than 20% were able to do this. The order that the identifying features of a rip current were selected for Q7 is consistent with data collected by Woodward (2015). It has been argued that communicating methods of rip current identification is key to reducing rip current incidents and fatalities, to allow beach users to avoid entering a rip in the first place (Sherker et al., 2010; Brander et al., 2014).

Q8: TRUE or FALSE - Shark attacks, lightning, and tornadoes combined kill more people than rip currents?

a) True; b) False

Several studies have identified that fatalities due to rip currents can exceed those caused by other, more publicised natural hazards in countries such as the U.S. and Australia (Lascody, 1998; Fletemeyer and Leatherman, 2010; Brander et al., 2013). The majority of survey respondents (73%; n = 122) correctly said that this statement was false (Fig. 3). The remaining 44 (26%) were surprised to find out that rip currents can cause more deaths than these other hazards. However, this is likely not the case in the UK context. The relatively high proportion of correct responses may be due to bias because the survey was about rip currents. Rip currents are high frequency and low impact hazards, and rarely cause more than one fatality in a single incident. As such, elements of complacency are often associated between the rip current hazard and public and media perception (Drozdzewski et al., 2012; SLSA, 2014). Rips also do not generally threaten infrastructure, cannot be managed by engineering, and the immediate impacts of drowning and injuries tend to be restricted to the family and local authorities such as lifeguards and emergency services (Short and Hogan, 1994). Therefore, the rip current hazard is often disregarded by governments and coastal managers (Lascody, 1998; Brander and MacMahan, 2011).

Q9: In the UK, you are more likely to get caught in a rip if you are:

(a) Male teenager; (b) Child <5 years old; (c) Female teenager; (d) Adult >18 years old

In the UK, male teenagers (aged 13–17 years) are the most likely demographic to be involved in rip current incidents (Woodward et al., 2013). Normalised data showed that teenagers in general were the most at risk, with 39% males and 24% females. Studies elsewhere also show that males are more at risk compared to females, including in Australia where 85% of coastal drowning were male (Brighton et al., 2013), and the U.S., where males account for 84% of all rip current fatalities, and are 6 times more likely than females to be caught in rips (Gensini and Ashley, 2010). In Australia, of the 266 drownings in 2013–2014, 13% (n = 34) were on beaches, and 81% were male (Royal Life Saving, 2014). The most common age range on beaches was 25–34 years of age, followed by 18–24 years (21%). Males are more likely to report a higher level of water confidence and exposure to risk behaviours (Gulliver and Begg, 2005), as well as overestimate their ability and underestimate risk (McCool et al., 2009). In water related incidents, Morgan et al. (2009) attributed the male gender bias to increased frequency and exposure to water based activity, and anecdotal evidence from UK lifeguards suggests males outweigh females in the water. However, from a study in New Zealand, Moran (2011) argues that it is less about exposure and more about male understanding and their behaviour and practice of water safety. In this survey, 46% (n = 78) of respondents answered correctly that you are most likely to be caught if you are a male teenager (Fig. 3). Twenty seven percent (n = 45) said if you are older than 18, 23% said less than 5 years old (n = 39), and 4% said female teenager (n = 6).

Q10: In the UK, rip incidents are more common where?

(a) Bournemouth; (b) South Wales; (c) Great Yarmouth; (d) North Cornwall and North Devon

The majority (81%) of RNLI beach lifeguard rip current incidents occur on the north coast of North Devon and Cornwall (Woodward et al., 2013). This is due to the combination of large tidal range, consistent swell, and beaches with sand bar morphologies where rips are common (Scott et al., 2011). These high occurrence rates were elevated by the large number of seasonal visitors (Woodward et al., 2013). For Q10, 4 options were given, which are popular seaside holiday destinations. Most respondents in this survey (65%; n = 122) selected that rip current rescues are more common in North Cornwall and North Devon, with 12% (n = 21) saying Bournemouth, 13% (n = 22) South Wales, and 9% (n = 16) Great Yarmouth (Fig. 3). North Cornwall and Devon are approximately 300 km driving from Southampton. Further research is required to determine how people know rips are common in this area; where it may relate to the fact that the north coast of Devon and Cornwall is a popular holiday destination in the UK, particularly for families, or respondents may associate rip currents with surf, which is dominant in those areas.

4. Conclusions

The rip current hazard is globally significant, yet many long-standing misconceptions and myths about rips exist, which can have potential negative consequences for beachgoers. However, to date, evidence regarding how prevalent and persistent these misconceptions are in the general public has been largely anecdotal.

This opportunistic study has described and quantified public perceptions of these myths for a representative sample of visitors to an open day at the National Oceanography Centre, Southampton, on the central south coast of the UK. The survey was undertaken as a fun but informative quiz aimed at families visiting the research-facility, and explored using such events as a conduit to gain valuable knowledge on the understanding of rip currents. In general, this mixed group of adults and children showed an awareness of the scale of the rip hazard, in terms of rescues, where rips occur, and how to escape a rip current if caught in one. However, of concern, is that only 11% of this group knew why rips are dangerous (due to panic), with 44% incorrectly stating that rips 'suck you under'. This relates to the persistence of the ongoing myth and incorrect use of the term 'undertow' to describe rip currents (Brander et al., 2013). Similarly, although most respondents knew the visual identifiers associated with rips, 40% still chose the rip current as the safest place to swim when shown a picture of one.

This study provides evidence that there are still misunderstandings about rip currents in the UK and existing detachments between the public and safety messages that needs to be addressed. In particular, there is a need to improve public awareness of how rip currents behave, what makes them dangerous, and how to identify them. Future communication efforts via rip current education interventions should attempt to dispel the myth of the 'undertow', and promote the 'don't panic' response. They should also emphasise the visual contrast between white water (non-rip), and calm water (rip location), to assist in rip identification. In the case of the latter, the use of slogans such as 'white is nice, green is mean' advocated in Australia (Brander, 2010), or the use of imagery and footage of coloured dye releases (Brander et al., 2013) may be useful. Ultimately, the best approach to mitigate the rip hazard is to encourage beachgoers to swim only on lifeguard patrolled beaches and in designated supervised areas. However, 34% of the survey respondents did not know what the red and yellow beach flags mean, further illustrating the need for continued public beach safety education in the UK at the most fundamental level.

References

Arozarena, I., Houser, C., Echeverria, A.G., Brannstrom, C., 2015. The rip current hazard in Costa Rica. Nat. Hazards 77 (2), 753–768. http://dx.doi.org/10.1007/s11069-015-1626-9.

Arun Kumar, S.V.V., Prasad, K.V.S.R., 2014. Rip current-related fatalities in India: a new predictive risk scale for forecasting rip currents. Nat. Hazards 71 (1), 313–335. http://dx.doi.org/10.1007/s11069-013-0812-x.

Austin, M., Scott, T., Brown, J., Brown, J., MacMahan, J., Masselink, G., Russell, P., 2010. Temporal observations of rip current circulation on a macro-tidal beach. Cont. Shelf Res. 30 (9), 1149–1165. http://dx.doi.org/10.1016/j.csr.2010.03.005.

Ballantyne, R., Carr, N., Hughes, K., 2005. Between the flags: an assessment of domestic and international university students' knowledge of beach safety in Australia. Tour. Manag. 26 (4), 617–622. http://dx.doi.org/10.1016/j.tourman.2004.02.016.

Bradley, B., 2012, August 7. Warning about Rip Currents on Lake Michigan. ABC Eyewitness News. Retrieved from. http://abc7chicago.com/archive/8765524/.

Bradstreet, A.J., Brander, R.W., McCarroll, J.R., Brighton, B., Dominey Howes, D., Drozdzewski, D., Sherker, S., Turner, I., Roberts, A., MacMahan, J., 2014. Rip current survival principles: towards consistency. J. Coast. Res. 72 (Special issue), 85–92. http://dx.doi.org/10.2112/SI72-016.1.

Branche, C.M., Stewart, S., 2001. Lifeguard Effectiveness: a Report of the Working Group. Centers for Disease Control and Prevention, National Center for Injury Prevention and Control, Atlanta, GA. Retrieved from. http://stacks.cdc.gov/view/cdc/11284.

Brander, R.W., 1999. Field observations on the morphodynamics evolution of a low-energy rip current system. Mar. Geol. 157 (3–4), 199–217. http://dx.doi.org/10.1016/S0025-3227(98)00152-2.

Brander, R.W., 2010. Dr Rip's Essential Beach Book: Everything You Need to Know about Surf, Sand and Rips. University of New South Wales Press Ltd, Sydney, NSW.

Brander, R.W., 2015. Rip currents. In: Ellis, J., Sherman, D. (Eds.), Sea and Ocean Hazards, Risks and Disasters. Treatise in Hazards and Disasters. Elsevier, Amsterdam, pp. 335–380.

Brander, R.W., Bradstreet, A., Sherker, S., MacMahan, J., 2011. Responses of swimmers caught in rip currents: perspectives on mitigating the global rip current hazard. Int. J. Aquatic Res. Educ. 5, 476–482.

Brander, R.W., Drozdzewski, D., Dominey-Howes, D., 2014. "Dye in the water": a visual approach to communicating the rip current hazard. Sci. Commun. 36 (6), 802–810. http://dx.doi.org/10.1177/1075547014543026.

Brander, R.W., Dominey-Howes, D., Champion, C., Del Vecchio, O., Brighton, B., 2013. Brief Communication: a new perspective on the Australian rip current hazard. Nat. Hazard Earth Sys. 13, 1687–1690. http://dx.doi.org/10.5194/nhess-13-1687-2013.

Brander, R.W., MacMahan, J.H., 2011. Future challenges for rip current research and outreach. In: Leatherman, S., Fletemeyer, J. (Eds.), Rip Currents — Beach Safety, Physical Oceanography, and Wave Modelling. CRC Press, Boca Raton, FL, pp. 1–29.

Brander, R.W., Short, A.D., 2001. Flow kinematics of low-energy rip current systems. J. Coast. Res. 17 (2), 468–481.

Brannstrom, C., Trimble, S., Santos, A., Brown, H.L., Houser, C., 2014. Perception of the rip current hazard on Galverston Island and North Padre Island, Texas, USA. Nat. Hazards 72 (2), 1123–1138. http://dx.doi.org/10.1007/s11069-014-1061-3.

Brighton, B., Sherker, S., Brander, R., Thompson, M., Bradstreet, A., 2013. Rip current related drowning deaths and rescues in Australia 2004–2011. Nat. Hazard Earth Sys. 13, 1069–1075. http://dx.doi.org/10.5194/nhess-13-1069-2013.

Bruneau, N., Bertin, X., Castelle, B., Bonneton, P., 2013. Tide-induced flow signature in rip currents on a meso-macrotidal beach. Ocean. Model. 74, 53–59. http://dx.doi.org/10.1016/j.ocemod.2013.12.002.

Caldwell, N., Houser, C., Meyer-Arendt, K., 2013. Ability of beach users to identify rip currents at Pensacola Beach, Florida. Nat. Hazards 68 (2), 1041–1056. http://dx.doi.org/10.1007/s11069-013-0673-3.

Daily Mail, 2014, January 9. Pictured: the Moment Panicked Anne Hathaway Got Caught in a Riptide and Screamed for Help in Choppy Hawaii Waters. Daily Mail. Retrieved from. http://www.dailymail.co.uk/tvshowbiz/article-2536733/Moment-panicked-Anne-Hathaway-gets-caught-riptide-screams-help-choppy-Hawaii-waters.html.

Davis, W.M., 1925. The undertow myth. Science 61 (1573), 206–208. http://dx.doi.org/10.1126/science.61.1573.206.

Drozdzewski, D., Shaw, W., Dominey-Howes, D., Brander, R., Walton, T., Gero, A., Sherker, S., Goff, J., Edwick, B., 2012. Surveying rip current survivors: preliminary insights into the experiences of being caught in rip currents. Nat. Hazard Earth Sys. 12, 1201–1211. http://dx.doi.org/10.5194/nhess-12-1201-2012.

Drozdzewski, D., Roberts, A., Dominey-Howes, D., Brander, R., 2015. The experiences of weak and non-swimmers caught in rip currents at Australian beaches. Aust. Geogr. 46 (1), 15–32. http://dx.doi.org/10.1080/00049182.2014.953735.

Fenner, P., 2000. Drowning awareness. Prevention and treatment. Aust. Fam. Physician 29 (11), 1045–1049.

Fletemeyer, J., Leatherman, S., 2010. Rip currents and beach safety education. J. Coast. Res. 26 (1), 1–3. http://dx.doi.org/10.2112/09A-0005.1.

Gallop, S.L., Bryan, K.R., Coco, G., Stephens, S.A., 2011. Storm-driven changes in rip channel patterns on an embayed beach. Geomorphology 127 (3–4), 179–188. http://dx.doi.org/10.1016/j.geomorph.2010.12.014.

Gensini, V.A., Ashley, W.S., 2010. An examination of rip current fatalities in the United States. Nat. Hazards 54 (1), 159–175. http://dx.doi.org/10.1007/s11069-009-9458-0.

Giordano, C., 2014, September 15. Family Day Out Turned to Horror as Rip Current Pulled Plymouth Swimmers Underwater. Plymouth Herald. Retrieved from. http://www.plymouthherald.co.uk/family-day-turned-horror-rip-current-pulled/story-22928256-detail/story.html.

Gulliver, P., Begg, D., 2005. Usual water-related behaviour and 'near-drowning' incidents in young adults. Aust. N. Z. J. Publ. Heal 29 (3), 238–243.

Harper, J., 2014, July 7. 3 girls Escape Terrifying Rip Current on Sandwich Beach. WCVB. Retrieved from. http://www.wcvb.com/news/3-girls-escape-terrifying-rip-current-on-sandwich-beach/26828688.

Hartmann, D., 2006. Drowning and beach-safety management (BSM) along the Mediterranean beaches of Israel—a long term perspective. J. Coast. Res. 22 (6), 1505–1514. http://dx.doi.org/10.2112/05-0497.1.

Hatfield, J., Williamson, A., Sherker, S., Brander, R., Hayen, A., 2012. Development and evaluation of an intervention to reduce rip current related beach drowning. Accid. Anal. Prev. 46, 45–51. http://dx.doi.org/10.1016/j.aap.2011.10.003.

International Lifesaving Federation of Europe (ILFE), 2005. Safety on European Beaches: Operational Guidelines, first ed. Retrieved from. http://europe.ilsf.org/sites/europe.ilsf.org/files/Safety.pdf.

Johnson, D., Pattiaratchi, C., 2004. Transient rip currents and nearshore circulation on a swell-dominated beach. J. Geophys. Res. Oceans 109, C02026. http://dx.doi.org/10.1029/2003JC001798.

Klein, A. H. da F., Santana, G.G., Diehl, F.L., de Menezes, J.T., 2003. Analysis of hazards associated with sea bathing: results of five years work in oceanic beaches of Santa Catarina state, southern Brazil. J. Coast. Res. 35, 107–116.

Lascody, R.L., 1998. East central Florida rip current program. Natl. Weather Dig. 22 (2), 25–30. Retrieved from. http://www.srh.noaa.gov/images/mlb/pdfs/EastCentralFloridaRipCurrentProgram_NWA.pdf.

Leatherman, S.P., 2012. Undertow, rip current, and riptide. J. Coast. Res. 28 (4), iii–iiv. http://dx.doi.org/10.2112/JCOASTRES-D-12-00052.1.

Leatherman, S.P., 2013. Rip currents. In: Finkl, C. (Ed.), Coastal Hazards. Springer, New York, pp. 811–831.

Lippmann, T.C., Holman, R.A., 1989. Quantification of sand bar morphology: a video technique based on wave dissipation. J. Geophys. Res. Oceans 94 (C1), 995–1011. http://dx.doi.org/10.1029/JC094iC01p00995.

Longuet-Higgins, M.S., Stewart, R.W., 1964. Radiation stresses in water waves, a physical discussion with applications. Deep Sea Res. 11 (4), 529–563. http://dx.doi.org/10.1016/0011-7471(64)90001-4.

MacMahan, J., Brown, J., Brown, J., Thornton, E., Reniers, A., Stanton, T., Henriquez, M., Gallager, E., Morrison, J., Austin, M.J., Scott, T.M., Senechal, N., 2010. Mean lagrangian flow behaviour on an open coast rip-channeled beach: a new perspective. Mar. Geol. 268 (1–4), 1–15. http://dx.doi.org/10.1016/j.margeo.2009.09.011.

MacMahan, J., Reniers, A., Brown, J., Brander, R., Thornton, E., Stanton, T., Brown, J., Carey, W., 2011. An introduction to rip currents based on field observations. J. Coast. Res. 27 (1), iii–ivi. http://dx.doi.org/10.2112/JCOASTRES-D-11-00024.1.

MacMahan, J.H., Thornton, E.B., Reniers, J.H.M., 2006. Rip current review. Coast. Eng. 53 (2–3), 191–208. http://dx.doi.org/10.1016/j.coastaleng.2005.10.009.

Martínez, M.L., Intralawan, A., Vázquez, G., Pérez-Maqueo, O., Sutton, P., Landgrave, R., 2007. The coasts of our world: ecological, economic and social importance. Ecol. Econ. 63 (2–3), 254–272. http://dx.doi.org/10.1016/j.ecolecon.2006.10.022.

Matthews, B., Andronaco, R., Adams, A., 2014. Warning signs at beaches: do they work? Saf. Sci. 62, 312–318. http://dx.doi.org/10.1016/j.ssci.2013.09.003.

McCarroll, R.J., Brander, R.W., MacMahan, J.H., Turner, I.L., Reniers, A.J.H.M., Brown, J.A., Bradstreet, A., Sherker, S., 2014a. Evaluation of swimmer-based rip current escape strategies. Nat. Hazards 71, 1821–1846. http://dx.doi.org/10.1007/s11069-013-0979-1.

McCarroll, R.J., Brander, R.W., Turner, I.L., Power, H.E., Mortlock, T.R., 2014b. Lagrangian observations of circulation on an embayed beach with headland rip currents. Mar. Geol. 355, 173–188. http://dx.doi.org/10.1016/j.margeo.2014.05.020.

McCarroll, R.J., Castelle, B., Brander, R.W., Scott, T., 2015. Modelling rip current flow and bather escape strategies over a transverse bar and rip channel morphology. Geomorphology 246, 502–518. http://dx.doi.org/10.1016/j.geomorph.2015.06.041.

McCool, J., Ameratunga, S., Moran, K., Robinson, E., 2009. Taking a risk perception approach to improving beach swimming safety. Int. J. Behav. Med. 16 (4), 360–366. http://dx.doi.org/10.1007/s12529-009-9042-8.

Moran, K., 2011. (Young) Men behaving badly: dangerous masculinities and risk of drowning in aquatic leisure activities. Ann. Leis. Res. 14 (2–3), 260–272. http://dx.doi.org/10.1080/11745398.2011.615719.

Morgan, D., Ozanne-Smith, J., Triggs, T., 2009. Direct observation measurement of drowning risk exposure for surf beach bathers. J. Sci. Med. Sport 12 (4), 457–462. http://dx.doi.org/10.1016/j.jsams.2008.04.003.

National Water Safety Forum, 2014. National Water Safety Forum 2013 Water Related Fatalities Statistics Release. http://www.nationalwatersafety.org.uk/waid/info/waid_fatalincidentreport_2013.xls.

Ranasinghe, R., Symonds, G., Black, K., Holman, R., 2004. Morphodynamics of intermediate beaches: a video imaging and numerical modelling study. Coast. Eng. 51 (7), 629–655. http://dx.doi.org/10.1016/j.coastaleng.2004.07.018.

Reniers, A.J.H.M., MacMahan, J., Beron-Vera, F.J., Olascoaga, M.J., 2010. Rip-current pulses tied to Lagrangian coherent structures. Geophys. Res. Lett. 37 (5), L05605. http://dx.doi.org/10.1029/2009GL041443.

Royal Life Saving, 2014. National Drowning Report 2014. Retrieved from. http://www.royallifesaving.com.au/__data/assets/pdf_file/0007/11995/RLS_NDR2014_LR.pdf.

Royal National Lifeboat Institution, 2014. Operational Statistics 2013. Retrieved from. http://rnli.org/aboutus/aboutthernli/Documents/ops-stats-report.pdf.

Scott, T., Masselink, G., Austin, A.J., Russell, P., 2014. Controls on macrotidal rip current circulation and hazard. Geomorphology 214, 198–215. http://dx.doi.org/10.1016/j.geomorph.2014.02.005.

Scott, T., Masselink, G., Russell, P., 2011. Morphodynamic characteristics and classification of beaches in England and Wales. Mar. Geol. 286 (1–4), 1–20. http://dx.doi.org/10.1016/j.margeo.2011.04.004.

Scott, T., Russell, P., Masselink, G., Wooler, A., Short, A., 2007. Beach rescue statistics and their relation to nearshore morphology and hazards: a case study for southwest England. J. Coast. Res. 50 (Special issue), 1–6.

Scott, T., Russell, P., Masselink, G., Wooler, A., 2009. Rip current variability and hazard along a macro-tidal coast. J. Coast. Res. 59 (Special issue), 895–899.

Scott, T., Russell, P., Masselink, G., Wooler, A., Short, A., 2008. High volume sediment transport and its implications for recreational beach risk. In: Proceedings of the 31st International Conference on Coastal Engineering, pp. 4250–4262. http://dx.doi.org/10.1142/9789814277426_0353. Hamburg.

Shepard, F.P., Emery, K.O., La Fond, E.C., 1941. Rip currents: a process of geological importance. J. Geol. 49, 337–369. Retrieved from. http://www.jstor.org/stable/30063339.

Sherker, S., Williamson, A., Hatfield, J., Brander, R., Hayen, A., 2010. Beachgoers' beliefs and behaviours in relation to beach flags and rip currents. Accid. Anal. Prev. 42 (6), 1785–1804. http://dx.doi.org/10.1016/j.aap.2010.04.020.

Short, A.D., 1985. Rip current type, spacing and persistence, Narrabeen beach, Australia. Mar. Geol. 65 (1–2), 47–71. http://dx.doi.org/10.1016/0025-3227(85)90046-5.

Short, A.D., 1999. Handbook of Beach and Shoreface Morphodynamics. John Wiley and Sons, New York.

Short, A.D., 2007. Australian rip systems—friend or foe? J. Coast. Res. 50 (Special issue), 7–11.

Short, A.D., Hogan, C.L., 1994. Rip currents and beach hazards, their impact on public safety and implications for coastal management. J. Coast. Res. 12 (Special issue), 197–209. Retrieved from. http://www.jstor.org/stable/25735599.

Smith, J.A., Largier, J.L., 1995. Observations of nearshore circulation: rip currents. J. Geophys. Res. 100 (C6), 10967–10975. http://dx.doi.org/10.1029/95JC00751.

Stronge, W.B., 2005. Economic value of beaches. In: Schwartz, M. (Ed.), Encyclopedia of Coastal Science. Springer, Dordrecht, pp. 401–403.

Surf Life Saving Australia (SLSA), 2014. National Coastal Safety Report 2014. Retrieved from. https://sls.com.au/sites/sls.com.au/files/NCSR%202014_101114_final.pdf.

White, K.M., Hyde, M.K., 2010. Swimming between the flags: a preliminary exploration of the influences on Australians' intentions to swim between the flags at patrolled beaches. Accid. Anal. Prev. 42 (6), 1831–1838. http://dx.doi.org/10.1016/j.aap.2010.05.004.

Wilks, J., DeNardi, M., Wodarski, R., 2007. Close is not close enough: drowning and rescues outside flagged beach patrol areas in Australia. Tour. Mar. Environ. 4 (1), 57–62. http://dx.doi.org/10.3727/154427307784835651.

Williamson, A., Hatfield, J., Sherker, S., Brander, R., Hayen, A., 2008. Improving beach safety: the science of the surf research project. In: Proceedings of 2008 Australian Water Safety Conference, pp. 102–103. Sydney. Retrieved from. http://www.ripcurrents.com/SymposiumDocuments/Improving%20Beach%20Safety-%20The%20Science%20of%20the%20Surf%20Research%20Project.pdf.

Woodward, E.M., 2015. Rip Currents in the UK: Incident Analysis, Public Awareness, and Education (Unpublished doctoral dissertation). Plymouth University, Plymouth, United Kingdom.

Woodward, E., Beaumont, E., Russell, P., Macleod, R., 2015. Public understanding and knowledge of rip currents and beach safety in the UK. Int. J. Aquatic Res. Educ. 9, 49–69. http://dx.doi.org/10.1123/ijare.2014-0067.

Woodward, E.M., Beaumont, E., Russell, P.E., Wooler, A., Macleod, R., 2013. Analysis of rip current incidents and victim demographics in the UK. J. Coast. Res. 65 (Special issue), 850–855.

Wright, L.D., Short, A.D., 1984. Morphodynamic variability of surf zones and beaches: a synthesis. Mar. Geol. 56 (1–4), 93–118. http://dx.doi.org/10.1016/0025-3227(84)90008-2.

Appendix C: Rip current observations paper

This paper was published as a result of the fieldwork undertaken for this PhD.

Rip current observations on a low-sloping dissipative beach

Shari L. Gallop[1,2], Karin R. Bryan[3], Sebastian Pitman[2], Roshanka Ranasinghe[4,5,6], Dean Sandwell[3]
[1] Department of Environmental Sciences, Macquarie University, NSW, Australia; shari.gallop@mq.edu.au
[2] Ocean and Earth Science, University of Southampton, Southampton, United Kingdom
[3] School of Science, University of Waikato, Hamilton, New Zealand
[4,5,6] UNESCO-IHE and Deltares, Delft, The Netherlands; and Australian National University, Canberra, Australia

Abstract
Rip currents are the main cause of beach rescues and fatalities. Key drivers of rip current hazard are: (1) fast current speeds; and (2) the exit rate of floating material from inside to outside of the surf zone. Exit rates may vary temporally, such as due to Very Low Frequency (VLF) motions, which have a period on the order of 10 minutes. However, there is little field data to determine the driver(s) of exit rate. Therefore, the aim of this research was to determine rip current circulation patterns, and specifically, determine their relationship to surf zone exits, on a high-energy dissipative beach. Three days of field measurements were undertaken at Ngarunui Beach, New Zealand. Three daily surf zone flow patterns were found: (1) alongshore; (2) surf zone eddy with high exit rate; and (3) surf zone eddy with no exits. There were strong infragravity peaks in energy within the surf zone, at 30-45s, although none at VLF (~10 minute) frequencies. Further research is underway to determine what drove the high surf zone exit rate observed at Ngarunui Beach.

Keywords: rip currents, video imagery, dissipative beach, surf zone, infragravity waves

1. Introduction

Rip currents are the leading global cause of rescues and fatalities of beach users [1; 2]. Rips are jet-like flows that flow seaward across the surf zone [3; 4], and are a common feature on beaches in an intermediate morphodynamic state [5]. The risk of rips to beach users is influenced by: (1) current speed inside the rip; and (2) the exit rate from the surf zone. Rip currents are generally strongest at low tide [6]. Rip circulation patterns often form eddies inside the surf zone, from which there may be occasional exits [7]. The rip current hazard is thought to increase with exit rate. Also, exit rate may be important for determining the best escape strategy for people caught in a rip [8]. Rip current velocities, and exit rates vary temporally, due to wave groups and other low frequency motions. However, there has been a lack of measurements to evaluate these relationships [9]. Therefore, the aim of this research was to determine rip current circulation patterns, and specifically, determine their relationship to surf zone exits, on a high-energy dissipative beach.

2. Study area

This research focused on Ngarunui Beach, Raglan, on the west coast of the North Island of New Zealand (Figure 1).

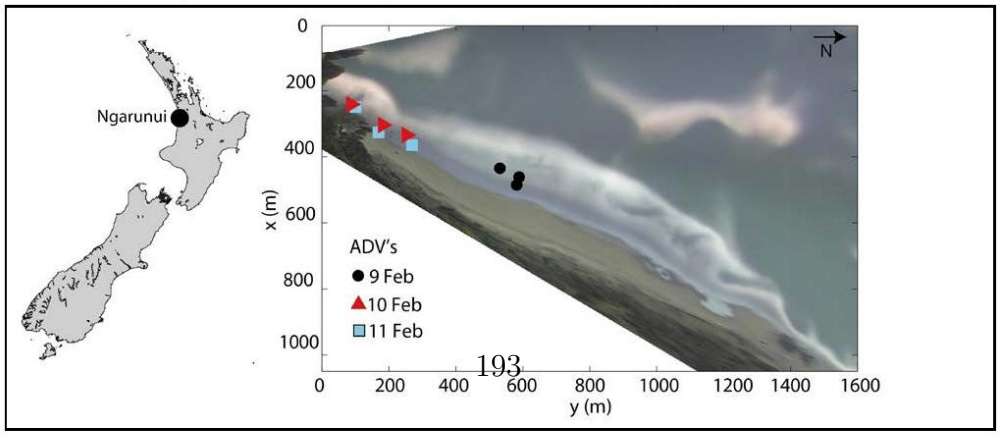

Figure 1 Location of Ngarunui Beach, New Zealand. Photo is geo-rectified, and averaged over 10 minutes from the Cam-Era video monitoring system, run by Waikato Regional Council and the National Institute of Water and Atmospheric Research (NIWA). White areas are breaking waves over sand bars. The symbols show ADV deployment locations on 9, 10 and 11 February 2015.

Ngarunui Beach is a 2 km-long, dissipative surf beach, bound by a tidal inlet to the north and a headland to the south. The beach consists of fine-medium iron sand [10] with median grain size of ~400 µm [11]. Tides are semidiurnal, with neap and spring ranges of around 1.8 and 2.8 m respectively [12]. The mean offshore significant wave height is 2 m, with period of 7 s [13].

3. Methods

Data were collected on 9–11 February 2015 using: (1) video imagery; (2) an offshore wave model; (3) three Acoustic Doppler Velocimeters (ADVs); and (4) ten GPS drifters (Figure 1). The Cam-Era video monitoring system has been in place at Ngarunui since 2007. This covers an area 1.5 km alongshore, and 150 to 800 m cross-shore. During daylight hours, a snapshot and ten-minute average image are collected half-hourly. Offshore wave data were obtained from the nzwave_12 forecast, which uses WAVEWATCH v3.14 and is run by NIWA. At the grid point closest to Ngarunui, hourly data are available from longitude -37.777834 and latitude 174.66760, at 53 m water depth. Three Triton Sontek ADVs were deployed in the surf zone (Figure 1), facing upwards. These were set to the maximum sampling rate for sea level and waves (4 Hz for 4086 samples). Ten GPS drifters were used, which were built based on the designs of [14] and [15]. The mean error and standard deviation for the QStarz BT-Q1000eX GPS was 3.78 ± 1.20 m, with velocity accuracy of ±0.05 m s^{-1}. These were deployed initially by wading out to waist-depth, and retrieved by swimmers and using a jet ski when they exited the surf zone, washed inshore, or went outside of the study area.

Figure 2 Photo showing the design of the GPS drifters used at Ngarunui Beach.

4. Results

4.1 Circulation patterns

Drifter deployments were made during the ebb tide on 9 Feb, and the flood tide on 10 and 11 Feb. Mean offshore H_s was 1.4 to 1.9 m during the deployments, with mean wave period between 7 and 12 s. Nearshore wave height measured with the ADVs ranged between 0.2 and 1 m at high tide. On 9 Feb, all the drifters travelled northwards, alongshore (Figure 3a). On 10 and 11 Feb, a clockwise surf zone eddy was revealed (where the offshore-directed flows are the rip current). On 10 Feb, it was common for drifters to circulate, then exit the surf zone (Figure 3b). On 11 Feb, the dominant behaviour was circulatory within the surf zone, with some drifters exiting the eddy to head northwards alongshore (Figure 3c).

4.2 Infragravity waves

Spectral analysis of ADV data revealed strong infragravity signals inside the surf zone, in the rip channel and feeder channels. There was a clear peak around 0.06–0.07 Hz (~14–17 s), and between 0.03–0.02 Hz (30 to 45 s) which is within the frequency range of infragravity waves.

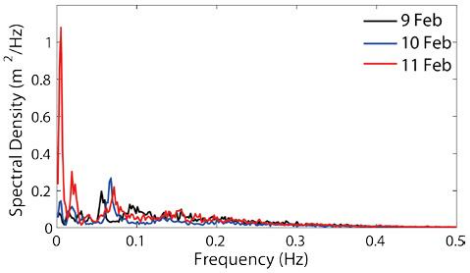

Figure 4 Mean spectra of pressure recorded by ADV1 on each day.

5. Discussion and conclusions

There were three main types of surf zone circulation patterns revealed at Ngarunui Beach. These are the first measurements of circulation at this popular surf beach. The dominant flow patterns on each day were: (1) alongshore; (2) circulation cell with high exit rate; and (3) circulation cell with no exits. This range of circulation patterns is similar to those observed in other (very different) environments. For example, three flow patterns were observed on the wind-wave dominated Dutch coast which were: circulation cell; an offshore-directed current deflected shore-parallel outside the surf zone; and (3) a meandering longshore current [16]. The longshore current at Ngarunui Beach was relatively linear rather than meandering (Figure 3a). The large variation in the dominant flow patterns over the 3 days would lead to different levels of risk to

beach users. The high exit rate from the surf zone observed on 10 Feb suggests that the topographic and hydrodynamic conditions posed a greater risk to beach users than the other 2 days. Exits from the main rip current circulation cell have been documented elsewhere [17; 7]. It has been suggested that such exits are due to pulsations in the rip current surface velocity field [18]. [18] and [19] showed using numerical modelling, that the main driver for the exit of floating material in a rip current was Very Low Frequency (VLF) motions, on the order of 10 minutes. At Ngarunui Beach, measurements with ADV's inside the rip and feeder channels revealed a strong spectral peak within the infragravity band (Figure 4), although there do not appear to be any peaks in the VLF band. Further analysis is underway to understand what could be driving the exits of drifters from the surf zone that occurred on 10 Feb (Figure 3b), in the absence of VLF motions. This will help understand drivers of rip current risk to beach users.

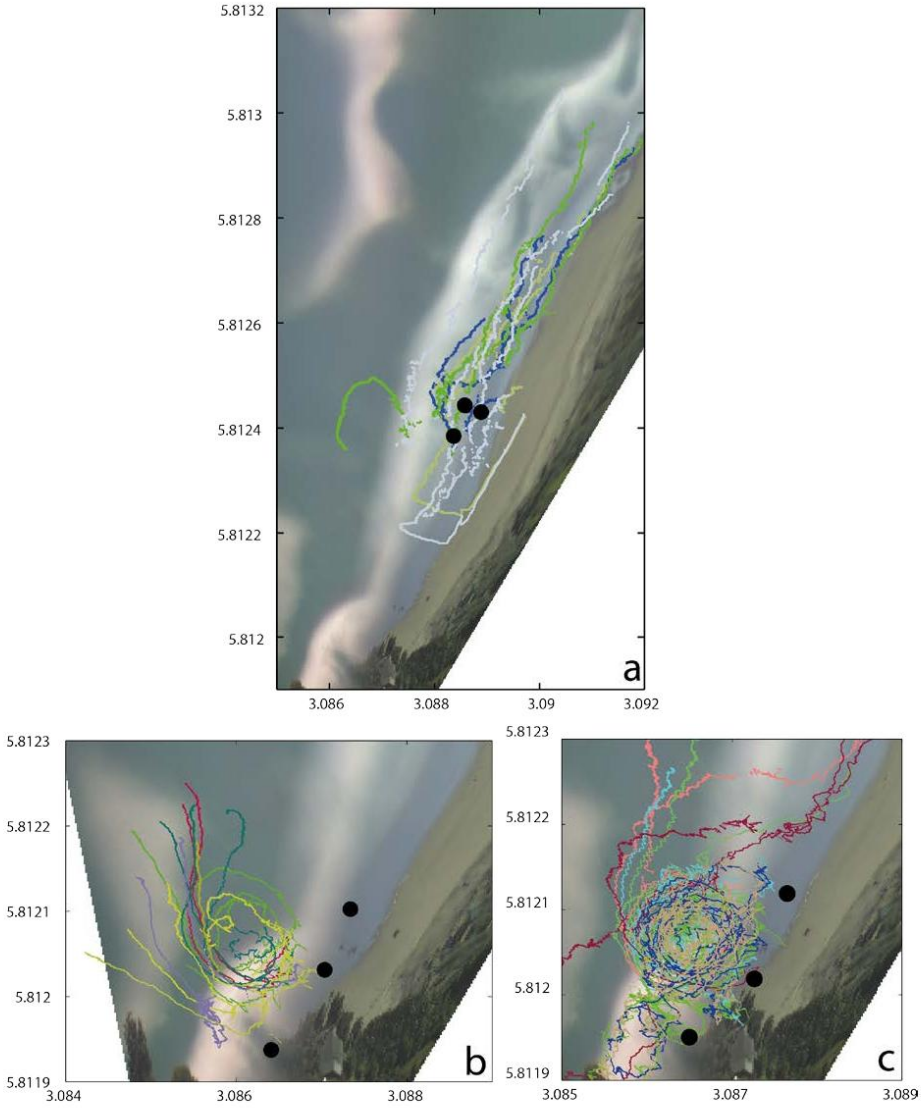

195

Figure 3 GPS drifter paths at Ngarunui Beach on: (a) 9 Feb; (b) 10 Feb; and (c) 11 Feb 2015. Black dots show locations of ADVs (Figure 1). Coordinates are in UTM where x is 10^5 and y 10^6.

6. Acknowledgements

Thanks to: the field volunteers including Mélanie Biausque, Carey Conn, Nicky Gallop, Steve Hunt, Jaco Labuschagne, Nicola Lovett, Chris Morcom, Julia Mullarney, Renaud Panier, Emily Woodhouse; the Raglan Coast Guard for helping us with their jetski, particularly Ed Aktin and Sebastian Boulay; the Raglan Surf Life Saving Club for being supportive; Brice Blossier for building and testing the drifters; Waikato Regional Council and NIWA for the Cam-Era video system; and Richard Gorman (NIWA) for providing offshore model wave data; and the Institute of Marine Engineering, Science & Technology (IMarEST) Laurie Prandolini Fellowship Award for funding the field work.

7. References

[1] Short, A.D. (1999). Beach hazards and safety, in: Short A.D. (Ed), Beach and shoreface morphodynamics, John Wiley and Sons, Chichester, pp. 292–304.

[2] Woodward, E., Beaumont, E. and Russell, P. (2015). Public understanding and knowledge of rip currents and beach safety in the UK, International Journal of Aquatic Research, Vol. 9, pp. 49-69.

[3] Aagaard, T., Greenwood, B. and Nielsen, J. (1997). Mean currents and sediment transport in a rip channel, Marine Geology, Vol. 140, pp. 25-45.

[4] Gallop, S.L., Bryan, K.R., Coco, G. and Stephens, S.A. (2011). Storm-driven changes in rip channel patterns on an embayed beach, Geomorphology, Vol. 127, pp. 179-188.

[5] Wright, L.D. and Short, A.D. (1984). Morphodynamic variability of surf zones and beaches: A synthesis, Marine Geology, Vol. 56, pp. 93-118.

[6] Brander, R.W. (1999). Field observations on the moprhodynamic evolution of a low-energy rip current system, Marine Geology, Vol. 15, pp. 199-217.

[7] Scott, T., Masselink, G., Austin, M.J. and Russell, P. (2014). Controls on macrotidal rip current circulation and hazard, Geomorphology, Vol. 214, pp. 198-215.

[8] McCarroll, R.J., Brander, R.W., MacMahan, J.H., Turner, I.L., Reniers, A.J.H.M., Brown, J.A. and Bradstreet, A. (2013). Assessing the effectiveness of rip current swimmer strategies, Shelly Beach, NSW, Australia, Journal of Coastal Research, Special Issue 65, pp. 784-789.

[9] MacMahan, J., Reniers, A.J.H.M., Thornton, E.B. and Stanton, T. (2004). Infragravity rip current pulsations, Journal of Geophysical Research, Vol. 109, C01033.

[10] Sherwood, A.M. and Nelson, C.S. (1979). Surficial sediments of Raglan Harbour, N.Z., Journal of Marine and Freshwater Research, Vol. 13, No. 4, pp. 475-496.

[11] Guedes, R.M.C., Bryan, K.R. and Coco, G. (2013). Observations of wave energy fluxed and swash motions on a low-sloping, dissipative beach, Journal of Geophysical Research: Oceans, Vol. 118, pp. 3651-3669.

[12] Walters, R.A., Goring, D.G., Bell, R.G. (2001). Ocean tides around New Zealand, New Zealand Journal of Marine and Freshwater Research, Vol. 35, No. 3, pp. 567-580.

[13] Gorman, R., Bryan, K.R. and Laing, A.K. (2003). Wave hindcast for the New Zealand region: Nearshore validation and coastal wave climate, New Zealand Journal of Marine and Freshwater Research, Vol. 37, pp. 567-588.

[14] Schmidt, W.E., Woodward, B.T., Millikan, K.S., Guza, R.T., Raubenheimer, B. and Elgar, S. (2003). A GPS-tracked surf zone drifter, Journal of Atmospheric and Oceanic Technology, Vol. 20, No. 7, pp. 1069-1075.

[15] MacMahan, J., Brown, J. and Thornton, E. (2009). Low-cost handheld global positioning system for measuring surf-zone currents, Journal of Coastal Research, Vol. 25, No. 3, pp. 744-754.

[16] Winter, G., van Dongeren, A.R., de Schipper, M.A. and van Thiel dr Vries, J.S.M. (2014). Rip currents under obliquely incident wind waves and tidal longshore currents, Coastal Engineering, Vol. 89, pp. 106-119.

[17] MacMahan, J., Brown, J., Brown, J., Thornton, E., Reniers, A., Stanton, T., Henriquez, M., Gallagher, E., Morrison, J., Austin, M.J., Scott, T.M. and Senechal, N. (2010). Mean Lagrangian flow behaviour on an open coast rip-channeled beach: A new perspective, Marine Geology, Vol.268, pp. 1-15.

[18] Castelle, B., Reniers, A. and MacMahan, J. (2013). Numerical modelling of surfzone retention in rip current systems: On the impact of the surfzone sandbar morphology, Proceedings of Coastal Dynamics 2013 (24-28 June, Arcachon).

[19] Reniers, A.J.H.M., MacMahan, J.H., Beron-Vera, F.J. and Olascoaga, M.J. (2010). Rip-current pulses tied to Lagrangian coherent structures, Geophysical Research Letters, Vol.37, L05605.

Appendix D: Pulsations in surfzone currents paper

This paper was published as a result of the fieldwork undertaken for this PhD.

Journal of Coastal Research	SI	75	378-382	Coconut Creek, Florida	2016

Pulsations in Surf Zone Currents on a High Energy Mesotidal Beach in New Zealand

Shari L. Gallop [†§*], Karin R. Bryan[‡], Sebastian J. Pitman[§], Roshanka Ranasinghe[††], and Dean Sandwell[‡]

[†]Department of Environmental Sciences, Macquarie University, Australia

[‡]School of Science, University of Waikato, New Zealand

[§]Ocean and Earth Science, University of Southampton, United Kingdom

[††]Department of Water Engineering, UNESCO-IHE, The Netherlands; Research School of Earth Sciences, Australian National University Australia; Harbour, Coastal and Ocean Engineering, Deltares, The Netherlands

www.cerf-jcr.org

www.JCRonline.org

ABSTRACT

Gallop, S.L.; Bryan, K.R.; Pitman, S.J.; Ranasinghe, R., and Sandwell, D., 2016. Pulsations in surf zone currents on a high energy mesotidal beach in New Zealand. *In:* Vila-Concejo, A.; Bruce, E.; Kennedy, D.M., and McCarroll, R.J. (eds.), *Proceedings of the 14th International Coastal Symposium* (Sydney, Australia). *Journal of Coastal Research*, Special Issue, No. 75, pp. 378-382. Coconut Creek (Florida), ISSN 0749-0208.

The exchange of material between the surf zone and continental shelf can be driven by pulsations in rip current velocities. However, there is a poor understanding of the relationship of these pulsations to surf zone morphology and material exchange. Moreover, understanding of rip current dynamics has focused mainly on single-barred beaches in an intermediate state, and there have been few studies on high energy beaches. Therefore, this paper undertakes preliminary research on surf zone current velocity pulsations, on a high energy beach in New Zealand. This initial analysis presents results from two days of measurements using Acoustic Doppler Velocimeters and Lagrangian GPS drifters. Drifters revealed pulsations in current velocities on the order of ~0.5–2 m s^{-1} throughout the surf zone, whether inside a rip current circulation cell or not. More infragravity wave energy was associated with constant pulsations in current velocity, and lower infragravity energy with pulsation bursts, lasting 5–10 minutes, interspersed with periods of relatively constant velocity lasting 15–25 minutes. However, higher wave conditions also reduced the exit rate from the surf zone.

ADDITIONAL INDEX WORDS: *rip channels, surf zone, beach morphodynamics, Raglan, infragravity.*

INTRODUCTION

Rip currents are jet-like flows in the surf zone that generally head in an offshore direction (Aagaard *et al.*, 1997). They are often present on beaches in an intermediate morphodynamic beach state (Wright and Short, 1984), and adjacent to structures such as headlands and groynes (Gallop *et al.*, 2011; McCarroll *et al.*, 2014; Short, 1985). It is important to understand the variability and drivers of rip current flows because: (1) globally, they are the leading cause of rescues and fatalities on beaches (Short, 1999; Woodward *et al.*, 2015); and (2) they are a key mechanism transporting material between the surf zone and continental shelf, such as larvae (Fujimura *et al.*, 2014), diatoms (Talbot and Bate, 1987), and sediments (Aagaard *et al.*, 1997). Therefore, they are an important sediment transport conduit contributing to coastal sediment budgets (Goodwin *et al.*, 2013; Wright, 1987). Recent research suggests that the exit rate of material from the surf zone to offshore is an important control of: (1) hazard to beach users (Scott *et al.*, 2013); (2) the best escape strategy for people caught in a rip (McCarroll *et al.*, 2013); and (3) rates of cross- shore exchange of water (Smith and Largier, 1995), and materials (Loureiro *et al.*, 2013; Thorpe *et al.*, 2013).

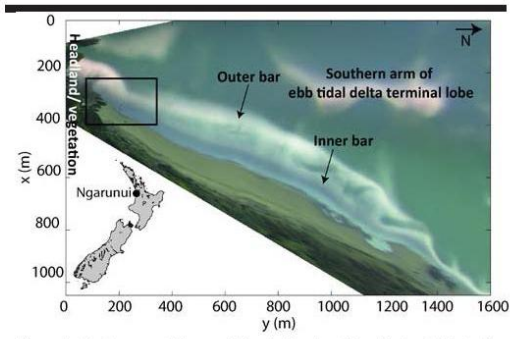

Figure 1. Study area at Ngarunui Beach, Raglan, New Zealand. Photo is a rectified, 10-minute average image from the Cam-Era video monitoring system. The box shows the area where ADVs and GPS drifters were deployed on 10 and 11 February 2015. White areas show breaking waves over shallow bathymetry. The dark area at the top of the beach is a shadow from the headland.

DOI: 10.2112/SI75-076.1 received 15 October 2015; accepted in revision 15 January 2016.

*Corresponding author: shari.gallop@mq.edu.au

Surf zone exits may be driven by pulsations in rip current velocity. Pulsation of surf zone currents can occur at infragravity (IG) frequencies (25–250 s) due to standing IG waves (MacMahan *et al.*, 2004a; Sonu, 1972) or wave groups (Munk, 1949; Reniers *et al.*, 2010; Shephard and Inman, 1950). In addition, recent research has revealed the presence of vortical motions at Very Low Frequency (VLF) (4–10 min) motions (Castelle *et al.*, 2013; MacMahan *et al.*, 2004b; Reniers *et al.*, 2010). A range of generation mechanisms for VLF motions have been suggested. The dominant mechanism appears to be surf zone eddies due to wave groups (MacMahan *et al.*, 2004b; Peregrine, 1998; Reniers *et al.*, 2007).

There is a lack of measurements (MacMahan *et al.*, 2004a) to understand the relationship of current pulsations to rip current generation, surf zone morphology, material exchange, and hazard. Therefore, the aim of this paper is to undertake preliminary research on the influence of IG wave energy on rip current flows on a high energy beach.

METHODS

This section introduces the study site, field experiment, and data analysis methods.

Study site

Ngarunui Beach on the west coast of New Zealand (Figure 1) has fine-medium iron sand (Sherwood and Nelson, 1979). The tide is semidiurnal, with neap and spring ranges of ~1.8 and 2.8 m (Walters *et al.*, 2001). Offshore mean significant wave height is 2 m, with a period of 7 s (Gorman *et al.*, 2003). The southern arm of the ebb tidal delta, terminal lobe to Whaingaroa Harbor acts as the outer bar during large swell events. Further inshore, there are inner (high tide) and outer (low tide) bars which are often cut by rip channels (Figure 1).

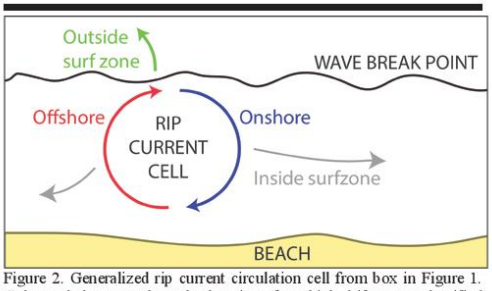

Figure 2. Generalized rip current circulation cell from box in Figure 1. Color coded arrows show the locations for which drifters are classified in Figures 3c and 4c.

Field experiment

A field experiment was undertaken between 9 and 11 February 2015 and included the deployment of three Triton Sontek Acoustic Doppler Velocimeters (ADVs), and ten GPS drifters. This paper focuses on data collected on February 10 and 11 collected in the rip current cell at the south end (Figure 1).

ADVs were deployed upward-facing within the rip current, and were set to the maximum sampling rate of 4 Hz for 4086 samples. GPS drifters were based on the design of Schmidt *et al.* (2003) and MacMahan *et al.* (2009). The GPS logger was the QStarz BT-Q100eX, which has a velocity accuracy of ±0.05 m s^{-1} (Thomson, 2012). One drifter was left in a static position on a benchmark to estimate the mean horizontal error and standard deviation of 3.78 ± 1.20 m. Drifters were deployed by wading out to waist-depth. They were retrieved using a combination of shore-retrieval, and a jetski when they: (1) washed onshore and dragging on the bed; (2) travelled alongshore outside of the study area; (3) exited the surf zone; and (4) entered busy surfing/swimming areas. All times are given in New Zealand Standard Time (NZST).

Data analysis

As in other studies of surf zone currents using GPS drifters (e.g., Johnson and Pattiaratchi, 2004; McCarroll *et al.*, 2014), velocity data were low-pass filtered using a Butterworth filter with a low-pass cutoff of 0.05 Hz, to average wave motion and other noise.; including an algorithm to reduce end effects. For this preliminary investigation, results are presented of individual drifter velocities and their location within the surf zone circulation system, and compared with IG wave energy. Drifter velocities are color coded by location: (1) offshore- and (2) onshore-directed flow in the rip current circulation cell; (4) elsewhere inside the surf zone (Figure 2); or (3) offshore.

Offshore wave conditions were obtained from the nzwave_12 wave forecast which used WAVEWATCHv3.14, and was run by NIWA. Drifter velocities were compared to the energy in the IG band of: pressure (water level); x (cross-shore); and y (longshore) currents recorded by ADVs in the surf zone. These were obtained by calculating wave power spectra on the detrended time-series, which were then smoothed using a Hanning window of 4096 data points. The total IG energy was summed for each window, within the frequency band of 0.0033–0.05 Hz (20–300 s); suggested infragravity wave frequency cutoffs vary but generally range within this window (e.g. Holman, 1981; MacMahan *et al.*, 2004a). Periods of pulsations in surf zone current velocities were identified by calculating the standard deviation of the low pass-filtered velocity in 2 minute windows. Pulsations were defined as occurring when the standard deviation was greater than the 50th percentile standard deviation of filtered drifter velocities.

RESULTS

Here, results are summarized for 10 and 11 February.

10 February

On 10 February, mean offshore significant wave height was 1.4 m, and period was 8.7 s. There was significantly more IG energy in cross-shore currents compared to sea level and long-shore currents (Figure 3a). IG energy gradually increased during late morning, with energy in cross-shore currents increasing from ~10 m^2/Hz, to peak at 15 m^2/Hz after 13:00 h (Figure 3a). Pulsation bursts of drifter velocity were identified by periods of high standard deviation (Figure 3b). During these pulsations, the drifters reached velocities on the order of ~0.5–2 m s^{-1} (Figure 3c). Drifter velocities alternated between pulsation bursts lasting around 5–10 minutes (Figure 3c), interspersed with periods of relatively constant, lower velocity of <0.5 m s^{-1}. Pulsations were not associated with the position within the surf zone, as this occurred at all locations sampled, *i.e.* in the offshore and onshore

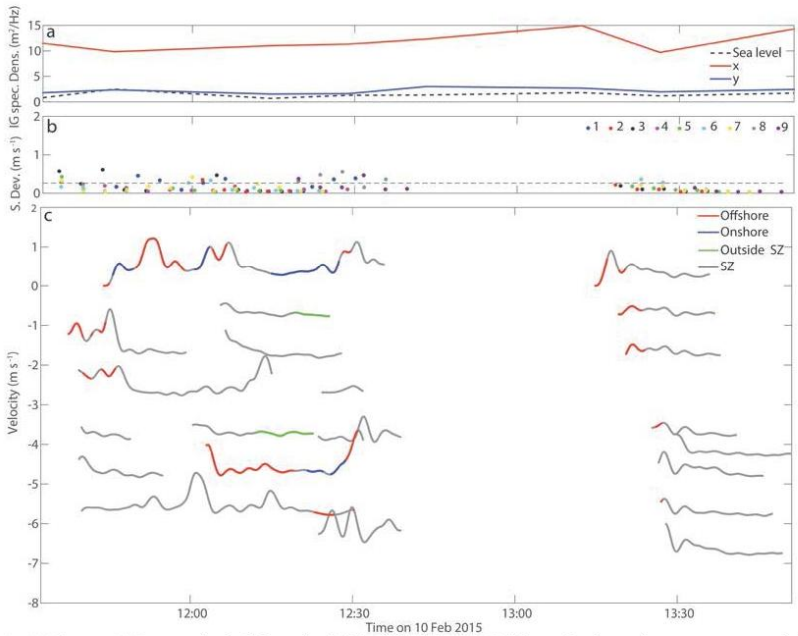

Figure 3. (a) On 10 February 2015, energy in the infragravity (IG) band (0.0033–0.05 Hz) for sea level, *x*, and *y* currents measured with an ADV; (b) standard deviation in drifter velocity for drifters 1 to 9, for 2 minute windows where the dashed line shows the 50th percentile; and (c) filtered GPS drifter velocity for 1 (top) to 9 (bottom), with plotting successively offset by -1 m s^{-1}. Color code corresponds to the areas shown in Figure 2.

flows within the rip current circulation cell, and others areas of the surf zone. Due to a lack of temporal drifter coverage, it is also not clear if more pulsing occurred as IG energy increased on this day.

11 February

On 11 February, mean offshore significant wave height increased to 1.9 m, and mean period to 11.7 s. This higher wave energy was reflected in cross-shore IG energy that was an order of magnitude greater than the day before, reaching 130 m^2/Hz (Figure 4a) compared to 13 m^2/Hz on 10 February (Figure 3a). Total IG energy was variable. For cross-shore currents, it reached local maxima in spectral density of ~80, 100, and 130 m^2/Hz at 12:30, 13:10, and 14:20 respectively; and local minima of ~50 m^2/Hz at 12:45 and 14:10. Unlike on the previous day, there were almost constant pulsations in GPS drifter velocities (Figure 4b). During these pulsations, drifters reached velocities on the order of 0.5–2 m s^{-1} (Figure 4c). These oscillations occurred regardless of location within the surf zone.

DISCUSSION

IG frequency energy was an order of magnitude greater on 11 February compared to 10 February. If rip current pulsations are driven by IG waves (MacMahan *et al.*, 2004a; Reniers *et al.*, 2010), then it is expected that more IG wave energy would lead to more pulsations in rip current velocity. This relationship is confirmed by differences between the two days, where pulsations in rip current velocities were constant on 11 February (Figure 4c), when IG wave energy was much greater (Figure 4a). Conversely, on 10 February when IG wave energy was relatively lower (Figure 3a), surf zone current pulsations were intermittent (Figure 3c) and occurred in bursts lasting for 5–10 minutes, interspersed by periods of relatively constant velocity, lasting 15–25 minutes. The magnitude of the velocity pulsations was similar between the two days, on the order of 0.5–2 m s^{-1}. If IG pulsations in rip current velocity are the main driver of surf zone exits, then more exits should have occurred on 11 February. However, there were significantly less exits on 11 February (6 %) compared to 10 February (71 %) (Gallop *et al.*, 2015). Offshore significant wave height was higher on the second day, at 1.9 m compared to 1.4 m on the first day. This relationship is consistent with findings elsewhere that more drifter exits occur during lower wave conditions (MacMahan *et al.*, 2010; Scott *et al.*, 2014).

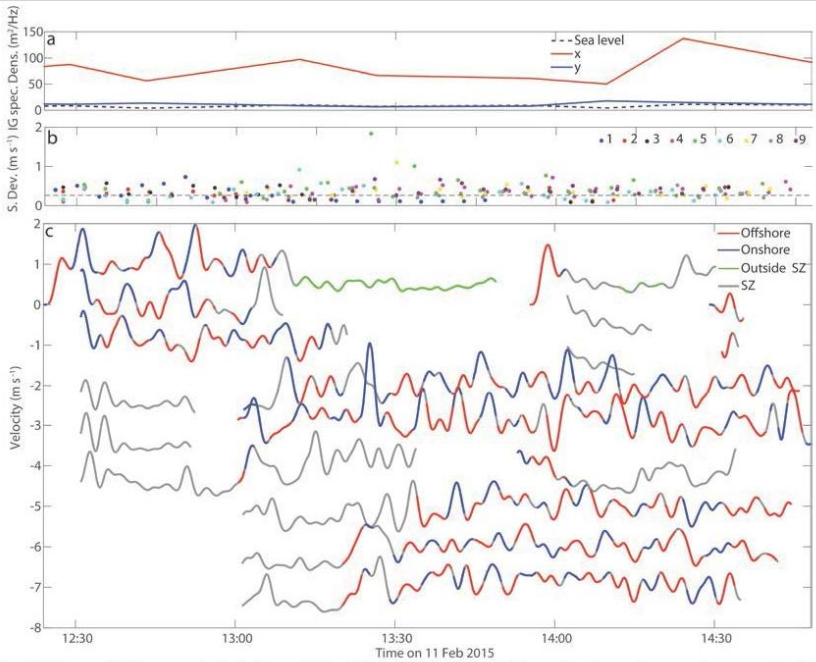

Figure 4. (a) On 11 February 2015, energy in the infragravity band (IG) (0.0033–0.05 Hz) for sea level, *x*, and *y* currents measured with an ADV; (b) standard deviation in drifter velocity for drifters 1 to 9, for 2 minute windows where the dashed line shows the 50th percentile; and (c) filtered GPS drifter velocity for 1 (top) to 9 (bottom), with plotting successively offset by -1 m s^{-1}. Color code corresponds to the areas shown in Figure 2.

This may be caused by larger waves breaking further offshore which induce current vortices that are coupled to the surf zone morphology, and encourage material retention (MacMahan *et al.*, 2010). Further research is required to understand the effect of rip current pulsations and incident wave conditions on rip current flows, particularly on high energy beaches.

CONCLUSIONS

This paper presented a preliminary study on rip current velocity pulsations, on a high energy, mesotidal beach in New Zealand. There were strong pulsations in surf zone current velocity on the order of ~0.5–2 m s^{-1}. These pulsations occurred in 5-10 minute bursts interspersed with 15-20 minute periods of relatively constant velocity, during lower total wave energy, and lower IG energy conditions. Conversely, during higher wave energy conditions, and when there was more IG wave energy present, the pulsations were constant. More pulsations did not lead to increased surf zone exits, possibly because the higher incident wave conditions encouraged the retention of material in the surf zone. Further research is planned to understand the balance of rip current velocity pulsations and incident wave conditions on rip current flows and surf zone exits on high energy beaches

ACKNOWLEDGMENTS

Thanks to the field volunteers: M. Biausque, C. Conn, N. Gallop, S. Hunt, J. Labuschagne, N. Lovett, C. Morcom, J. Mullarney, R. Panier, E. Woodhouse; the Raglan Coast Guard (E. Aktin and S. Boulay); B. Blossier for the drifters; Waikato Regional Council and NIWA for Cam-Era; S. Harrison for image assistance; R. Gorman (NIWA) for nzwave_12; and the IMarEST Laurie Prandolini Fellowship.

LITERATURE CITED

Aagaard, T.; Greenwood, B., and Nelson, J., 1997. Mean currents and sediment transport in a rip channel. *Marine Geology*, 140, 25-45.

Castelle, B.; Reniers, A., and MacMahan, J., 2013. Numerical modelling of surfzone retention in rip current systems: On the impact of the surfzone sandbar morphology. *Proceedings of Coastal Dynamics 2013* (24-28 June, Arcachon).

Fujimura, A.G.; Reniers, A.J.H.M.; Paris, C.B.; Shanks, A.L.; MacMahan, J.H., and Morgan, S.G., 2014. Numerical

simulations of larval transport into a rip-channeled surf zone. *Limnology and Oceanography*, 59(4), 1434-1447.

Gallop, S.L.; Bryan, K.R.; Coco, G., and Stephens, S.A., 2011. Storm-driven changes in rip channel patterns on an embayed beach. *Geomorphology, 127*(3–4), 179-188.

Gallop, S.L.; Bryan, K.R.; Pitman, S.; Ranasinghe, R., and Sandwell, D., 2015. Rip current observations on a low-sloping dissipative beach. *Proceedings of Coasts and Ports* (15-18 September, Auckland).

Goodwin, I.D.; Freeman, R., and Blackmore, 2013. An insight into headland sand bypassing and wave climate variability from shoreface bathymetric change at Byron Bay, New South Wales, Australia. *Marine Geology*, 341, 29-45.

Gorman, R.; Bryan, K.R., and Laing, A.K., 2003. Wave hindcast for the New Zealand region: Nearshore validation and coastal wave climate. *New Zealand Journal of Marine and Freshwater Research*, 27, 567-588.

Holman, R.A., 1981. Infragravity energy in the surf zone. *Journal of Geophysical Research* 86(C7), 6442-6450.

Johnson, D. and Pattiaratchi, C., 2004. Transient rip currents and nearshore circulation on a swell-dominated beach. *Journal of Geophysical Research*, 109, C02026.

Loureiro, C.; Ferreira, Ó., and Cooper J.A.G., 2012. Extreme erosion on high-energy embayed beaches: Influence of megarips and storm grouping. *Geomorphology,* 139–140, 155–171.

MacMahan, J.; Reniers, A.J.H.M.; Thornton, E.B., and Stanton, T., 2004a. Infragravity rip current pulsations. *Journal of Geophysical Research*, 109, C01033.

MacMahan, J.H.; Reniers, A.J.H.M.; Thornton, E.B., and Stanton, T.P., 2004b. Surf zone edits coupled with rip current morphology. *Journal of Geophysical Research*, 109, C07004.

MacMahan, J.; Brown, J., and Thornton, E., 2009. Low-cost handheld global positioning system for measuring surf-zone currents. *Journal of Coastal Research*, 25(3), 744-754.

MacMahan, J.; Brown, J.; Brown, J.; Thornton, E.; Reniers, A.; Stanton, T.; Henriquez, M.; Gallager, E.; Morrison, J.; Austin, M.J.; Scott, T.M., and Senechal, N., 2010. Mean Lagrangian flow behaviour on an open coast rip-channeled beach: A new perspective. *Marine Geology,* 268(1-4): 1-15.

McCarroll, R.J.; Brander, R.W.; MacMahan, J.H.; Turner, I.L.; Reniers, A.J.H.M.; Brown, J.A., and Bradstreet, A., 2013. Assessing the effectiveness of rip current swimmer strategies, Shelly Beach, NSW, Australia. *Journal of Coastal Research*, Special Issue 65, 784-789.

McCarroll, R.J.; Brander, R.W.; Turner, I.L.; Power, H.E., and Mortlock, T.R., 2014. Lagrangian observations of circulation on an embayed beach with headland rip currents. *Marine Geology, 355*, 173-188.

Munk, W.H., 1949. Surf beats. *EOS Transactions*, AGU. 30(6), 849-854.

Peregrine, D.H., 1998. Surf zone currents. *Theoretical and Computational fluid dynamics*, 10, 295-309.

Reniers, A.J.H.M.; MacMahan, J.H.; Beron-Vera, F.J., and Olascoaga, M.J., 2010. Rip-current pulses tied to Lagrangian coherent structures. *Geophysical Research Letters*, 37, L05605.

Reniers, A.J.H.M.; MacMahan, J.H.; Thornton, E.B., and Stanton, T.P., 2007. Modeling of very low frequency motions during RIPEX. *Journal of Geophysical Research* 112, C07013.

Schmidt, E.W.; Woodward, B.T.; Millikan, K.S.; Guza, R.T.; Raubenheimer, B., and Elgar, S., 2003. A GPS-tracked surf zone drifter. *Journal of Atmospheric and Oceanic Technology*, 20(7), 1069-1075.

Shepard, F.P. and Inman, D.L., 1950. Nearshore water circulation related to bottom topography and wave refraction. *EOS Transactions*, AGU, 31(1), 196-212.

Sherwood, A.M. and Nelson, C.S., 1979. Surficial sediments of Raglan Harbour, N.Z. *Journal of Marine and Freshwater Research*, 15(4), 475-496.

Short, A.D., 1985. Rip current type, spacing and persistence, Narrabeen beach, Australia. *Marine Geology*, 65(1-2), 47-71.

Short, A.D., 1999. Beach hazards and safety. In: Short, A.D. (ed.). *Beach and shoreface morphodynamics.* Chichester: John Wiley and Sons, pp. 292-304.

Scott, T.; Masselink, G.; Austin, M.J., and Russell P., 2014. Controls on macrotidal rip current circulation and hazard. *Geomorphology,* 214, 198–215.

Smith, J.A. and Largier, J.L., 1995. Observations of nearshore circulation: Rip currents. *Journal of Geophysical Research-Oceans,* 100(C6), 10967–10975.

Sonu, C.J., 1972. Field observation of nearshore circulation and meandering currents. *Journal of Geophysical Research*, 79, 3065-3071.

Talbot, M.M.B. and Bate, G.C., 1987. Rip current characteristics and their role in the exchange of water and surf diatoms between the surf zone and nearshore. *Estuarine, Coastal and Shelf Science*, 25(6), 707-720.

Thomson, J., 2012. Wave breaking dissipation and 'SWIFT' drifters. *Journal of Atmospheric and Oceanic Technology*, 29, 1866-1882.

Thorpe, A.; Miles, J.; Masselink, G.; Russell, P.; Scott, T., and Austin, M., 2013. Suspended sediment transport in rip currents on a macrotidal beach. *Journal of Coastal Research,* Special Issue 65, 1880–1885.

Walters, R.A.; Goring, D.G., and Bell, R.G., 2001. Ocean tides around New Zealand. *New Zealand Journal of Marine and Freshwater Research,* 35(3), 567-580.

Woodward, E.; Beaumont, E., and Russell, P., 2015. Public understanding and knowledge of rip currents and beach safety in the UK. *International Journal of Aquatic Research*, 9, 49-69.

Wright, L.D., 1987. Shelf-surfzone coupling: Diabathic shoreface transport. *Proceedings of Coastal Sediments 1987* (12-14 May, New Orleans).

Wright, L.D. and Short, A.D., 1984. Morphodynamic variability of surf zones and beaches: A synthesis. *Marine Geology*, 56, 93-118.

References

Aagaard, T., Greenwood, B., 1995. Longshore and cross-shore suspended sediment transport at far infragravity frequencies in a barred environment. Continental Shelf Research 15, 1235 – 1249.

Aagaard, T., Greenwood, B., Nielsen, J., 1997. Mean currents and sediment transport in a rip channel. Marine Geology 140, 25–45.

Aarninkhof, S., Turner, I., Dronkers, T., Caljouw, M., Nipius, L., 2003. A video-based technique for mapping intertidal beach bathymetry. Coastal Engineering 49, 275–289.

Alexander, P., Holman, R., 2004. Quantification of nearshore morphology based on video imaging. Marine Geology 208, 101–111.

Almar, R., Coco, G., Bryan, K., Huntley, D., Short, A., Senechal, N., 2008. Video observations of beach cusp morphodynamics. Marine Geology 254, 216–223.

Arozarena, I., Houser, C., Echeverria, A.G., Brannstrom, C., 2015. The rip current hazard in costa rica. Natural Hazards 77, 753–768.

Arun Kumar, S.V.V., Prasad, K.V.S.R., 2014. Rip current-related fatalities in india: a new predictive risk scale for forecasting rip currents. Natural Hazards 70, 313–335.

Austin, M., Masselink, G., Scott, T., Russell, P., 2014. Water-level controls on macro-tidal rip currents. Continental Shelf Research2 75, 28–40.

Austin, M., Scott, T., Brown, J., Brown, J.A., MacMahan, J., Masselink, G., Russell, P., 2010. Temporal observations of rip current circulation on a macro-tidal beach. Continental Shelf Research 30, 1149–1165.

Austin, M., Scott, T., Brown, J., MacMahan, J., 2009. Macrotidal Rip Current Experiment: Circulation And Dynamics. 10th International Coastal Symposium (ICS 2009) 2009, 24–28.

Austin, M., Scott, T., Russell, P., Masselink, G., 2013. Rip Current Prediction: Development, Validation, and Evaluation of an Operational Tool. Journal of Coastal Research 29, 283–300.

Barlas, B., Beji, S., 2016. Rip current fatalities on the black sea beaches of istanbul and effects of cultural aspects in shaping the incidents. Natural Hazards 80, 811–821.

Barry, R.G., Kiladis, G., Bradley, R.S., 1981. Synoptic climatology of the western united states in relation to climatic fluctuations during the twentieth century. Journal of Climatology 1, 97–113.

Bergsma, E., Conley, D., Davidson, M., O'Hare, T., 2016. Video-based nearshore bathymetry estimation in macro-tidal environments. Marine Geology 374, 31 – 41.

Bergsma, E., Conley, D., Davidson, M., O'Hare, T., Holman, R., 2014. An assessment of video-based bathymetry estimation in a macro tidal environment. Coastal Engineering Proceedings 1, 38.

Blair, D., 1998. The kirchhofer technique of synoptic typing revisited. International Journal of Climatology 18, 1625–1635.

Blenkinsopp, C., Turner, I., Masselink, G., 2011. Swash zone sediment fluxes: Field observations. Coastal Engineering 58, 28–44.

Blossier, B., Bryan, K.R., Daly, C.J., Winter, C., 2016. Nearshore sandbar rotation at single-barred embayed beaches. Journal of Geophysical Research: Oceans 121, 2286–2313.

Bogle, J., Bryan, K., Black, K., Hume, T., Healy, T., 2000. Video Observations of Rip Formation and Evolution, in: 6th International Coastal Symposium, Hamilton, New Zealand. pp. 117–127.

Bovik, A., 2005. Introduction to digital image and video processing, in: Bovik, A. (Ed.), Handbook of image and video processing. 2nd ed.. Elsevier Academic Press, Burlington, MA, USA. chapter 1.1, pp. 3–20.

Bowen, A., 1969. Rip currents: 1. Theoretical investigations. Journal of Geophysical Research 74, 5467–5478.

Bowen, A., Inman, D., 1969. Rip Currents: 2. Laboratory and Field Observations. Journal of Geophysical Research 74, 5479–5490.

Brander, R., 1999. Field observations on the morphodynamic evolution of a low-energy rip current system. Marine Geology 157, 199–217.

Brander, R., Bradstreet, A., Sherker, S., MacMahan, J., 2011. The behavioural responses of swimmers caught in rip currents: new perspectives on mitigating the global rip current hazard. International Journal of Aquatic Research and Education 5, 476–482.

Brander, R., MacMahan, J., 2011. Future challenges for rip current research and outreach, in: Leatherman, S., Fletemeyer, J. (Eds.), Rip Currents: Beach safety, physical oceanography, and wave modelling. CRC Press, Florida, USA, pp. 1–26.

Brander, R., Scott, T., 2016. Science of the rip current hazard. The Science of Beach Lifeguarding , 67.

Brander, R., Short, A., 2000. Morphodynamics of a large-scale rip current system at Muriwai Beach, New Zealand. Marine Geology 165, 27–39.

Brewster, B.C., Gould, R., 2014. Comment on "rip current related drowning deaths and rescues in australia 2004–2011" by brighton et al. (2013). Natural Hazards and Earth System Sciences 14, 2203–2204.

Brighton, B., Sherker, S., Brander, R., Thompson, M., Bradstreet, A., 2013. Rip current related drowning deaths and rescues in australia 2004-2011. Natural Hazards and Earth System Sciences 13, 1069–1075.

Browne, M., Strauss, D., Tomlinson, R., Blumenstein, M., 2006. Objective beach-state classification from optical sensing of cross-shore dissipation profiles. IEEE Transactions on Geoscience and Remote Sensing 44, 3418–3426.

Bruneau, N., Bonneton, P., Castelle, B., Pedreros, R., 2011. Modeling rip current circulations and vorticity in a high-energy mesotidal-macrotidal environment. Journal of Geophysical Research 116, doi:10.1029/2010JC006693.

Castelle, B., Bonneton, P., Sénéchal, N., Dupuis, H., Butel, R., Michel, D., 2006. Dynamics of wave-induced currents over an alongshore non-uniform multiple-barred sandy beach on the Aquitanian Coast, France. Continental Shelf Research 26, 113–131.

Castelle, B., McCarroll, R., Brander, R., Scott, T., Dubarbier, B., 2016a. Modelling the alongshore variability of optimum rip current escape strategies on a multiple rip-channelled beach. Natural Hazards: Journal of the International Society for the Prevention and Mitigation of Natural Hazards 81, 663–686.

Castelle, B., Reniers, A., MacMahan, J., 2014. Bathymetric control of surf zone retention on a rip-channelled beach. Ocean Dynamics 64, 1221–1231. Cited By 8.

Castelle, B., Scott, T., Brander, R., McCarroll, R., 2016b. Rip current types, circulation and hazard. Earth-Science Reviews 163, 1 – 21.

Chow, J.C.F., Soda, K., 1972. Laminar flow in tubes with constriction. The Physics of Fluids 15, 1700–1706.
arXiv:http://aip.scitation.org/doi/pdf/10.1063/1.1693765.

Cook, D.O., 1970. The occurrence and geologic work of rip currents off southern california. Marine Geology 9, 173 – 186.

Dalrymple, R., 1975. A mechanism for rip current generation on an open coast. Journal of Geophysical Research 80, 3485–3487.

Dalrymple, R., Lozano, C., 1978. Wave-current interaction models for rip currents. Journal of Geophysical Research 83, 6063–6071.

Dalrymple, R., MacMahan, J., Reniers, A., Nelko, V., 2011. Rip Currents. Annual Review of Fluid Mechanics 43, 551–581.

Dalrymple, R.A., Martin, P.A., 1990. Wave diffraction through offshore breakwaters. Jouranl of waterway, port and coastal engineering 116, 727–741.

Dean, R., 1973. Heuristic models of sand transport in the surf zone, in: Proceedings of Conference on Engineering Dynamics in the Surf Zone, pp. 208–214.

Dean, R., Thieke, R., 2011. Surf zone hazards: Rip currents and waves, in: Leatherman, S., Fletemeyer, J. (Eds.), Rip Currents: Beach safety, physical oceanography, and wave modelling. CRC Press, Boca Raton, FL, pp. 107–124.

Drozdzewski, D., Shaw, W., Dominey-Howes, D., Brander, R., Walton, T., Gero, A., Sherker, S., Goff, J., Edwick, B., 2012. Surveying rip current survivors: preliminary insights into the experiences of being caught in rip currents. Natural Hazards and Earth System Sciences 12, 1201–1211.

Feddersen, F., 2014. The generation of surfzone eddies in a strong alongshore current. Journal of Physical Oceanography 44, 600–617. arXiv:http://dx.doi.org/10.1175/JPO-D-13-051.1.

Fowler, R., Dalrymple, R., 1990. Wave group forced nearshore circulation. Coastal Engineering Proceedings 1.

Gal, Y., Browne, M., Lane, C., 2014. Long-term automated monitoring of nearshore wave height from digital video. IEEE Transactions on Geoscience and Remote Sensing 52, 3412–3420.

Gallop, S., Bryan, K., Coco, G., 2009. Video observations of rip currents on an embayed beach, in: International Coastal Symposium, pp. 49–53.

Gallop, S., Bryan, K., Coco, G., Stephens, S., 2011. Storm-driven changes in rip channel patterns on an embayed beach. Geomorphology 127, 179–188.

Gallop, S., Bryan, K., Pitman, S., Ranasinghe, R., Sandwell, D., 2015. Rip current observations on a low-sloping dissipative beach, in: Australian Coasts and Ports 2015 Conference, pp. 304 – 307.

Gallop, S., Bryan, K., Pitman, S., Ranasinghe, R., Sandwell, D., 2016a. Pulsations in surf zone currents on a high energy mesotidal beach in New Zealand. Journal of Coastal Research 1.

Gallop, S., Woodward, E., Brander, R., Pitman, S., 2016b. Perceptions of rip current myths from the central south coast of England. Ocean and Coastal Management 119.

Gensini, V.A., Ashley, W.S., 2010. An examination of rip current fatalities in the united states. Natural Hazards 54, 159–175.

Gevers, T., Smeulders, A., 1999. Colour based object recognition. Pattern Recognition 32, 453–464.

Gevers, T., Stokman, H., 2003. Robust histogram construction from colour invariants for object recognition. IEEE Transactions on pattern analysis and machine intelligence 25, 1–6.

Gonzalez, R., Woods, R., 2008. Digital Image Processing. 3rd ed., Pearson Education Ltd, New Jersey, USA.

Gorman, R., Bryan, K., Laing, A., 2003. Wave hindcast for the New Zealand region: nearshore validation and coastal wave climate. New Zealand Journal of Marine and Freshwater Research 37, 567–588.

Gourlay, M., 1968. Beach and Dune Erosion Tests. Technical report Report no. M935/M936. Delft Hydraulics Laboratory.

Guedes, R., Bryan, K., Coco, G., 2013. Observations of wave energy fluxes and swash motions on a low-sloping, dissipative beach. Journal of Geophysical Research 118, 3651–3669.

Guedes, R., Calliari, L., Holland, K., Plant, N., Pereira, P., Alves, F., 2011. Short-term sandbar variability based on video imagery: Comparison between Time-Average and Time-Variance techniques. Marine Geology 289, 122–134.

Haller, M.C., Honegger, D., Catalan, P.A., 2014. Rip current observations via marine radar. Journal of Waterway, Port, Coastal, and Ocean Engineering 140, 115–124. arXiv:http://dx.doi.org/10.1061/(ASCE)WW.1943-5460.0000229.

Harrison, S., Hunt, S., 2014. Whaingaroa Harbour, New Zealand. Hydrographic Chart. Technical Report. Distributed by University of Waikato and Waikato Regional Council at NZCS 2014.

Hatfield, J., Williamson, A., Sherker, S., Brander, R., Hayen, A., 2012. Development and evaluation of an intervention to reduce rip current related beach drowning. Accident Analysis & Prevention 46, 45 – 51.

Hemer, M., Simmonds, I., Keay, K., 2008. A classification of wave generation characteristics during large wave events on the southern australian margin. Continental Shelf Research 28, 634 – 652.

Holland, K., Holman, R., Lippmann, T., Stanley, J., Plant, N., 1997. Practical use of video imagery in nearshore oceanographic field studies. Journal of Oceanic Engineering 22, 81–92.

Holman, R., Plant, N., Holland, K., 2013. cBathy: A robust algorithm for estimating nearshore bathymetry. Journal of Geophysical Research: Oceans 118, doi:10.1002/jgrc.20199.

Holman, R., Sallenger, A., Lippmann, T., Haines, J., 1993. The application of video image processing to the study of nearshore processes. Oceanography 6, 78–86.

Holman, R., Stanley, J., Özkan-Haller, T., 2003. Applying video sensor networks to nearshore environment modelling. IEEE Pervasive Computing 2, 14–21.

Holman, R., Stanley, L., 2007. The history and technical capabilities of Argus. Coastal Engineering 54, 477–491.

Holman, R., Symonds, G., Thornton, E., Ranasinghe, R., 2006. Rip spacing and persistence on an embayed beach. Journal of Geophysical Research 111, doi:10.1029/2005JC002965.

Houser, C., Arnott, R., Ulzhfer, S., Barrett, G., 2013. Nearshore circulation over transverse bar and rip morphology with oblique wave forcing. Earth Surface Processes and Landforms 38, 1269–1279.

Huisman, C., Bryan, K., Coco, G., Ruessink, B., 2011. The use of video imagery to analyse groundwater and shoreline dynamics on a dissipative beach. Continental Shelf Research 31, 1728–1738.

Huntley, D., Saulter, A., Kingston, K., Holman, R., 2009. Use of video imagery to test model predictions of surf heights, in: WIT Transactions on Ecology and the Environment, WIT Press. pp. 39–50.

Inman, D., Quinn, W., 1952. Currents in the surf zone, in: Proceedings of the 2nd Conference on coastal Engineering, Council on Wave Research. pp. 24–36.

Ishikawa, T., Komine, T., Aoki, S.I., Okabe, T., 2014. Characteristics of rip current drowning on the shores of japan. Journal of Coastal Research , 44–49arXiv:http://dx.doi.org/10.2112/SI72-009.1.

Johnson, D., Pattiaratchi, C., 2004. Transient rip currents and nearshore circulation on a swell-dominated beach. Journal of Geophysical Research 109, doi:10.1029/2003JC001798.

Kirchofer, W., 1974. Classification of european 500-mb patterns, in: Arbeitsbericht der Schweizerischen Meteorologischen Zentralanstalt, Geneva. pp. 1–32.

Komar, P., 1998. Beach processes and sedimentation. 2nd ed., Prentice-Hall, Upper Saddle River, New Jersey.

van de Lageweg, W., Bryan, K., Coco, G., Ruessink, B., 2013. Observations of shoreline-sandbar coupling on an embayed beach. Marine Geology 344, 101–114.

Leatherman, S.P., 2011. Future challenges for rip current research and outreach, in: Leatherman, S., Fletemeyer, J. (Eds.), Rip Currents: Beach safety, physical oceanography, and wave modelling. CRC Press, Florida, USA, pp. 259–271.

Lee, J.S., 1980. Digital image enhancement and noise filtering by use of local statistics. IEEE Trans. Pattern Anal. Mach. Intell. 2, 165–168.

Li, Z., 2016. Rip current hazards in south china headland beaches. Ocean & Coastal Management 121, 23–32.

Lippmann, T., Holman, R., 1989. Quantification of Sand Bar Morphology : A Video Technique Based on Wave Dissipation. Journal of Geophysical Research 94, 995–1011.

Lippmann, T., Holman, R., 1991. Phase Speed and Angle of Breaking Waves Measured with Video Techniques, in: Coastal Sediments (1991), ASCE. pp. 542–556.

Long, J.W., Ozkan-Haller, H.T., 2005. Offshore controls on nearshore rip currents. Journal of Geophysical Research: Oceans 110, n/a–n/a. C12007.

Longuet-Higgins, M., Stewart, R., 1964. Radiation stress in water waves, a physical discussion with applications. Deep-Sea Research 11, 529–563.

Longuet-Higgins, M.S., 1970. Longshore currents generated by obliquely incident sea waves: 1. Journal of Geophysical Research 75, 6778–6789.

MacMahan, J., Brown, J., Brown, J.A., Thornton, E., Reniers, A., Stanton, T., Henriquez, M., Gallagher, E., Morrison, J., Austin, M., Scott, T., Senechal, N., 2010. Mean Lagrangian flow behavior on an open coast rip-channeled beach: A new perspective. Marine Geology 268, 1–15.

MacMahan, J., Brown, J., Thornton, E., 2009. Low-Cost Handheld Global Positioning System for Measuring Surf-Zone Currents. Journal of Coastal Research 25, 744–754.

MacMahan, J., Reniers, A., Thornton, E., Stanton, T., 2004. Infragravity rip current pulsations. Journal of Geophysical Research 109, doi:10.1029/2003JC002068.

MacMahan, J., Thornton, E., Reniers, A., 2006. Rip current review. Coastal Engineering 53, 191–208.

Masselink, G., Austin, M., Scott, T., Poate, T., Russell, P., 2014. Role of wave forcing, storms and {NAO} in outer bar dynamics on a high-energy, macro-tidal beach. Geomorphology 226, 76 – 93.

Masselink, G., Evans, D., Hughes, M.G., Russell, P., 2005. Suspended sediment transport in the swash zone of a dissipative beach. Marine Geology 216, 169 – 189.

Masselink, G., Pattiaratchi, C., 2001. Seasonal changes in beach morphology along the sheltered coastline of perth, western australia. Marine Geology 172, 243 – 263.

Masselink, G., Puleo, J., 2006. Swash-zone morphodynamics. Continental Shelf Research 26, 661–680.

Masselink, G., Russell, P., 2006. Flow velocities, sediment transport and morphological change in the swash zone of two contrasting beaches. Marine Geology 227, 227 – 240.

Masselink, G., Short, A., 1993. The effect of tide range on beach morphodynamics and morphology: A conceptual beach model. Journal of Coastal Research 9, 785–800.

McCarroll, R., Brander, R., Turner, I., Power, H., Mortlock, T., 2014. Lagrangian observations of circulation on an embayed beach with headland rip currents. Marine Geology 355, 173–188.

McCarroll, R.J., Brander, R.W., MacMahan, J.H., Turner, I.L., Reniers, A.J., Brown, J.A., Bradstreet, A., 2013. Assessing the effectiveness of rip current swimmer escape strategies, shelly beach, nsw, australia. Journal of Coastal Research 65, 784–789.

McCarroll, R.J., Castelle, B., Brander, R.W., Scott, T., 2015. Modelling rip current flow and bather escape strategies across a transverse bar and rip channel morphology. Geomorphology 246, 502–518.

McGregor, G.R., Bamzelis, D., 1995. Synoptic typing and its application to the investigation of weather air pollution relationships, birmingham, united kingdom. Theoretical and Applied Climatology 51, 223–236.

McKay, C., Brander, R.W., Goff, J., 2014. Putting tourists in harms way–coastal tourist parks and hazardous unpatrolled surf beaches in new south wales, australia. Tourism Management 45, 71–84.

Miloshis, M., Stephenson, W.J., 2011. Rip current escape strategies: lessons for swimmers and coastal rescue authorities. Natural Hazards 59, 823–832.

Molinari, R., Kirwan, Jr., A.D., 1975. Calculations of Differential Kinematic Properties from Lagrangian Observations in the Western Caribbean Sea. Journal of Physical Oceanography 5, 483–491.

Murray, T., Cartwright, N., Tomlinson, R., 2013. Video-imaging of transient rip currents on the Gold Coast open beaches, in: 12th International Coastal Symposium, pp. 1809–1814.

Orzech, M.D., Reniers, A.J., Thornton, E.B., MacMahan, J.H., 2011. Megacusps on rip channel bathymetry: Observations and modeling. Coastal Engineering 58, 890 – 907.

Orzech, M.D., Thornton, E., MacMahan, J., O'Reilly, W.C., Stanton, T., 2010. Alongshore rip channel migration and sediment transport. Marine Geology 271, 278–291.

Pitman, S., Gallop, S., Haigh, I., Mahmoodi, S., Masselink, G., Ranasinghe, R., 2016. Synthetic imagery for the automated detection of rip currents. Journal of Coastal Research 1.

Plant, N.G., Aarninkhof, S.G.J., Turner, I.L., Kingston, K.S., 2007. The performance of shoreline detection models applied to video imagery. Journal of Coastal Research , 658–670arXiv:http://dx.doi.org/10.2112/1551-5036(2007)23[658:TPOSDM]2.0.CO;2.

Price, T., Ruessink, B., 2011. State dynamics of a double sandbar system. Continental Shelf Research 31, 659 – 674.

Quartel, S., 2009. Temporal and spatial behaviour of rip channels in a multiple-barred coastal system. Earth Surface Processes and Landforms 176, 163–176.

Quartel, S., Addink, E., Ruessink, B., 2006. Object-oriented extraction of beach morphology from video images. International Journal of Applied Earth Observation and Geoinformation 8, 256 – 269.

Ranasinghe, R., Symonds, G., Black, K., Holman, R., 2004. Morphodynamics of intermediate beaches: a video imaging and numerical modelling study. Coastal Engineering 51, 629 – 655.

Ranasinghe, R., Symonds, G., Holman, R., 1999. Quantitative characterisation of rip currents via video imaging, in: Kraus, N., McDougal, W. (Eds.), Coastal Sediments '99. American Society of Civil Engineers, Reston, USA, pp. 987–1002.

Reniers, A., MacMahan, J., Thornton, E., Stanton, T., Henriquez, M., Brown, J., Brown, J.A., Gallagher, E., 2009. Surf zone surface retention on a rip-channeled beach. Journal of Geophysical Research 114, doi:10.1029/2008JC005153.

Reniers, A.J.H.M., MacMahan, J.H., Beron-Vera, F.J., Olascoaga, M.J., 2010. Rip-current pulses tied to lagrangian coherent structures. Geophysical Research Letters 37, n/a–n/a. L05605.

Reniers, R.L.E.P., Murphy, L., Lin, A., Bartolom, S.P., Wood, S.J., 2016. Risk perception and risk-taking behaviour during adolescence: The influence of personality and gender. PLOS ONE 11, 1–14.

Russ, J.C., 2011. Image Processing Handbook, Sixth Edition. 6th ed., CRC Press, Inc., Boca Raton, FL, USA.

Schmidt, W.E., Woodward, B.T., Millikan, K.S., Guza, R.T., Raubenheimer, B., Elgar, S., 2003. A gps-tracked surf zone drifter. Journal of Atmospheric and Oceanic Technology 20, 1069–1075. arXiv:http://dx.doi.org/10.1175/1460.1.

Scott, T., Austin, M., Masselink, G., Russell, P., 2016. Dynamics of rip currents associated with groynes — field measurements, modelling and implications for beach safety. Coastal Engineering 107, 53 – 69.

Scott, T., Masselink, G., Austin, M., Russell, P., 2014. Controls on macrotidal rip current circulation. Geomorphology 214, 198–215.

Scott, T., Russell, P., Masselink, G., Austin, M., Wills, S., Wooler, A., 2011. Rip Current Hazards on the United Kingdom, in: Leatherman, S., Fletemeyer, J. (Eds.), Rip Currents: Beach safety, physical oceanography, and wave modelling. CRC Press, Boca Raton, FL. 1999, pp. 225–244.

Scott, T., Russell, P., Masselink, G., Wooler, A., 2009. Rip current variability and hazard along a macro-tidal coast. Journal of coastal research , 895.

Scott, T., Russell, P., Masselink, G., Wooler, A., Short, A., 2008. High volume sediment transport and its implications for recreational beach risk, in: Proceedings of the International Conference on Coastal Engineering, Hamburg. pp. 4250–4262.

Shaw, W., Goff, J., Brander, R., Walton, T., Roberts, A., Sherker, S., 2014. Surviving the surf zone: Towards more integrated rip current geographies. Applied Geography 54, 54–62.

Shepard, F., 1936. Rip tide or "rip current". Science 84, 181–182.

Shepard, F., Emery, K., LaFond, E., 1941. Rip currents: a process of geological importance. Journal of Geology 49, 337–369.

Shepard, F., Inman, D., 1950. Nearshore circulation related to the bottom topography and wave refraction. Transactions of the American Geophysial Union 31, 555–565.

Shepard, F., Inman, D., 1951. Nearshore circulation, in: ASCE (Ed.), Proceedings of the 1st Coastal Engineering Conference, New York. pp. 50–59.

Sherker, S., Williamson, A., Hatfield, J., Brander, R., Hayen, A., 2010. Beachgoers' beliefs and behaviours in relation to beach flags and rip currents. Accident; analysis and prevention 42, 1785–1804.

Sherwood, A.M., Nelson, C.S., 1979. Surficial sediments of raglan harbour. New Zealand Journal of Marine and Freshwater Research 13, 475–496. arXiv:http://dx.doi.org/10.1080/00288330.1979.9515825.

Short, A., 1985. Rip-current type, spacing and persistence, Narrabeen beach, Australia. Marine Geology 65, 47–71.

Short, A., 2007. Australian Rip Systems – Friend or Foe ? Journal of Coastal Research SI50, 7–11.

Short, A.D., 1979. Three dimensional beach-stage model. The Journal of Geology 87, 553–571. arXiv:http://dx.doi.org/10.1086/628445.

da Silva, J.C., Sancho, F., Quaresma, L., 2006. Observation of rip currents by synthetic aperture radar. Proceedings of SEASAR .

Singley, J.A., 2004. Hazard versus risk. Chemical Health and Safety 11, 14 – 16.

SLSA, 2011. 2010-11 National Surf Safety Report. Technical Report. Surf Life Saving Australia.

SLSNZ, 2016. Patrol and Memberships Database. techreport. Surf Life Saving New Zealand. Wellington, New Zealand.

Smit, M., Aarninkhof, S., Wijnberg, K., Gonzaléz, M., Kingston, K., Southgate, H., Ruessink, B., Holman, R., Siegle, E., Davidson, M., Medina, R., 2007. The role of video imagery in predicting daily to monthly coastal evolution. Coastal Engineering 54, 539–553.

Smith, R.K., Bryan, K.R., 2007. Monitoring beach face volume with a combination of intermittent profiling and video imagery. Journal of Coastal Research , 892–898arXiv:http://dx.doi.org/10.2112/04-0287.1.

Sonu, C., 1972. Field observations of nearshore circulation and meandering currents. Journal of Geophysical Research 77, 3232–3247.

Spydell, M., Feddersen, F., Guza, R.T., Schmidt, W.E., 2007. Observing surf-zone dispersion with drifters. Journal of Physical Oceanography 37, 2920–2939. arXiv:http://dx.doi.org/10.1175/2007JPO3580.1.

Spydell, M.S., 2016. The suppression of surfzone cross-shore mixing by alongshore currents. Geophysical Research Letters 43, 9781–9790.

Stockdon, H., Holman, R., 2000. Estimation of wave phase speed and nearshore bathymetry from video imagery. Journal of Geophysical Research 105, 22015.

Thorpe, A., Miles, J., Masselink, G., Russell, P., Scott, T., Austin, M., 2013. Suspended sediment transport in rip currents on a macrotidal beach. Journal of Coastal Research , 1880–1885arXiv:http://dx.doi.org/10.2112/SI65-318.1.

Tomasi, C., Manduchi, R., 1998. Bilateral filtering for gray and color images, in: Sixth International Conference on Computer Vision (IEEE Cat. No.98CH36271), pp. 839–846.

Turner, I., Aarninkhof, S., Holman, R., 2006. Coastal imaging applications and research in Australia. Journal of Coastal Research 22, 37–48.

Turner, I., Whyte, D., Ruessink, B., Ranasinghe, R., 2007. Observations of rip spacing, persistence and mobility at a long, straight coastline. Marine Geology 236, 209–221.

Van Leeuwen, B.R., McCarroll, R.J., Brander, R.W., Turner, I.L., Power, H.E., Bradstreet, A.J., 2016. Examining rip current escape strategies in non-traditional beach morphologies. Natural Hazards 81, 145–165.

Vos, R.G., 1976. Observations on the formation and location of transient rip currents. Sedimentary Geology 16, 15 – 19.

Wang, J.Y.A., Adelson, E.H., 1994. Representing moving images with layers. IEEE Transactions on Image Processing 3, 625–638.

Whyte, D., Turner, I., Ranasinghe, R., 2005. Rip characterisation on the gold coast, australia: An analysis using coastal imaging techniques, in: Coasts and Ports 2005: Coastal Living - Living Coast, Adelaide, Australia. pp. 233–238.

Winter, G., van Dongeren, A., de Schipper, M., van Thiel de Vries, J., 2014. Rip currents under obliquely incident wind waves and tidal longshore currents. Coastal Engineering 89, 106 – 119.

Woodward, E., Beaumont, E., Russell, P., Wooler, A., Macleod, R., 2013. Analysis of rip current incidents and victim demographics in the uk. Journal of Coastal Research 65, 850–855.

Wright, L., Chappell, J., Thom, B., Bradshaw, M., Cowell, P., 1979. Morphodynamics of reflective and dissipative beach and inshore systems: Southeastern australia. Marine Geology 32, 105 – 140.

Wright, L., Short, A., 1984. Morphodynamic variability of surf zones and beaches: A synthesis. Marine Geology 56, 93 – 118.

Wright, L., Short, A., Boon, J., Hayden, B., Kimball, S., List, J., 1987. The morphodynamic effects of incident wave groupiness and tide range on an energetic beach. Marine Geology 74, 1 – 20.

Yarnal, B., 1992. Synoptic Climatology in Environmental Analysis: A Primer. Studies in Climatology, Wiley.

Yu, J., Slinn, D., 2003. Effects of wave-current interaction on rip currents. Journal of Geophysical Research 108, doi:10.1029/2001JC001105.